AD-A089 142 LOCKHEED MISSILES AND SPACE CO INC PALO ALTO CA PALO --ETC F/G 22/2
ACOSS THREE (ACTIVE CONTROL OF SPACE STRUCTURES), PHASE I.(U)
MAY 80 M G LYONS, J N AUBRUN, G MARGULIES F30602-79-C-0087
UNCLASSIFIED RADC-TR-80-131 NL

1 OF 3
AD A 089 142

LEVEL II

RADC-TR-80-131
Final Technical Report
May 1980

ACOSS THREE (ACTIVE CONTROL OF SPACE STRUCTURES) PHASE I

Lockheed Missiles & Space Company, Inc.

Sponsored by
Defense Advanced Research Projects Agency (DoD)
ARPA Order No. C654

APPROVED FOR PUBLIC RELEASE; DISTRIBUTION UNLIMITED

The views and conclusions contained in this document are those of the authors and should not be interpreted as necessarily representing the official policies, either expressed or implied, of the Defense Advanced Research Projects Agency or the U. S. Government.

ROME AIR DEVELOPMENT CENTER
Air Force Systems Command
Griffiss Air Force Base, New York 13441

(15) F30602-79-C-0087

UNCLASSIFIED

SECURITY CLASSIFICATION OF THIS PAGE (When Data Entered)

(19) REPORT DOCUMENTATION PAGE		READ INSTRUCTIONS BEFORE COMPLETING FORM
1. REPORT NUMBER (18) RADC-TR-80-131	2. GOVT ACCESSION NO. AD-A089	3. RECIPIENT'S CATALOG NUMBER 742
4. TITLE (and Subtitle) (1) ACOSS THREE (ACTIVE CONTROL OF SPACE STRUCTURES), PHASE I		5. TYPE OF REPORT & PERIOD COVERED (9) Final Technical Report 2 Jan [redacted] - 30 Sep 79
		6. PERFORMING ORG. REPORT NUMBER N/A
7. AUTHOR(s) (10) Michall G. Lyons, Narenda K. Gupta, Jean N. Aubrun, et al, Gabriel Margulies		8. CONTRACT OR GRANT NUMBER(s) F30602-79-C-0087
9. PERFORMING ORGANIZATION NAME AND ADDRESS (1) Lockheed Missiles & Space Company, Inc. Lockheed Palo Alto Research Laboratory 3251 Hanover Street, Palo Alto CA 94304		10. PROGRAM ELEMENT, PROJECT, TASK AREA & WORK UNIT NUMBERS 62301E C6540103 (17) 01
11. CONTROLLING OFFICE NAME AND ADDRESS (11) Defense Advanced Research Projects Agency 1400 Wilson Blvd Arlington VA 22209		12. REPORT DATE May [redacted]80 13. NUMBER OF PAGES 205 (12) 212
14. MONITORING AGENCY NAME & ADDRESS (if different from Controlling Office) Rome Air Development Center (OCSE) Griffiss AFB NY 13441		15. SECURITY CLASS. (of this report) UNCLASSIFIED 15a. DECLASSIFICATION/DOWNGRADING SCHEDULE N/A

16. DISTRIBUTION STATEMENT (of this Report)

Approved for public release; distribution unlimited.

17. DISTRIBUTION STATEMENT (of the abstract entered in Block 20, if different from Report)

Same

18. SUPPLEMENTARY NOTES

RADC Project Engineer: Richard Carman (OCSE)

19. KEY WORDS (Continue on reverse side if necessary and identify by block number)

control theory, large space structures, structural dynamics, flexible vehicles, stability augmentation, micro-vibration suppression, low and high authority control

20. ABSTRACT (Continue on reverse side if necessary and identify by block number)

The theory of stability augmentation (active control of vehicle dynamics) for large space structures is developed and tested analytically on a number of strawman configurations including large surveillance and HEL weapons platforms. It is shown that active control is potentially feasible for micro-vibration stabilization of precision large structures; performance of several experimental breadboards is illustrated to enhance the theory.

DD FORM 1 JAN 73 1473 EDITION OF 1 NOV 65 IS OBSOLETE

UNCLASSIFIED

SECURITY CLASSIFICATION OF THIS PAGE (When Data Entered)

210118 slt

FOREWORD

This final report for Active Control of Space Structures (Phase I) represents work performed by the Lockheed Missiles & Space Company, Inc., and its subcontractor Systems Control, Inc. for the Defense Advanced Research Projects Agency under Contract No. F30602-79-C-0087. Synergistic Technology, Inc. and Dr. R. E. Skelton served as principal contributing consultants.

CONTENTS

Section		Page
1	INTRODUCTION	1-1
	1.1 Background	1-1
	1.2 Outline of Report	1-2
2	APPROACH	2-1
	2.1 Introduction and Methodology	2-1
	2.2 Basic Controller Forms	2-2
	2.3 Features of the Control Synthesis Methodology	2-5
	References	2-7
3	STRUCTURAL MODELING TECHNIQUE	3-1
	3.1 Finite-Element Models	3-1
	3.2 Distributed Models	3-4
4	CONTROL SYNTHESIS TECHNIQUES	4-1
	4.1 Low Authority Control Synthesis	4-1
	4.2 High Authority Control Methods	4-6
	4.2.1 Control Problem	4-6
	4.2.2 Model Reduction	4-11
	4.2.3 Control Design	4-18
	References	4-38
	4.2.4 Orthogonal Filters	4-39
	References	4-44
	4.2.5 Controller Simplification	4-45
	4.3 Selection of Actuator Locations	4-49
	4.3.1 Introduction	4-49
	4.3.2 Problem Statement	4-49
	4.3.3 Optimality Criteria	4-50
	4.3.4 General Form For The Controllability Matrix	4-51

CONTENTS (Cont.)

Section		Page
	4.3.5 Numerical Procedure	4-56
	4.3.6 Conclusion	4-56
5	APPLICATIONS TO DARPA STRAWMEN	5-1
	5.1 The Charles Stark Draper Laboratory (CSDL) Example	5-1
	5.1.1 The CSDL Example Structural Model	5-1
	5.1.2 The CSDL Example Control Problem	5-4
	5.1.3 The CSDL Example: Centralized Low Authority Controller Design	5-5
	5.1.4 The CSDL Example: Decentralized Low Authority Controller Design	5-12
	5.1.5 Generalized Collocated Control Design	5-15
	5.1.6 Modal Cost Analysis (MCA) Results for the CSDL Example	5-23
	5.2 Adopt 5/4 System	5-26
	5.2.1 System Description	5-26
	5.2.2 SAS Performance	5-26
	5.3 MM-Wave System	5-32
	5.3.1 System Description	5-32
	5.3.2 SAS Performance	5-32
	5.4 Halo/Walrus System	5-38
	5.4.1 System Description	5-38
	5.4.2 SAS Performance	5-38
	5.5 Tilting Telescope System (Adopt-12)	4-45
6	EXPERIMENTAL RESULTS	6-1
	6.1 Proof-Mass Damped Beam (Minibeam)	6-1
	6.1.1 Experimental Set-Up	6-1
	6.1.2 Analytical Model and Actuator Dynamics	6-3
	6.2 Gyrodamped Beam (Maxibeam)	6-5
	6.2.1 Experimental Set-Up	6-5
	6.2.2 Analytical Model and Actuator Dynamics	6-9

CONTENTS (Cont.)

Section		Page
	6.2.3 Control Equations for Active Augmentation of Passive Gyrodamper	6-11
	6.3 TOYSAT Experiments	6-15
	6.3.1 Introduction	6-16
	6.3.2 Optimal Slew Maneuver	6-17
	6.3.3 Low Authority Control	6-18
	6.3.4 High Authority Control	6-25
	6.4 Microvibration Sensing	6-37
	6.4.1 Introduction	6-37
	6.4.2 Theory	6-38
	6.4.3 Digital Signal Processor	6-44
	6.4.4 Experimental Apparatus	6-50
	6.4.5 Experimental Results	6-54
	6.4.6 Conclusions and Recommendations	6-60
7	CONCLUSIONS AND FUTURE WORK	7-1
	7.1 Conclusions	7-1
	7.2 Future Work	7-1
Appendix		
A	MODAL STRUCTURE OF OSCILLATORY SYSTEMS	A-1
B	INVERSE OPTIMAL CONTROL FOR GENERALIZED COLLOCATED CONTROL	B-1
C	DESIGN OF CONTROL LAWS WITH FREQUENCY SHAPED COST FUNCTIONALS	C-1
D	MINIMUM ENERGY CONTROL	D-1

Section 1
INTRODUCTION

1.1 BACKGROUND

Increasing threat of global warfare has created a significant need for large space platforms both for surveillance and for deployment of space based defensive weapon systems. Because these systems may operate in optical or mm-wave regimes, the structures must maintain accurate geometric shapes. The presence of active systems onboard the spacecraft also may require the minimization of vibration from random disturbances. Self-defense may demand that the platform be maneuvered without structural damage or loss of performance.

Insuring that such performance can be met using passive techniques (e.g., structural stiffening, material selection) generally poses unacceptable weight penalties or performance uncertainties even when such techniques may be feasible. For high performance maneuvering, passive methods can totally fail to provide adequate performance. Active control techniques, however, may be effectively used to create so-called control configured spacecraft where the structural dynamic properties including structural damping are strongly influenced by active closed-loop control systems placed on the basic structure. In this way, requirements on passive stiffness and damping may be considerably relaxed with potential savings in weight, material costs, and payload subsystem complexity. The technology of active structural control however is still immature and poorly understood.

The performance potential for control configured spacecraft is the motivation for the DARPA/ACOSS (Active control of Space Structures) program . This report, covering the activities of the LMSC Phase I effort, summarizes the analytical investigations, control synthesis methods, and experimental results (funded by IRAD) achieved during this 1978 program. Contributions of individual team members, including Lockheed, Palo Alto Research Lab, the LMSC Space Systems

Division, Systems Control, Inc., Synergistic Technology, Inc., and Prof. R. E. Skelton (Purdue), were critical to the progress made during Phase I. To keep this report to a reasonable length, many techniques are only summarized or briefly discussed as indicated in the sections below.

1.2 OUTLINE OF REPORT

Section 2 is a brief exposition of the technical approach taken in Phase I of ACOSS.

Section 3 deals with the important subject of modeling techniques for flexible spacecraft and the relative merits and pitfalls of continuum or discrete models and the effects of closed-loop controls.

Section 4 comprises the bulk of the control synthesis methodology in both low- and high authority control techniques. Section 5 provides summaries of the analytical designs for stability augmentation systems for the DARPA Strawmen configurations studied under Phase I. Finally, experimental results developed under IRAD which are relevant to Phase I objectives and, in particular, to follow-on efforts are included in Section 6.

Section 2
APPROACH

2.1 INTRODUCTION AND METHODOLOGY

Stability augmentation or the addition of closed-loop damping to large flexible space structures has been the subject of numerous recent papers (Refs [1-5]). These publications have focused, for the most part, on single methodologies or techniques for synthesizing a control law. This report is a synopsis of research work performed over the past year and endeavors to match various synthesis techniques and controller forms to specific system performance requirements. In so doing, it evolves a general approach to structural stability augmentation. Moreover, this combination of techniques permits guarantees of system robustness, if not performance, which would otherwise be unattainable. The methodology advocated here requires several complex techniques indicated below.

The general requirements for stability augmentation are listed in Table 1. It should be noted that shape control is a different process from removal of vibrational energy from the structure as noted in the table. The first two categories require large increases in structural damping at low frequency either because the attitude control system is interacting with the structure or because maneuver induced structural ringing must be removed to meet mission requirements. Modifying structural admittance functions at specific low frequencies generally requires substantial knowledge of mode shapes and frequency quantities which are known less accurately at higher frequency. The third category arises from the need to control high frequency settling times and to suppress vibration propagation from sources imbedded in the structure (e.g., coolers, CMG's, etc.).

Table 1

STABILITY AUGMENTATION REQUIREMENTS

- STABILITY AUGMENTATION - STRUCTURAL DEFLECTION VELOCITY SUPPRESSION
  - FEW SENSORS / ACTUATORS, ALL BROADBAND
- VEHICLE SHAPE / DIRECT FIGURE CONTROL
  - VERY LOW BANDWIDTH SENSING
  - LARGE NUMBER OF ACTUATORS

STRUCTURAL DISTURBANCE	CONTROL REQUIREMENT	A PRIORI KNOWLEDGE OF SYSTEM DYNAMICS
ATTITUDE CONTROL	HIGH DAMPING IN OVERLAPPED MODES	EXCELLENT ($10\%\ f_o$)
MANEUVERING / TRANSIENT SETTLING	MINIMUM EXCITATION, HIGH DAMPING IN SELECTED MODES	GOOD TO POOR ($\geq 10\%\ f_o$) DEGRADES WITH FREQUENCY
VIBRATION SUPPRESSION	BROADBAND, LOW TO MODERATE DAMPING	POOR FOR ALL CASES, OPEN-LOOP DAMPING $\zeta > 100\%$ ERROR

2.2 BASIC CONTROLLER FORMS

Two basic classes of controls emerge from these requirements. Low-Authority Structural Controls (LASC) which provide limited (broadband) modal damping may be synthesized using perturbation techniques as shown by Aubrun [Ref 2 and Section 4.1]. For systems restricted to collocated rate sensing and complementary actuation (decentralized, no cross-coupling), Aubrun shows that stability is guaranteed over the system bandwidth and, with suitable precautions as discussed below, the system is always stable. High-Authority Structural Control (HASC) which provides arbitrary damping ratios in low frequency modes by exploiting knowledge of system dynamics is generally synthesized as a multi-input/multi-output (centralized) control. A direct application of standard control design procedures leads to serious stability problems. Within the HASC bandwidth, spillover in modeled and unmodeled modes must be bounded by reduction of parameter sensitivity or, ultimately, by system identification prior to imposing the control. Beyond the HASC bandwidth uncontrolled phase shifts introduced by lightly damped modes can cause system instability. Synthesis of the HASC system which forces rapid control effort roll-off with increasing frequency coupled with an overlapped LASC system to lower modal q in the crossover region significantly increases system robustness. This relationship is illustrated in Fig. 1. The methods for guaranteeing stability are summarized in Table 2. Fundamentally, HASC stability due to interaction with high frequency modes is assured by limited high frequency HASC authority and a decentralized LASC system for which critical modes at HASC crossover are controllable (fixed by LASC actuator placement).

The selection of a control law using a centralized form (LASC or HASC) may proceed either by using perturbation techniques based on a formula by Jacobi or by minimization of a quadratic cost functional with state and control weighting which are frequency dependent. This frequency dependence forces a dynamic controller form with an augmented state vector dictated by the frequency roll-off selected by the designer.

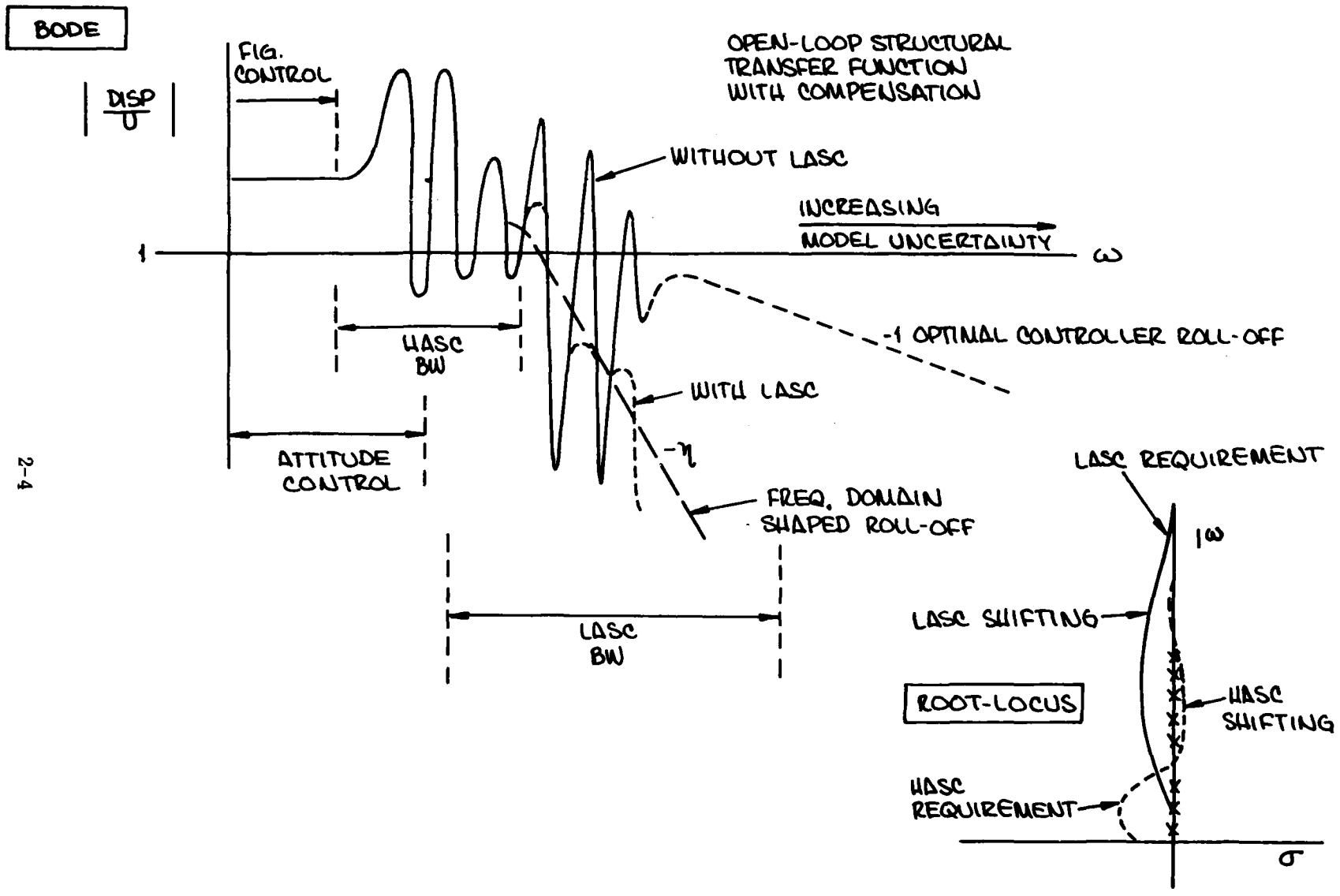

Fig. 1 Integrated LASC/HASC Stability Augmentation

2.3 FEATURES OF THE CONTROL SYNTHESIS METHODOLOGY

The following features of the control design methodology provide a systematic approach to meet system performance goals.

(a) The basic method consists of three steps, (i) model reduction, (ii) filter/control law specification, and (iii) control law simplification. This provides a good model in the control design stage. The resulting controller may be further simplified in the last step.

(b) Specific attention is given to poles, zeros and residues in the model reduction stage. This resulting reduced order model then provides a good approximation of system behavior in the frequency range of interest.

(c) For collocated systems (sensors and actuators at the same location), a general control design approach is proposed based both on modern control theory and root perturbation techniques.

(d) A unique linear quadratic – Gaussian design method is developed in which the performance index is shaped with frequency. This results in control laws which have minimum influence on high frequency modes. This provides a mechanism to minimize the possibility of high frequency modes going unstable.

(e) The controller is treated as a dynamic model with specified inputs and outputs. The model reduction methods are then used to simplify the controller.

(f) Techniques for optimal actuator/sensor locations are studied.

Table 2

SUMMARY OF STABILITY AUGMENTATION APPROACH

REQUIREMENT	CONTROLLER FORM	METHODS TO INSURE STABILITY
HIGH DAMPING RATIOS IN SELECTED MODES > 20 %	HIGH-AUTHORITY NON-COLOCATED (CENTRALIZED) (HASC)	WITHIN HASC BANDWIDTH (PARAMETER ERRORS): • FREQ. WEIGHTING (STATE WEIGHTING) • ACTUATOR/SENSOR PLACEMENT • SYSTEM IDENTIFICATION OUTSIDE HASC BANDWIDTH (TRUNCATION, MODELING ERRORS): • FREQ. WEIGHTING - DYNAMIC CONTROLLERS • OVERLAPPED LOW-AUTHORITY SYSTEM TO SUPPRESS HIGH Q MODES AT CROSSOVER
LOW TO MODERATE 5-25 % * (* HIGH VALUES ACHIEVED IN SPECIAL CASES)	LOW-AUTHORITY COLOCATED (DECENTRALIZED) (LASC)	WITHIN LASC BANDWIDTH: • STABLE UNDER ANY CONDITIONS • PERFORMANCE MINIMIZED BY ACTUATOR PLACEMENT, FEEDBACK "TUNING" OUTSIDE LASC BANDWIDTH: • RESONANCE WITH HIGH Q STRUCTURAL MODES CONTROLLED WITH PARALLEL PASSIVE DAMPER

INCREASING ROBUSTNESS ↓

REFERENCES

1. R. E. Skelton, "Adaptive Orthogonal Filters for Compensation of Truncated Modes and Other Model Data Uncertainty in Spacecraft," AIAA 17th Aerospace Sciences Meeting, Jan. 15-17, 1979, paper No. 79-0197

2. J. N. Aubrun, "Theory of the Control of Structures by Low Authority Controllers," AIAA Conference on Large Space Platforms: Future Needs and Capabilities, Los Angeles, Calif., Sept. 27-29, 1978, paper No. 78-1689

3. J. N. Aubrun, "General Theory of Low Authority Control" (in preparation)

4. M. J. Balas, "Reduced Order Control of Large Structures in Space," 17th AIAA Aerospace Sciences Meeting, Jan. 1979, paper No. 79-0196

5. P. V. Kokotovic, et. al., "Singular Perturbation Methods for Reducing the Model Order in Optimal Control Design," IEEE Transactions on Auto Control, Vol. AC-13, No. 4, August 1969

6. N. K. Gupta, "Frequency Shaping Techniques in Modern Control Design Methods," Systems Control, Inc. Technical Memo, June 1978

Section 3
STRUCTURAL MODELING TECHNIQUE

3.1 FINITE-ELEMENT MODELS

A central issue in the active control of space structures is the development of "correct" mathematical models for the open and closed loop dynamical plants. While a great deal of polemic has been generated in recent times against finite-element structural programs and their assorted pitfalls, programs such as NASTRAN, SPAR, ASTRO, etc., are never-the-less the primary tools for generating dynamical models of conceptual spacecraft whose structure cannot be idealized by simple models of beams, plates, beams with lumped masses, and so on.

Finite-element structural programs were used extensively during Phase I of the ACOSS Program in order to model the DARPA Strawmen dynamical plants (HALO, MM WAVE, ADOPT's 5/4 and 12, CSDL example) to which various controllers were applied. While this modeling was not heavily emphasized by the contract requirements, it turned out to be an important activity in the sense that insights were gained into the various aspects of the process and the emergence of a general methodology was identified. The essential observation was made that a single finite-element model of a structure, postulated in an a priori fashion, was not necessarily the best modal representation suitable for the closed-loop model. After insight was gained into the control policy to be applied, and, in particular, into the type of actuctors (and their locations) required to implement it, it became very plausible that a more refined open-loop model would improve modal convergence of the closed-loop model and hence alleviate the difficulties of modal truncation. Implicit in this approach is the requirement that a structure can be examined geometrically by computer-graphic animation techniques which clarify the physical interaction between actuators and the local structural deformations which they impose. In this sense, a structure-to-be-controlled becomes much more than a set of constant coefficient matrices given once and for all.

The structural design iteration procedure identified at the end of Phase I of the ACOSS program, could typically involve the following steps:

1. Design the global structure, and "tune" local substructures. In the HALO design, for example, the tuning of the flexible mirror substructures was to a large extent independent of the overall design which would treat these mirrors, in a first approximation, as rigid plates interconnected by elastic beams.

2. Examine the elastic behavior (generally via the undamped, free/free eigenmodes) using computer-graphic animation such as available on the ADAGE computer in LMSC's STARLAB. What is required here is the observation of the physical motions occurring locally in the neighborhood of nodal and antinodal points of the dominant structural modes.

3. Infer from these geometrical motions (translations, rotations, and combinations of both) preliminary actuator locations and actuator types to be used. These could consist of forces, force couples, torques, torque couples, etc. Depending upon the structural design and the mission requirements, trade-offs can be made between inertial and intrastructural actuators. This step is particularly important for decentralization colocated LAC sensor/actuator pairs, and serves indirectly to corroborate the information derived from Aubrun's controller effectiveness coefficients*

$$e_{an} \equiv \phi^{A}_{an} \, \phi^{R}_{rn} = \left(\phi_n\right)^2$$

or, equivalently, from the Skelton-Hughes controllability maps when these can be constructed.

4. Synthesize preliminary controls and test performance via closed-loop eigenanalysis. Performance criteria may be derived from the insensitivity of the zeroes of closed-loop transfer functions to modal truncation (see next section), from convergence of phase and/or gain measures vs number of modes, or from other measures. If performance is not satisfactory, proceed to next step.

5. Modify the boundary conditons of the structure by introducing, at actuator locations, "fictitious" inertias (translational or rotational) whose D'Alembert reactions (forces or torques) will mimic the effect of the corresponding actuators. In structural dynamics this procedure is equivalent to the use of certain classes of quasi-static modes. For example, a beam which is torque-controlled at one end is better represented by modes which correspond to the presence of a suitable rotary inertia at the controlled end rather than by free-free modes, even if a lumped mass is added at the controlled end to model the actuator.

*See eg (8) in Section 4.1, Low Authority Control Synthesis:

6. Repeat eigenanalysis of the modified structure to generate faster converging modes vis-a-vis performance criteria.

The above design iteration steps represent, in general, extensive work, but experience gained in Phase I of the ACOSS program clearly indicates that the integration between controls and structural dynamics expertise is far from complete. The effectiveness of procedures such as outlined above can only be evaluated in detailed applications.

3.2 DISTRIBUTED MODELS

Such models may be obtained for structures that can be conveniently described by partial differential equations (PDEs). Although it seems unlikely that a complex space structure will ever fall into that category, interest in this type of modeling is threefold: 1) for laboratory experiments, where the test structures may be simple enough, an analytical model would be the most accurate and therefore of greater value for evaluating the experimental results; 2) PDEs may be used directly for control synthesis; and 3) PDEs offer a direct way for evaluating the finite-element models and understand their deficiencies.

Distributed models may be used in two different ways, both starting with partial differential equations which are assumed to be a complete description of the dynamical characteristics of the system.

The first method converts these PDEs and associated boundary conditions into an infinite set of ordinary differential equations. A small subset of these ODEs is then chosen as a model, and this is strictly equivalent to the finite-element approach, except that a finite set of modes is obtained analytically and not via a numerical eigensystem decomposition. This method was used in all the beams and experiments described in Section 6 and were found to be very accurate and useful.

The second method starts with the same PDEs but does not expend the solution into modes. Better, it directly obtains an exact analytical transfer function which can be used in classical control theory, or in the more elaborate – distributed optimal control theory if desired.*

Since approximate transfer functions can also be obtained from model expansion of the first method, comparisons can be made between finite-element representations (identical to the first method) and the exact model (second method). The

*J. A. Breakwell, "Automatic Control of Flexible Spacecraft," Ph.D. Thesis, Stanford University, to appear Dec 1979.

particular problem of a free-free beam was treated using these two approaches and analytical expressions obtained for the continuous and discrete (modal) transfer functions are shown in Fig. 1. Two types of transfer function appear in Fig. 1, i.e., displacement/force and rotation/torque at one end. All symbols are defined in Fig. 1. The discrete transfer function $T_d(\beta;n)$ is a function of the number n of modes retained in the series expansion.

Figure 2 shows a graphical comparison of the exact rotation-to-torque transfer function $T_c(\beta)$ (obtained from the continuous model) and the truncated (discrete) transfer functions $T_d(\beta;n)$ when 7 terms or 20 terms are retained, i.e., the beam is modeled by one rigid body mode and either 6 or 19 structural modes. The graph clearly shows the error in the zero-crossings, while the other parts of the curves are in excellent agreement. Because the zeroes of the open-loop system play an important part in the closed-loop system, their insensitivity to modal truncation is of prime importance to the control design. Zero crossing errors can be reduced by increasing the number n of modeled modes, but a satisfactory result will require a very large value for n. These curves indicate that a much better approximation could be obtained by adding a constant bias term (negative in this case) to the discrete transfer function.

A more systematic view of this problem can be seen in Fig. 3 which shows the partitioning of the infinite series representing the exact transfer function for the case of a general undamped structure. The ϕ_i's are the mode shapes at the location where the displacement-to-force ratio is measured (or rotation-to-torque, etc.). The number of modes to be controlled is n_c, the number of modes retained in the model of the structure is n_r.

In the straight truncation case one has $n_r = n_c$, and a substantial error is committed in representing the zeroes of the system, leading to erroneous control design. The expanded truncation uses a larger model, but still a significant error may remain. The "rounded" transfer function approximates the remainder of the infinite series by a constant bias term. (For these terms, s is indeed much less than the ω's, hence the approximation.)

ρ: BEAM DENSITY
A: CROSS-SECTIONAL AREA
E: YOUNG'S MODULUS
I: CROSS-SECTIONAL INERTIA
ℓ: BEAM LENGTH

S: LAPLACE TRANSFORM VARIABLE

$$\beta^4 \equiv -\ell^4 \rho A s^2 / EI$$

y: BEAM DEFLECTION AT ONE END
θ: BEAM SLOPE AT THAT END
f: FORCE APPLIED TO BEAM AT THAT END
τ: TORQUE APPLIED TO BEAM AT THAT END

(DEF.)

$$\begin{cases} T(\beta) \equiv y(s,\ell)/f(s,\ell) & \text{(CONTINUOUS OR DISCRETE)} \\ T'(\beta) \equiv \theta(s,\ell)/\tau(s,\ell) & \text{(CONTINUOUS OR DISCRETE)} \end{cases}$$

TRANSLATION/FORCE	$T_c(\beta) = \frac{3}{EI\beta^3} \frac{\sin\beta\cosh\beta - \cos\beta\sinh\beta}{1 - \cosh\beta\cos\beta}$	(CONTINUOUS)
	$T_d(\beta;n) = \frac{4\ell^3}{EI}\left[\frac{1}{\beta^4} + \sum_{i=1}^{n} \frac{1}{\beta^4 - \beta_i^4}\right]$	(DISCRETE)
ROTATION/TORQUE	$T_c'(\beta) = \frac{\ell}{EI\beta} \frac{\sin\beta\cosh\beta + \cos\beta\sinh\beta}{1 - \cosh\beta\cos\beta}$	(CONTINUOUS)
	$T_d'(\beta;n) = \frac{4\ell}{EI}\left[\frac{3}{\beta^4} + \sum_{i=1}^{n} \frac{\beta_i^2}{\beta^4 - \beta_i^4}\left(\frac{\cos\beta_i - \cos\beta_i}{\sin\beta_i - \sin\beta_i}\right)\right]$	(DISCRETE)

CONTINUOUS AND DISCRETE OPEN-LOOP TRANSFER FUNCTIONS FOR BEAM (I)

Fig. 1 Continuous and Discrete Open-Loop Transfer Functions for Beam (I)

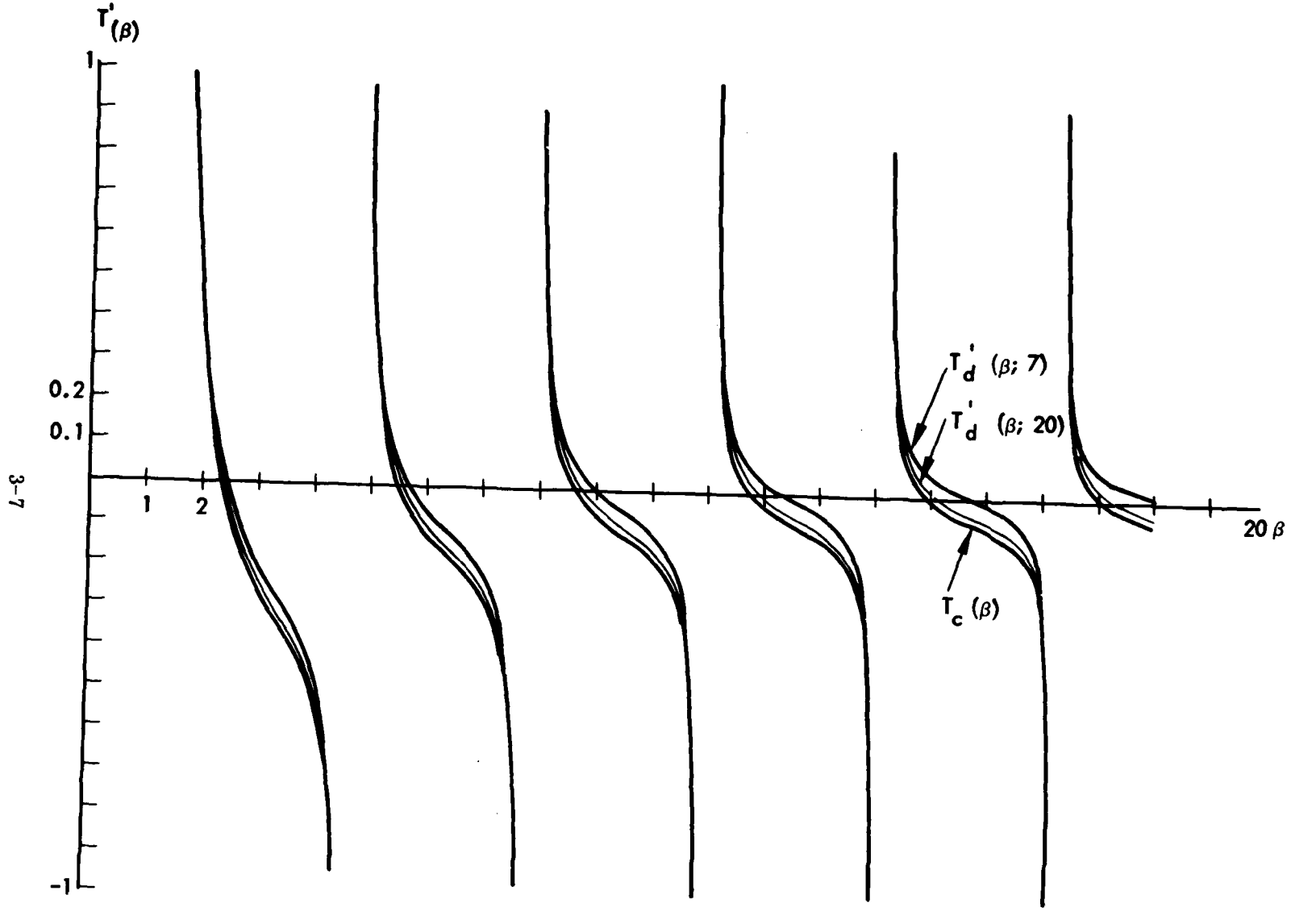

Fig. 2 Continuous and Discrete Open-Loop Transfer Functions for Beam (II)

MODES	TO BE CONTROLLED	RETAINED IN MODEL	NOT RETAINED IN MODEL
TRANSFER FUNCTION	$S \geq \omega_i$	$S \leq \omega_i$	$S \ll \omega_i$
EXACT $T_e(S) =$	$\sum_{i=1}^{n_c} \frac{\phi_i^2}{\omega_i^2 + S^2}$	$+ \sum_{n_c+1}^{n_r} \frac{\phi_i^2}{\omega_i^2 + S^2}$	$+ \sum_{n_r+1}^{\infty} \frac{\phi_i^2}{\omega^2 + S^2}$
TOTAL TRUNCATION $T_d(S, n_c) =$	$\sum_{i=1}^{n_c} \frac{\phi_i^2}{\omega_i^2 + S^2}$		
EXPANDED TRUNCATION $T_d(S, n_r) =$	$\sum_{i=1}^{n_c} \frac{\phi_i^2}{\omega_i^2 + S^2}$	$+ \sum_{n_c+1}^{n_r} \frac{\phi_i^2}{\omega_i^2 + S^2}$	
ROUNDED $T_d^R(S, n_r) =$	$\sum_{i=1}^{n_c} \frac{\phi_i^2}{\omega_i^2 + S^2}$	$+ \sum_{n_c+1}^{n_r} \frac{\phi_i^2}{\omega_i^2 + S^2}$	$+ \sum_{n_r+1}^{\infty} \frac{\phi_i^2}{\omega_i^2}$

Fig. 3 Modal Partitioning and Approximate Transfer Functions

Because all these approximations depend on the convergence of the series, there are open questions regarding the use of other kinds of mode shape functions which may improve convergence. For instance mode shape derivatives (used to express rotation and torque properties) converge much slower than the usual displacement mode when free-free modes are used. However, using mode shapes which reflect better the boundary conditions imposed by a torquer may drastically improve convergence.

Figure 4 shows an example of a more general 6th order system transfer function and three different ways to obtain reduced order transfer functions. Numerical values are displayed in Fig. 5. The best results are obtained with the rounded-off T.F. where not only the zeroes are well represented but also the residues of the retained poles (which is not the case for the zero-retaining T.F.).

EXAMPLE

$$T(s) = \frac{2\,(s^2 + 1)\,(s^2 + 3)}{(s^2 + 2)\,(s^2 + 5)\,(s^2 + 6)}$$

$$= \frac{\frac{1}{8}\,(s^2 + 1)\,(s^2/_3 + 1)}{(s^2/_2 + 1)\,(s^2/_4 + 1)\,(s^2/_6 + 1)} \quad \text{(factor form)}$$

$$= \frac{-1/4}{s^2 + 2} + \frac{-1\ 1/2}{s^2 + 4} + \frac{-3\ 3/4}{s^2 + 6} \quad \text{(residue form)}$$

APPROXIMATIONS

Truncated TF $\quad \dfrac{-1/4}{s^2 + 2} + \dfrac{-1\ 1/2}{s^2 + 4} = \dfrac{-1/2\,(s^2/_{2.3} + 1)}{(s^2/_2 + 1)\,(s^2/_4 + 1)}$

Round-Off TF $\quad \dfrac{-1/4}{s^2 + 2} + \dfrac{-1\ 1/2}{s^2 + 4} + \dfrac{S}{B} = \dfrac{\frac{1}{8}\,(s^2/_{0.65} + 1)\,(s^2/_{2.55} + 1)}{(s^2/_2 + 1)\,(s^2/_4 + 1)}$

Zero Retaining TF $= \dfrac{1}{8}\,\dfrac{(s^2/_{2.55} + 1)}{(s^2/_2 + 1)\,(s^2/_4 + 1)}$

Fig. 4 Transfer Function Simplifications (Truncation vs Round-Off)

SUMMARY OF EXAMPLE

	GAIN	ZEROES	RESIDUE AT $\pm \sqrt{2}\, j$	RESIDUE AT $\pm 2j$
COMPLETE SYSTEM	1/8	$\pm j$, $1.7j$	-1/4	-1 1/2
TRUNCATED T.F.	-1/2	$\pm 1.5j$	-1/4	-1 1/2
ROUNDED-OFF T.F.	1/8	$\pm .81j$, $\pm 1.6j$	-1/4	-1 1/2
ZERO RETAINING T.F.	1/8	$\pm j$, $\pm 1.7j$	-1/6	-1/2

Fig. 5 Transfer Function Simplifications (Truncation vs Round-Off)

Section 4

CONTROL SYNTHESIS TECHNIQUES

4.1 LOW AUTHORITY CONTROL SYNTHESIS

The following controller design synthesis is based on J. N. Aubrun's Low Authority Control (LAC) Theory (Ref [*]). To describe the methodology, only an outline of the required theory will be given; for proofs and additional details, see Ref [*].

Consider the system described in state-space form by:

$$\left\{\begin{array}{lll} \text{Dynamics:} & \dot{X} = FX + Gu \\ \text{Sensors:} & y = HX \\ \text{Controls:} & u = Cy \end{array}\right\} \Longrightarrow \dot{X} = (F + GCH)\,X \qquad (1)$$

(Closed-Loop Dynamics)

For sufficiently "small" controls C (see Ref [*]), let

$$GCH \equiv dF \qquad (2)$$

be considered as a perturbation of F, so that the closed-loop dynamics may be written as

$$\dot{X} = (F + dF)\,X \qquad (3)$$

Let λ_n denote the n-th (complex) root of F, and denote by L_n , R_n respectively the corresponding left and right eigenvectors of F, i.e.

[*] J. N. Aubrun, "Theory Of The Control Of Structures By Low Authority Controllers", AIAA Conference On Large Space Platforms: Future Needs And Capabilities, Los Angeles, Calif/Sept 27-29, 1978, Page No. 78-1689; also, AIAA J., Guidance and Control, revised version (in press), 1979.

$$F^T L_n = \lambda_n L_n$$
$$F R_n = \lambda_n R_n \qquad (4)$$

normalized so that $L_n^T R_n = 1$.

For "small" C, let $d\lambda_n$ denote the eigenvalue shift corresponding to dF. Then, as shown in egs (19) and (27) of Ref [*], Jacobi's formula leads to the fundamental LAC root shift formula

$$\begin{aligned} d\lambda_n &\cong L_n^T \; dF \; R_n \\ &\equiv L_n^T \; GCH \; R_n \\ &\equiv \left(\phi_n^A \right) C \left(\phi_n^R \right) \end{aligned} \qquad (5)$$

where $\phi_n^A \equiv L_n^T G$ and $\phi_n^R \equiv HR_n$ are generalized actuator and sensor modes respectively. The fundamental LAC formula expresses then the eigenvalue shifts by the bilinear form

$$d\lambda_n \cong \sum_{a,r} C_{ar} \; \phi_{an}^A \; \phi_{rn}^R \qquad (6)$$

where $a = 1, 2, \ldots, N_a$ and $r = 1, 2, \ldots, N_r$ are indices describing, respectively, actuator and sensor locations (nodes).

Consider next the case where:

(i) sensors and actuators are physically colocated *)

(ii) sensors and actuators are of "corresponding types" (i.e. translation/force, rotation/torque)

(iii) sensors measure rates

*) This does not necessarily require that the sensor-to-actuator feedback is also colocated.

then it can be shown (Ref [*]) that $H = G^T$. If, furthermore, there exists a right and left eigenvector for root n, it can also be shown that

$$G^T L_n = H R_n \tag{7}$$

and thus

$$\phi_n^A = G^T L_n = H R_n = \phi_n^R \ (\equiv \phi_n) \tag{8}$$

which is an equivalent re-statement of the classical reciprocity relations between actuators and sensors for colocated systems of the type considered above.

From (8), the fundamental LAC formula (6) becomes then the following quadratic form (for each n):

$$d\lambda_n \cong \sum_{a,r} C_{ar} \ \phi_{an} \ \phi_{rn} \tag{9}$$

The above formula is the basic LAC prediction formula for the root shifts (hence closed-loop damping) produced by sufficiently "small" control gains C_{ar} (see Ref [*]). To synthesize the gains C_{ar}, let $(d\lambda_n)_P$ denote the predicted root shifts given by the above formula, and let $(d\lambda_n)_D$ (given numbers) denote the desired root shifts imposed by the LAC controller design. Then the gains C_{ar} are chosen so as to minimize the weighted quadratic cost functional

$$J(C) \equiv \sum_n W_n \left[(d\lambda_n)_P - (d\lambda_n)_D \right]^2 + \sum_{a,r} C_{ar}^2 \tag{10}$$

in which the modal weights W_n help specify pole locations, and the term $\sum_{a,r} C_{ar}^2$ improves robustness of the controller. Since the cost functional J(C) is quadratic in C, the gains can be obtained algebraically by solving the linear equations

$$" \frac{\partial J}{\partial C} = O \ " \quad \text{for C .}$$

In order to carry out this procedure, we need to (i) relabel the gain matrix C_{ar} ($a = 1, \ldots, N_a$, $r = 1, \ldots, N_r$) as a gain vector C_α ($\alpha = 11, 12, \ldots 1N_r, 21, 22, \ldots, \ldots -N_a N_r$), (ii) relabel the multiply-indexed modal coefficients ϕ_{an} ϕ_{rn} as a modal coefficient matrix $\Phi^{(2)}_{n\alpha}$, using the same correspondence between the single index α and the pair of indices a, r as used in (i), and finally (ii) define a diagonal weighting matrix W whose elements are W_n. For simplicity, denote the desired root-shifts $(d\lambda_n)_D$ by d_n, considered as components of a vector d.

With the above relabeling, the weighted quadratic cost functional (10) can be rewritten as

$$J(C) = \sum_n W_n \left[\sum \Phi^{(2)}_{n\alpha} C_\alpha - d_n \right]^2 + \sum_\alpha C_\alpha C_\alpha \qquad (11)$$

or in matrix form

$$J(C) = (\Phi^{(2)} C - d)^T W (\Phi^{(2)} C - d) + C^T C \qquad (12)$$

From (11) we can calculate the partial derivatives (where β is an index having the same range as α):

$$\frac{1}{2} \frac{\partial J}{\partial C_\beta} = \sum_n W_n \left[\sum_\alpha \Phi^{(2)}_n C - d_n \right] \Phi_{n\beta} + C_\beta \qquad (13)$$

or equivalently in matrix form (I: identity matrix)

$$\frac{1}{2} \frac{\partial J}{\partial C} = \left[(\Phi^{(2)})^T W \Phi^{(2)} + I \right] C - (\Phi^{(2)})^T W d \qquad (14)$$

Thus the condition $\frac{\partial J}{\partial C} = 0$ leads to the LAC gain synthesis formula

$$C = \left[(\Phi^{(2)})^T W \Phi^{(2)} + I \right]^{-1} (\Phi^{(2)})^T W d \qquad (15)$$

The above LAC gain systhesis procedure was carried out for the CSDL tetrahedral truss example, using rate-feedback only and an upper triangular form for the gain matrix C. The CSDL example will be discussed in Section 5.1 below.

4.2 HIGH-AUTHORITY CONTROL METHODS

4.2.1 Control Problem

Introduction

The application of advanced control design techniques requires the use of models. Dynamics of continuous structures is, in general, described by a set of partial differential equations of the wave type. These equations may be derived for simple structures like beams and plates but are difficult for practical structures used in space. In addition, even though control laws can be designed for such structures, in concept, the solutions are too difficult for implementation.

A more practical approach for modeling the structures uses the modal approach. In this approach the basic functions describing the dynamic system behavior are written in terms of spatial expansions and the dynamics of the basis function is described by a coupled ordinary differential equation. This differential equation forms the basis of control design approaches.

4.2.1.1 Modal Representation. Finite order modal representations are obtained either from simplification of partial differential equations representing the dynamics of the structures or a direct derivation based on finite element analysis. In the finite element analysis, the structure is divided into a set of lumped masses and the differential equations are derived with appropriate boundary conditions at each lumped mass. The details of the finite element approach may be found in other references.

A finite order lumped mass model for the structure is written as

$$M\ddot{\xi} + C\dot{\xi} + K\xi = Gu \qquad (1)$$

where ζ are translational or rotational deflections and u is the input. M, C, K and G are mass, damping, spring and input distribution matrices. This model is typically of high order, depending upon the number of elements used in finite element analysis or the grid size used to convert the partial differential equation into an ordinary differential equation.

The model may be converted into a state space formulation by defining the state vector as follows:

$$X = \begin{pmatrix} \zeta \\ \dot{\zeta} \end{pmatrix} \tag{2}$$

$$\frac{d}{dt}\begin{bmatrix} \zeta \\ \dot{\zeta} \end{bmatrix} = \begin{bmatrix} O & I \\ -M^{-1}K & -M^{-1}C \end{bmatrix}\begin{bmatrix} \zeta \\ \dot{\zeta} \end{bmatrix} + \begin{bmatrix} O \\ -M^{-1}G \end{bmatrix} u \tag{3}$$

The states may alternately be defined as follows, where $M^{1/2}$ is a symmetric square root of M.

$$X = \begin{bmatrix} M^{1/2}\zeta \\ M^{1/2}\dot{\zeta} \end{bmatrix} \tag{4}$$

The corresponding state equations are

$$\frac{d}{dt}\begin{bmatrix} M^{1/2}\zeta \\ M^{1/2}\dot{\zeta} \end{bmatrix} = \begin{bmatrix} O & I \\ -M^{-1/2}KM^{-1/2} & -M^{-1/2}CM^{-1/2} \end{bmatrix}\begin{bmatrix} M^{1/2}\zeta \\ M^{1/2}\dot{\zeta} \end{bmatrix} + \begin{bmatrix} O \\ M^{-1/2}G \end{bmatrix} \tag{5}$$

With this selection of the state, the damping and the spring matrices are symmetric. These equations are written as:

$$\frac{d}{dt}\begin{bmatrix} \xi \\ \dot{\xi} \end{bmatrix} = \begin{bmatrix} O & I \\ -A & -D \end{bmatrix}\begin{bmatrix} \xi \\ \dot{\xi} \end{bmatrix} + \begin{bmatrix} O \\ B \end{bmatrix} u \tag{6}$$

The following transformation could convert A into a diagonal matrix.

$$\begin{pmatrix} \xi \\ \dot{\xi} \end{pmatrix} = \begin{bmatrix} T & O \\ O & T \end{bmatrix}\begin{bmatrix} \xi \\ \dot{\xi} \end{bmatrix} \tag{7}$$

where T is any matrix which makes TAT^{-1} diagonal. The state equations then become

$$\frac{d}{dt}\begin{bmatrix}\bar{\xi}\\ \dot{\bar{\xi}}\end{bmatrix} = \left[\begin{array}{c|c} O & I \\ \hline -A_o & -D_o \end{array}\right]\begin{bmatrix}\bar{\xi}\\ \dot{\bar{\xi}}\end{bmatrix} + \begin{bmatrix}O\\ B_o\end{bmatrix} \tag{8}$$

where A_o is a diagonal matrix.

Inertial devices measure absolute values of translational or rotational positions. velocities or accelerations at several points on the structure. Optical devices or other systems may measure relative position, velocity or acceleration at two or more points on the structure. The measurements are written as

$$\text{position:} \quad y = C_1 \bar{\xi} = \left[C_1 \vdots O\right]\begin{bmatrix}\bar{\xi}\\ \dot{\bar{\xi}}\end{bmatrix}$$

$$\text{velocity:} \quad y = C_2 \dot{\bar{\xi}} = \left[O \vdots C_2\right]\begin{bmatrix}\bar{\xi}\\ \dot{\bar{\xi}}\end{bmatrix}$$

$$\text{acceleration:} \quad y = C_3 \ddot{\bar{\xi}} = \left[-C_3 A_o \vdots -C_3 D_o\right]\begin{bmatrix}\bar{\xi}\\ \dot{\bar{\xi}}\end{bmatrix} + C_3 B_o u$$

In general, therefore, the measurements are expressed as:

$$y = C\begin{bmatrix}\bar{\xi}\\ \dot{\bar{\xi}}\end{bmatrix} + Du \tag{9}$$

4.2.1.2 Control Problems and Requirements. The basic problem with many structural dynamics problems is the low damping ratios of system modes. The systems of interest to us must perform several tasks which require both model following and stability augmentation.

The structure models are often known accurately at low frequencies. In addition, the low frequency modes have large settling times. Therefore, control activity is more efficiently utilized in controlling low frequency modes. A model reduction

approach is required to reduce the partial differential equation model or high order lumped parameter model into a low order model. These techniques must not only represent low frequency behavior faithfully but must also include the impact of high frequency behavior in low frequency models.

The control design problem is complicated because the model being lumped mass and of low order, approximates the dynamic behavior of the structure. The control design procedure must appreciate this limitation of the model. A direct application of the linear-quadratic Gaussian methods produces the control and observation spillover problem, where the control law adversely affects one or more unmodeled modes. The control structure must avoid or minimize the spillover problem.

The general control law resulting from the above developments is likely to be of high order. Techniques are developed to reduce controller order without compromizing closed loop performance, if possible.

Figure 1 shows the overall control design procedure. The overall procedure consists of three major steps:

(1) Model Reduction: Development of control design models from distributed parameter or finite element descriptions.

(2) Control Design: Design of a controller/filter or output feedback logic to specify the control structure.

(3) Controller Simplification: Reduction of the controller obtained in the previous step to simplify implementation and for rebustification.

The steps in the overall procedures must be carefully integrated to support assumptions and approximations made in each of the steps. This integration and the development of specific design methodologies which support this integration is the basis of our approach for design of control system for space structures.

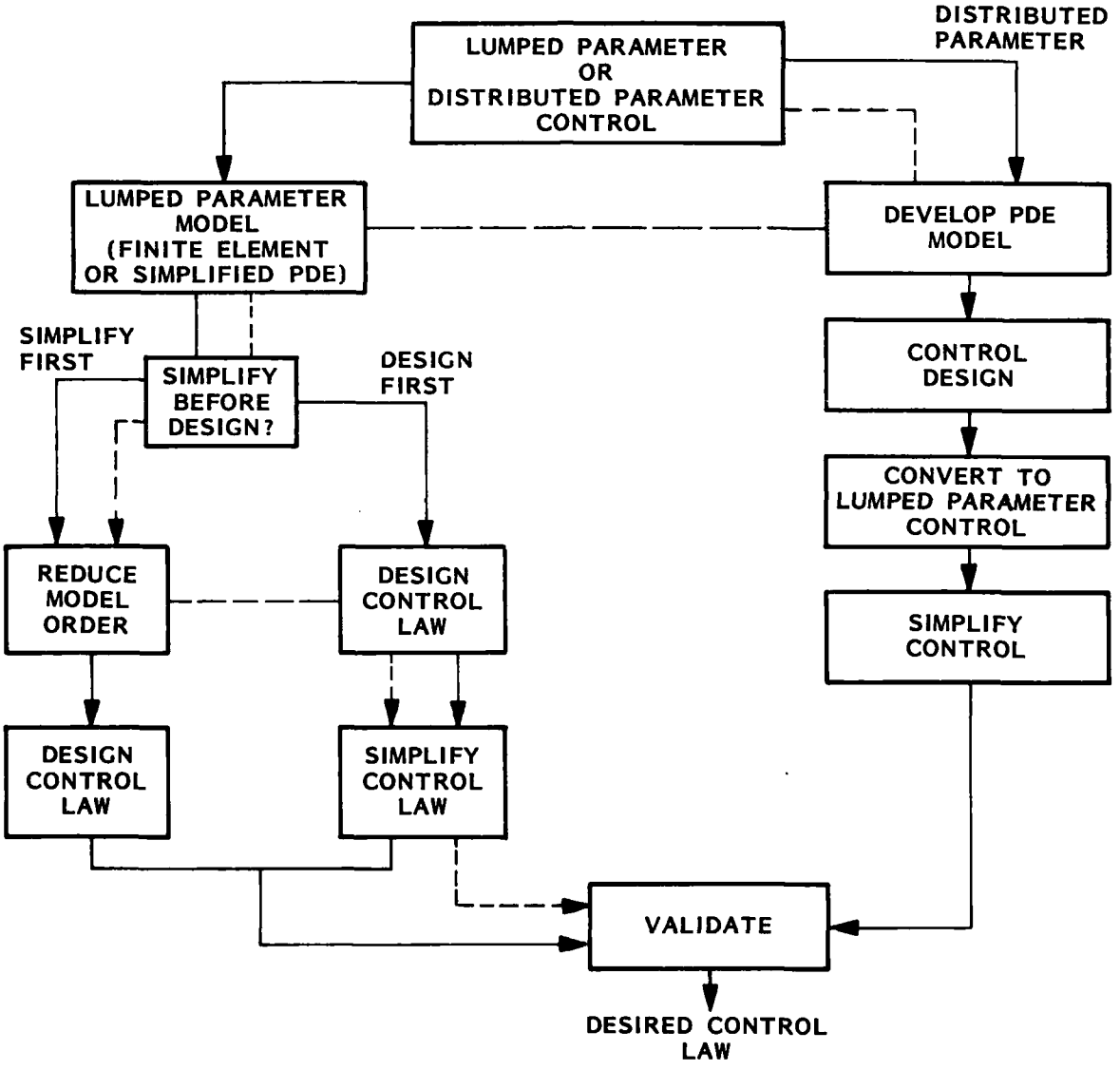

Fig. 1 Control Synthesis Approaches

4.2.2 Model Reduction

4.2.2.1 Requirements. Partial differential operations describe the dynamics of large space structures. Lumped mass approximation of this dynamics via finite element analysis or direct discretization leads to high order ordinary differential equation models. Though this model form is suitable for the application of many well developed control design methods, the high order creates a problem both of computation and of implementation. In addition, higher order modes in continuous structures are more sensitive to microscopic changes in the physical structure than low order modes. The description of high order modes, therefore, has large errors resulting from the finitie element analysis and approximations in modeling the physical structure. Lumping of two truss elements may have a minor effect on the first mode but may completely alter the mode shape of a high frequency system mode.

Model reduction is required for robustness and to simplify control law computation and implementation.

Criteria and computation procedures for model reduction are discussed in this chapter. The reduced model must contain essential elements of the dynamics such that the resulting control law is suitable for the continuous structure described by partial differential equations. Roles of poles, zeros and residues of transfer functions in closed loop control design are discussed first followed by selection of specific criteria and numerical procedures.

4.2.2.2 Poles, Zeros and Residues. In linear systems, the closed loop behavior is dictated significantly by several transfer function properties. Three of the most significant properties are the poles, the zeros, and the residues.

The roles of transfer function properties are best explained by considering a single input single output (SISO) system with output y and input u.

$$y(s) = T(s)\, u(s) \tag{1}$$

The characteristic values λ_i, $i = 1, 2 \cdots n$ of the T(s) denominator are the open loop system eigenvalues and indicate system stability properties. The transfer function may be written in terms of zeros Z_i, $i = 1, 2 \cdots n$ or residues r_i, $i = 1, 2 \cdots n$ as follows

$$T(s) = \frac{K(s - Z_1)\,(s - Z_2) \cdots (s - z_m)}{(s - \lambda_1)\,(s - \lambda_2) \cdots (s - \lambda_n)} \quad : \text{Zeros Representation}$$

$$= \sum_{i=1}^{n} \frac{r_i}{s - \lambda_i} \quad : \text{Residue Representation} \tag{2}$$

Consider now a feedback matrix C(s) with gain α. The closed loop transfer function is

$$T_c(s) = \frac{T(s)}{1 + \alpha C(s)\, T(s)} \tag{3}$$

which may be written as

$$T_c(s) = \frac{\bar{K}(s - \bar{z}_1) \cdots (s - \bar{z}_{\bar{m}})}{(s - \bar{\lambda}_1)\,(s - \bar{\lambda}_2) \cdots (s - \bar{\lambda}_{\bar{n}})} \tag{4}$$

It is easy to see that for smaller α,

$$\left.\frac{\partial \lambda_i}{\partial \alpha}\right|_{\alpha \to 0} = \alpha C(\lambda_i)\, r_i \tag{5}$$

Thus r_i dictates the behavior of the pole for small gain. When α is large, the finite closed loop poles are the zeros of C(s) and T(s).

To summarize, the residues of the transfer function describe the low gain properties and the zeros the high gain properties. Both zeros and residues are important in closed loop control design.

4.2.2.3 Numerical Procedures. Consider a Nth order linear system with x, input u and output y

$$\dot{x} = Fx + Gu \tag{6}$$

$$y = Hx + Du \tag{7}$$

The input-output transfer function is given by

$$y = (H(sI - F)^{-1}G + D)u \tag{8}$$

or

$$\frac{y(s)}{u(s)} = \frac{1}{\Delta(s)} \sum_{i=0}^{N} B(i)s^i \tag{9}$$

The eigenvalues of $\Delta(s)$ define system poles, while B(i) are matrices of numerator polynomial. The zeros of y_k and u_l transfer function is

$$\frac{y_k(s)}{u_l(s)} = \frac{1}{\Delta(s)} \sum_{i=0}^{N} B_{kl}(i)s^i$$

$$\triangleq \frac{K_{kl}\,(s - Z_{1kl})\,(s - Z_{2kl}) \cdots (s - Z_{Nkl})}{(s - \lambda_1)\,(s - \lambda_i) \cdots (s - \lambda_N)}$$

$$\triangleq \sum_{i=1}^{N} \frac{r_{ikl}}{(s - \lambda_i)} \tag{10}$$

Different approaches are useful for maintaining zeros or residues in reduced order models.

Maintaining Residues and Poles

A modal decomposition provides the framework for reducing arbitrary linear models to design models with same residues and poles as the high order models. The procedures are well known [2] and their application to model reduction is described below.

The linear Eqs. (6) and (7) can be transformed to block diagonal form assuming the n x n dynamics matrix, F, has no repeated eigenvalues:

$$x = Tz\,\Xi \tag{11}$$

$$\dot{z} = \Lambda z + u \tag{12}$$

$$y = HTz + Du \tag{13}$$

where A is an n x n block diagonal matrix, T is an n x n matrix composed of the column eigenvectors of F, Z is an n x 1 modal coordinate vector, and Ξ is the n x m modal control distribution matrix. Also,

$$FT = TA \tag{14}$$

The system of Eqs. (11) through (13) can be partitioned into a set of q states and q eigenvalues (time constants) and n-q states and eigenvalues as follows:

$$\left[\begin{array}{c} x_1 \\ \hline x_2 \end{array}\right] = \left[\begin{array}{c|c} T_{11} & T_{12} \\ \hline T_{22} & T_{22} \end{array}\right]\left[\begin{array}{c} z_1 \\ \hline z_2 \end{array}\right] \tag{15}$$

$$\left[\begin{array}{c} \dot{z}_1 \\ \hline \dot{z}_2 \end{array}\right] = \left[\begin{array}{c|c} A_1 & 0 \\ \hline 0 & A_2 \end{array}\right]\left[\begin{array}{c} z_1 \\ \hline z_2 \end{array}\right] + \left[\begin{array}{c} \Xi_1 \\ \hline \Xi_2 \end{array}\right] u \tag{16}$$

where x_1 and z_1 are n x 1 vectors partitioning the states and modes and x_2 and z_2 are (N-n) x 1 vectors partitioning the remaining states and modes.

In the representation of the above equation it is easy to verify that the residues of the poles are appropriate products of terms in matrices HT and Ξ. The residue maintaining model reduction procedure is simply derived as in the following.

N-n poles are eliminated by setting $Z_2 = 0$. This gives

$$Z_2 = -\Lambda_2^{-1} \Xi u \tag{17}$$

The reduced order model is

$$\dot{Z}_1 = \Lambda_1 Z_1 + \Xi_1 u \tag{18}$$

$$Y = HT \begin{bmatrix} Z_1 \\ \hline -\Lambda_2^{-1} \Xi u \end{bmatrix} + Du$$

$$= H'Z_1 + D'u \tag{19}$$

Many model reduction procedures do not modify the coefficient of u in the measurement equation. It is clear from the above equations and subsequent examples that such a change is essential.

Maintaining Zeros and Poles

If the transfer function between output y_k and input u_l is simplified to keep the first w poles and m zeros, the following form is obtained.

If the first n poles and m zeros the simplified transfer function is

$$\frac{y_{k(s)}}{u_{l(s)}} = \frac{K_{kl} \prod_{i=m+1}^{N} (-Z_{ikl})}{\prod_{i=n+1}^{N} (-\lambda_i)} \cdot \frac{(s - Z_{1kl}) \cdots (s - Z_{mkl})}{(s - \lambda_i) \cdots (s - \lambda_n)} \tag{20}$$

Note that the gain has to be modified because high frequency poles and zeros have steady state effects.

The reduced model is obtained by performing a similar reduction on each transfer function and then detaining a state space realization from the complete transfer function. The process of obtaining the minimum state space realization is not simple (except for single input multi output or multi input and single output system). In fact in multi output systems, this procedure may even lead to an increase in model order.

Model reduction procedures which maintain zeros have not been used extensively except in single input single output systems.

4.2.2.4 Selections of Significant Poles. The procedures of the previous section may be used once poles to be retained in the reduced order model are specified. This specification has usually been based on two considerations:

1. Frequency separation
2. Performance evaluation

The frequency separation approach keeps poles in a prespecified frequency range depending on the actuator/sensor bandwidth, control requirements and modeling accuracy. In most large space structures control design problems, all these considerations lead to retention of low frequency poles. One exception is the elimination of forced vibration at specified frequencies (e.g., motors).

The performance evaluation approach evaluates the effect of elimination of each combinations of modes on the performance of the closed loop system. Significant work has been done on this problem by Skelton [Sec. 5.1.6]. The concept of open loop modal cost analysis provides an integrated framework for selecting modes which will effect the feedback control law.

The selection of the poles to be eliminated will consist of two steps. In the first step, all poles and zeros not in the frequency range of interest will be eliminated. In the second step, modal cost analysis will be used to selectively eliminate those modes which have minimum effect on performance.

With the simplified model for large space structures, we are now ready for control design.

4.2.3 Control Design

4.2.3.1 Control Approach. Design of feedback control laws for large space structures is dictated by the following considerations:

(i) Model: Because of modeling accuracy as well as computational considerations, the model is of low order. The neglected modes have low damping and can be unstable if not properly considered in control design.

(ii) Sensors and Actuators: Though structures have significant response up to infinite frequency, physical actuators/sensors have finite bandwidth. In addition actuators and sensors have dead zeros, hysterisis and non-linearities.

(iii) Model Uncertainties: The behavior of structures is known only approximately at high frequency. Therefore, it is difficult to assess the behavior of high frequency poles.

(iv) Space Application: Because of weight and volume considerations in space applications, optimization of sensors and actuators is critical in control of space structures.

The control design approach developed addresses these issues in the feedback law specification. The integrated approach is based on an extension of the work of Aubrun [sec 4.1] on collocated sensors/actuators and on frequency shaping filter/controller design methods.

The collocated sensor/actuator based control design approach has been called the low-authority structural control (LASC) because of the limited amount of structural damping which it can produce. The LASC theory has been generalized to include many sensor/actuator pairs with possible cross feedback among pairs.

The general feedback controller/filter design problem considers general sensor/actuator location with general signal flow structure. The validity of the model over a small frequency range is used directly in the control design approach.

The resulting controller provides maximum robustness against truncated modes. High damping ratios can be obtained in selected modes. The stability of unmodeled modes cannot be guaranteed even with perfect actuators and sensors.

4.2.3.2 Generalization of Colocated Control. Collocated control is generalized for multi-input multi-output systems. It is shown that the solution is closely related to an inverse optimal control solution. A design procedure is discussed followed by controller robustness properties.

Inverse Optimal Control Problem

This section considers the control problem with collocated actuators and sensors. In addition, all sensor/actuator pairs are complimentary to each other (e.g., velocity sensor/force actuator, rate sensor/moment actuator). The output vector, y, is obtained then through

$$y(t) = G^T x(t),\ y \in R^m \tag{1}$$

Neglecting the low natural damping of the flexible system, the finite order* linear oscillatory system is described through

$$\dot{x}(t) = F x(t) + G u(t),\ x \in R^{2n},\ u \in R^m \tag{2}$$

where

$$F = \left[\begin{array}{c|c} 0 & I_n \\ \hline -A_o & 0 \end{array}\right] \qquad G = \left[\begin{array}{c} 0 \\ \hline B_o \end{array}\right] \tag{3}$$

and A_o is an n x n symmetric positive definite (p.d.) matrix, and B_o is an n x m matrix of full rank m ($m \leq n$).

*Refer to chapter 3 for further details on model derivation.

The state vector, x, of the system described in (2) is defined by

$$x \triangleq [q, \dot{q}] \tag{4}$$

where q and $\dot{q}$ are generalized displacements and velocities respectively. Using the output of (1) in implementing an output feedback control law will result in a velocity (rate) feedback only due to the structure of G in (3). This is an important property of collocated controls for systems described as in (2); it will be exploited in deriving the analytical foundations for the design procedure.

Consider now the case where the system in (1) and (2) is a single-input, single-output (SISO) system. Then, it can be shown that the use of a collocated reate feedback control will result in an eigenvalue shift to the left in the complex plane (increased damping). The proof of this property is based on Jacobi's formula for eigenvalues perturbations and the modal structure of the system in (2) and (3) (see Sec. 4.1).

Can collocated rate feedback control provide increased damping in multi-input, multi-output (MIMO) systems too?

The answer is provided through the application of inverse optimal control theory.

We consider an objective function quadratic in state and control over an infinite time period, i.e.,

$$J(x, u) = \int_0^\infty \left[x^T(t)Qx(t) + u^T(t)R\,u(t)\right]dt \tag{5}$$

and

$$Q \geq 0,\ R > 0 \tag{6}$$

The problem of inverse optimal control to be considered is the following. Given a stabilizing output feedback control law described by

$$u(t) = Ky(t) = KG^T x(t) \tag{7}$$

for what weighting matrices Q and R in (5) is this control also optimal?

Appendix A derives the solution to this problem; a summary of results is provided in Table 1.

The solution to the inverse optimal control problem as formulated above will allow us to generalize the stabilization properties of a collocated rate feedback control to MIMO systems. This is discussed next.

Properties of Solution

The stabilization of a linear system by a state feedback control law requires the system in (2) to be controllable* [5]. This is an important structural property that will be assumed for the system under consideration.

It is well known [5] that if $Q = L^T L$, where (F, L) is an observable pair, the optimal control obtained through the solution of the ARE yields a stable closed-loop system. In the case discussed in Appendix A we have

$$Q = L^T L \tag{8}$$

where the m x 2n matrix L is given by

$$L = \left[0 \,\vdots\, \alpha B^{-1/2} B_o^T\right] \tag{9}$$

It is simple to show that if (F, G) is a controllable pair, R and A_o are symmetric p.d matrices and $\alpha \neq 0$, then (F, L) is an observable pair too. This shows that selecting any symmetric negative definite matrix for the output feedback gain matrix will result in a stabilizing collocated control. In addition, this control is also optimal for a specific optimization problem as discussed in Appendix A. This result provides the required generalization to MIMO systems.

*This requirement can be relaxed to that of stabilizability [5].
+Algebraic Ricatti Equation.

Table 1

SUMMARY

Given

$$\dot{x}(t) = Fx(t) + Gu(t) \ , \ x \in R^{2n} \ , \ u \in R^{m}$$
$$u(t) = KG^{T} x(t) \text{ (rate feedback)}$$
$$K = K^{T} < 0 \text{ (a given gain matrix)}$$

$$F = \begin{bmatrix} 0 & I_n \\ -\bar{A}_o & \bar{0} \end{bmatrix} \ , \ G = \begin{bmatrix} 0 \\ \bar{B}_o \end{bmatrix} \ , \ A_o = A_o^{T} \quad 0$$

$$x \triangleq [q, \dot{q}]^{T} \ , \ x(0) = x_o$$

Problem:

For what Q and R matrices is u the optimal control for a linear quadratic objective function given by

$$J^* = \min_{u \in \mathcal{U}} \int_o^{\infty} (x^{T}(t)Qx(t) + u^{T}(t)Ru(t))\, dt$$

Solution of ARE:†

$$P = \begin{bmatrix} A_o & 0 \\ 0 & I_n \end{bmatrix}$$

Input Penalty Matrix:

$$R = -\alpha K^{-1} \ , \ \alpha > 0$$

State Penalty Matrix:

$$Q = \begin{bmatrix} 0 & 0 \\ 0 & \alpha^2 B_o R^{-1} B_o^{T} \end{bmatrix}$$

Optimal Cost:

$$J^* = x_o^{T} P x_o = \alpha \left(q_o^{T} A_o q_o + \| \dot{q}_o \|^2 \right)$$

†Algebraic Riccati Equation

The results presented in Table 1 can be used to yield a physical interpretation of the solution to the inverse optimal control problem.

The optimal performance is written as

$$J^* = \min_u [J_1 + J_2] \tag{10}$$

where

$$J_1 = \alpha^2 \int_0^\infty q^T B_o R^{-1} B_o^T \, q \, dt \tag{11}$$

$$J_2 = \int_0^\infty u^T R u \, dt \tag{12}$$

The interpretation suggested above is that the cost functional is the total energy of the system. The term contributed by the state is the kinetic energy where

$$E = \dot{q}^T M \dot{q} \tag{13}$$

and the "mass," M, is given by

$$M = \alpha^2 B_o R^{-1} B_o^T \tag{14}$$

Also, the use of velocity feedback where the actuators and sensors are collocated results in an LQ problem where only kinetic energy is weighted.

The solution of the inverse optimal control problem as presented above has a theoretical and practical significance. On the theoretical side we have been able to show that this solution results in a stable closed-loop system. This solution can also be used to answer the question of control "spillover". The practical aspect of the inverse optimal control problem lends itself to an implementable design procedure discussed in the following section.

Design Procedure

It was shown above that the solution of the inverse optimal control problem results in a state weighting matrix given by

$$Q = \left[\begin{array}{c|c} 0 & 0 \\ \hline 0 & \alpha^2 B_o R^{-1} B_o^T \end{array}\right] \tag{15}$$

In practice, however, one starts the design procedure by specifying the weighting matrices rather than obtaining them as an end result. This specification results from the performance levels the system is required to achieve.

The use of low-authority controllers (collocated sensors and actuators) to-date was concerned mainly with the question of stability. The results obtained above allow us to extend the scope of these controllers beyond that of stability.

Let the state weighting matrix Q, be specified as

$$Q = \left[\begin{array}{c|c} 0 & 0 \\ \hline 0 & Q_o \end{array}\right] \tag{16}$$

where Q_o is any n x n symmetric p.s.d matrix.

Given Q as in (16), the design is concerned with solving

$$-\alpha B_o K B_o^T = Q_o \tag{17}$$

for the symmetric gain matrix K.

If the n x m matrix B_o is square and nonsingular, i.e., n = m, then the required gain is obtained from (17) as

$$K = -\left(\frac{1}{\alpha}\right) B_o^{-1} Q_o \left(B_o^T\right)^{-1} \tag{18}$$

In practice, however, one finds that $m<n$ in which case (18) will not be available. A valid assumption that can still be made is that B_o is of full rank equal to m.

In this case we can solve (17), so that the solution is approximate in the least squares sense.

Let

$$J = tr\left[\left(Q_o + \alpha B_o K B_o^T\right)\left(Q_o + \alpha B_o K B_o^T\right)^T\right] \tag{19}$$

then, setting

$$\left.\frac{\partial J}{\partial K}\right|_{K=K^*} = 0 \tag{20}$$

we find

$$K^* = -\left(\frac{1}{\alpha}\right)\left(B_o^T B_o\right)^{-1} B_o^T Q_o B_o \left(B_o^T B_o\right)^{-1} \tag{21}$$

Remarks:

1. Since Q_o is p.d, and $\alpha > 70$, the gain matrix obtained in (21) is symmetric. negative definite as required.
2. Since the objective function of (19) is convex, the gain matrix of (21) is globally optimal.

Using the gain as given in (21) for the control of the system in (2) through the application of (7) will result in a solution of an inverse optimal control problem where the actual state weighting matrix is given by

$$\hat{Q} = \left[\begin{array}{c|c} 0 & 0 \\ \hline 0 & Q^* \end{array}\right] \tag{22}$$

and

$$Q^* = B_o\left(B_o^T B_o\right)^{-1} B_o^T Q_o B_o \left(B_o^T B_o\right)^{-1} B_o^T \tag{23}$$

The actual weighting matrix Q^* of (23) can be rewritten as

$$Q^* = CQ_oC \tag{24}$$

where

$$C = B_o\left(B_o^T B_o\right)^{-1} B_o^T = C^T \tag{25}$$

The design procedure is concerned with specifying Q_o so that the resulting Q^* as given in (24) will approach a desired weighting structure i.e.,

$$Q^* \approx Q_d \tag{26}$$

The above discussion can be summarized into a numerical procedure.

The numerical procedure is motivated by equation (26). The matrix Q_o is the design matrix to be chosen in an iterative manner until system's closed-loop performance is acceptable.

The procedure is as follows:

Step 1: Read: A_o, B_o, Q_o, m, n, α

Step 2: Set: $k = 1$

$$Q_k = Q_o$$

$$D = B_o\left(B_o^T B_o\right)^{-1}$$

$$C = DB_o^T$$

Step 3: $Q^* = CQ_kC$

$$K_k^* = (1/\alpha)\, D^T Q_k D$$

Find eigenvalues of $\left[\begin{array}{c|c} 0 & I_n \\ \hline -A_o & B_o K_k B_o^T \end{array}\right]$

Step 4: If eigenvalue distribution is acceptable (damping ratios, frequencies, etc.) go to 5 , otherwise find the diagonal difference of Q^* and Q_k

$$\gamma_i = Q^*(i,i) - Q_k(i,i), \quad 1 \leq i \leq n$$

then

$$Q_{k+1}(i,i) = Q_k(i,i) - \zeta_i \, \mathrm{sgn}(\gamma_i), \quad \zeta_i > 0$$

$k \longrightarrow k + 1$

go to 3 .

Step 5: STOP.

Remark: The choice of the parameter ζ_i can be varying depending present eigenvalue distribution.

This numerical procedure will be used in section 5 to design a controller for a flexible structure (a pyramid).

Robustness Properties of Generalized Collocated Control

A problem associated with control design for large space structures is that of truncated modes. The dimension of the model described in Eq. (2) depends on the fineness of grid used in the application of the finite element method. Usually, however, the dimension is quite large and some reduction in order will result in modes that are truncated from the final model used for design. The effect of the control derived from the reduced-order model on the truncated modes ("control spillover," Ref. 4 in sec. 2) is of extreme importance in the overall evaluation of the control system.

Another problem to be considered is the effect of parameter variations (or uncertanity) on performance quality. The solution to the inverse optimal control problem will be used to demonstrate design robustness in regard to the following two specific problems.

Problem 1:

To what extent, if any, is the solution to the inverse optimal control problem sensitive to truncated modes?

Problem 2:

How are closed-loop stability properties affected by parameter variations (or uncertainty) in system matrices?

The problem of truncated modes will be considered first. The matrix describing the dynamics of the flexible system, given by Eq. (2) has eigenvalues distributed on the imaginary axis. The process of mode truncation is carried out by ignoring eigenvalues that are far from the origin on the imaginary axis (high-frequencies). Analytically, the problem of mode truncation is as follows. Let the full-order finite linear system* be described by

$$\dot{z}(t) \triangleq \begin{bmatrix} \dot{x}(t) \\ \dot{x}_T(t) \end{bmatrix} = \left[\begin{array}{c|c|c} 0 & & I \\ \hline -A_o & 0 & \\ \hline 0 & -A_T & 0 \end{array}\right] z(t) + \begin{bmatrix} 0 \\ \hline B_o \\ \hline B_T \end{bmatrix} u(t) \qquad (27)$$

where the subscript T stands for the part of the system to be truncated. The output used for control is given by

$$y(t) = B_o^T x(t) + B_T^T x_T(t), \; y \in R^m \qquad (28)$$

The matrix A_T contributes to the full order system frequencies higher than those contributed by A_o and, therefore, can be truncated to yield the reduced order model described by

$$\dot{x}(t) = \left[\begin{array}{c|c} 0 & I_n \\ \hline -A_o & 0 \end{array}\right] x(t) + \begin{bmatrix} 0 \\ \hline B_o \end{bmatrix} u(t) \qquad (29)$$

*The real flexible system is described through a second order PDE (wave equation). In linear form, the flexible system is of infinite dimension. Equation (1), therefore, considers only a finite number of these modes.

Robustness Property 1:

The full order system described in Eq. (27) under the control

$$u(t) = Ky(t), -K = -K^T > 0 \tag{30}$$

and y given by Eq. (28) will remain stable for every A_T provided that (A_o, B_o), (A_T, B_T) are controllable pairs.

The proof of this property is by using the control as derived from the reduced order system and noting that the full order system assumes the form given by

$$\dot{z}(t) = \left[\begin{array}{c|cc|c} 0 & & & K \\ \hline -A_o & 0 & \left(\begin{array}{c} B_o \\ \hline B_T \end{array}\right) & K(B_o : B_T)^T \\ 0 & -A_T & & \end{array}\right] z(t)$$

Appendix B indicates that this system will be asymptotically stable provided (A_o, B_o) and (A_T, B_T) form controllable pairs.

This result shows how the inverse optimal control solution can be put to use to answer the question of control spillover (Ref. 4 in sec. 2).

Observing the proof of Appendix B we can arrive at the second robustness result. This result shows how stability properties of the closed-loop system are affected by parameter variations in the system matrix A_o.

Robustness Property 2:

Consider the dynamic system described in Eq. (28) and where the n x n matrix A_o can have uncertain parameters that belong to certain set. Applying the output feedback control of Eq. (4) will result in a stable closed-loop system for every A_o in the give range of possible parameter variation provided A_o is always symmetric and p.d. over its entire range.

Remark: In the case when A_o is a diagonal n x n matrix, the above result guarantees stability of the closed-loop system provided the diagonal of A_o remains positive over all possible variations.

4.2.3.3 General Controller/Filter Design. With collocated sensors and actuators output feedback may be used to increase the damping ratio of all modes up to a certain level. In many systems it is not possible to place actuators and sensors at the same place. Often also higher damping ratio is desired in certain selected modes. General controller/filter design theory is the desired.

Design Procedure

Since the models are of high order with multi-inputs and -outputs, Linear-Quadratic-Gaussian LQG techniques are useful. LQG methods must be modified such that they account for the following factors.

(i) Model unvalidity at high frequencies
(ii) Bandlimited actuators/sensors, and
(iii) Control requirements at low frequency

This section describes a completely new theoretical development to extend LQG methods for large space structure applications.

LQG techniques are based on state description models of

$$\begin{aligned} \dot{x} &= Fx + Gu \\ y &= Hx \end{aligned} \tag{31}$$

The function to be optimized is quadratic in states x and input u. A direct optimization of the performance index gives the desired control law. These methods require many assumptions.

1. The model is valid for all values of inputs and states. In addition, the dynamics is well described at all input and state frequencies.

2. The filter uses values of F, G and H matrices explicitly in the implementation stage (in addition to the gain K which also depends on the state definition matrices). The filter design also assumes that the dynamics is known equally accurately at all frequencies. This may make the combination of the filter and the control law extremely sensitive to errors, see also Doyle [2].

3. The optimality of the filter is strongly dependent on the accuracy of noise statistics.

Classical control design methods are based on frequency domain descriptions of systems and account for model uncertainty at high frequencies by the use of gain and phase margin comcepts. Gain and phase margins provide a measure of uncertainty in the model at high frequency for which stability can be guaranteed.

It has been shown by Anderson and Moore [5] and Athans and Safonov [6] that the LQG controller has a 60° phase margin and 50% to infinite gain margin. The phase and gain margin properties provide for a constant phase error in all channels and for individual variations in gain. The system may be extremely sensitive if two gains change in opposite directions. In general, the phase and gain margin property does not relate directly to parameter sensitivity. The performance of the LQG controllers degrades further when a filter is used for state estimation. The gain and phase margin properties are no longer valid. In addition, the filter dynamics, dictated by specified noise characteristics, may be too fast, leading to interaction with unmodeled terms.

To understand the concept of frequency shaping, it is necessary to write the standard LQG cost functional in the frequency domain. With inifinte time horizon and no weighting on the final state, the cost functional may be written as:

$$J = 1/2\int_{\infty}^{\infty} [x^*(j\omega)Ax(j\omega) + u^*(j\omega)Bu(j\omega)]d\omega \qquad (32)$$

where * implies complex conjugate. Clearly, in this formulation, the weighting matrices are not functions of frequency, i.e., the state and control excursions at all frequencies are equally unacceptable. In many systems, on the other hand,

inputs in the neighborhood of a particular frequency are not desirable because of poor sensor or actuator characteristics at that frequency. Historically, this constraint of constant weighting at all frequencies has resulted because of the difficulty of shaping the weighting functional with frequency in the conventional time domain LQG formulation. Representation of the cost functional, Eq. (32), provides a clue to the frequency domain approach for using frequency shaping ideas in modern control theory techniques. Matrices A and B in Eq. (32) may be made functions of frequency to give a generalized cost function of the form

$$J = 1/2 \int_{\infty}^{\infty} [x^*(j\omega)A(j\omega)x(j\omega) + u^*(j\omega)B(j\omega)u(j\omega)]d\omega \qquad (32)$$

$A(j\omega)$ and $B(j\omega)$ are Hermitian matrices at all frequencies.

A design procedure based on this weighting is given in Appendix C.

The frequency shaped weighting matrices are used in large space structure control as follows. Maximum control activity is desired at low frequency with minimum on no control activity at high frequency. This may be achieved, for example, by selecting $B(j\omega)$ small at low frequency and large at high frequencies. If the model is not valid at high frequency, we may also want to minimize state excursions in that region. This may require large state weighting at high frequency. Table 2 gives a set of weighting functions which may be useful in space structure control. As shown in Appendix C and with examples in Section 5, such weighting functions lead to general compensation structures in the feedback loop.

Filter Design

States required for feedback control are often not measured directly. Reliable estimators should then be designed to extract the state time history from the measured data. In general states corresponding to the modes retained in the model must be estimated with minimium contamination from high frequency model states.

Table 2

A USEFUL SET OF FREQUENCY SHAPED WEIGHTING FUNCTIONS

STATE WEIGHTING	CONTROL WEIGHTING	COMMENTS
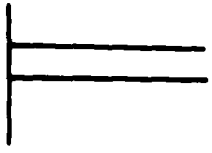 A = CONSTANT	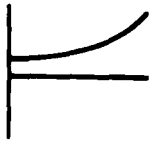 $B = \omega^2$ (1) $\omega^2 + \omega_1^2$ (2) $\omega^4 + \omega_1^4$ (3)	MINIMIZES CONTROL ACTIVITY AT HIGH FREQUENCY
 $A = \omega^2$ (1) $\omega^4 + \omega_1^4$ (2)	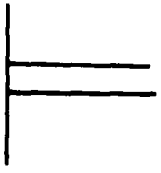 B = 1	MINIMIZES STATE EXCURSIONS AT HIGH FREQUENCY
 A = 1	 $B = \frac{1}{\omega^2}$ $B = \frac{\omega^2 + \omega_1^2}{\omega^4 + \omega_2^4}$	AVOIDS CONTROL SATURATION IN INERTIAL ACTUATORS. REDUCES FEEDBACK OF LOW FREQUENCY NOISE
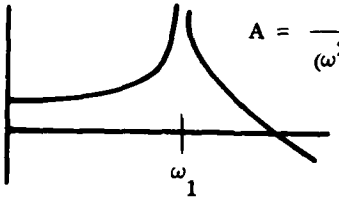 $A = \frac{1}{(\omega^2 - \omega_1^2)^2}$ ω_1	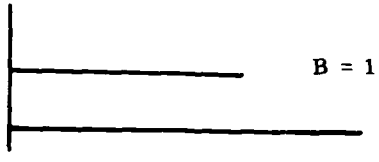 B = 1	ELIMINATES THE EFFECTS OF EXTERNAL VIBRATION AT ω_i
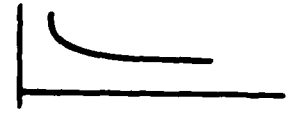 $A = \frac{1}{\omega^2}$	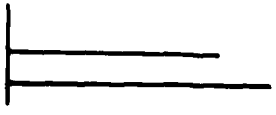 B = 1	INTEGRAL CONTROL

Skelton has developed an orthogonal filter approach for state estimation in systems with unknown non-white noise. Consider the dyanmic system

$$\dot{x} = Fx + Gu + w \tag{34}$$

where w is a vector of nonwhite and nonstationary noise. The concept involves approximating w by a vector of onthogonal functions, E

$$w = \sqrt{E} \tag{35}$$

Chekychev polynomials could be selected as the set of approximating orthogonal function.

In Kalman filter or observer formulation, it is advantageous to select approximating functions which can be generated by a set of differential equations. Fourier series and orthogonal polynomials both satisfy this requirement, E then follows a differential equation

$$\dot{E} = F'E + W' \tag{36}$$

where W is white noise source introduced to account for changes in the error terms.

A nonwhite error term may also be introduced in the measurement equation

$$y = Hx + v \tag{37}$$

and v may be approximated by the same set of orthogonal functions and a pure white noise term 'v'

$$v = DE + v' \tag{38}$$

Equations (34) through (38) may be formulated into a Kalman filter for estimating the states. As a by product, the orthogonal error knows E will also be estimated. If necessary Γ and D may also be estimated in realtime. This method is described later in greater detail.

Another approach for state estimation is based on frequency shaping of state and measurement noise. In Eq. (34), for example, noise W is primary high frequency corresponding to truncated modes. The noise spectrum is then selected to be a function which is small in the model frequency range and high in regions of truncated modes. The measurement noise is treated in a similar manner.

The negative log likelihood function for state estimation becomes

$$\text{NLLF} = \int_{\infty}^{\infty} \left(W^* Q^{-1}(j\omega) W + v^* R^{-1}(j\omega) v \right) d\omega$$

Much work has been done on guidelines for selecting the weighting functions. Once appropriate shaping functions have been selected, the filter design procedure is similar to the control design procedure outlined in Appendix C.

Relationship Between Orthogonal Filter and Frequency Shaping Methods

Orthogonal filters and frequency shaping state estimation methods try to correct for inadequacy of the model in certain frequency ranges. The orthogonal filter approach models the error by a series of orthogonal functions in time domain while the frequency shaping approach approximates the error by a series of functions in the frequency domain. Both methods require additional states to model the nonwhite error. If the set of orthogonal functions and the frequency shaped weights are appropriately selected, the two methods should give identical results. Figure 2 compares the frequency domain and time domain algorithms.

4.2.3.4 Robustness Properties. In analyzing the effect of control on unmodeled modes we need to look at their motion in the complex plane. Let us introduce a scaling parameter γ in the feedback loop. For small γ, a pole at α_i moves from open loop value at the rate

$$R_i \frac{N_C(-\alpha_i)}{D_C(-\alpha_i)}$$

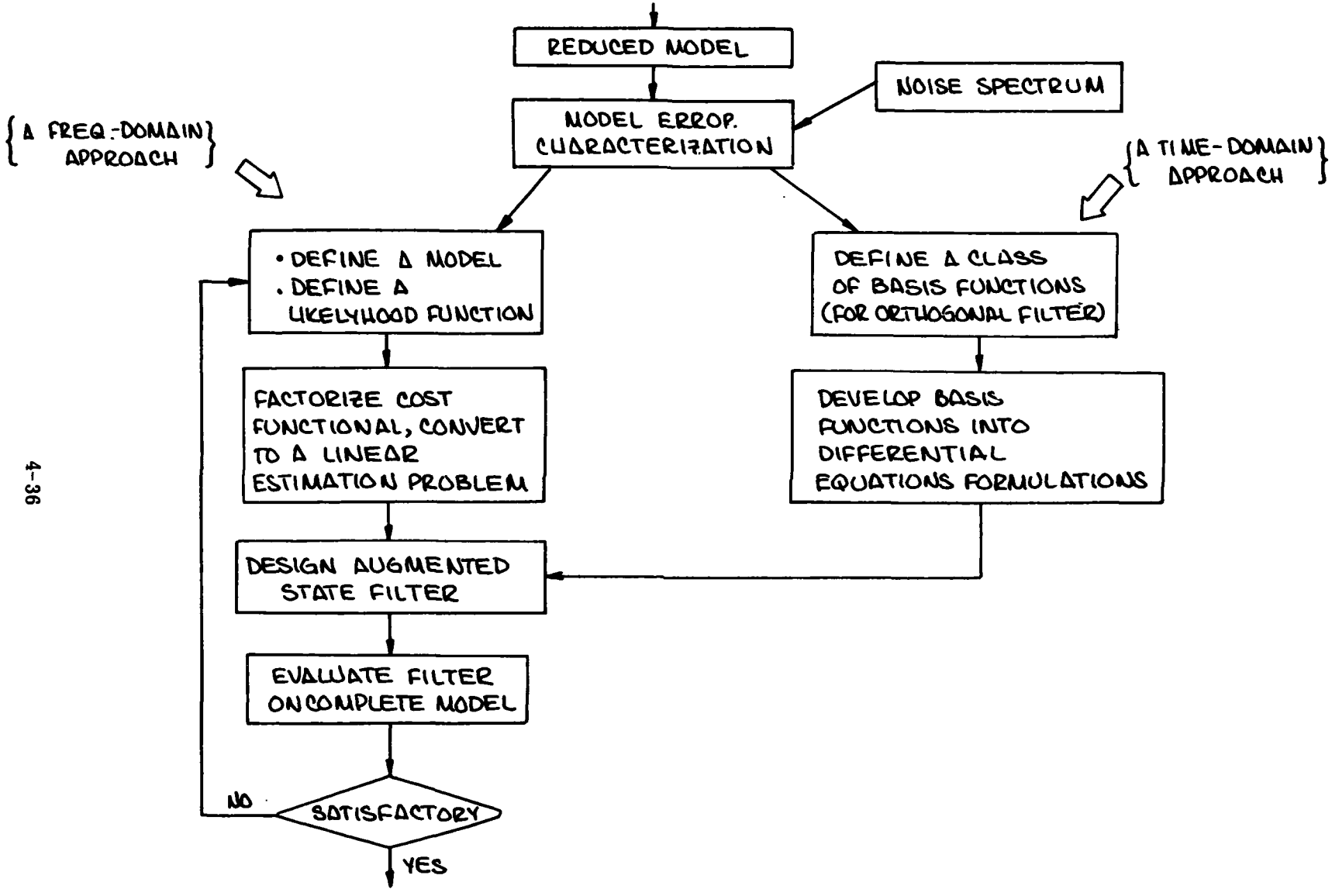

Fig. 2 Frequency Weighted Cost Functional and Orthogonal Filter Approaches to Estimator Design

where R_i is the residue of the pole in the open loop system. If the reduced model maintains residues of the modeled modes, the small gain behavior of retained modes is not affected by model reduction. The behavior of the unmodeled modes is dictated by the residue at the pole (a property of the system and actuator/sensor locations) and the controller transfer function at the pole (a property of the controller). The sign of the residue is often not known precisely but its magnitude can be bounded. This provides a bound on the rate at which each eigenvalue moves for small gains.

The high gain properties of the closed loop system are difficult to analyze. All poles will ultimately move into a zero or go to infinity. The closed-loop behavior is extremely sensitive to zero locations whose computed position depends, in a sensitive way, on the modal functions selected for the truncated model.

Frequency shaping approach ensures robustness of unmodeled modes by designing control laws such that the rate of movement of unmodeled modes is much smaller compared to the rate at which modeled poles move. This is achieved by designing controllers such that $T_C(s)$ is high at low frequency and small in the high frequency region. This is realized by frequency-shaped weighting functions in which the weights increase with frequency. If, in addition, the low frequency poles do not move in the high frequency region, the residues R_i on unmodeled modes will not change significantly. If the residue of the ith mode is of magnitude smaller than $|R_i|$, the closed-loop pole α_i will be contained within a circle with center at α_i and radius $|R_i|$ abs $\left(T_C(-\alpha_i)\right)$. To guarantee stability, this circle must lie in the left half plane.

REFERENCES

1. Bryson, A. E., and Ho. Y. C., Applied Optimal Control, Xerox Blaisdell, Massachusetts, 1974

2. Doyle, J. C., "Guaranteed Margins for LQG Regulations," IEEE Trans. Auto Control Vol. AC-23, No. 4, 756-757, August 1978 (Technical Note).

3. Rosenbrock, H. H., Computer Aided Control System Design, Academic Press, 1974

4. McFarlane, A. G. J., and Postlethwaite, I., "The Generalized Nyquist Stability Criteria and Multivariable Root Loci," Int. Journal of Control, No. 25, pp 81-127, 1977

5. Anderson, B. D. O. and Moore, J. B., Linear Optimal Control, Englewood Cliffs, NJ, Prentice Hall, 1971

6. Safonov, M. G., and Athans, M., "Gain and Phase Margin for Multiloop LQG Regulators," IEEE Trans. Auto. Control, Vol. 22, pp. 173-179, April 1977

4.2.4 Orthogonal Filters

Introduction

The orthogonal filter seeks to compensate for errors in the mathematical model of the structure in the state estimation problem. The potential of the method lies in the fact that the total model error is estimated rather than just the parameter errors available in present parameter adaptive and identification methods. First we show that modeling errors can always be decomposed into (1) parameter errors, (2) truncated modes, (3) disturbances, and (4) nonlinearities. Then the idea of the orthogonal filter is presented.

Model Errors for Matrix-Second-Order Systems

Let the nonlinear evaluation model of the structure be described by

$$M\ddot{q}_1 + (D_1 + G_1)q_1 + K_1 q_1 = B_1 u + f(q_1, \dot{q}_1, u, t) + {}_1 w_1$$

$$y_1 = P_1 q_1 + R_1 \dot{q}_1 + A_1 \ddot{q}_1 \quad q_1 \varepsilon R^{N_1}, u \varepsilon R^m \tag{1}$$

$$z_1 = P_1 q_1 + R_1 \dot{q}_1 + A_1 \ddot{q}_1 + g(q_1, \dot{q}_1, t) + v_1, \; z_1 \varepsilon R^{\ell}$$

where q_1 has dimension N_1, and $g(q_1, q_1, t)$ represents any nonlinearities in the measurement equations. Parameters of the matrices P_1, R_1, and A_1 are fixed by the location of displacement sensors, rate sensors, and accelerometers, respectively. $y_1 \varepsilon R^k$ represents the k variables we wish to control. For example, if we wish to control the entire state vector then y_1 becomes $y_1^T = (q_1^T, q_1^T)$ by appropriate choice of P_1, R_1, A_1.

$$P_1 = \begin{bmatrix} I \\ 0 \end{bmatrix}, \quad R_1 = \begin{bmatrix} 0 \\ I \end{bmatrix}, \quad A_1 = \begin{bmatrix} 0 \\ 0 \end{bmatrix} \tag{2}$$

The performance objectives might be stated in terms of $y_1(t)$ and $u(t)$, as in Ref 2, or they might be stated in terms of closed loop eigenvalue locations, as in Ref 3. This report is not specifically concerned with the control policy. Instead, it is concerned with the question of whether the model error vectors $e_q(t)$, $e_y(t)$, or $e_z(t)$ associated with any design model S_2

$$M_2\ddot{q}_2 + (D_2 + G_2)\dot{q}_2 + K_2q_2 = B_2u + e_q,\ q_2 \varepsilon R^{N_2}$$

$$y_1 = P_2q_2 + R_2\dot{q}_2 + A_2\ddot{q}_2 + e_y\ ,\ u \varepsilon R^m \tag{3}$$

$$z_1 = P_2q_2 + R_2\dot{q}_2 + A_2\ddot{q}_2 + e_z\ ,\ y_1 \varepsilon R^k\ ,\ z_1 \varepsilon R^\ell$$

can be reconstructed on-line at the same time the state vector $x_2^T = (q_2^T, \dot{q}_2^T)$ is reconstructed from the measurements $z_1(t)$. (By definition of the evaluation model (1) it is assumed throughout that $z_1(t)$ represents the actual measurements sufficiently accurately for controller evaluation purposes.)

Model error vectors $e_q(t) \varepsilon R^{N_2}$, $e_y(t) \varepsilon R^k$, $e_z(t) \varepsilon R^\ell$ exist such that the output vectors $y_1(t)$, and $z_1(t)$ of the reduced order model (3) are identically equal to the corresponding output vectors $y_1(t)$ and $z_1(t)$ of the higher order model (1). The model error vectors are

$$\begin{bmatrix} e_q \\ e_y \\ e_z \end{bmatrix} \triangleq e_\Delta + e_t + e_w + e_{NL} \tag{4}$$

where e_Δ is that contribution to the total model errors due to parameter errors in $(M_2, D_2, G_2, K_2, P_2, R_2, A_2, P_2, R_2, A_2)$, e_t is that contribution to the total model errors due to errors in model order (truncated modes), e_w is that contribution due to erroneously modeled disturbances, and e_{NL} is that contribution to the total model errors due to neglected nonlinearities. Furthermore, e_Δ, e_t, e_w, and e_{NL} have the explicit expressions

$$e_\Delta = \begin{bmatrix} -\Delta M_2 \\ \Delta A_2 \\ \Delta A_2 \end{bmatrix} \ddot{q}_2 + \begin{bmatrix} -\Delta D_2 & -\Delta G_2 \\ \Delta R_2 & \\ \Delta R_2 & \end{bmatrix} \dot{q}_2 + \begin{bmatrix} -\Delta K_2 \\ \Delta P_2 \\ \Delta P_2 \end{bmatrix} q_2 + \begin{bmatrix} \Delta B_2 \\ 0 \\ 0 \end{bmatrix} u \qquad (5a)$$

$$e_t = \begin{bmatrix} -\Omega_1^T M_1 \\ A_1 \\ A_1 \end{bmatrix} \Omega_2 \ddot{q}_t + \begin{bmatrix} -\Omega_1^T (D_1 + G_1) \\ R_1 \\ R_1 \end{bmatrix} \Omega_2 \dot{q}_t + \begin{bmatrix} -\Omega_1^T K_1 \\ P_1 \\ P_1 \end{bmatrix} \Omega_2 q_t \qquad (5b)$$

$$e_w = \begin{bmatrix} \Omega_1^T \Gamma_1 w_1 \\ 0 \\ v_1 \end{bmatrix} \qquad (5c)$$

$$e_{NL} = \begin{bmatrix} \Omega_1^T f \\ 0 \\ g \end{bmatrix} \qquad (5d)$$

where $q_t(t)$ is a $(N_1 - N_2)$-vector which satisfies

$$\begin{bmatrix} \Omega_1^T \\ \Omega_2^T \end{bmatrix} M_1 [\Omega_1 \ \Omega_2] \begin{bmatrix} \ddot{q}_2 \\ \ddot{q}_t \end{bmatrix} + \begin{bmatrix} \Omega_1^T \\ \Omega_2^T \end{bmatrix} (D_1 + G_1) [\Omega_1 \ \Omega_2] \begin{bmatrix} \dot{q}_2 \\ \dot{q}_t \end{bmatrix} +$$

$$\begin{bmatrix} \Omega_1^T \\ \Omega_2^T \end{bmatrix} K_1 [\Omega_1 \ \Omega_2] \begin{bmatrix} q_2 \\ q_t \end{bmatrix} = \begin{bmatrix} \Omega_1^T \\ \Omega_1^T \end{bmatrix} (B_1 u + \Gamma_1 W_1 + f) \qquad (6)$$

The transformation matrix $\Omega = [\Omega_1, \Omega_2]$ may be any nonsingular matrix, and the parameter errors $(\Delta M_2, \Delta D_2, \Delta G_2, \Delta K_2, \Delta B_2, \Delta P_2, \Delta R_2, \Delta A_2, \Delta \mathcal{P}_2, \Delta \mathcal{R}_2, \Delta \mathcal{A}_2)$ associated with the reduced model (3) will be defined by

$$
\begin{aligned}
\Delta P_2 &= P_1 \Omega_1 - P_2 \\
\Delta \mathcal{P}_2 &= \mathcal{P}_1 \Omega_1 - \mathcal{P}_2 \\
\Delta R_2 &= R_1 \Omega_1 - R_2 \\
\Delta \mathcal{R}_2 &= \mathcal{R}_1 \Omega_1 - \mathcal{R}_2 \\
\Delta A_2 &= A_1 \Omega_1 - A_2 \\
\Delta \mathcal{A}_2 &= \mathcal{A}_1 \Omega_1 - \mathcal{A}_2 \\
\Delta M_2 &= \Omega_1^T M_1 \Omega_1 - M_2 \\
\Delta D_2 &= \Omega_1^T D_1 \Omega_1 - D_2 \\
\Delta G_2 &= \Omega_1^T G_1 \Omega_1 - G_2 \\
\Delta K_2 &= \Omega_1^T K_1 \Omega_1 - K_2 \\
\Delta B_2 &= \Omega_1^T B_1 - B_2
\end{aligned}
\tag{7}
$$

Selection of Orthogonal Functions for Model Error Approximation

Under these conditions:

1. $$\int_{k\tau}^{(k+1)\tau} e^T(t)\, e(t)\, dt < \infty \quad , \quad \tau > 0, \quad k = 0, 1, 2, \ldots \tag{8}$$

for any set of functions satisfying

2. $$\int_{k\tau}^{(k+1)\tau} \gamma(t)\, \gamma^T(t)\, g(t)\, dt = \Lambda, \quad \gamma \in R^d \tag{9}$$

where Λ is nonsingular and $g(t)$ is a positive scalar weighting,

there exists, during any interval $\tau > 0$, a set of coefficients F_{ij} such that convergence in the mean squared sense is guaranteed.

$$\lim_{d \to \infty} \left\| e_i(t) - \sum_{j=1}^{d} F_{ij} \gamma_j(t) \right\| = 0 , \quad t \varepsilon [k\tau, (k+1)\tau] \tag{10}$$

Furthermore, the functions $\gamma_j(t)$, $j = 1, 2, \ldots d$ can be generated by

$$\dot{\gamma} = D \tag{11}$$

for some choice of D. Thus, by augmenting the model

$$\dot{x} = Ax + Bu + e_x \qquad \hat{e}_x = F\hat{\gamma}$$

$$z = Mx + v$$

with the model error system

$$\dot{\gamma} = D\gamma , \quad \hat{e}_x = F\hat{\gamma} \tag{12}$$

the estimator can be constructed

$$\begin{pmatrix} \dot{\hat{x}} \\ \dot{\hat{\gamma}} \end{pmatrix} = \begin{bmatrix} A & F \\ 0 & D \end{bmatrix} \begin{pmatrix} \hat{x} \\ \hat{\gamma} \end{pmatrix} + \begin{bmatrix} B \\ 0 \end{bmatrix} u + G'(z - M\hat{x})$$

which produces estimates of the state x and the model error vector e_x, where $\hat{e}_x = F\hat{\gamma}$.

The difference between the construction of the orthogonal filter and the construction of the estimator using frequency weighted costs is that the former requires selection of a set of basis functions in the time domain, whereas the latter requires selection of a set of basis functions in the frequency domain. Further research into the equivalence of the two points of view is required.

REFERENCES

1. Skelton, R. E. and P. C. Hughes, "Flexible Space Structure Model Reduction and Control Design by Modal Cost Analysis," 2nd AIAA/VPI Symposium on the Dynamics and Control of Large Flexible Spacecraft, Blanksburg, VA, June, 1979.

2. Hughes, P. C. and R. E. Skelton, "Controllability and Observability for Flexible Spacecraft," Proceedings, Second VPI/AIAA Symposium on Dynamics and Control of Large Flexible Spacecraft, Blanksburg, VA, 1979.

3. Highes, P. C. and Skelton, R. E., "Stability, Controllability, and Observability of Linear Matrix-Second Order Systems," JACC Proceedings, Denver, Col., June 1979.

4. Skelton, R. E. and C. Z. Gregory, "Measurement Feedback and Model Reduction by Modal Cost Analysis," Proceedings, Joint Automatic Control Conference, Denver, Col., 1979.

4.2.5 Controller Simplification

4.2.5.1 Problem Motivation. The modeling process for a large flexible structure can result in a dynamic system of prohibitive dimensions. Model order reduction is performed in two stages. The first stage, discussing earlier, consists of model reduction prior to control design. Further reduction in controller complexity is obtained by a direct simplification of the dynamic controller itself. This section discusses methods for control law simplification.

There are two aspects of controller reduction, (a) numerical procedure, and (b) criteria function. It is shown below that control laws resulting from modern control theory can be perceived as dynamic systems. Numerical procedures for reduction are, therefore, similar to those for model reduction. Criteria functions which may be used for controller simplification are given subsequently.

4.2.5.2 Controller as a Dynamic System. The controller can be viewed as a dynamic system to which model reduction techniques can be applied. When a state estimator is used in implementing the control law the controller is described by the following dynamic equations:

$$\begin{cases} \dot{\hat{x}} = F\hat{x} + Gu + K(y - H\hat{x}) & (1) \\ u = C\hat{x} & (2) \end{cases}$$

which can be rewritten as

$$\begin{cases} \dot{\hat{x}} = (F + Gc - KH)\hat{x} + Ky & (3) \\ u = C\hat{x} & (4) \end{cases}$$

This shows that the controller can be viewed as a dynamic system whose inputs are the (output) measurements and whose outputs are the control to be applied to the system.

This dynamic system is of the same order as the original system used in control design. One of the two methods may be used for reducing control law complexity (a) reduced order observers, or (b) dynamic system reduction.

Reduced Order Observers

The system described in (1) is a full-order Kalman filter on Luenberger observer. Therefore, one simple way to alleviate the possible dimensionality problem mentioned above is to use a reduced-order observer. This is described by:

$$\dot{z} = F_o z + K_o y + G_o u \tag{5}$$

where

$$z = Tx \tag{6}$$

$$TA - F_o T = K_o H \tag{7}$$

$$G_o = TB \tag{8}$$

and z is an $(n-m)$ dimensional vector (y is m-dimensional).

Defining

$$\left[\begin{array}{c} H \\ \hline T \end{array}\right]^{-1} = \left[\begin{array}{c:c} P & Q \end{array}\right] \tag{9}$$

the state estimate is given by

$$\hat{x} = Py + Qz \tag{10}$$

Therefore, the reduced-order controller is given by

$$\dot{z} = (F_o + G_o CQ)z + (K_o + CP)y \tag{11}$$

$$u = CPy + CQz \tag{12}$$

F_o may be chosen arbitrarily

The reduction of complexity was possible since the information available through the output, y, is not reconstructed in the reduced-order observer. The order of the system cannot be reduced by more than the number of outputs.

Controller Simplification

Let us consider the controller through the following general dynamic equation

$$\dot{\hat{x}} = F^*\hat{x} + Ky \tag{13}$$

$$u = C\hat{x} \tag{14}$$

This dynamic system may have real on complex poles.

A simple structure for a reduced controller is offered by

$$\dot{u} = F_1 u + G_1 y \tag{15}$$

This, however, requires that

$$CF^* = F_1 C \tag{16}$$

$$G_1 = CB \tag{17}$$

Equation (17) presents no special problems but (16) is not always solvable. It can be shown that a necessary and sufficient conditon for (16) to be solvable

is that the gain matrix C be the left eigenvectors of the full order observer matrix F* in (13). This condition could perhaps be met approximately in many systems. The benefits in doing so are clear but how to actually carry it out is still an open question.

4.2.5.3 Criteria for Model Reduction. In general, controller simplification should be such that the resulting control will yield satisfactory performance with not much degradation compared to the following criteria are available to minimize loss in performance because of controller simplifications.

(a) Residues: Elimate controller poles with small residues

(b) Pole-Zero Cancellation: Eliminate poles which approximately cancel controller zeros

(c) Frequency Range: Approximate controller poles and zeros outside the frequency range of interest

(d) Modal Cost Analysis: Discard controller poles which have minimal effects on system performance. This methodology has been firmalized by modal cost analysis, developed by Skelton [ ]. This method considers a cost functional given by

$$V = \lim_{\gamma \to \infty} E\left\{ \| \hat{y} \|_Q^2 + \| u \|_R^2 \right\} = \sum_{i=1}^{\gamma} V_i$$

the simplification is based on eliminating modes whose contribution to the over all cost (V_i) is small compared to others. This is the most sophisticated controller simplification method.

Summary

This section shows methods for controller simplification. Since the controller can be treated as a dynamic system, controller simplification is very similar to model reduction.

4.3 SELECTION OF ACTUATOR LOCATIONS

4.3.1 Introduction

The problem of actuator/sensor locations in dynamic systems has received little attention, despite its importance. Often, actuator locations are selected before the control design or, are specified based on other considerations. In these cases the designer is faced with the problem of constructing an acceptable control law to best satisfy a predetermined objective, with the constraints of actuator/sensor locations.

As increasing demands are placed on feedback control, it is necessary to manipulate actuator locations to meet design requirements.

The large space structure has a low natural damping and behaves almost like a pure oscillatory system. The actuators on this system are required to increase the damping of the naturally flexible structure. It is up to the designer to determine actuator/sensor locations that best meet the design objective.

This section considers the problem of optimal actuator locations for an oscillatory dynamic system. It will be shown that closed-form expressions concerning the modal structure of the dynamic system can be obtained. This modal information can then be used in developing the design procedure of this report.

4.3.2 Problem Statement

The oscillatory dynamic system to be considered in this section is described by

$$\dot{x}(t) = F_m x(t) + G u(t), \; x \epsilon R^{2n}, \; u \epsilon R^m \qquad (1)$$

where

$$F = \left[\begin{array}{c|c} 0 & I_n \\ \hline -A & 0 \end{array}\right], \quad G = \left[\begin{array}{c} 0 \\ \hline B \end{array}\right] \tag{2}$$

and A is a symmetric, positive-definite (p.d) n x n matrix I_n is the n x n identity matrix, and B is an n x m matrix.

The system matirx, F, is determined by the physics of the problem, but the input matrix, G, can be selected subject to some criteria and the structure given by Eq. (2). The next section will describe a particular criterion to be employed as a measure of optimality in actuator location, i.e., the specification of G. The problem of sensor location, even though not treated here, can be similarly defined and solved by duality.

4.3.3 Optimality Criteria

The state vector of the oscillatory system given in Eq. (1) contains the displacements and velocities at various nodes of the system. In placing the actuators, it is desirable that control energy will be such that after some finite time both displacements and velocities will be zero, i.e.,

$$x(T) = 0 \quad \text{for some finite} \quad T > 0 \tag{3}$$

An additional requirement is that the control energy exerted by the actuators will be minimal.

Kalman, Ho, and Narendra [1] have shown that the minimal energy control[†] is given by

$$u^*(t) = G^T(t)\,\phi(t_o,t)W^{-1}(t_o,T)\,[\phi(t_o,T)x(T)-x_0] \tag{4}$$

where $\phi(.)$ is the transition matrix and W(.) is the controllability matrix defined by

[†]For details. see Appendix D

$$W(t_o,T) = \int_{t_o}^{T} \phi(t_o,\tau)G\ G^T\phi^T(t_o,\tau)d\tau \qquad (5)$$

If the final desired state is the origin, the minimal control energy will be given by

$$J^* \triangleq \min_u \int_{t_o}^{T} ||u(\tau)||^2 d\tau = x_o^T W^{-1}(t_o,T)x_o \qquad (6)$$

Since the controllability matrix, W depends on the actuator locations, the control energy can be affected by properly choosing these locations.

The general measure of optimality to be used in selecting the actuator locations is given by

$$J_k = \min_B [t_r(M_o W^{-k})]^{1/k} \qquad (7)$$

where the weighting matrix M_o is used to eliminate the effect of initial conditions on the performance index.

For $M_o = I$ we get the following special cases

$$\underline{k = 0:}\ J_o = \max_B [\det(W)] \qquad (8)$$

$$\underline{k = 1:}\ J_1 = \max_B [n/t_r(W^{-1})] \qquad (9)$$

$$k = \infty:\ J_\infty = \max_B [\lambda\min(W)] \qquad (10)$$

4.3.4 General Form For The Controllability Matrix

The n x n matrix A in Eq. (2) is a symmetric p.d. matrix. As will be demonstrated shortly, the transition matrix as well as the controllability matrix can be written

rather easily in closed form if A is a diagonal matrix. Therefore, the first step in the analysis will be to define a transformation that will result in an equivalent system with this property. Let

$$z \triangleq T_x \tag{11}$$

where

$$T = \left[\begin{array}{c|c} U^{-1} & 0 \\ \hline 0 & U^{-1} \end{array}\right] \tag{12}$$

and U is the n x n matrix of eigenvectors of A, i.e.

$$AU = U \Lambda_A \tag{13}$$

$$\Lambda_A = \text{diag}\,(a_1, \ldots, a_n) \tag{14}$$

Then the equivalent system is given by

$$\dot{z} = F_o z + G_o u \tag{15}$$

where

$$F_o = TA_oT^{-1},\ G_o = TB_o = \left[\begin{array}{c} 0 \\ \hline G \end{array}\right] \tag{16}$$

and

$$G = U^{-1}B \tag{17}$$

Furthermore, if

$$\phi_X(t,t_o) \triangleq e^{F(t-t_o)} \tag{18}$$

$$\phi_z(t,t_o) \triangleq e^{F_o(t-t_o)} \tag{19}$$

then

$$\phi_x(t,t_o) = T^{-1} \phi_z(t,t_o)T \tag{20}$$

If

$$W_x(0,T) = \int_o^T \phi_x(0,\tau)G\ G^T \phi^T(0,\tau)d\tau \tag{21}$$

and

$$W_z(0,T) = \int_o^T \phi_z(0,\tau)G_o\ G_o^T \phi^T(0,\tau)d\tau \tag{22}$$

then, using Eqs. (15) and (20)

$$W_x(0,T) = T^{-1} W_z(0,T)(T^{-1})^T \tag{23}$$

The measure of optimality will now be given by

$$J_k = \min \left[\text{tr } MW_z^{-k}\right]^{1/k} \tag{24}$$

where

$$M = T^k M_o(T^T)^k \tag{25}$$

The modal structure for the system described by (15) is derived in Appendix A. This structure results in a closed form expresssion for the transition matrix given by

$$\Phi_z(0,t) = \begin{bmatrix} \alpha_1 & & 0 & B_1 & & 0 \\ & \ddots & & & \ddots & \\ 0 & & \alpha_n & 0 & & B_n \\ \hline \alpha_1 & & 0 & \alpha_1 & & 0 \\ & \ddots & & & \ddots & \\ 0 & & \alpha_n & 0 & & \alpha_n \end{bmatrix} \tag{26}$$

where

$$\left.\begin{aligned} \alpha_i &= \cos\sqrt{a_i}\, t \\ \beta_i &= -\frac{1}{\sqrt{a_i}} \sin\sqrt{a_i}\, t \\ \alpha_i &= \sqrt{a_i}\, \sin\sqrt{a_i}\, t \end{aligned}\right\} \quad i = 1, 2, \ldots, n \tag{27}$$

Using the definition for the controllability matrix as given in Eq. (22), the expression for the transition matrix as given in Eqs. (26) and (27) and, in addition, the following definition

$$G_o G_o^T = \begin{bmatrix} G_{11} & G_{12} & \cdots & G_{1n} \\ \vdots & & & \\ G_{n1} & \cdots & & G_{nn} \end{bmatrix} \tag{28}$$

we obtain the following expression for $W_z(0,T)$,

$$W_z(0,T) = \left[\begin{array}{c|c} W_{11} & W_{12} \\ \hline W_{12} & W_{22} \end{array}\right] \tag{29}$$

The four n x n symmetric blocks are described as follows:

$$W_{11} = \int_o^T \begin{bmatrix} G_{11}\beta_1^2 & G_{12}\beta_1\beta_2 & \cdots & G_{1n}\beta_1\beta_n \\ & G_{22}\beta_2^2 & & \\ & & \ddots & \\ & & & G_{nn}\beta_n^2 \end{bmatrix} dt$$

$$W_{12} = \int_o^T \begin{bmatrix} G_{11}\beta_1\alpha_1 & G_{12}\beta_1\alpha_2 & \cdots & G_{1n}\beta_1\alpha_n \\ & G_{22}\beta_2\alpha_2 & & \\ & & \ddots & \\ & & & G_{nn}\beta_n\alpha_n \end{bmatrix} dt = W_{21}^T$$

$$W_{22} = \int_o^T \begin{bmatrix} G_{11}\alpha_1^2 & G_{12}\alpha_1\alpha_2 \cdots\cdots G_{1n}\alpha_1\alpha_n \\ & G_{22}\alpha_2^2 \\ & \ddots \\ & G_{nn}\alpha_n^2 \end{bmatrix} dt$$

Using the expression for the controllability matrix we obtain the main result.

Theorem 1: For terminal time, T, large enough (10 sec) the controllability matrix given in Eq. (29) becomes diagonally dominant and can be approximated by

$$W_{ii}(0,T) = \begin{cases} \dfrac{G_{ii}T}{2_{ai}} & 1 \le i \le n \\ \dfrac{G_{ii}T}{2} & n < i \le 2n \end{cases} \qquad (30)$$

Proof: The diagonal elements of $W_z(o,T)$ are given by

$$W_{ii}(0,T) = \begin{cases} \dfrac{G_{ii}T}{a_i}\left(\dfrac{T}{2} - \dfrac{\sin 2T\sqrt{a_i}}{2\sqrt{a_i}}\right) & 1 \le i \le n \\ \dfrac{G_{ii}}{2}\left(T + \dfrac{\sin 2T\sqrt{a_i}}{2\sqrt{a_i}}\right) & n < i \le 2n \end{cases}$$

for T large enough the second term becomes negligible and hence we get Eq. (30). The off-diagonal elements are a product of sine and cosine functions only without the additive term of the terminal time as found for the diagonal terms. Therefore, for T large enough the matrix W becomes diagonally dominant with terms given by Eq. (30).

With this expression for the controllability matrix we can turn now toward the numerical problem of solving for the actuator locations Eq. (7) or Eq. (24).

4.3.5 Numerical Procedure

The optimal location of actuators will be established through the solution of

$$J_k = \min \left[tr(MW_z^{-k}) \right]^{1/k}$$

The steps of the algorithm are as follows:(also see enclosed flow chart, Fig. 1):

Step 1: Read A, M_o, n, m, k, ϵ, T

Step 2: Find U, Λ_A such that

$$AU = U\,\Lambda_A$$

Step 3: Construct T as in Eq. (12) and find M as in Eq. (25)

Step 4: Make an initial guess for the parameters vector θ.

Step 5: Find the matrix B from known analytical relationship with θ, tables, etc.

Step 6: Find the diagonal terms of

$$G_2 = U^{-1}BB^T (U^{-1})^1$$

Step 7: Construct the diagonal of the controllability matrix W_z, via Eq. (30)

Step 8: $\min(tr\, MW_z^{-k})^{1/k}$ to find an update to the parameters vectors θ.

Step 9: If the update $\Delta\theta$ is small, i.e., $\|\Delta\theta\| \leq \epsilon$ STOP; otherwise, GO TO Step 5.

Remark: In step 3 only the diagonal terms of M have to be found.

4.3.6 Conclusion

The problem of actuator location for oscillatory system was considered. It was shown that through the controllability matrix one can arrive at an actuator location that is derived via the solution of the minimum energy control.

A similar approach can be used for the solution of the sensor location problem.

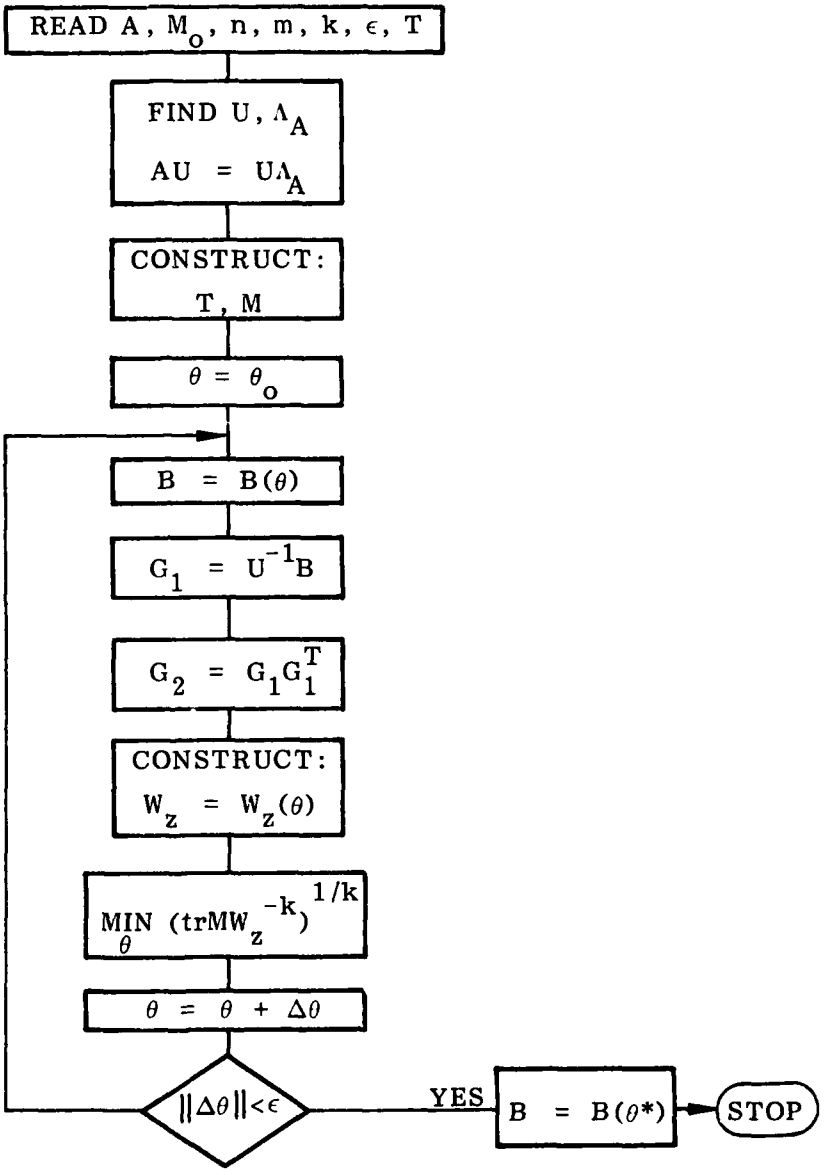
READ A , M_o, n, m, k, ϵ, T
FIND U, Λ_A
AU = $U\Lambda_A$
CONSTRUCT:
T, M
$\theta = \theta_o$
B = B(θ)
$G_1 = U^{-1}B$
$G_2 = G_1G_1^T$
CONSTRUCT:
$W_z = W_z(\theta)$
$\min_\theta (trMW_z^{-k})^{1/k}$
$\theta = \theta + \Delta\theta$
$\|\Delta\theta\| < \epsilon$
YES
B = B(θ^*)
STOP

Fig. 1

Section 5
APPLICATIONS TO DARPA STRAWMEN

5.1 THE CHARLES STARK DRAPER LABORATORY (CSDL) EXAMPLE

5.1.1 The CSDL Example Structural Model

The model illustrated in Fig. 1 is a conceptual structure recently designed by Dr. Keto Soosaar and R. Strunce of the Charles Stark Draper Laboratory (CSDL). The CSDL example consists of a (regular) tetrahedral truss supported on a ground by three right-angled bipods. The bipod legs are pinned to ground, and all other nodes are clamped. The individual truss members, including the bipods, have elastic flexibility in their axial directions only, i.e., they can undergo compression and elongation but no lateral bending. The four vertices of the tetrahedron each have three degrees of freedom, so that the entire model can be completely represented by 12 structural modes.

The structural model is described in consistent, but unspecified units. The edges of the (regular) tetrahedron are each 10 units long, and the bipod legs are each $2\sqrt{2}$ units long. (The "horizontal" base of the tetrahedron is therefore situated 2 units above ground, i.e., above the x,y plane.) The top vertex is defined as LOS (line-of-sight), and the six bipod legs are defined to act as "member dampers," i.e., active axial spring/dashpots, each equipped with a rate and position sensor. The three bipods represent therefore 6 colocated actuator/sensor pairs, each pair being identified with a bipod leg. Sensor measurements and actuator forces are thus confined to the axial elongation/compression motions and rates of the bipod legs.

The stiffness properties of the structure are non-uniform, and are given in terms of the truss members' cross-sectional areas. Two sets of values are given, one for a "nominal" model, and the other for a "perturbed" model, as follows: (see Fig. 1 for truss element numbers)

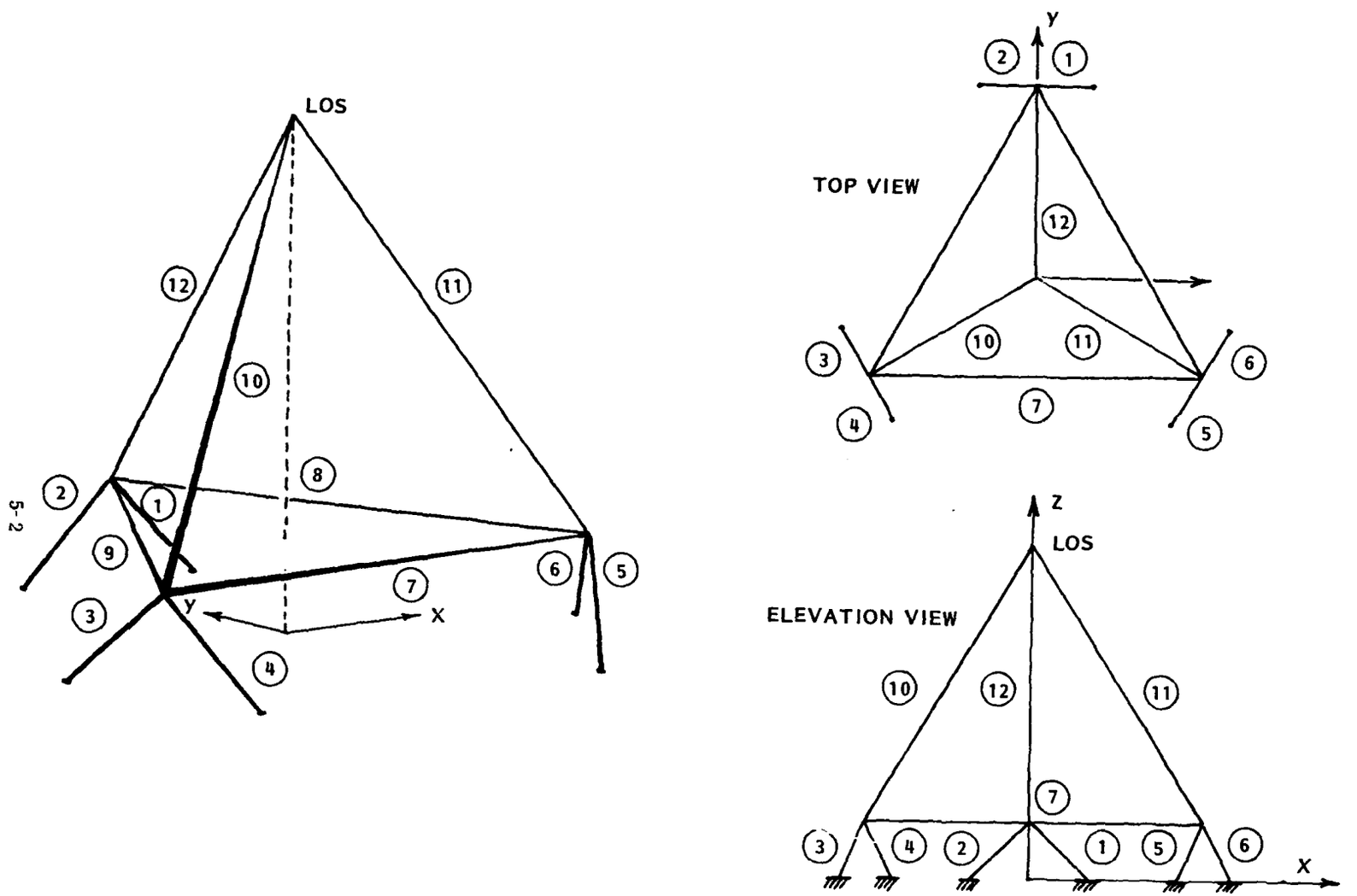

Fig. 1 The CSDL Example Structural Model

Truss Element No.	Area (Nominal Model)	Area (Perturbed Model)
1	100	150
2	100	150
3	100	150
4	100	150
5	100	150
6	100	150
7	1000	1200
8	1000	1200
9	1000	1200
10	1000	1200
11	100	150
12	100	150

where, for both models, Young's modulus is E = 1.0. Finally, there are lumped masses of 2 units at each vertex of the tetrahedron for the nominal model. For the perturbed model, the lumped mass at the LOS vertex (see Fig. 1) is changed to 4 units, and the others remain the same.

The structural frequencies (open-loop eigenvalues) of the two 12-mode models can be obtained from a finite-element structural program (e.g., NASTRAN, SPAR, ASTRO, etc.) and are as follows:

	Frequency (Hz)	
Model No.	Nominal Model	Perturbed Model
1	0.213588	0.186316
2	0.264949	0.233445
3	0.460071	0.471833
4	0.470687	0.566233
5	0.540840	0.612490
6	0.669164	0.819555
7	0.741991	0.903348
8	0.756823	0.908903
9	1.35909	1.42279
10	1.47227	1.63987
11	1.63687	1.73851
12	2.05391	2.22286

5.1.2 The CSDL Example Control Problem

As described in the previous subsection, there are two structural models: one is the nominal model, and the other is the perturbed model (nominal model with parameter variations). It is assumed that all 12 modes have 0.5 percent inherent structural damping. By definition, modes 9, 10, 11, and 12 are to be treated as unmodelled modes, so that they cannot be used in any controller design process. However, they are to be used for the full-order evaluation model for all designs.

The physical model to be used in the controller design process consists of the first eight modes of the nominal model. The evaluation of the various controller designs is then based on the full 12-mode models for both the nominal and perturbed structures. By "construction", good performance is obtained when modes 1, 2, 4, and 5 are actively controlled so that they acquire at least 10 percent damping. When that is achieved, the closed-loop response of the structure to certain initial conditions is such that the x-LOS error (LOSX) and y-LOS error (LOSY) (i.e., the x and y components of the LOS vertex) have magnitudes less than 0.0004 and 0.00025 units of length, respectively, after 20 seconds.

The rationale for the statements above is based on the following simulation experiment: 10 percent modal damping is assigned to modes 1, 2, 4, and 5, and 0.5 percent to the remaining modes of the 12-mode nominal model. The structure is then subjected to an initial condition at t = -1 sec by giving a unit displacement along the x-axis to the front base vertex of the tetrahedron (see Fig. 1). The transient response is then simulated to t = 20 sec, and it is observed that the LOS requirements are met.

To make the problem more challenging, a "snapshot" of the transient response is taken at t = 0 sec, and values of the modal coordinates (displacement and velocity) are recorded. These values are then modified by setting to zero the modal coordinates corresponding to the unmodelled modes 9 through 12. The resulting initial conditions to be used at t = 0 sec are then the following:

Mode No.	Displacement (Q)	Velocity (Q)
1	-0.0001	-0.003
2	0.0006	0.01
3	0.0001	0.03
4	-0.0009	-0.02
5	0.0008	0.02
6	-0.0001	-0.02
7	-0.0002	0.003
8	0.0002	0.004
9	0.0	0.0
10	0.0	0.0
12	0.0	0.0

The CSDL example control problem consists then of two parts: (1) design an "acceptable" controller using all 6 colocated sensors/actuators, and (2) design an "acceptable" controller that works without using colocated sensors and actuators. (This is to be achieved by eliminating either a sensor or an actuator – or both – from each bipod leg so that no colocated sensor/actuator pairs remain in the system. Many combinations are obviously possible.) In both cases, the controller design is "acceptable" if the LOS requirements are essentially met for both the nominal and perturbed 12-mode models, with the controller design based only on the first 8 (or fewer) modes. The primary objective of the CSDL example is to provide a well-defined, non-trivial dynamical plant which serves as a common "test-bed" to illustrate, compare, and evaluate various controller designs. In that context, the exact verification of the LOS requirements is only secondary, and the given LOS specifications serve as approximate evaluation guidelines.

5.1.3 The CSDL Example: Centralized Low Authority Controller Design

This centralized controller design is based on the Low Authority Control Gain Synthesis procedure previously described in Section 4.1. While sensors and actuators are physically colocated, the feedback in this design is not colocated, and hence (by definition) is called centralized. (Note: A decentralized low authority controller, i.e., using colocated feedback, may of course also be considered. If, however, sensors are further assumed to measure rates only*

*Low Authority Control Theory is valid for full state-feedback. Restriction of this design to rate-feedback only was assumed here in order to achieve the simplest controller design leading to acceptable performance vis a vis the LOS requirements.

```
***C MATRIX IS  9X 9    NON-ZERO ELEMENTS FOLLOW (GAIN MATRIX C IS UPPER TRIANGULAR)

C( 1, 1)= -5.570+00 C( 1, 2)= -4.570+00 C( 1, 3)=  1.210+00 C( 1, 4)=  8.880+00
C( 1, 5)=  5.670+00 C( 1, 6)= -9.820+00 C( 2, 2)= -1.120+01 C( 2, 3)= -1.190+01
C( 2, 4)=  1.100+01 C( 2, 5)=  1.820+01 C( 2, 6)=  5.670+00 C( 3, 3)= -6.690+00
C( 3, 4)=  1.810+00 C( 3, 5)=  1.100+01 C( 3, 6)=  8.890+00 C( 4, 4)= -6.690+00
C( 4, 5)= -1.190+01 C( 4, 6)=  1.210+00 C( 5, 5)= -1.120+01 C( 5, 6)= -4.570+00
C( 6, 6)= -5.580+00
```

NOMINAL MODEL

*** ROOTS OF THE CLOSED-LOOP SYSTEM ***

MODE	IND	FREQUENCY	DAMPING	TIME CONST.	REAL PART	IMAGINARY
→ 1	1	2.3686-01	.115365	5.8244+00	-1.7169-01	1.4783+00
→ 2	1	2.7056-01	.171780	3.4243+00	-2.9203-01	1.6747+00
3	1	3.3980-01	.292132	1.6033+00	-6.2372-01	2.0419+00
→ 4	1	4.5676-01	.105136	3.3142+00	-3.0173-01	2.8540+00
→ 5	1	5.4926-01	.126561	2.2895+00	-4.3678-01	3.4234+00
6	1	7.1263-01	.052593	4.2465+00	-2.3549-01	4.4714+00
7	1	7.8119-01	.302852	4.0515-01	-2.4682+00	4.2427+00
8	1	8.4789-01	.691555	2.7143-01	-3.6842+00	3.8482+00
9	1	1.3561+00	.168382	6.9698-01	-1.4348+00	8.3992+00
10	1	1.4281+00	.214249	5.2018-01	-1.9224+00	8.7644+00
11	1	1.6346+00	.037089	2.6252+00	-3.8092-01	1.0263+01
12	1	2.0522+00	.008904	8.7100+00	-1.1481-01	1.2894+01

PERTURBED MODEL

*** ROOTS OF THE CLOSED-LOOP SYSTEM ***

MODE	IND	FREQUENCY	DAMPING	TIME CONST.	REAL PART	IMAGINARY
→ 1	1	1.9116-01	.073184	1.1376+01	-8.7902-02	1.1979+00
→ 2	1	2.3540-01	.076797	8.8037+00	-1.1359-01	1.4747+00
3	1	4.3082-01	.185411	1.9925+00	-5.0189-01	2.6600+00
→ 4	1	5.1960-01	.109628	2.7940+00	-3.5791-01	3.2451+00
→ 5	1	6.3963-01	.095613	2.6024+00	-3.8426-01	4.0005+00
6	1	8.0808-01	.029404	6.6982+00	-1.4929-01	5.0751+00
7	1	9.3761-01	.449716	3.7745-01	-2.6494+00	5.2619+00
8	1	9.8457-01	.580253	2.7858-01	-3.5896+00	5.0383+00
9	1	1.4856+00	.221133	4.8445-01	-2.0642+00	9.1035+00
10	1	1.5813+00	.147145	6.8401-01	-1.4620+00	9.8273+00
11	1	1.7212+00	.059084	1.5651+00	-6.3895-01	1.0795+01
12	1	2.2219+00	.007304	9.8067+00	-1.0197-01	1.3960+01

Fig. 2 Centralized Low Authority Control (LAC) Design for the CSDL Example. Control Gains and Closed-Loop Eigenvalues for Nominal and Perturbed Models

the inherent nature of the CSDL example structure, together with a a priori fixed selection of sensors and actuators, are such that the LOS performance requirements cannot be met. Indeed, synthesis of such a controller has shown that it is limited to approximately 4 percent (maximum) damping in modes 1, 2, 4, and 5, and hence not acceptable. This result is physically not surprising: indeed, infinite gains for such a controller would completely rigidify the bibods and the base of the tetrahedron while leaving the elastic motions of the top (LOS) vertex essentially unaffected. As will be shown in Section 5.1.4, a modification of the CSDL control problem, whereby different sensor/actuator types and locations can be used, leads to an acceptable decentralized, rate-feedback low authority controller design.)

For the centralized LAC rate-feedback controller design, an upper triangular form for the gain matrix C was used. Figure 2 gives the values of the gains and shows the resulting damping ratios, for both nominal and perturbed models, obtained by a full system eigenanalysis. The comparison between the LAC-theory predicted and the actual closed-loop damping (for the nominal model) is shown in Fig. 3, where the model weights W_n are also displayed. (Note: As in most gain synthesis procedures, some trial-and-error iterations are required to determine acceptable gains. In this case, iterations were made on the values of the W_n and of the desired damping ratios $(2\zeta_n W_n)_D = (d\lambda_n)_D \equiv d_n$ appearing in Eq. (15) of Section 4.1. A key feature of the LAC theory is that its closed-loop performance prediction formula, Eq. (9) of Section 4.1, provides a simple and numerically fast method to evaluate the effect of these iterations prior to final verification by full system eigenanalysis.)

Figures 4, 5, and 6 show the results of LOS transient response to the CSDL initial conditions, including time-histories of LOSX, LOSY, physical motion of LOS, and the actuator force levels developed in the bipod actuators. These levels are only about 1-1/2 times higher than those obtained with the optimal controller designs discussed in Section 5.1.5.

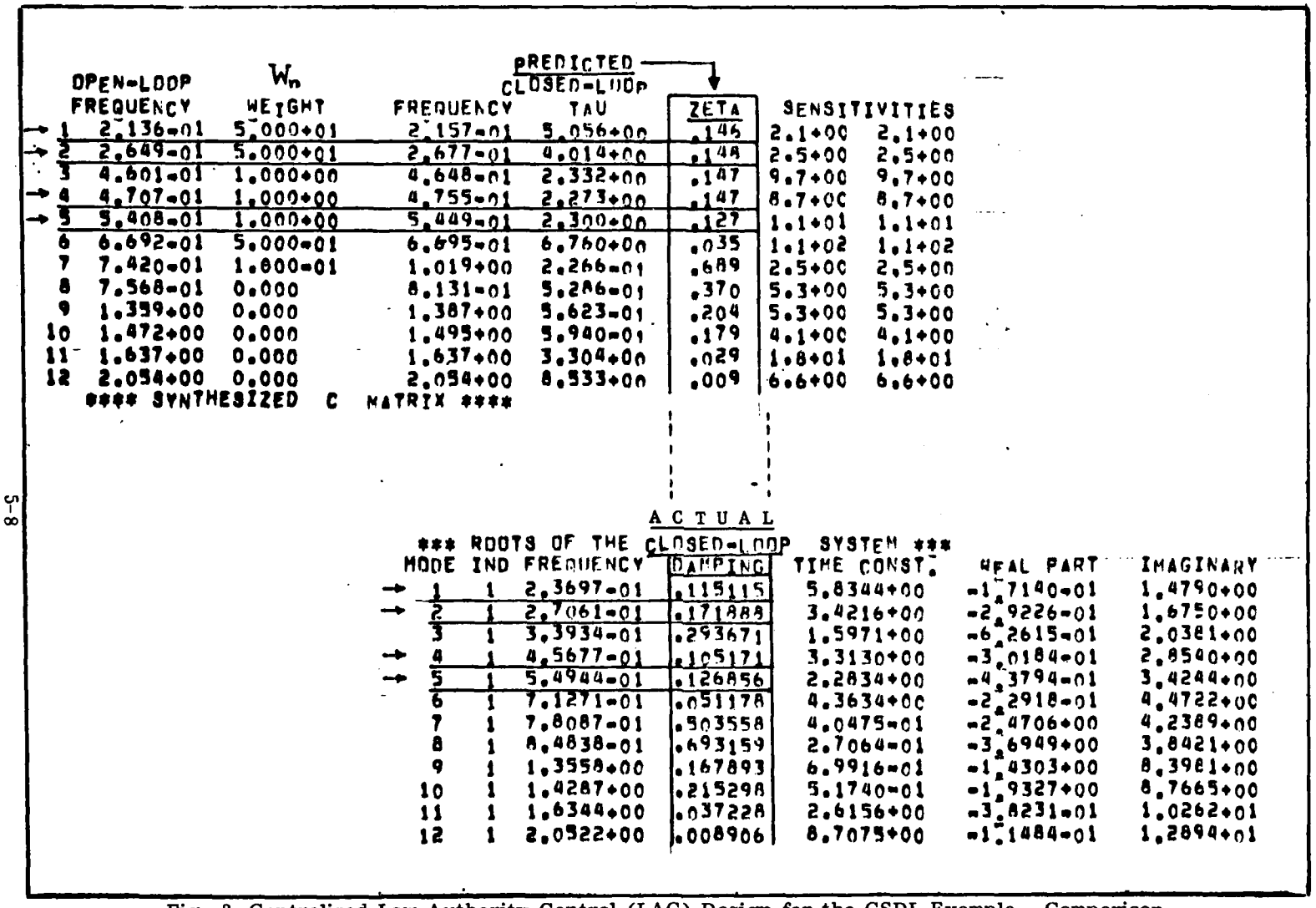

	OPEN-LOOP FREQUENCY	W_n WEIGHT	PREDICTED CLOSED-LOOP FREQUENCY	TAU	ZETA	SENSITIVITIES	
→ 1	2.136-01	5.000+01	2.157-01	5.056+00	.146	2.1+00	2.1+00
→ 2	2.649-01	5.000+01	2.677-01	4.014+00	.148	2.5+00	2.5+00
3	4.601-01	1.000+00	4.648-01	2.332+00	.147	9.7+00	9.7+00
→ 4	4.707-01	1.000+00	4.755-01	2.273+00	.147	8.7+00	8.7+00
→ 5	5.408-01	1.000+00	5.449-01	2.300+00	.127	1.1+01	1.1+01
6	6.692-01	5.000-01	6.695-01	6.760+00	.035	1.1+02	1.1+02
7	7.420-01	1.000-01	1.019+00	2.266-01	.689	2.5+00	2.5+00
8	7.568-01	0.000	8.131-01	5.286-01	.370	5.3+00	5.3+00
9	1.359+00	0.000	1.387+00	5.623-01	.204	5.3+00	5.3+00
10	1.472+00	0.000	1.495+00	5.940-01	.179	4.1+00	4.1+00
11	1.637+00	0.000	1.637+00	3.304+00	.029	1.8+01	1.8+01
12	2.054+00	0.000	2.054+00	8.533+00	.009	6.6+00	6.6+00

**** SYNTHESIZED C MATRIX ****

ACTUAL

*** ROOTS OF THE CLOSED-LOOP SYSTEM ***

	MODE	IND	FREQUENCY	DAMPING	TIME CONST.	REAL PART	IMAGINARY
→	1	1	2.3697-01	.115115	5.8344+00	-1.7140-01	1.4790+00
→	2	1	2.7061-01	.171888	3.4216+00	-2.9226-01	1.6750+00
	3	1	3.3934-01	.293671	1.5971+00	-6.2615-01	2.0381+00
→	4	1	4.5677-01	.105171	3.3130+00	-3.0184-01	2.8540+00
→	5	1	5.4944-01	.126856	2.2834+00	-4.3794-01	3.4244+00
	6	1	7.1271-01	.051178	4.3634+00	-2.2918-01	4.4722+00
	7	1	7.8087-01	.503558	4.0475-01	-2.4706+00	4.2389+00
	8	1	8.4838-01	.693159	2.7064-01	-3.6949+00	3.8421+00
	9	1	1.3558+00	.167893	6.9916-01	-1.4303+00	8.3981+00
	10	1	1.4287+00	.215298	5.1740-01	-1.9327+00	8.7665+00
	11	1	1.6344+00	.037228	2.6156+00	-3.8231-01	1.0262+01
	12	1	2.0522+00	.008906	8.7075+00	-1.1484-01	1.2894+01

Fig. 3 Centralized Low Authority Control (LAC) Design for the CSDL Example. Comparison Between Predicted and Actual Damping Ratios Obtained for the Nominal Model

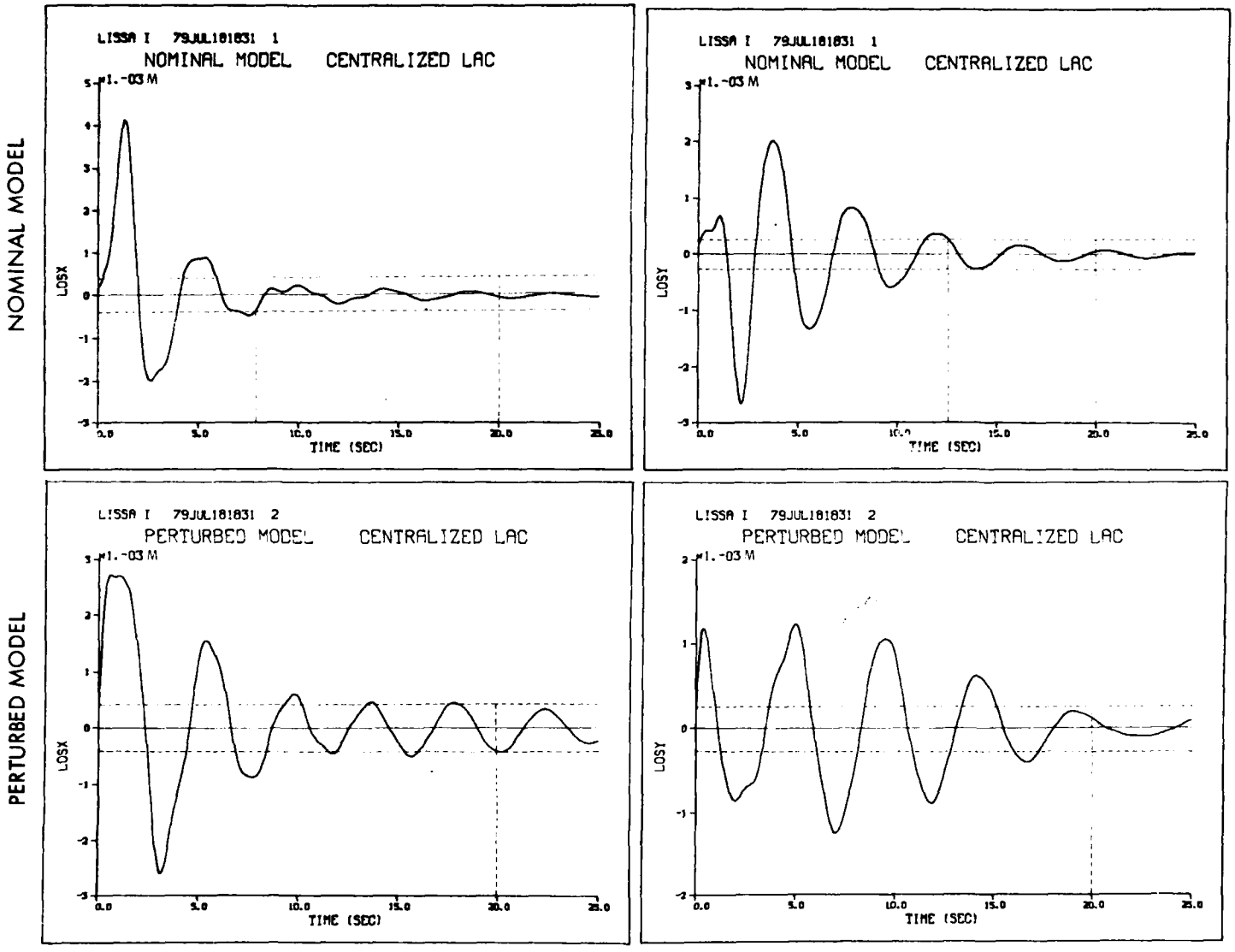

Fig. 4 Centralized LAC Design Evaluation (CSDL Example) – Closed-Form Solution of LOS Transient Responses to the CSDL Initial Conditions. (Dashed Lines Represent LOS Requirements

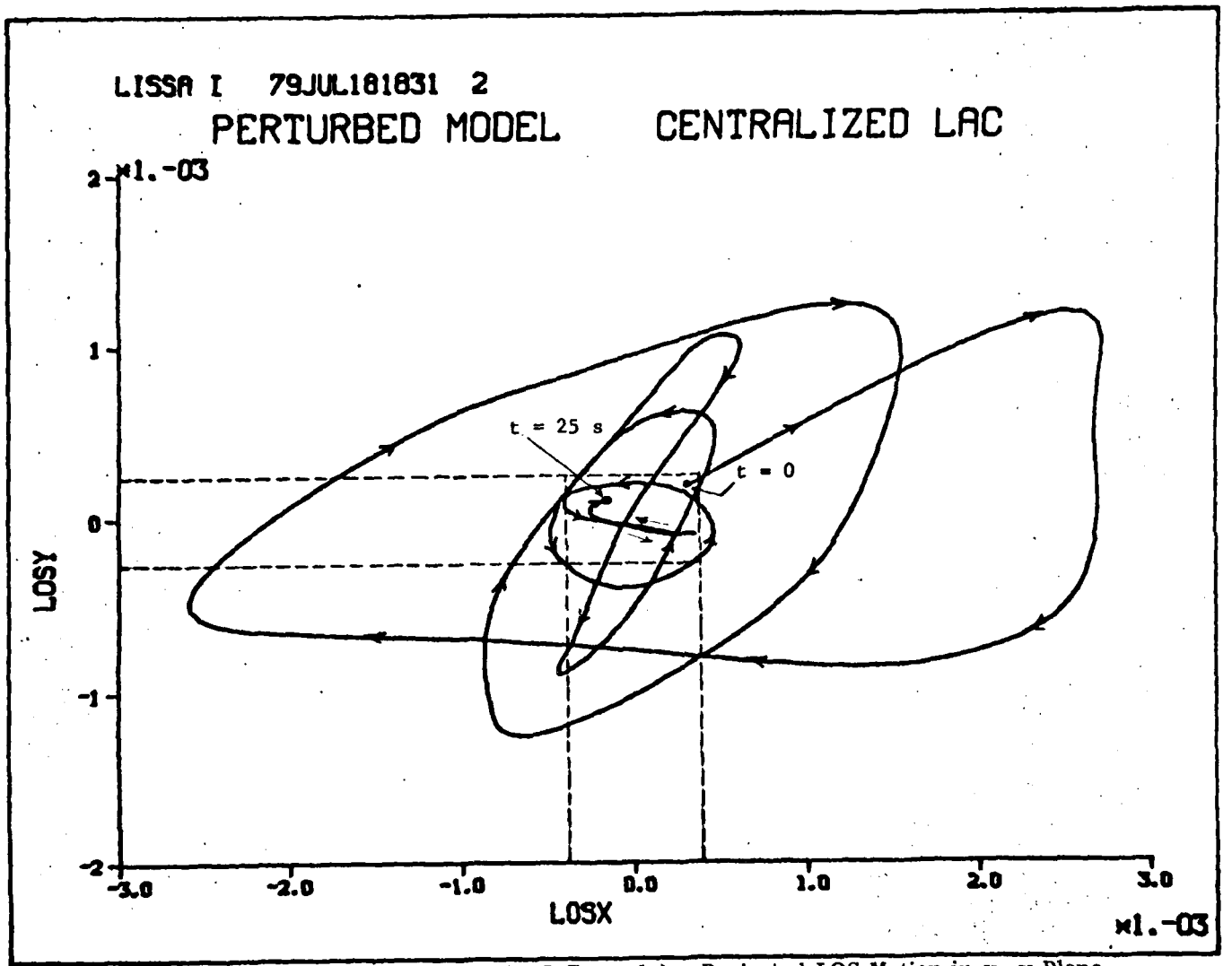

Fig. 5 Centralized LAC Design (CSDL Example) - Projected LOS Motion in x, y Plane Dashed Lines Represent LOS Requirements After 20 sec. LOS Trajectory Enters Target Area at About 18 sec

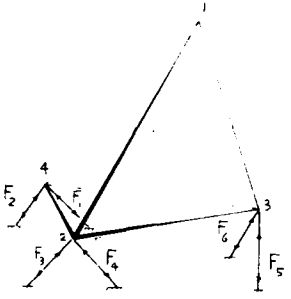

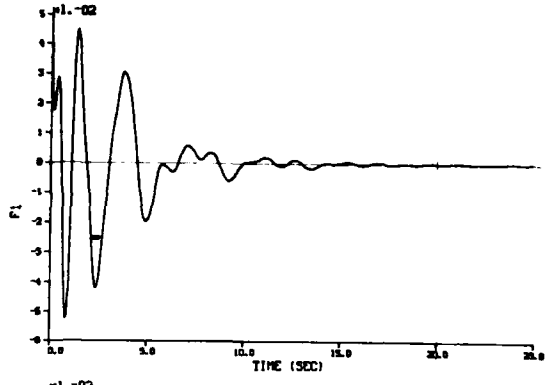

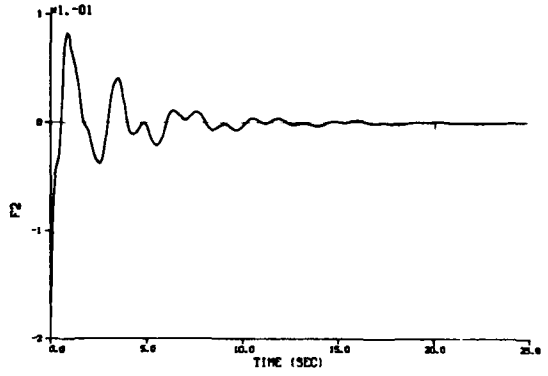

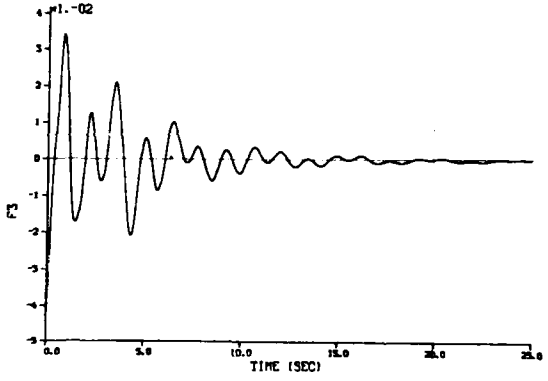

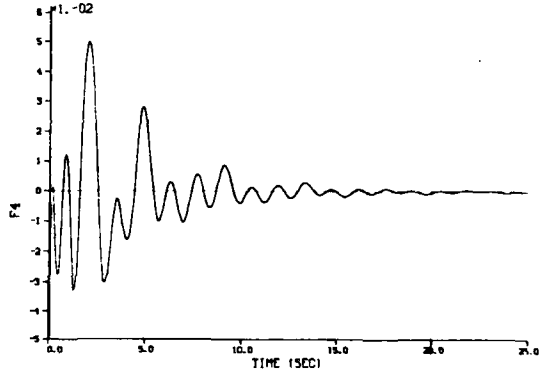

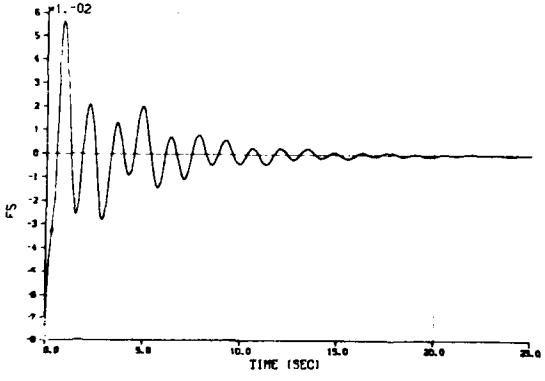

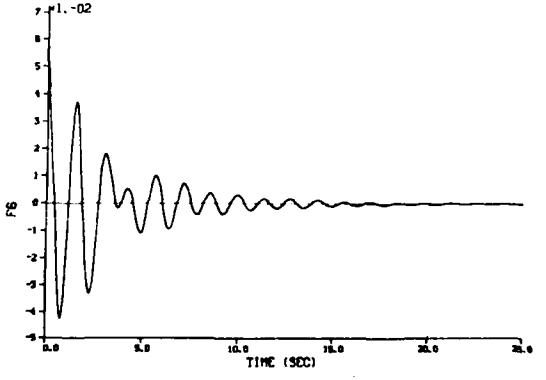

Fig. 6 Centralized LAC Design for the CSDL Example – Actuator Force Levels

5.1.4 The CSDL Example: Decentralized Low Authority Controller Design

This controller design is not restricted to the sensor/actuator pairs postulated in the CSDL example control problem (Section 5.1.2). Instead, it is based on the use of 5 sensor/actuator pairs, three of which are one "leg" of each bipod, shown in Fig. 7 as F_1 , F_3 , F_5 , and the remaining two are inertial proof-mass dampers, designated as F_7 , F_8 , acting translationally along the x and y directions , respectively.

Figure 7 shows the nominal model open-loop frequencies, the synthesized diagonal gain matrix C, the LAC-predicted and the actual closed-loop damping ratios obtained from full system eigenanalysis.

Figure 8 shows the actual damping ratios for both the nominal and perturbed models, and the LOS transient response evaluations to the CSDL initial conditions, also for both nominal and perturbed models. Since the latter were obtained by "vector exponential" closed-form solution methods, LOSX, and LOSY are tabulated directly for the time interval 19 sec $\leq t \leq$ 25 sec. As can be seen, the LOS requirements are easily met at $t = 20$ sec.

AD-A089 142 LOCKHEED MISSILES AND SPACE CO INC PALO ALTO CA PALO --ETC F/G 22/2
ACOSS THREE (ACTIVE CONTROL OF SPACE STRUCTURES). PHASE I.(U)
MAY 80 M G LYONS, J N AUBRUN, G MARGULIES F30602-79-C-0087
UNCLASSIFIED RADC-TR-80-131 NL

2 OF 3
AD A089142

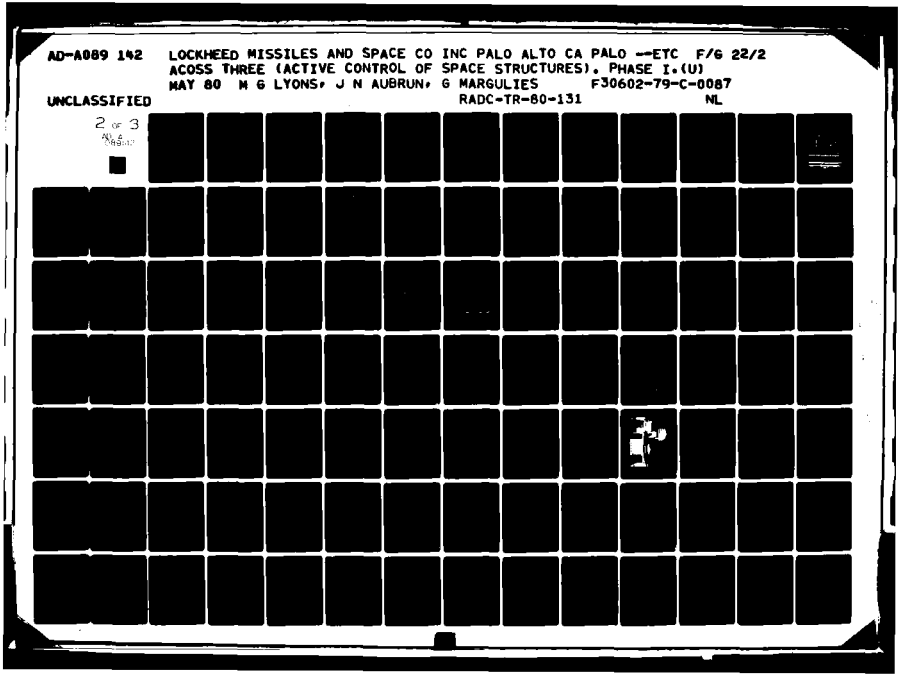

```
OPEN-LOOP    SYSTEM'S ROOTS
MODE  IND  FREQUENCY   DAMPING
  1    2  2.1359-01   .005000
  2    2  2.6495-01   .005000
  3    2  4.6007-01   .005000
  4    2  4.7069-01   .005000
  5    2  5.4084-01   .005000
  6    2  6.6916-01   .005000
  7    2  7.4199-01   .005000
  8    2  7.5682-01   .005000
  9    2  1.3591+00   .005000
 10    2  1.4723+00   .005000
 11    2  1.6369+00   .005000
 12    2  2.0539+00   .005000
HOW MANY ACTUATORS WILL BE USED?5
HOW MANY SENSORS  WILL  BE USED? 5
DO YOU WANT COLOCATION?
YES
 ENTER ACTUATOR # & SENSOR #
 ?? 1,1
 ?? 3,3   CSDL ACTUATORS
 ?? 5,5
 ?? 7,7   PROOF-MASS DAMPER
 ?? 8,8   X,Y AXES, TOP VERTEX
 NEW ZETAS ?
YES
 ENTER MODE# AND DESIRED ZETA
 ?? 1,.12
 ?? 2,.12
 ?? 3,.12   <-
 ?? 4,.12
 ?? 5,.12
 ??
 CHANGE MODAL WEIGHTS?
YES
 ENTER MODE# AND NEW WEIGHT
 ?? 1,1
 ?? 2,2
 ?? 4,4
 ??
 CAR (DIAGONAL GAIN MATRIX)
  101 -6.82+00   303 -6.03+00   505 -5.83+00
 GAINS OK?       707 -7.12-01   808 -5.50-01
YES
```

Nominal Model

```
  OPEN-LOOP                    PREDICTED CLOSED-LOOP
   FREQUENCY   WEIGHT     FREQUENCY  TAU       ZETA    SENSITIVITIES
 1 2.14-01   1.00+00      2.15-01   6.0+00     .124    1.9+00 1.2-03
 2 2.65-01   2.00+00      2.67-01   5.0+00     .118    1.9+00 1.1-03
 3 4.60-01   1.00+00      4.62-01   3.9+00     .089    1.9+00 8.4-04
 4 4.71-01   4.00+00      4.73-01   3.0+00     .113    1.9+00 1.1-03
 5 5.41-01   1.00+00      5.46-01   2.1+00     .142    1.9+00 1.4-03
 6 6.69-01   0.00         6.81-01   1.3+00     .187    1.9+00 1.9-03
 7 7.42-01   0.00         7.52-01   1.3+00     .165    1.9+00 1.6-03
 8 7.57-01   0.00         7.66-01   1.3+00     .157    1.9+00 1.5-03
 9 1.36+00   0.00   <-    1.36+00   1.7+00     .067    1.9+00 6.2-04
10 1.47+00   0.00         1.47+00   2.0+00     .055    1.8+00 5.0-04
11 1.64+00   0.00         1.64+00   2.9+00     .033    1.7+00 2.8-04
12 2.05+00   0.00         2.05+00   9.1+00     .008    8.2-01 3.5-05
OK SO FAR?
YES
 *** MATRIX C STORED ON FILE 20

***** S,G & H WRITTEN ON FILE
```

7, 8 Inertial Dampers

ACTUAL

```
CLOSED-LOOP  SYSTEM'S ROOTS
MODE  IND  FREQUENCY   DAMPING
  1    1  2.1430-01   .124672
  2    1  2.6756-01   .117694
  3    1  4.7936-01   .076734
  4    1  4.9134-01   .116105
  5    1  5.5486-01   .119237
  6    1  6.7630-01   .322390
  7    1  7.0575-01   .068695
  8    1  7.2100-01   .179587
  9    1  1.3470+00   .069437
 10    1  1.4501+00   .050216
 11    1  1.6211+00   .030363
 12    1  2.0518+00   .008127
```

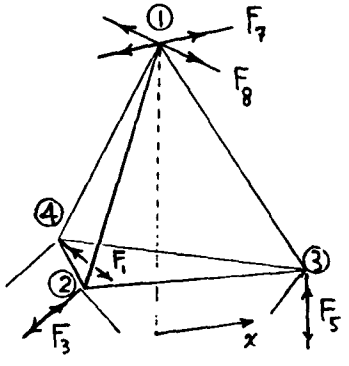

1, 3, 5 Member Dampers

```
*END
 *** GOOD-BYE .  LACSYS***
```

Fig. 7 Decentralized LAC Design (CSDL Example) – Design Procedure Illustration

Nominal Model

CLOSED-LOOP SYSTEM'S ROOTS

MODE	IND	FREQUENCY	DAMPING
1	1	2.1430-01	.124672
2	1	2.6756-01	.117694
3	1	4.7936-01	.076734
4	1	4.9134-01	.116105
5	1	5.5486-01	.119237
6	1	6.7630-01	.322390
7	1	7.0575-01	.068695
8	1	7.2100-01	.179587
9	1	1.3470+00	.069437
10	1	1.4501+00	.050216
11	1	1.6211+00	.030363
12	1	2.0518+00	.008127

Perturbed Model

CLOSED-LOOP SYSTEM'S ROOTS

MODE	IND	FREQUENCY	DAMPING
1	1	1.8651-01	.074401
2	1	2.3410-01	.070412
3	1	4.7938-01	.050130
4	1	5.8076-01	.089167
5	1	6.2327-01	.099579
6	1	8.4842-01	.261397
7	1	8.6348-01	.047423
8	1	8.9114-01	.147271
9	1	1.4149+00	.076658
10	1	1.6177+00	.047797
11	1	1.7170+00	.037068
12	1	2.2215+00	.006815

Nominal Model

P 40
**** NOMINAL MODEL ****
5 DECENTRALIZED CONTROLLERS
*** TRANSIENT RESPONSE ***

TIME	LOSX	LOSY
.000	1.679-04	1.621-04
19.000	3.631-05	-1.752-05
19.000	3.631-05	-1.752-05
19.200	6.304-05	-1.750-05
19.400	8.151-05	-1.750-05
19.600	9.167-05	-1.662-05
19.800	9.257-05	-1.517-05
20.000	8.466-05	-1.335-05
20.200	7.028-05	-1.086-05
20.400	5.007-05	-8.748-06
20.600	2.714-05	-6.777-06
20.800	2.822-06	-5.619-06
21.000	-2.062-05	-5.143-06
21.200	-4.062-05	-4.674-06
21.400	-5.589-05	-3.920-06
21.600	-6.376-05	-1.508-06
21.800	-6.446-05	2.426-06
22.000	-5.788-05	7.998-06
22.200	-4.550-05	1.442-05
22.400	-3.015-05	2.011-05
22.600	-1.325-05	2.442-05
22.800	2.264-06	2.594-05
23.000	1.558-05	2.472-05
23.200	2.564-05	2.085-05
23.400	3.183-05	1.478-05
23.600	3.473-05	7.677-06
23.800	3.376-05	-1.273-07
24.000	3.015-05	-7.444-06
24.200	2.409-05	-1.394-05
24.400	1.643-05	-1.913-05
24.600	8.415-06	-2.250-05
24.800	1.279-07	-2.432-05
25.000	-6.991-06	-2.414-05

LISSA I 79JUL21 6 1

Perturbed Model

C / / / 40
*** PERTURBED MODEL ***
5 DECENTRALIZED CONTROLLERS
*** TRANSIENT RESPONSE ***

TIME	LOSX	LOSY
.000	3.053-04	1.886-04
19.000	1.610-04	1.432-04
19.000	1.610-04	1.432-04
19.200	3.310-05	1.363-04
19.400	-1.039-04	1.150-04
19.600	-2.382-04	8.324-05
19.800	-3.567-04	4.632-05
20.000	-4.426-04	1.307-05
20.200	-4.868-04	-1.124-05
20.400	-4.822-04	-2.175-05
20.600	-4.330-04	-1.963-05
20.800	-3.469-04	-7.335-06
21.000	-2.370-04	9.870-06
21.200	-1.172-04	2.676-05
21.400	4.893-07	3.950-05
21.600	1.049-04	4.470-05
21.800	1.916-04	4.277-05
22.000	2.563-04	3.384-05
22.200	3.010-04	2.131-05
22.400	3.253-04	6.591-06
22.600	3.306-04	-8.344-06
22.800	3.158-04	-2.369-05
23.000	2.799-04	-4.014-05
23.200	2.237-04	-5.784-05
23.400	1.489-04	-7.703-05
23.600	6.240-05	-9.524-05
23.800	-2.936-05	-1.107-04
24.000	-1.155-04	-1.194-04
24.200	-1.881-04	-1.191-04
24.400	-2.387-04	-1.072-04
24.600	-2.631-04	-8.350-05
24.800	-2.610-04	-4.948-05
25.000	-2.351-04	-8.176-06

LISSA I 79JUL21 6 2

Fig. 8 Decentralized Controllers – LOS Transient Response Evaluation

5.1.5 Generalized Collocated Control Design

The CSDL structure is described analytically by

$$\dot{x} = \begin{bmatrix} 0 & I_n \\ -A_o & 0 \end{bmatrix} x + \begin{bmatrix} 0 \\ B_o \end{bmatrix} u$$

where

A_o = diag (1.8, 2.7, 8.36, 8.75, 11.5, 17.7, 2.17, 22.6, 72.9, 85.6, 106, 167)

$$B_o = \begin{bmatrix} -0.023 & -0.067 & -0.439 \\ -0.112 & 0.017 & 0.069 \\ -0.077 & 0.271 & 0.046 \\ 0.189 & -0.050 & -0.249 \\ 0.156 & -0.049 & 0.351 \\ -0.289 & 0.289 & -0.289 \\ -0.320 & -0.369 & -0.049 \\ 0.365 & 0.299 & -0.069 \\ -0.229 & 0.250 & 0.231 \\ 0.167 & -0.150 & -0.317 \\ -0.145 & 0.146 & -0.220 \\ 0.025 & -0.013 & 0.114 \end{bmatrix}$$

The matrix Q_o to be used in the design procedure outlined above will be taken as a diagonal 12 x 12 matrix.

In the following iterations the diagonal of the matrix Q_o will be selected. Using the design procedure outlined in 4.2, Q and K will be found and, also, the resulting closed-loop eigenvalue system.

High Authority Control Design

In the high authority controller selection the following weighting matrices are selected

$$A(jW) = \Lambda$$

$$B(jW) = \text{Diag}\,[b_1(W^2 + W_1^2),\ b_2(W^2 + W_2^2).\ \ldots\ b_6(W^2 + W_6^2)]$$

A(jW) does not depend on the frequency. B(jW) can be factered as

$$B(jW) = \text{Diag}\,(-jW + W_1,\ -jW + W_2\ \ldots,\ -jW + W_6)\ x\ \text{Diag}\,(b_1,\ b_2\ \ldots,\ b_6)\ x\ \text{Diag}\,(jW + W_1,\ jW + W_2\ \ldots,\ jW + W_6)$$

If we define

$$\dot{U}_i + W_i\, U_i = Z_i$$

then

$$U^*\, B(jW)u = Z^T\, \text{Diag}\,(b_1,\ b_2\ \ldots\ b_6)Z$$

The control design problem is then described by the following set of equations.

$$\dot{x} = F_x + G_u \longrightarrow \text{16 Equations (8 modes)}$$

$$\dot{u}_i = W_i U_i + Z_i \longrightarrow \text{16 Equations}$$

Cost Functional

$$x^T \Lambda x + Z^T R Z$$

$$R = \text{Diag } (b_1, b_2 \ldots b_6)$$

Control Law

$$Z = C_1 \hat{x} + C_2 u$$

Filter

$$\dot{\hat{x}} = F\hat{x} + Gu + K (y - H\hat{x})$$

The following weighting functions were used with six actuators and six sensors (collocated system).

State Weighting = Diag (0.5, 0.5, 0.5, 0.5, 0.1, 0.1, 0.5, 0.5, 1.0, 1.0, 6* 0.001)

Modes in which 10% damping Ratio is desired

Control Weighting = Diag (0.01, 0.01, 0.01, 0.01, 0.01, 0.01)

All actuators are equally important

Process Noise = Diag (10, 10, 4, 4, 4, 0.4, 0.4, 0.0)

Meas Noise = Unity Matrix

Shaping Frequencies = (3.1, 3.2, 3.3, 3.4, 3.5, 3.6) Rad/Sec

Closed loop damping ratio for the nominal control design and evaluation modes are shown in Table 1 . Note the excellent behavior of high frequency modes not considered in control design model. Table 2 shows results on the perturbed model.

The control design procedure was repeated with the first three actuators and the last three sensors (noncolocated system). The following parameters were used in the design stage.

State Weighting = (4*1.0, 2*0.1, 4*1.0, 6*0.001)

Modes in which 10% damping Ratio is desired

Control Weighting = (3*0.01) First three actuators are used for control

Process Noise = (30, 30, 8, 8, 8, 0.8, 0.8, 0.0)

Meas Noise = Unity Matrix

Shaping Frequencies = (3.1, 3.2, 3.3) Rad/Sec

Table 3 compares the control design and evaluation models. Note again that the modes not considered in control design are not significantly effected. When the controller is used on the perturbed modes, satisfactory results are predicted (see Table 4).

Table 1

NOMINAL DAMPING RATIOS

FREQUENCY(Hz)	8 MODE MODEL		12 MODE MODEL	
	CONTROLLER	ESTIMATOR	CONTROLLER	ESTIMATOR
.214	.107	.141	.101	.146
.265	.123	.179	.113	.187
.460	.0528	.139	.0525	.136
.471	.127	.152	.115	.161
.541	.174	.161	.186	.149
.669	.00713	.0532	.00713	.0534
.742	.00652	.0532	.00652	.0471
.757	.0263	.005	.0262	.005
1.36	-	-	.00128	-
1.47	-	-	.00227	-
1.64	-	-	.00415	-
2.05	-	-	.00491	-

Table 2

COMPARISON OF NOMINAL AND PERTURBED CLOSED-LOOP SYSTEMS - COLOCATED CONTROL

NOMINAL			PERTURBED SYSTEM		
FREQUENCY (Hz)	CONTROLLER (ξ)	FILTER (ξ)	FREQUENCY (Hz)	CONTROLLER (ξ)	FILTER (ξ)
.214	.101	.147	.186	.0807	.183
.265	.113	.187	.233	.0734	.168
.460	.0525	.161	.472	.0311	.182
.471	.115	.137	.566	.0925	.133
.541	.109	.186	.612	.132	.173
.669	.00713	.0534	.820	.00517	.0324
.702	.00652	.0471	.903	.00327	.0577
.757	.0263	.005	.909	.0127	.005
1.36	.00128	-	1.42	.00101	-
1.47	.00227	-	1.64	.00479	-
1.64	.00415	-	1.71	.00468	-
2.05	.00491	-	2.22	.00213	-

Table 3

NOMINAL DAMPING RATIOS NONCOLOCATED DESIGN

FREQUENCY (Hz)	8 MODE MODEL		12 MODE MODEL	
	CONTROLLER	FILTER	CONTROLLER	FILTER
.214	.109	.173	.110	.173
.265	.125	.216	.124	.217
.460	.033	.101	.0332	.0987
.471	.126	.167	.139	.155
.541	.125	.158	.118	.163
.669	.00604	.0454	.00603	.0450
.742	.00550	.0462	.00550	.0462
.757	.0192	.005	.0193	.005
1.36	-	-	.00596	-
1.47	-	-	.00407	-
1.64	-	-	.00443	-
2.05	-	-	.00498	-

Table 4

COMPARISON OF NOMINAL AND PERTURBED CLOSED-LOOP SYSTEMS - NONCOLOCATED CONTROL

NOMINAL			PERTURBED SYSTEM		
FREQUENCY (Hz)	CONTROLLER (ξ)	FILTER (ξ)	FREQUENCY (Hz)	CONTROLLER (ξ)	FILTER (ξ)
.214	.110	.173	.186	.132	.154
.265	.124	.217	.233	.121	.173
.460	.0332	.0987	.472	.0118	.113
.471	.139	.154	.566	.142	.133
.541	.118	.164	.612	.108	.152
.669	.00603	.0119	.820	.00473	.0211
.742	.00550	.0462	.903	.00517	.0337
.757	.0193	.005	.909	.0073	.005
1.36	.00596	-	1.42	.00301	-
1.47	.00447	-	1.64	.00738	-
1.61	.00443	-	1.74	.00632	-
2.05	.00498	-	2.22	.00399	-

5.1.6 Modal Cost Analysis (MCA) Results for the CSDL Example

Here we ask for additional insight into the MCA (see Ref 1, Sec 4.2.4) methods by solving a standard optimal control problem with two different reduced models: Model S_3 is the 16th order model obtained by keeping the 8 lowest frequency modes; Model S_4 is the 16th order model obtained by keeping the 8 modes with the largest open loop modal cost. The nominal evaluation model is of order 24 and has the form

$$\begin{aligned} \dot{x} &= Ax + Cu + w, \quad \mathcal{E}\left|ww^T\right| = \left|X(0)x^T(0)\right| \\ y &= Px \qquad \text{line of sight errors at tip} \\ z &= Mx \qquad \text{displacement and rate measurements in legs} \end{aligned} \tag{1}$$

The quadratic cost for this problem is defined by

$$y^TQy = \underbrace{\eta_7^2 + \eta_8^2}_{\text{LOS Error}} + \underbrace{100\left(\eta_7^2 + \eta_8^2\right)}_{\substack{\text{Adds Damping} \\ \text{to LOS} \\ \text{Regulation}}}$$

The open loop modal costs V_{c_i} are defined by

$$V = \lim_{t \to \infty} y^TQy = \sum_{i=1}^{12} V_{c_i}$$

$$V_{c_i} = \frac{\theta_\alpha^T Q \theta_\alpha}{4\zeta_\alpha\omega_\alpha^3},$$

where θ_α are modal amplitudes and ω_α are modal frequencies.

Figure 1 shows the resulting modal costs for each mode. On the vertical scale the frequencies of the modes are shown. Thus, the eight modes contained in the design model S_3 lie below the dashed horizontal line. The eight modes contained

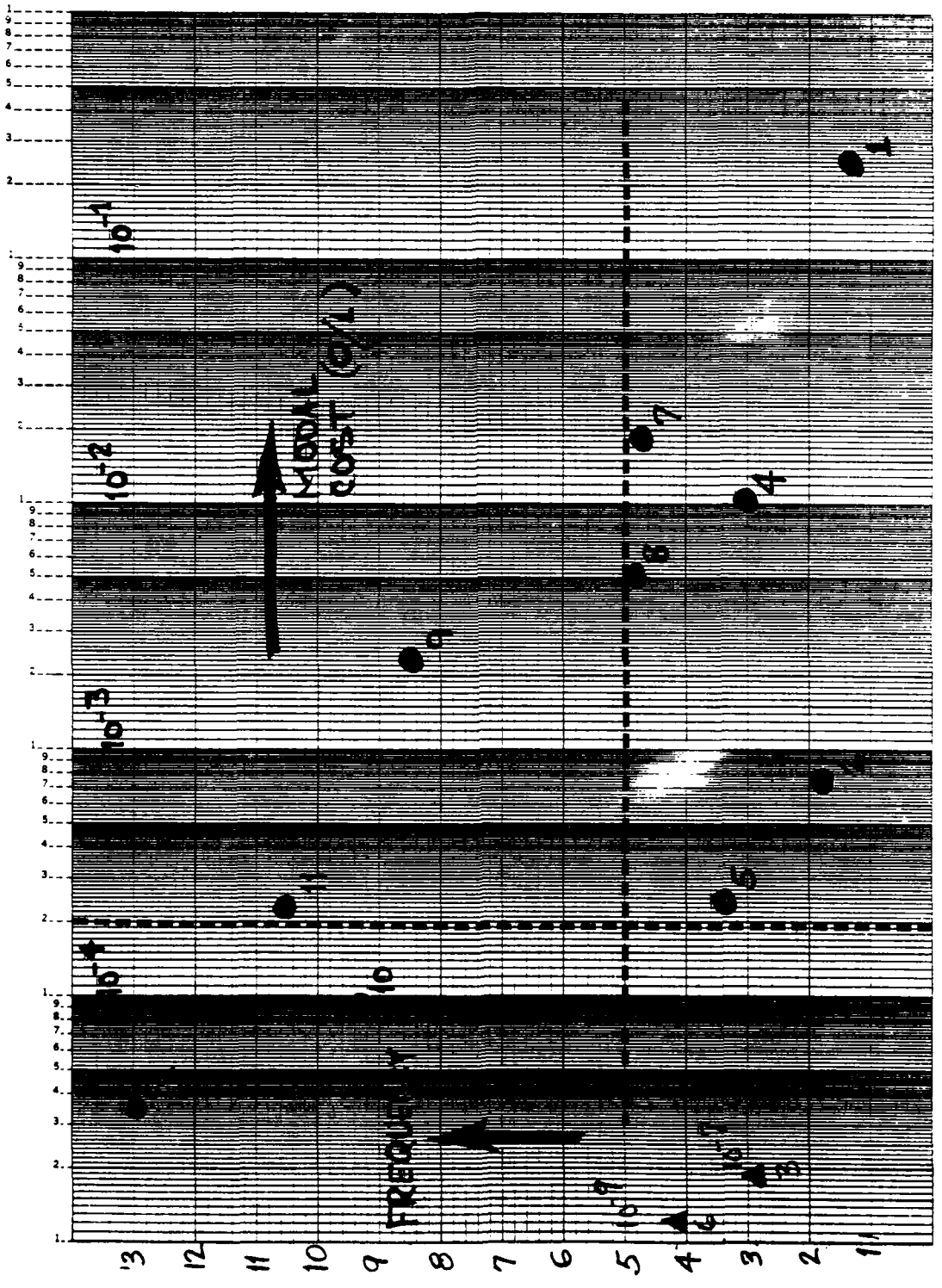

Fig. 1 Modal Costs, CSDL Example

in the design model S_4 lie to the right of the vertical dashed line. The modes in common to both models are 1, 2, 4, 5, 7. 8. Modal cost analysis indicates modes 3 and 6 are least significant among all modes, while modes 3 and 6 rank among the 8 most significant in the "dominant mode" model S_3. Table 1 shows that the damping added to each optimal design has approximately the same magnitude but is distributed differently among the modes. The MCA design selected modes 9 and 11 for additional damping, while the dominant mode design (with model S_3) attempted to add damping to modes 3 and 6. The control effort was approximately the same for both designs but the line of sight regulation was written better by 37 percent with the MCA design.

The results using MCA should be even better than the above results by using closed-loop modal cost analysis. Without such additional results, however, we can at least say that open-loop MCA has potential in the reduction of large models (obtained from finite element programs) to lower order models, before any closed-loop analysis is done.

Table 1

CSDL EXAMPLE

Dominant Mode Model		MCA	
Use Optimal Control for S_3 to Drive S_1:		Use Optimal Control for S_4 to Drive S_1:	
Mode	Damping	Mode	Damping
1	0.29	1	0.29
2	0.34	2	0.35
3	0.03	3	0.005
4	0.08	4	0.08
5	0.11	5	0.11
6	0.005	6	0.005
7	0.08	7	0.08
8	0.05	8	0.05
9	0.005	9	0.05
10	0.005	10	0.005
11	0.005	11	0.04
12	0.005	12	0.005
$V = \mathcal{E}\left\{y^T Q y + u^T u\right\}$			
LOS Regulation:	8.84		6.46
Control Effort:	6.17		6.34

5.2 LBET SYSTEM

5.2.1 System Description

The LBET strawman system provides an ideal test platform for active vibration suppression. Although on-board disturbances (state noise) do not excessively perturb the attitude control system nor do structural modes fall within the attitude control bandwidth, suppression of vibration due to on-board state noise sources is essential to meet mission requirements. The system is diagramed in Fig. 1 along with candidate locations for proof-mass actuator systems used to increase closed-loop damping of structural modes. The selection of structural materials and design rationale are fully discussed in the LMSC ADOPT TASK E final report and will not be addressed here. Some typical low-frequency modes from the finite-element model are illustrated in Fig. 2.

For worst case values, system pointing and wave front errors for the unaugmented system are approximately two orders-of-magnitude greater than specification requirements. Furthermore, these values assume 1 percent structural damping in the first 20 modes. This assumption is generally untenable for Gr-Ep structural designs where experimental evidence indicates that 0.3 percent is more realistic.*

5.2.2 SAS Performance

The principal modal interaction with pointing performance is due to the tracker attachment to the spacecraft. Several locations for proof-mass damping actuators were tried, as shown in the system sketch, with the most successful being location 1 at the tracker. Participation of other modes in performance was down by at least a factor of 10 and increased damping in these modes did not significantly

*Measurement of modal structural damping is a controversial issue which will be addressed in the LMSC ACOSS phase 1A study.

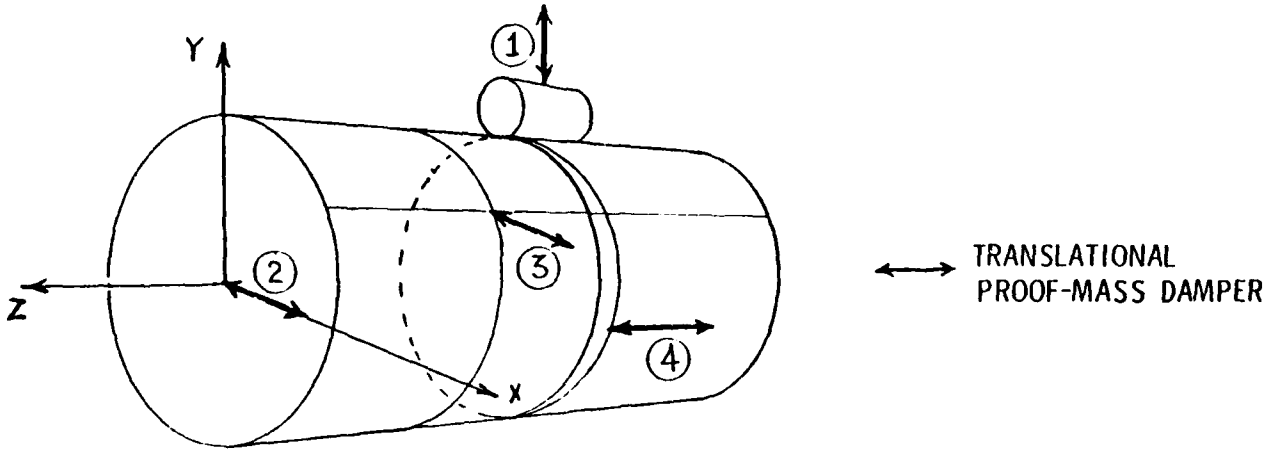

Fig. 1 LBET System – Proof-Mass Damper Locations and Control Axes

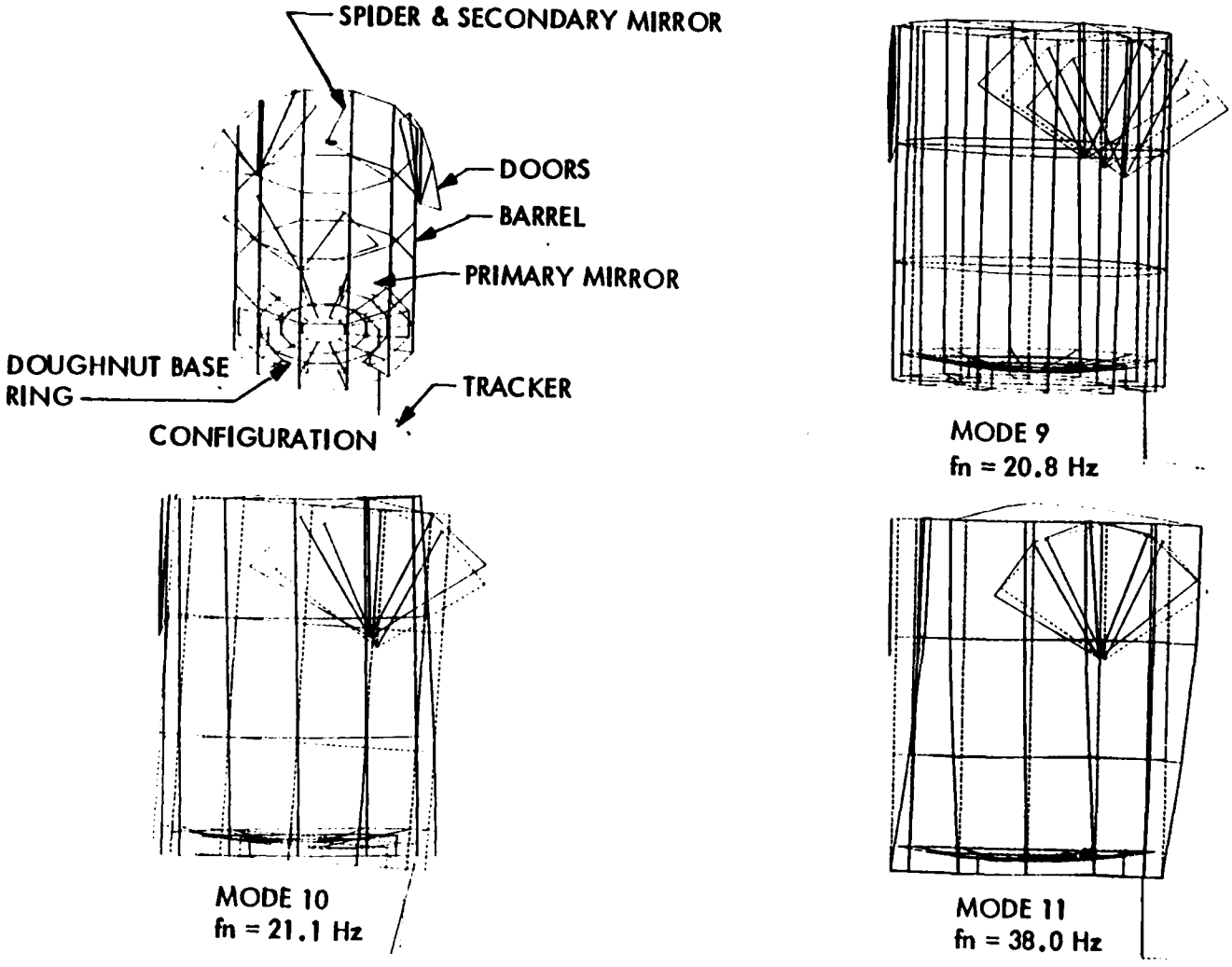

Fig. 2 LBET Baseline Dynamic Model and Dominant Modes

enhance performance. The open- and closed-loop damping performance obtained with a single collocated (decentralized) system is shown by the computer generated design in Table 1. Open-loop damping was assumed to be 0.5 percent and the significant modes are enclosed by the boxes. The synthesis procedure was asked to produce 10 percent in the two critical modes and 9 percent and 7.7 percent were produced as shown.

The principal advantages which accrue from this mechanization are relaxed system requirements and decreased sensitivity to knowledge of plant dynamics and disturbance sources.

Specifically, requirements to disable on-board noise sources, and to maintain high bandwidth figure control and steering mirrors may be eased considerably. Assumptions about passive structural damping no longer become so significant, tolerance to non-isolatable disturbances is high, and transient settling due to large, on-board disturbances becomes acceptable.

 (The reverse of this page is blank)

Table 2

LBET DECENTRALIZED LAC CONTROLLER- INERTIAL DAMPER ON TRACKER (X,Y AXES)

```
 OPEN-LOOP     SYSTEM'S ROOTS
 MODE  IND  FREQUENCY   DAMPING
   1    2   1.6034-01   .005000
   2    2   2.2374-01   .005000
   3    2   4.3743-01   .005000
   4    2   4.7953-01   .005000
   5    2   8.0601-01   .005000
   6    2   1.1361+00   .005000
   7    2   1.5624+01   .005000
   8    2   1.5729+01   .005000
   9    2   2.0796+01   .005000
  10    2   2.1051+01   .005000
  11    2   3.7955+01   .005000
  12    2   4.0773+01   .005000
  13    2   4.6672+01   .005000
  14    2   4.8039+01   .005000
  15    2   5.2344+01   .005000
  16    2   5.2501+01   .005000
  17    2   5.4159+01   .005000
  18    2   5.9595+01   .005000
  19    2   6.3249+01   .005000
  20    2   6.3538+01   .005000
 HOW MANY ACTUATORS WILL BE USED? 2
 HOW MANY SENSORS  WILL  BE USED? 2
 DO YOU WANT COLOCATION?
Y
 ENTER ACTUATOR # & SENSOR #
 ?? 1,1
 ?? 2,2
 NEW ZETAS ?
YES
 ENTER MODE# AND DESIRED ZETA
 ?? 9,.1
 ?? 10.,.1
```

```
 CLOSED-LOOP  SYSTEM'S ROOTS
 MODE  IND  FREQUENCY   DAMPING
   1    1   7.9247-03  1.000000
   2    1   1.7233-02  1.000000
   3    1   2.1404-01   .006603
   4    1   3.5630-01   .022732
   5    1   7.9626-01   .005516
   6    1   1.0198+00   .019744
   7    1   7.5298+00  1.000000
   8    1   1.5509+01  1.000000
   9    1   1.5612+01   .006768
  10    1   1.5725+01   .007156
  11    1   2.0141+01   .090614
  12    1   2.0251+01   .077703
  13    1   3.7956+01   .005271
  14    1   4.0799+01   .007431
  15    1   4.8001+01   .043115
  16    1   4.8039+01   .005000
  17    1   4.9575+01   .108298
  18    1   5.2501+01   .005009
  19    1   5.2602+01   .006493
  20    1   5.9595+01   .005015
  21    1   6.3249+01   .005001
  22    1   6.3532+01   .005075
*SET
*PRINT C
*GO


 ***C MATRIX IS  5X 5
  1, 1 -2.179+04  2, 2 -6.458+04
```

5.3 MM-WAVE SYSTEM

5.3.1 System Description

The MM-wave strawman system is a 30 m by 60 m curved platform originally proposed by CSDL. The configuration and moment of inertia properties are shown in Fig. 1. For convenience in modeling, the reflector back structure was modified to include the NASA-LRC octetruss configuration using Gr-Ep columns manufactured at LMSC. The new properties on the right of the figure represent the octetruss values. As shown in the accompanying Table 1, the octetruss reduces both back structure and feed support weight.

5.3.2 SAS Performance

To show SAS feasibility, the LASC synthesis procedure (see Section 4) was used to select feedback gains for actuators located by visually observing modal deflections to assess controllability. A two-axis gyro damper and a single proof-mass damper were installed on the reflector and a three-axis gyro damper was used to control the feed tower. These actuator locations are shown in Fig. 2 along with frequency and damping characteristics of the closed-loop system. The controls are all of the colocated decentralized low-authority type without consideration for bandwidth constraints. Moderate amounts of damping are introduced up to 20 Hz with the principal effects occurring in the low frequency modes below 1.6 Hz. In Figs. 3a and 3b the feed decenter transfer functions are compared for open- and closed-loop and it may be observed that peak responses are reduced by a factor of approximately 6 to 1.

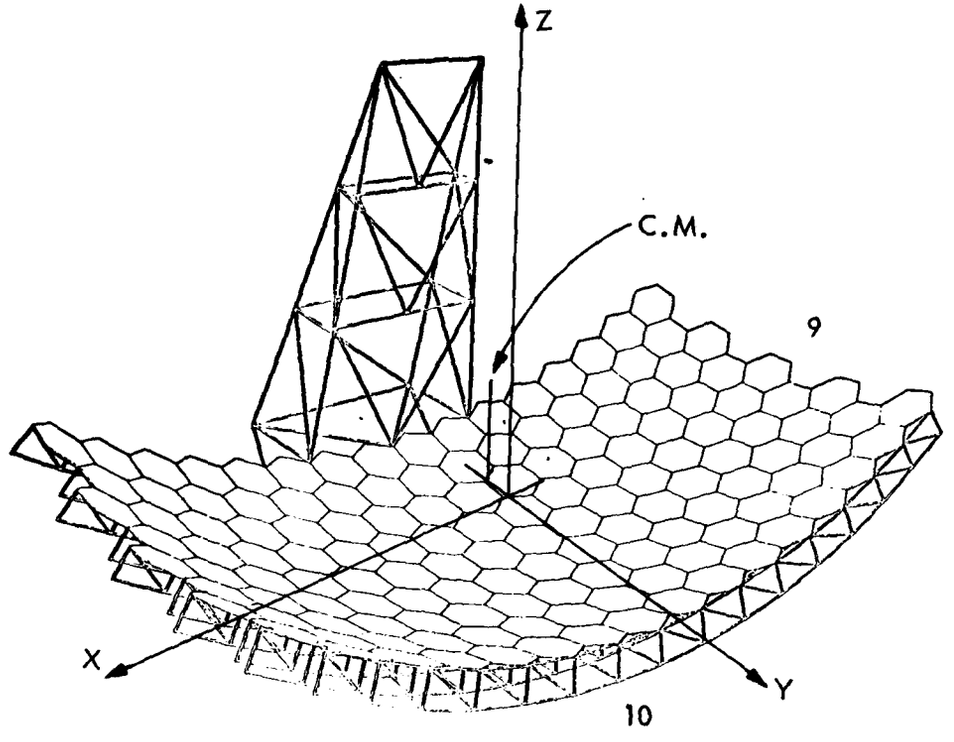

	ORIGINAL STRAWMAN DESIGN	NEW OCTETRUSS DESIGN
	TOTAL MASS	
M	= 17440 kg	11521 kg
	C.M. LOCATION	
X	= 0.0	0.0
Y	= 0.79 m	-3.231 m
Z	= 4.19 m	4.370 m
	INERTIAS ABOUT CENTER OF MASS	
IXX	= 2.137×10^6 kgm^2	4.221×10^6 kgm^2
IYY	= 5.550×10^6 kgm^2	1.583×10^6 kgm^2
IZZ	= 6.728×10^6 kgm^2	4.992×10^6 kgm^2

NOTE: ALTERED DATA REFLECTS RESULTS OF "REXBAT" MODEL AS CURRENTLY CONFIGURED

Fig. 1 mm-Wave Antenna Characteristics

Table 1

30 x 60 mm mm-WAVE ANTENNA MASS ALLOCATIONS

	STRAWMAN DESIGN (GIVEN)	OCTETRUSS STRUCTURE	
REFLECTOR PANELS	9,000 kg	9,000 kg	
BACKUP TRUSS	7,200 kg	2,018 kg	
FEED SUPPORT	940 kg	204 kg	
FEED EQUIPMENT	300 kg	300 kg	
	17,440 kg	11,522 kg	TOTALS

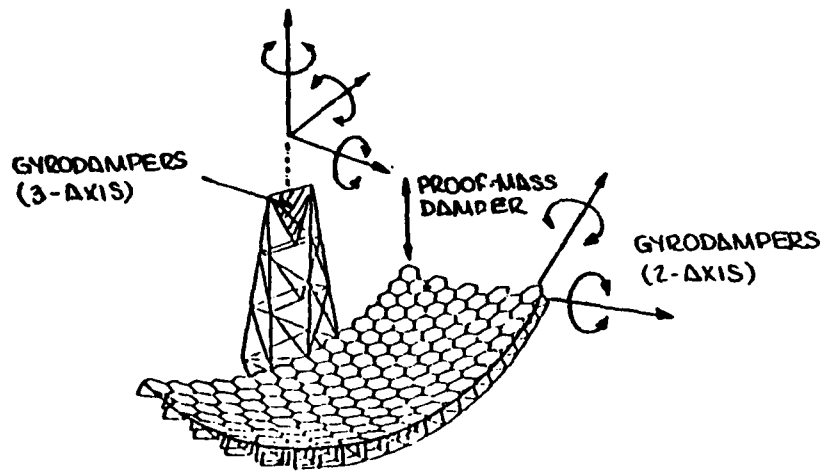

OPEN LOOP

SYSTEM'S ROOTS

ROOT	IND	FREQUENCY
1	2	2.4945-01
3	2	3.1194-01
5	2	5.5561-01
7	2	1.0100+00
9	2	1.6945+00
11	2	2.9754+00
13	2	3.1104+00
15	2	3.4119+00
17	2	5.1903+00
19	2	6.2370+00
21	2	1.8815+01
23	2	1.9443+01
25	2	1.9792+01
27	2	1.9953+01
29	2	2.0576+01

CLOSED-LOOP

*** ROOTS OF THE CLOSED-LOOP SYSTEM ***

ROOT	IND	FREQUENCY	DAMPING	TIME CONST.	REAL PART	IMAGINARY
1	1	3.1227-01	.021399	2.3818+01	-4.1985-02	1.9616+00
3	1	3.4367-01	.318345	1.4547+00	-6.8742-01	2.0470+00
5	1	4.2096-01	.795402	4.7533-01	-2.1038+00	1.6031+00
7	1	9.9956-01	.188701	8.4379-01	-1.1851+00	6.1676+00
9	1	1.6958+00	.051208	1.8328+00	-5.4562-01	1.0641+01
11	1	2.9668+00	.087360	6.1406-01	-1.6285+00	1.8570+01
13	1	3.1006+00	.058203	8.8192-01	-1.1339+00	1.9448+01
15	1	3.4147+00	.043342	1.0754+00	-9.2992-01	2.1435+01
17	1	5.1738+00	.077666	3.9607-01	-2.5248+00	3.2410+01
19	1	6.1005+00	.045048	5.7913-01	-1.7267+00	3.8292+01
21	1	1.9028+01	.062217	1.3444-01	-7.4383+00	1.1932+02
23	1	1.9371+01	.018772	4.3768-01	-2.2848+00	1.2169+02
25	1	1.9680+01	.016782	4.8188-01	-2.0752+00	1.2364+02
27	1	1.9930+01	.020617	3.8734-01	-2.5817+00	1.2520+02
29	1	2.0483+01	.016803	4.6240-01	-2.1625+00	1.2868+02

Fig. 2 mm-Wave Antenna (12 Modes) - LASC Actuators and Performance

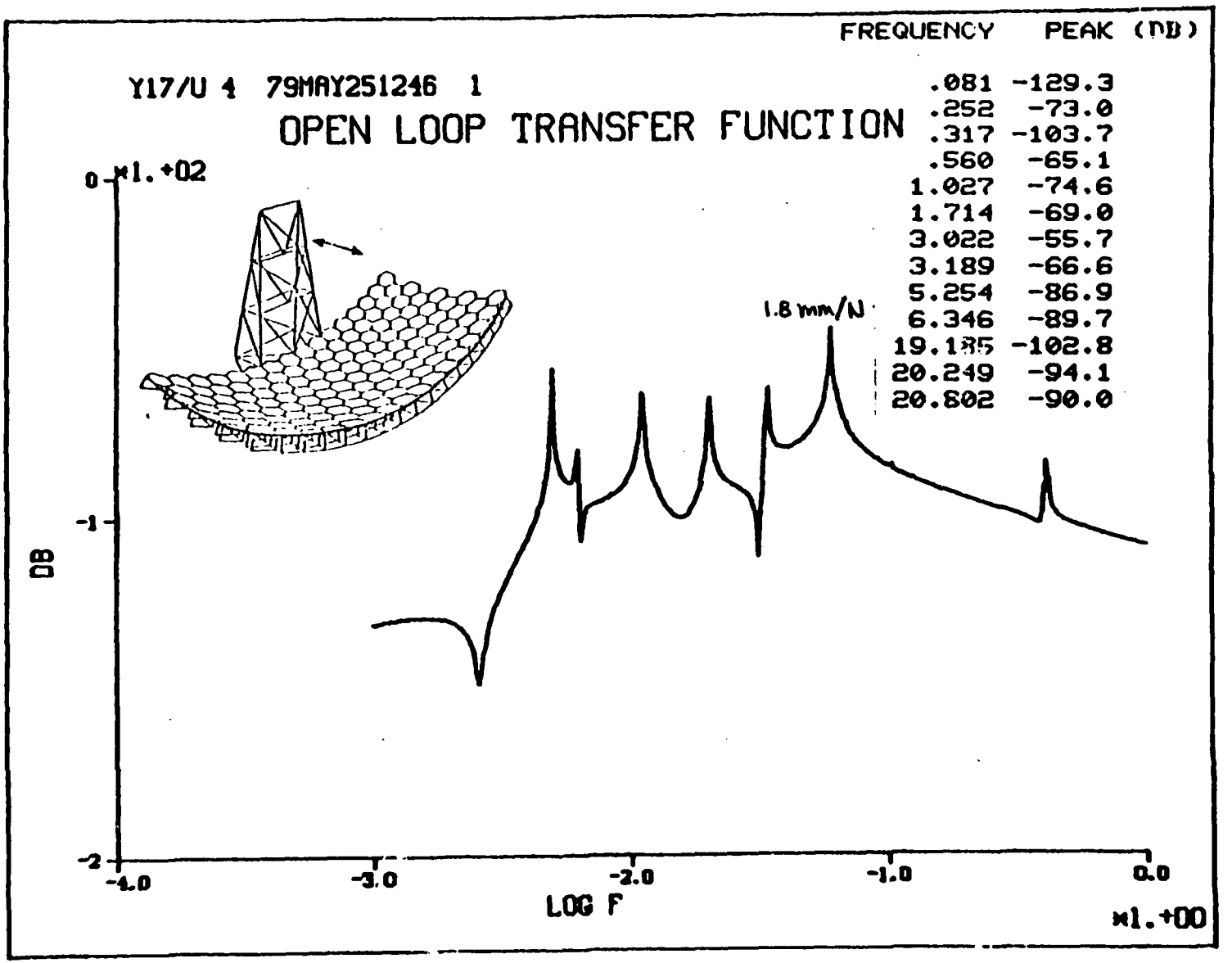

Fig. 3a mm-Wave Antenna (12 Modes) - Feed Decenter

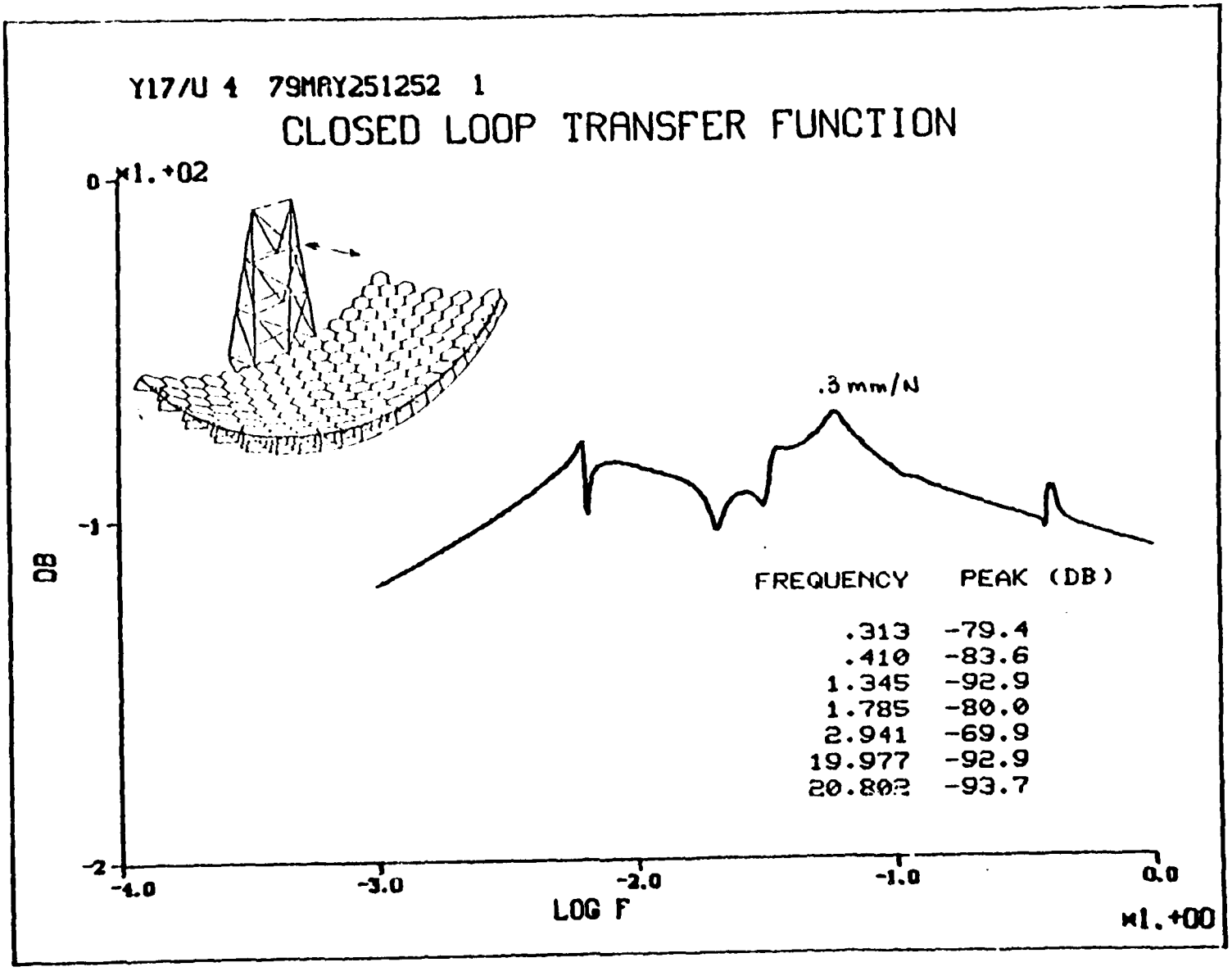

Fig. 3b mm-Wave Antenna (12 Modes) - Feed Decenter

5.4 HALO/WALRUS SYSTEM

5.4.1 System Description

The HALO (High Altitude Large Optics) System examined for stability augmentation was the HUGHES WALRUS (Wide-Angle Large Reflecting Unobscured System). The optical characteristics and required element tolerances are described in various HALO documents contained in the Riverside Research Library and in the LMSC proposal for An Actively Controlled Structure Program, Vol 1, 17 April 78, LMSC-L034034(S). The discussions here will be restricted to the feasibility and potential performance of active stability augmentation using only low-authority control. The basic configuration, shown in Fig. 1, uses an LMSC designed structure in lieu of the cable support system used on the original Hughes Configuration. The attitude control system, cryo-coolers, etc., are housed in the so-called "dirty box" which is not actively isolated but rather attached directly to the optical structure as shown. The mirrors are supported by pyramid structures which were weight optimized as shown in Fig. 2. The overall mass properties are reproduced in Table 1.

5.4.2 SAS Performance

A coarse finite-element model, illustrated in Fig. 3, was used to examine basic feasibility. Decentralized low-authority control (with no bandwidth constraints) of the fundamental low-frequency structural modes was attempted while higher frequency "mirror modes" were left uncontrolled. For a practical design, a more refined model is necessary and actuator/sensor bandwidth limitations would have to be included to insure that feedback compensation and passive low-authority actuator damping were appropriately selected. The actuator locations, characteristics and closed-loop damping performance are given in Fig. 4. The modes between 1 Hz and 16 Hz all exhibit damping greater than 10% except for a few uncontrolled modes; this is accomplished by 8 proof-mass systems and 1 (rotational) gyro damper. Individual mirror modes, all above 24 Hz, exhibited less than 1% damping, as expected, since these modes were uncontrollable by the actuators

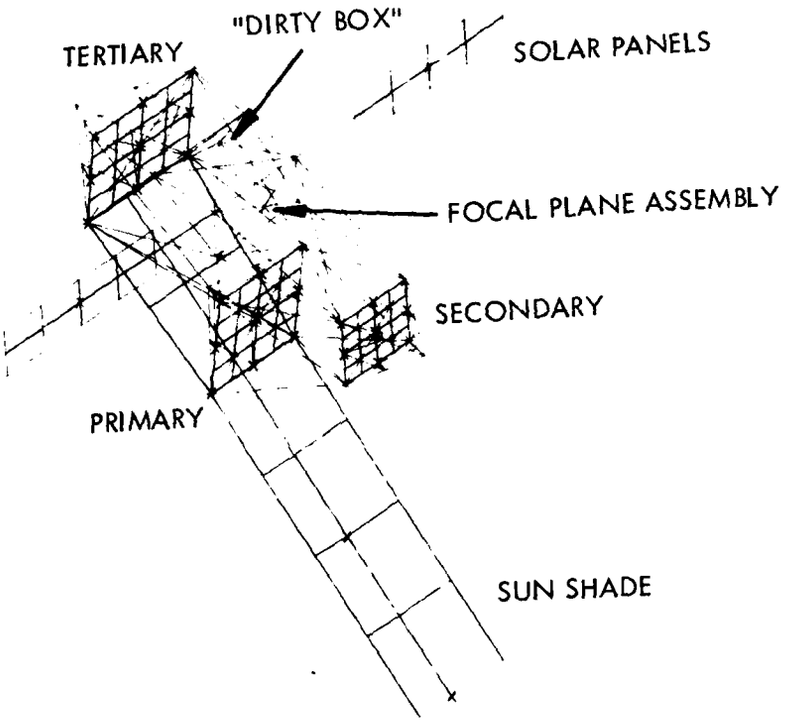

Fig. 2 Halo/Walrus Structural Model (General View)

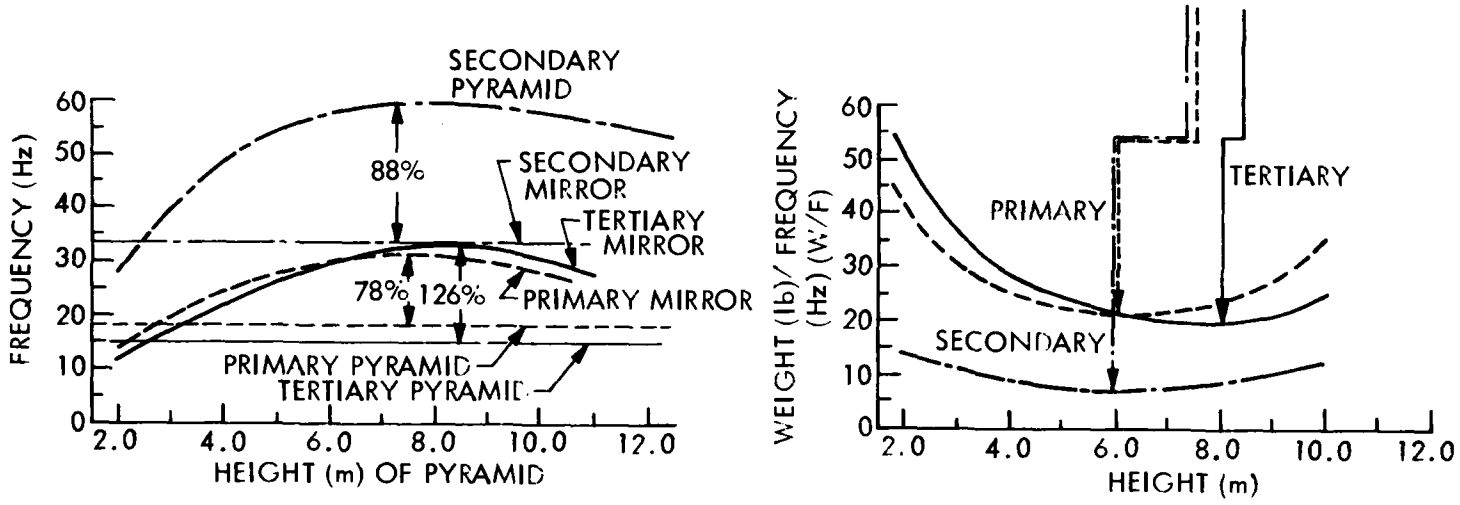

Fig. 2 Pyramid Structural Optimization

Table 1

HALO/WALRUS WEIGHTS (MASSES)

PARTITION NUMBER	STRUCTURE	WEIGHT (MASS) - lb (kg)		
		TOTAL =	NON-STRUCTURAL	+ STRUCTURAL
9	SOLAR DEVICES (ARRAYS & SHIELD)	3,080. (1,400.)	3,080. (1,400.)	0 (0)
8	TERTIARY MIRROR	7,260. (3,300.)	7,260. (3,300.)	0 (0)
7	SECONDARY MIRROR	3,520. (1,600.)	3,520. (1,600.)	0 (0)
6	PRIMARY MIRROR	6,820. (3,100.)	6,820. (3,100.)	0 (0)
5	TERTIARY PYRAMID	737. (335.)	0 (0)	737. (335.)
4	SECONDARY PYRAMID	497. (226.)	0 (0)	497. (226.)
3	PRIMARY PYRAMID	660. (300.)	0 (0)	660 (300.)
2	BACKUP STRUCTURE	12,814. (5,825.)	10,560. (4,800.)	2,254. (1,025.)
1	TOTAL STRUCTURE	35,388. (16,086.)	31,240. (14,200)	4,148. (1,886.) INCLUDES 20% CONTINGENCY FOR JOINTS

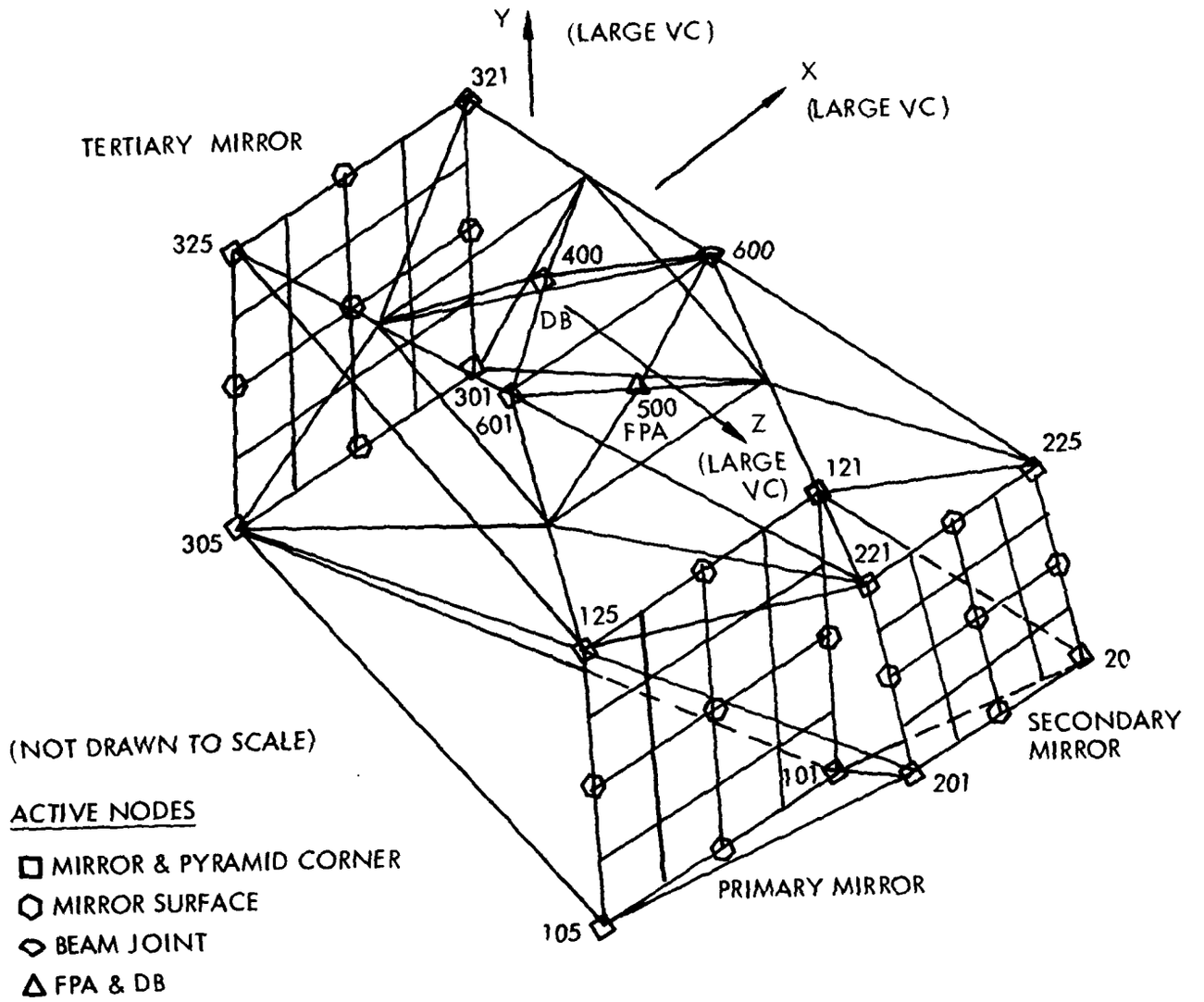

Fig. 3 Halo Model

selected. Reversal of high q structural resonances in this case eases significantly any requirements to isolate vibration sources on-board the spacecraft and permits greater freedom in synthesis of the attitude control system.

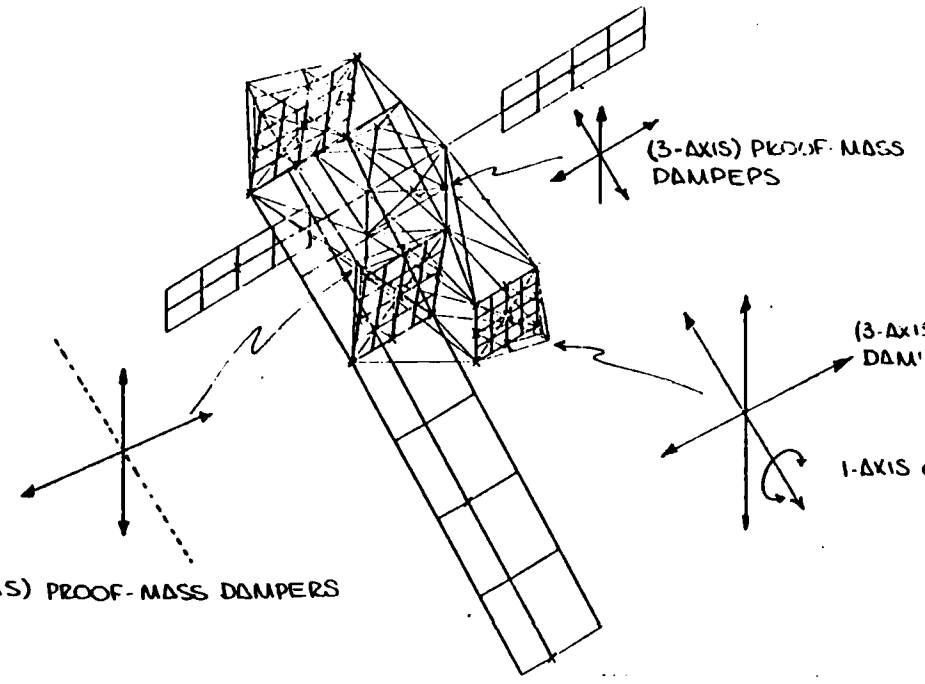

NOTE: ONLY FIRST 14 FLEXIBLE MODES SHOWN ON THIS CHART.

GAINS

PROOF-MASS: 10 N PER mm/SEC

GYRODAMPER: 10 Nm PER MRAD/SEC

*** ROOTS OF THE CLOSED-LOOP SYSTEM ***

ROOT	IND	FREQUENCY	DAMPING	TIME CONST.	REAL PART	IMAGINARY
13	2	3.9930-01	.016167	2.4654+01	-4.0561-02	2.5086+00
15	2	1.1702+00	.109328	1.2440+00	-8.0385-01	7.3085+00
17	2	1.2012+00	.128759	1.0290+00	-9.7179-01	7.4846+00
19	2	1.2170+00	.366890	3.5645-01	-2.8054+00	7.1133+00
21	2	1.6921+00	.125631	7.4868-01	-1.3357+00	1.0548+01
23	2	1.7716+00	.219156	4.0991-01	-2.4395+00	1.0861+01
25	2	2.0086+00	.344982	2.2969-01	-4.3537+00	1.1845+01
27	2	4.5440+00	.031951	1.0962+00	-9.1223-01	2.8537+01
29	2	9.0733+00	.068502	2.5606-01	-3.9053+00	5.6876+01
31	2	1.1516+01	.214701	6.4344-02	-1.5541+01	7.0670+01
33	2	1.1739+01	.025266	5.3660-01	-1.8636+00	7.3736+01
35	2	1.1968+01	.035254	3.7722-01	-2.6510+00	7.5150+01
37	2	1.5559+01	.233192	4.3866-02	-2.2797+01	9.5033+01
39	2	1.6130+01	.017116	5.7313-01	-1.7448+00	1.0133+02

Fig. 4 Halo/Walrus (30 Modes) - LASC Actuators and Performance

5.5 TILTING TELESCOPE SYSTEM (ADOPT-12)

The structural description of the system considered in this section is given in Fig. 1. The modes of this system are shown in Fig. 2. The model used in the control design has 26 states, 13 controls, and 26 measurements; these are detailed as follows:

26 State Model
- 2 rigid body modes
- 11 structural modes

13 Controls
- 12 surface controllers
- 3 back body torquer

26 Measurements
- 12 surface position 96 independent)
- 12 surface velocity (6 independent)
- 1 relative angle
- 1 average orientation angle

1 Disturbance Source
- Lateral force on back body

The control design for this system was concerned with the following problems:

1. Reduced-order model derivation
2. Comparison of LQG and frequency shaped cost functional design method
3. Filter design

In the derivation of the reduced-order model desired states are retained. In addtion the reduced order model has the same poles as the high order model. Due to symmetry, duplicate sensors/actuators can be eliminated in the control design based on the reduced model. Details of the reduction process are shown in Fig. 3. The effect of the states retained in the reduced model on the zero location is shown in Fig. 4.

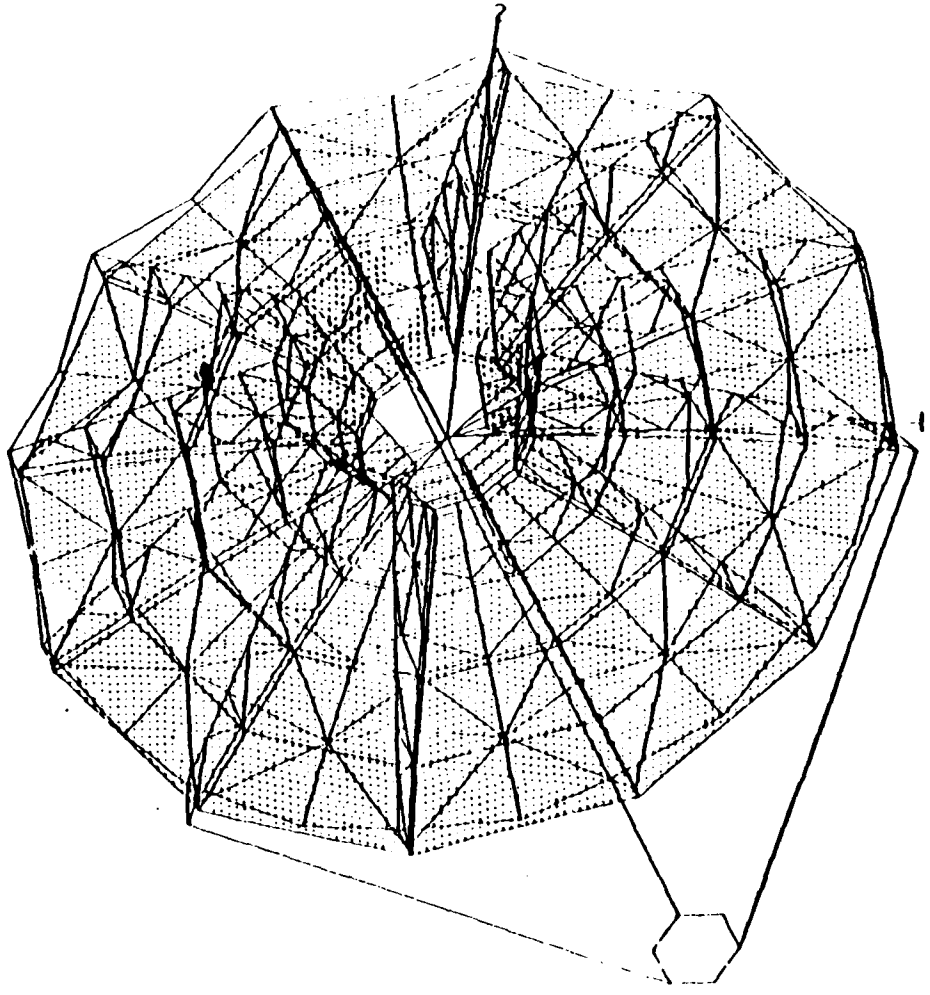

Fig. 1 Tilting Telescope Final Structural Design
Primary Mirror Support Structure

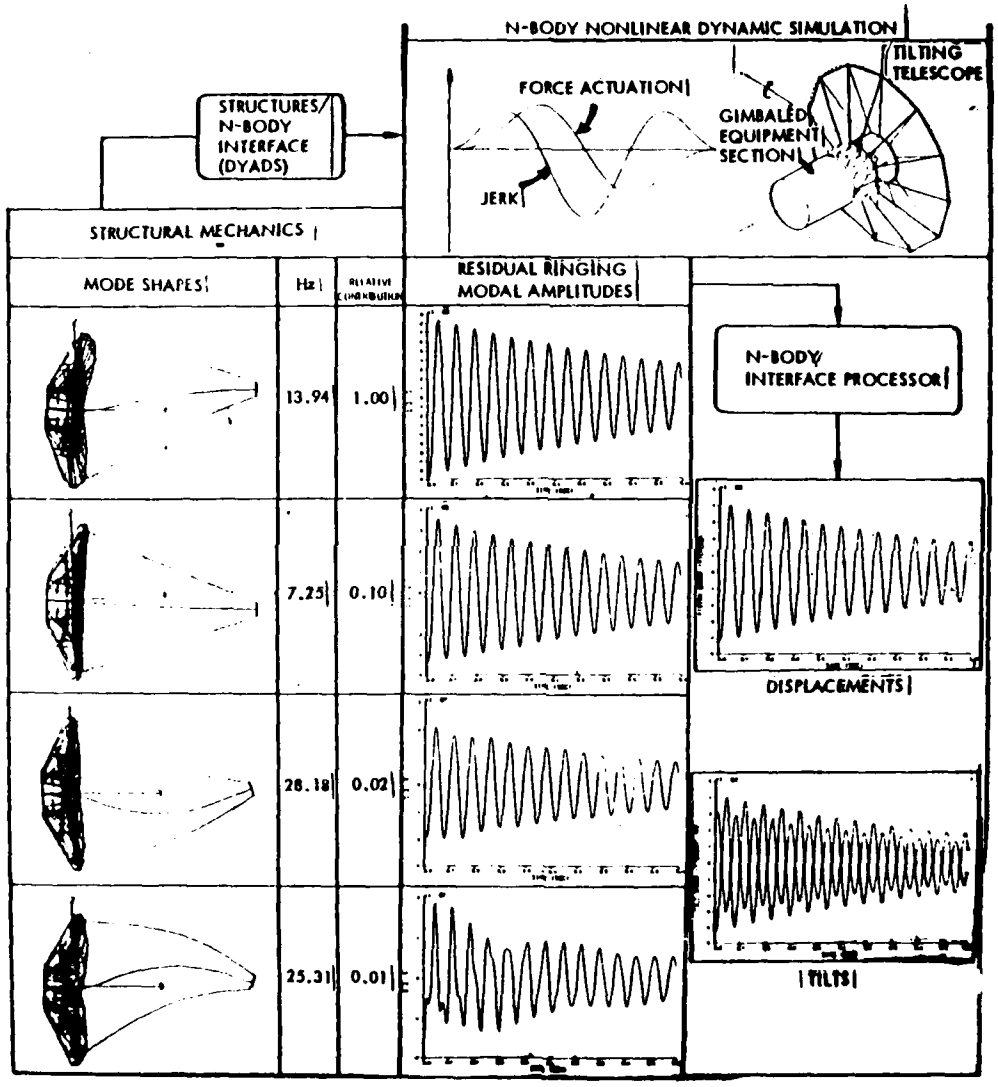

Fig. 2 Selected System Modes

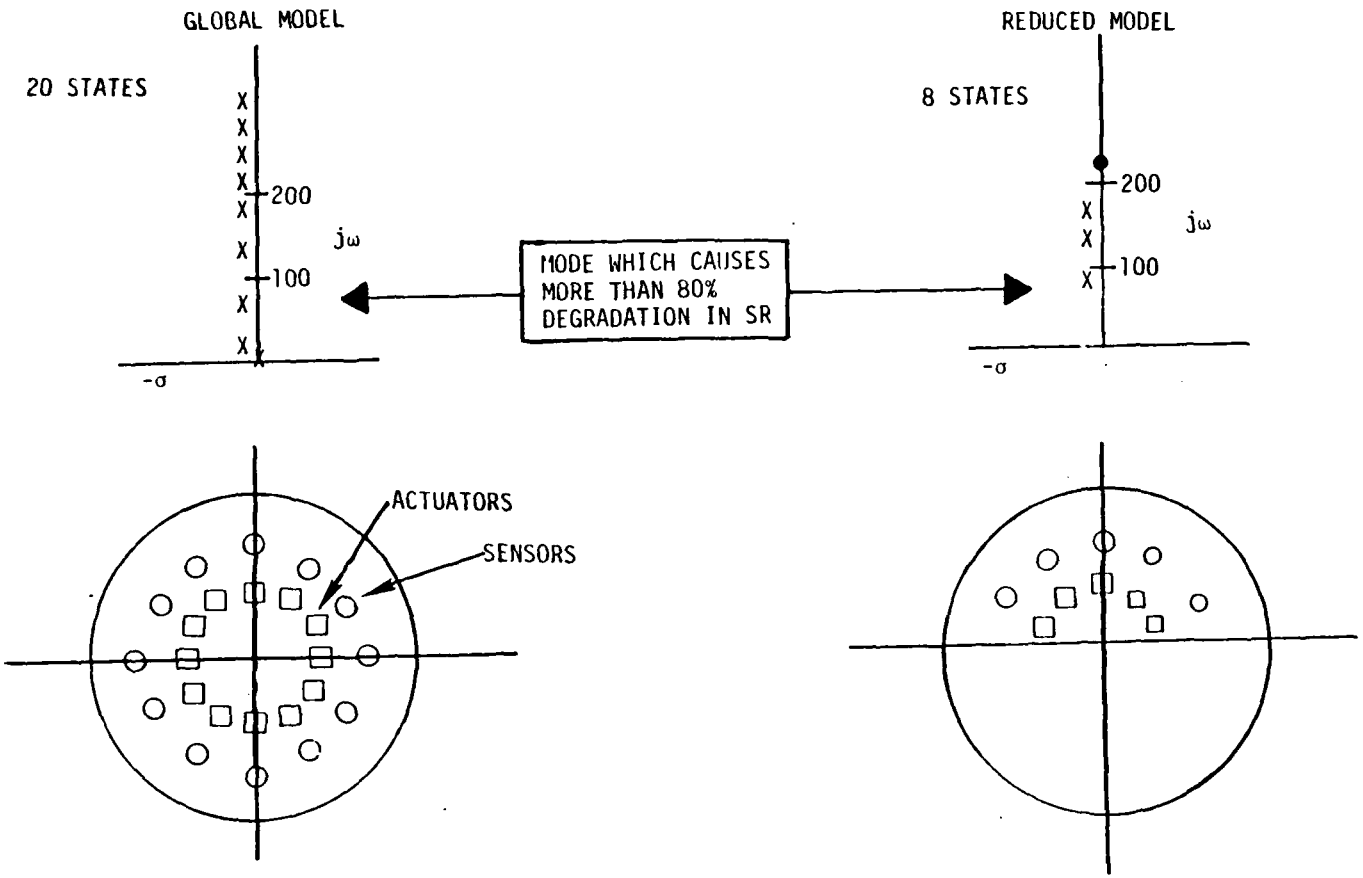

- REDUCED MODEL HAS DESIRED POLES SAME AS HIGH ORDER MODEL
- DESIRED STATES ARE RETAINED
- DUPLICATE SENSORS/ACTUATORS ARE ELIMINATED IN CONTROL DESIGN

Fig. 3 Tilting Telescope System Definition

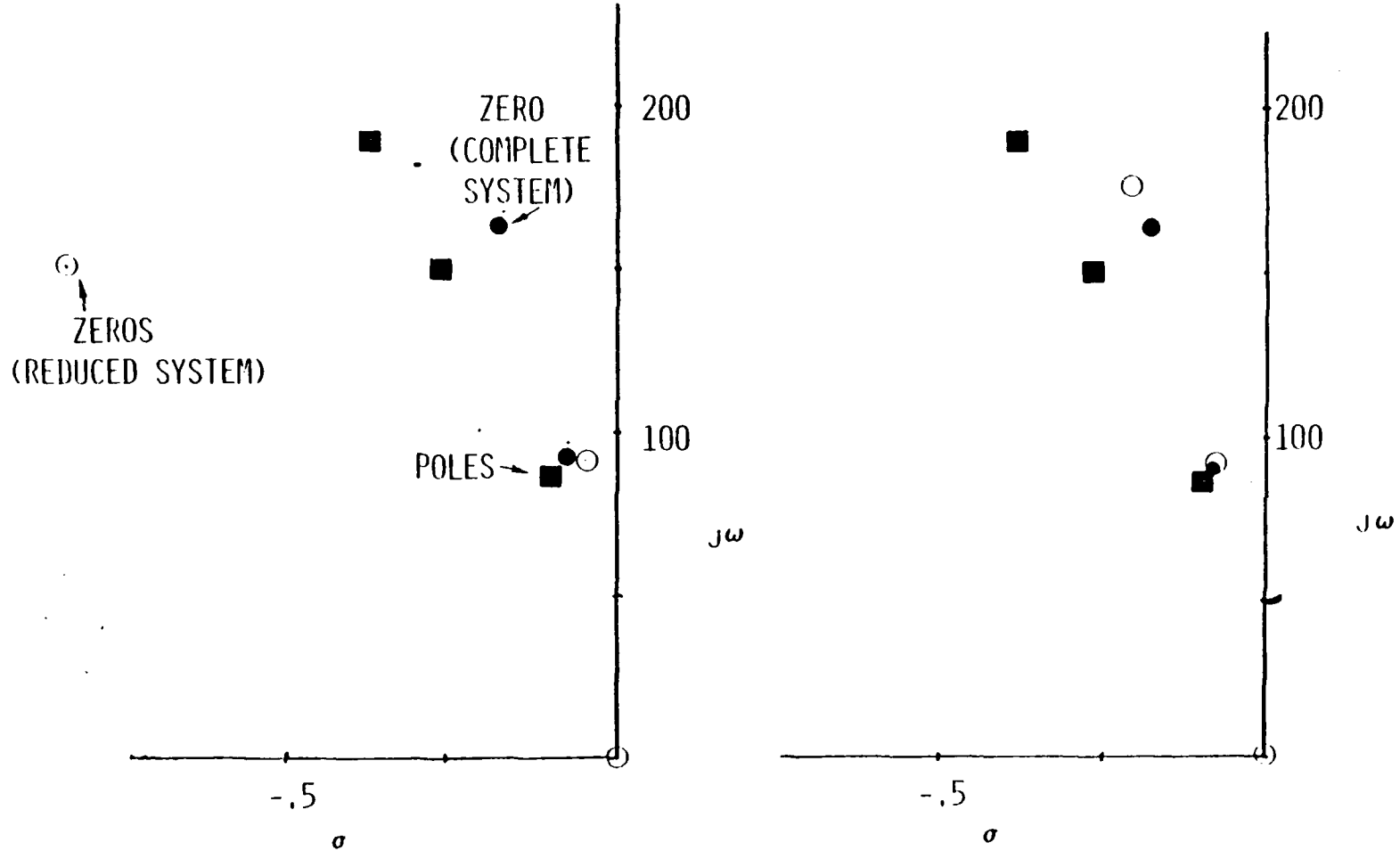

Fig. 4 Effect of State Selection on Reduced System Zero Location

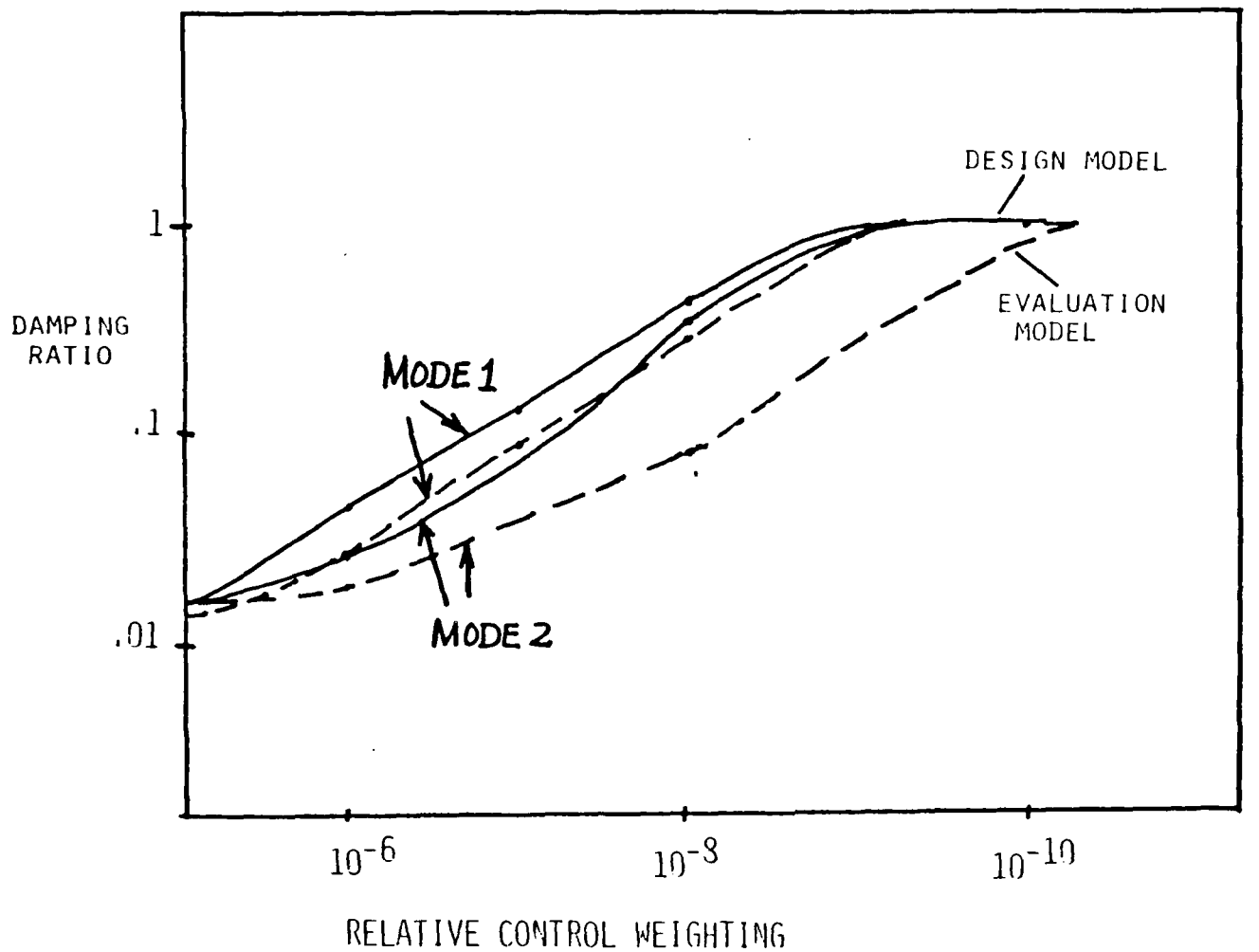

Fig. 5 Damping Ratio of Controlled Modes (LQG Design)

The next stage in the design was the comparison between frequency shaped cost functionals and the standard LQG design method. The basis of comparison was taken as the damping ratios of various modes. The results are given in Figs. 5 through 8.

An important issue in the application of frequency shaped cost functionals is the choice of these functionals. The choice must be adapted to the particular situation at hand.

As mentioned before, a problem associated with large space structures is that of truncated modes. An approach toward dealing with this problem is offered through the application of frequency shaped cost functionals. The weighting on the control is increased at high frequency to account for the model invalidity in that regim, see Fig. 9, leaving the state weighting constant the effect of control weighting can be observed. In Fig. 10 the change in damping raio as a function of control weighting is depicted.

The last topic considered for this structure was that of filter design. Filter must be designed for good transient as well as rms response. If only rms response is considered poor measurement responses may result (fast poles).

Additional requirements are:

- Very little change in the filter closed-loop poles based on original power spectral density of the noise
- Noise matrix scaled to improve system behavior
- Requires reduction of compensator for better design

Figures 11 and 12 illustrate these points.

Figure 13 shows the rms response in steady state. As the control weighting decreases (a) the damping ratio increases, (b) the rms furface deflection improves (i.e., becomes smaller), (c) the difference between low order and high order model increases, and (d) more actuator power is required. Note that this figure

does not include effects of actuator sensor noise. Those two effects could significantly degrade performance. Control force requirements are shown in Figs. 14 and 15. It can be observed that with decreased control weighting associated with increased damping ratio, the actuator requirements are more severe.

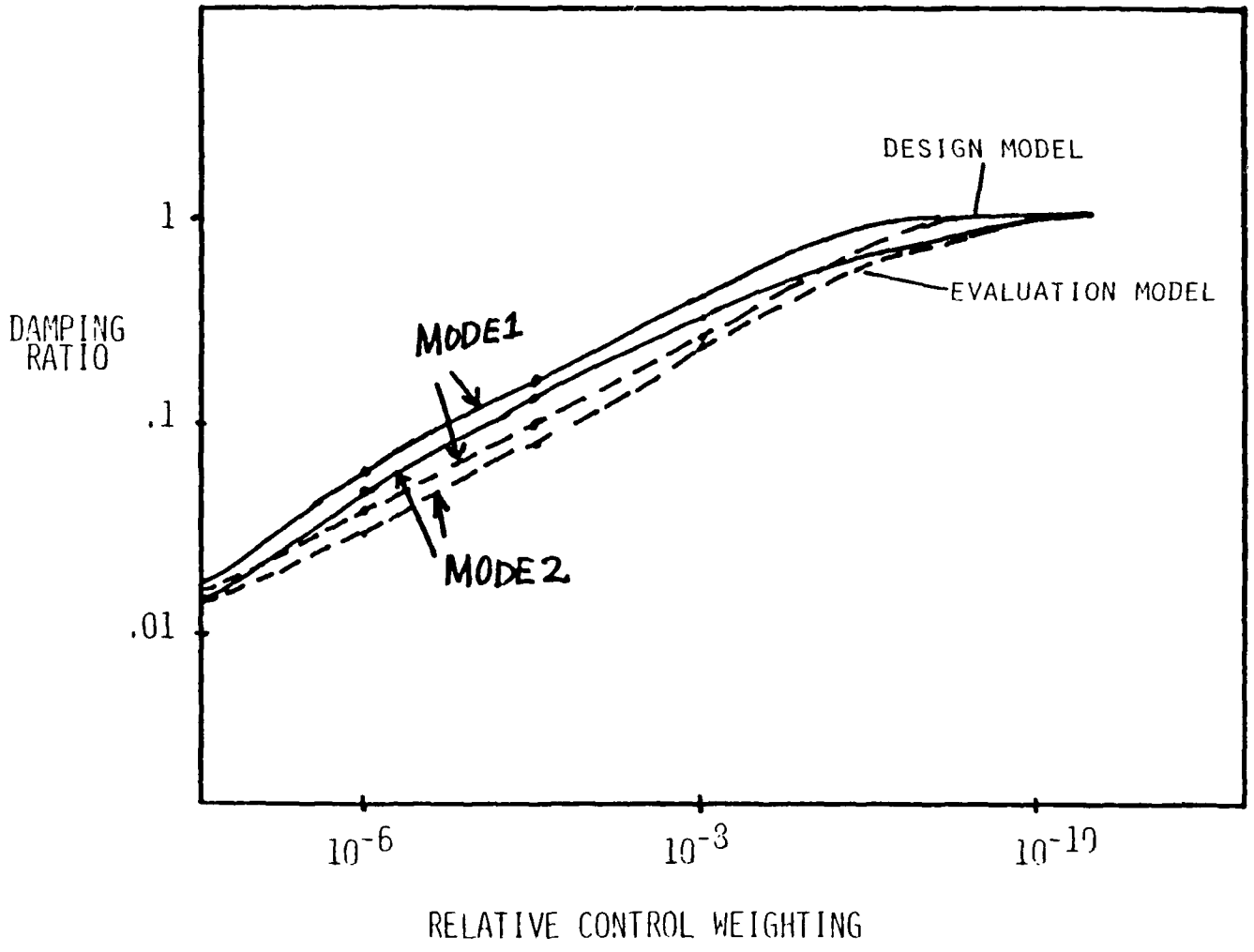

Fig. 6 Damping Ratio of Controlled Modes (Frequency Shaped Cost Functional)

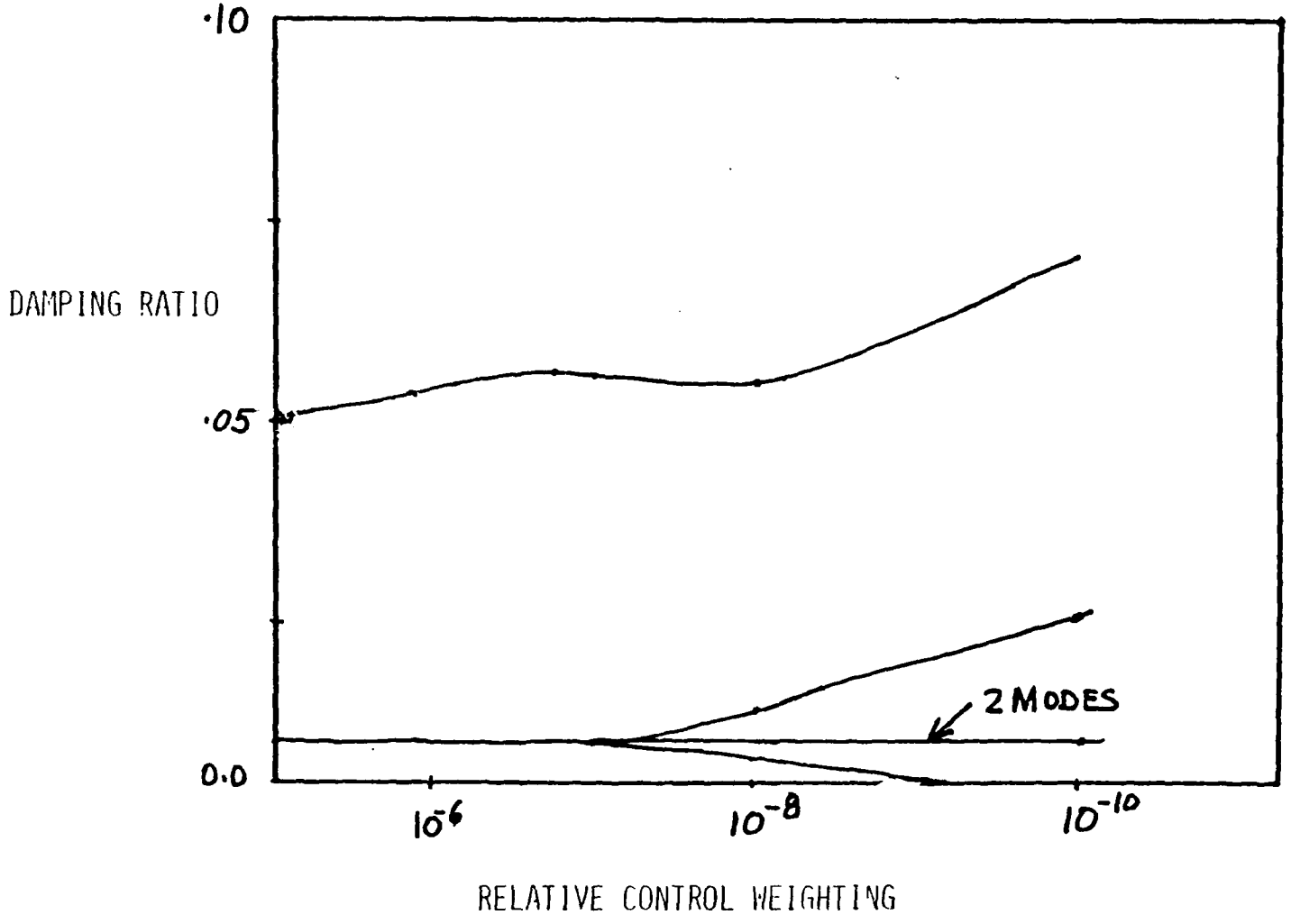

Fig. 7 Damping Ratio of Uncontrolled Modes (LQG Design)

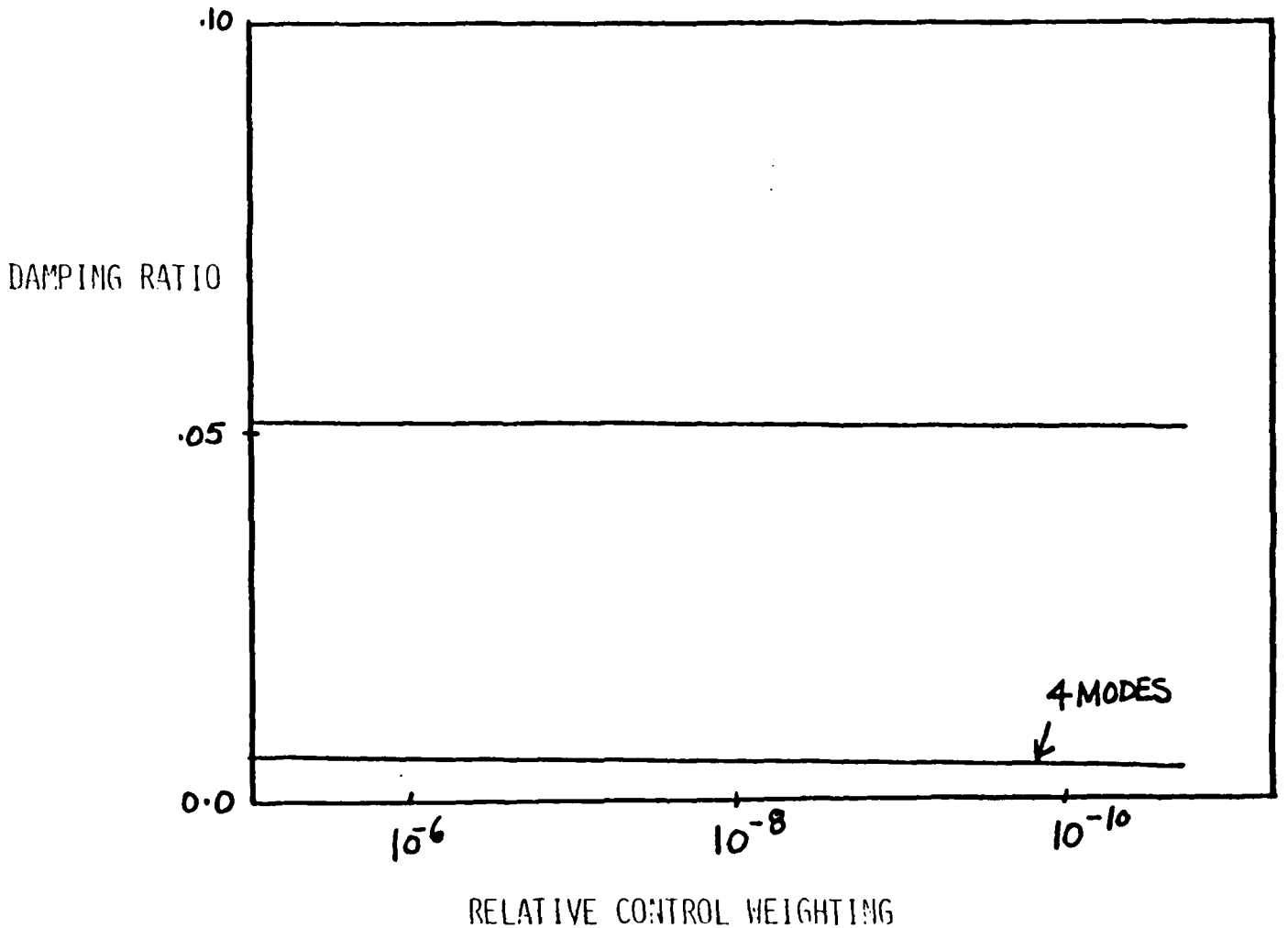

Fig. 8 Damping Ratio of Uncontrolled Modes (Frequency Shaped Cost Functional)

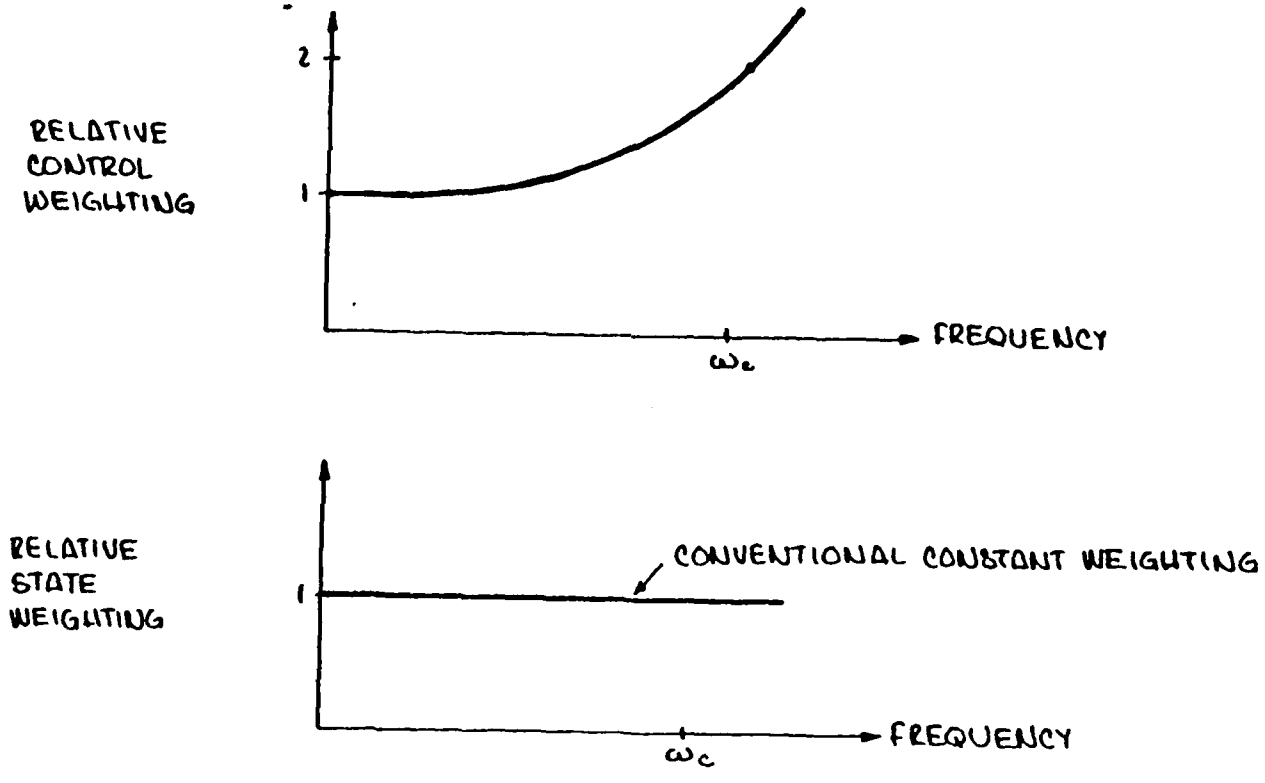

Fig. 9 Control Design Weighting Functions

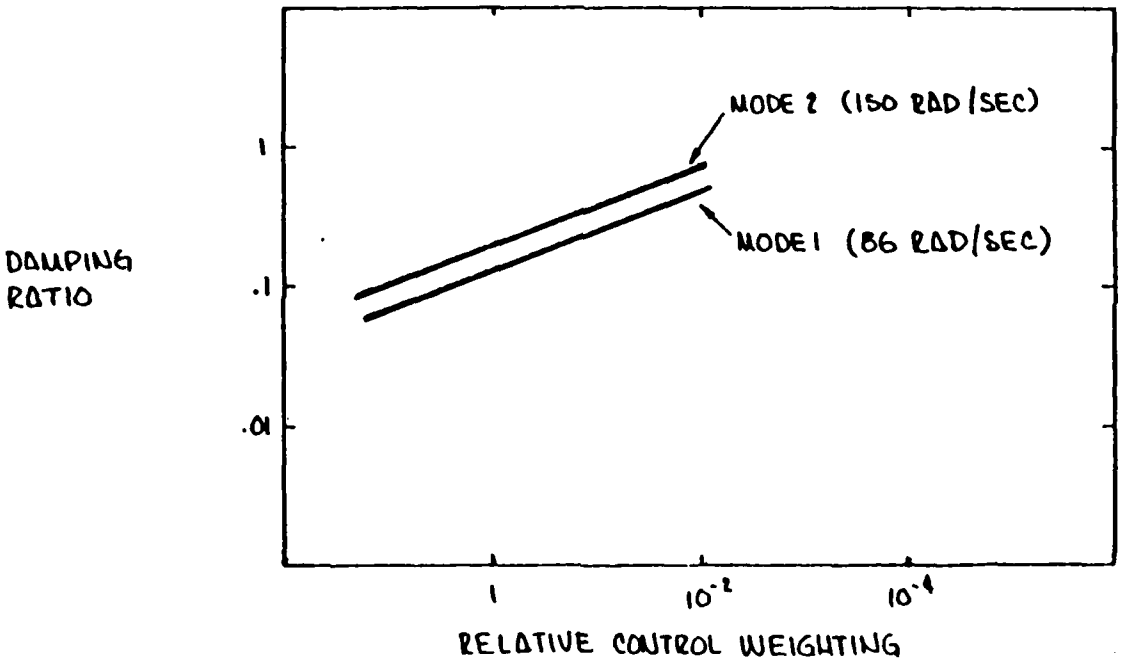

Fig. 10 Damping Ratio as a Function of Relative Control Weighting

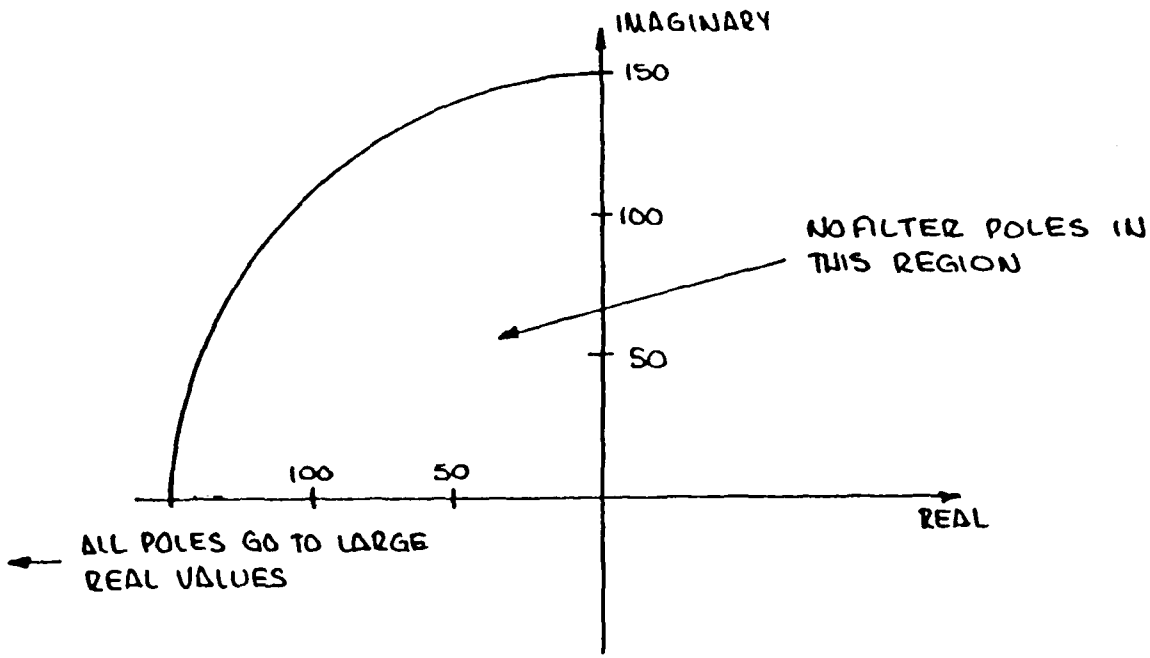

SOLUTION: (1) SELECT ARTIFICIAL NOISE WEIGHTING TO GET GOOD TRANSIENT RESPONSE IN ADDITION TO GOOD STEADY STATE RESPONSE

(2) DO A CONTROLLER REDUCTION TO SIMPLIFY THE FILTER

Fig. 11 Filter Closed Loop Poles with Original Noise PSD

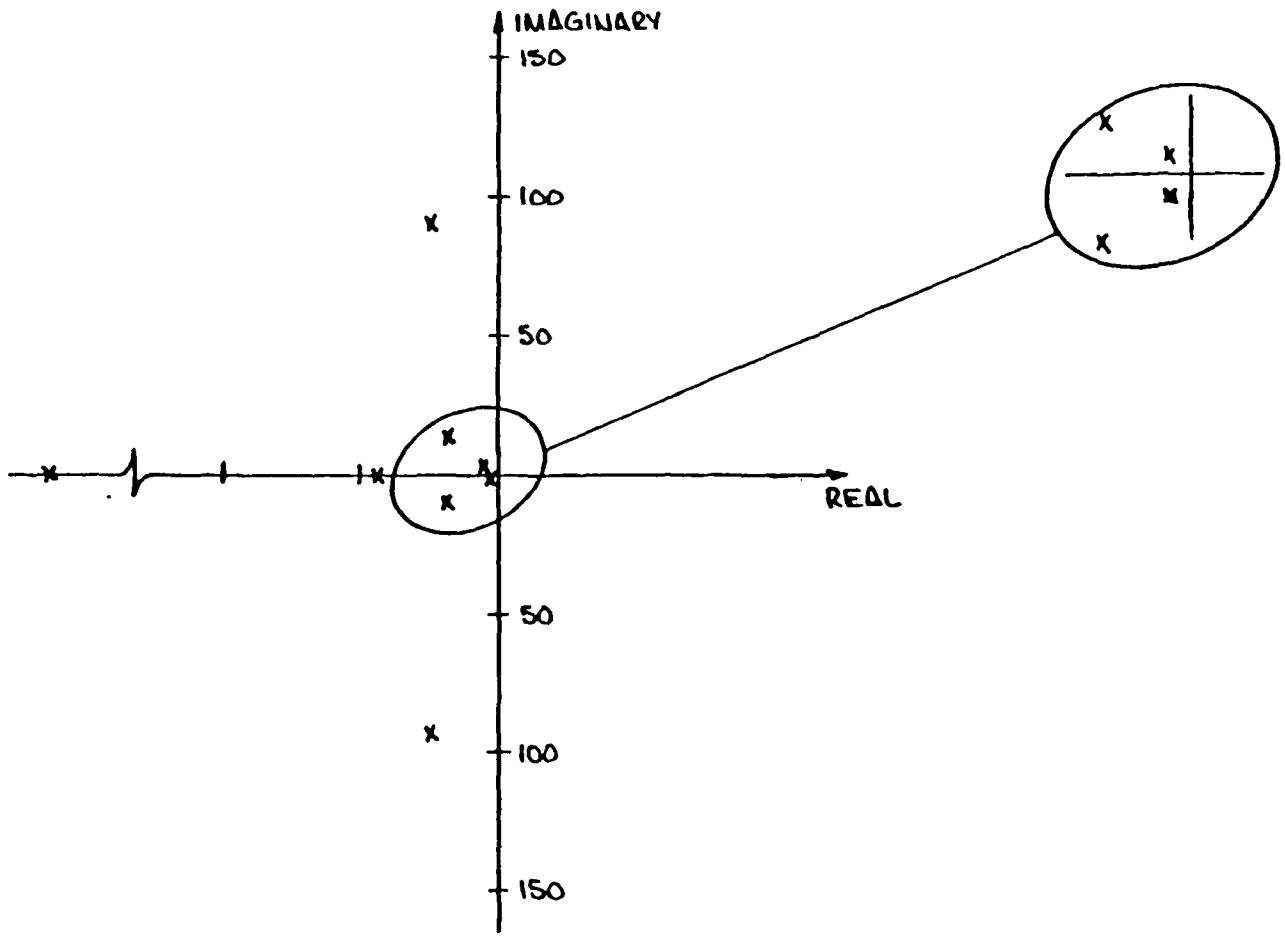

Fig. 12 Filter Closed Loop Poles with Scaled Noise Source

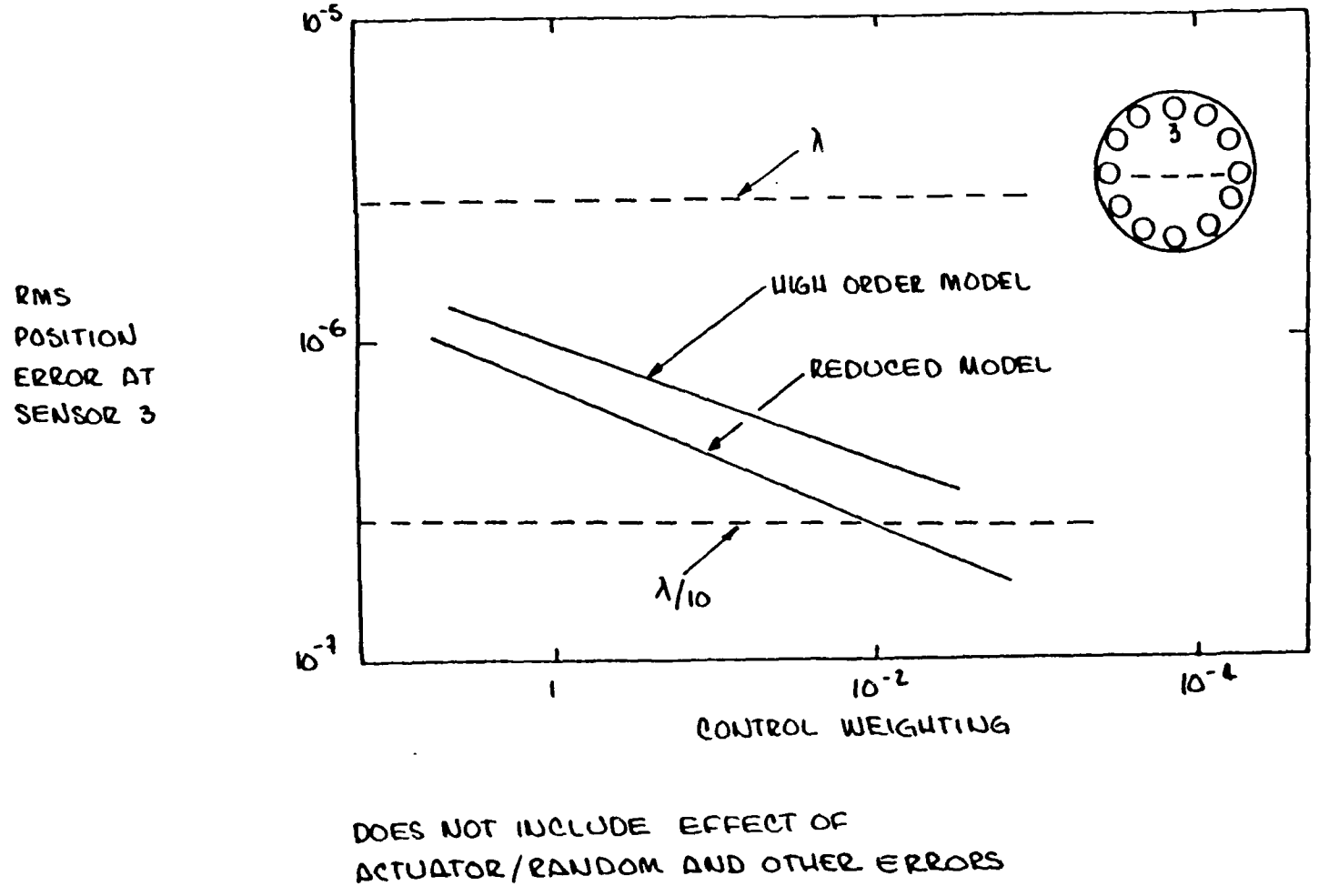

Fig. 13 Root Mean Square Response in Steady State (Laser PSD Disturbance)

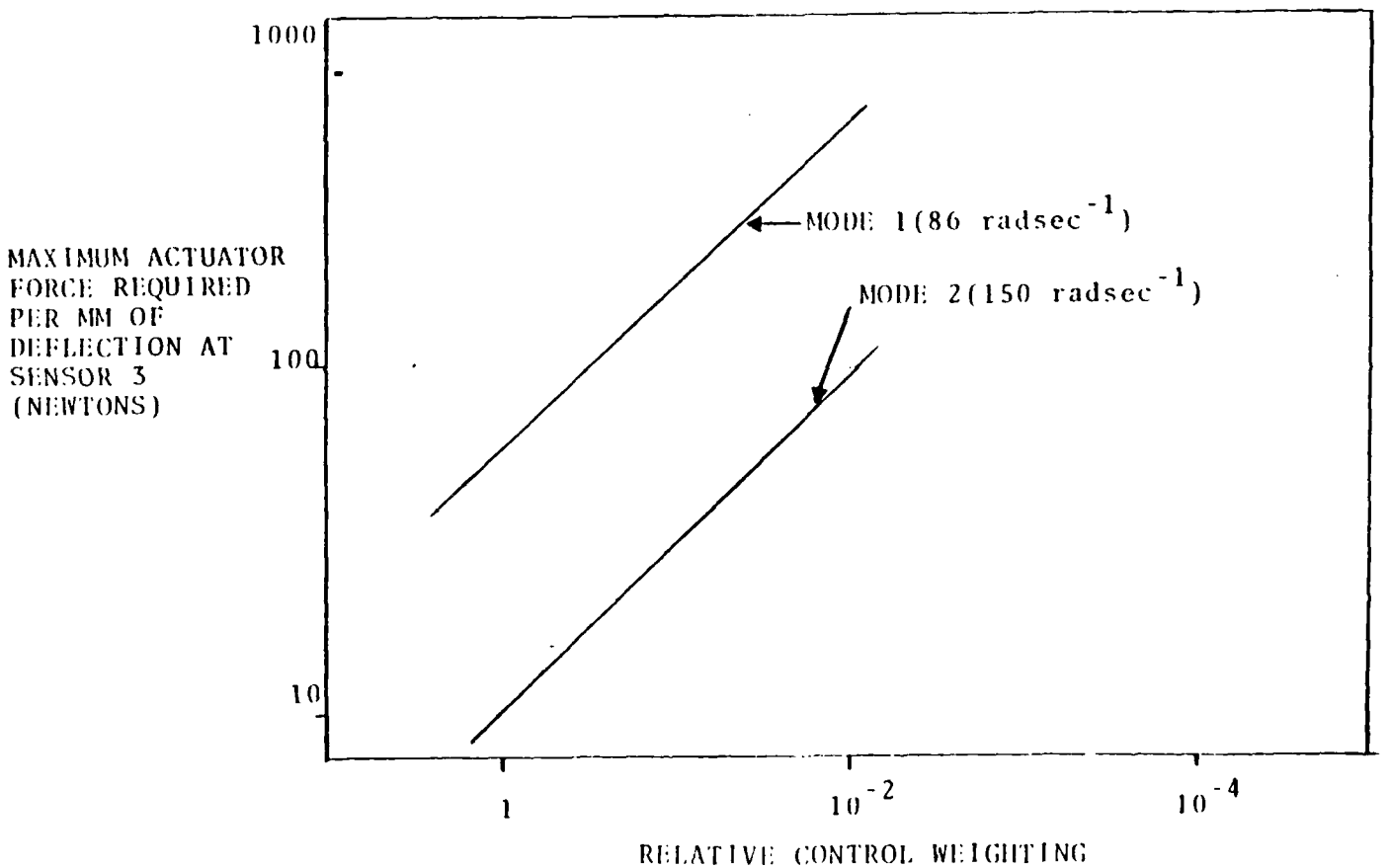

Fig. 14 Control Force Requirements (Maximum Values)

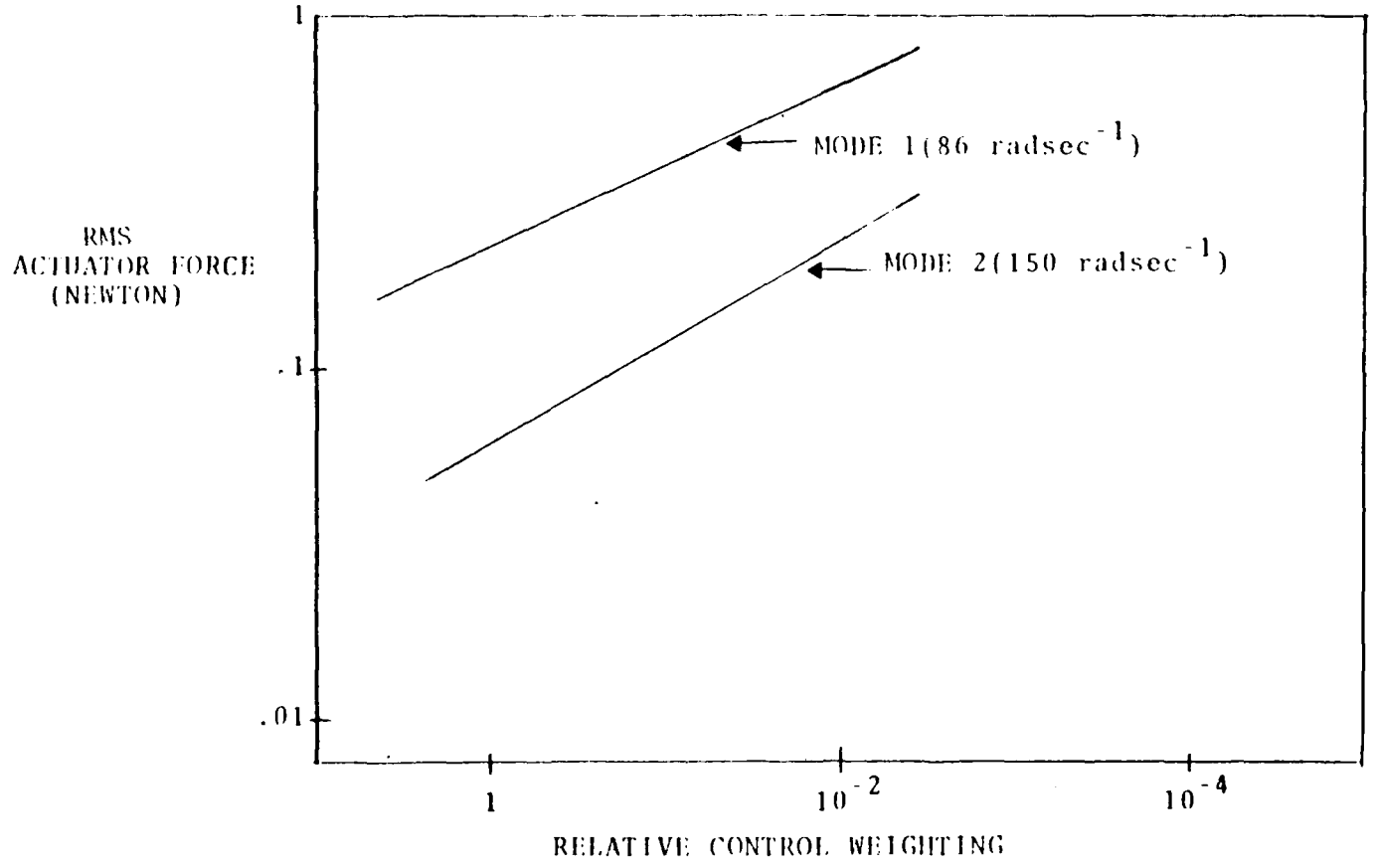

Fig. 15 Control Force Requirements (RMS Values)

Section 6
EXPERIMENTAL RESULTS

The experimental results presented in this section were created under LMSC IRAD funding in general support of this area of research and are included to clarify the applicability of the theoretical work described in earlier sections.

6.1 PROOF-MASS DAMPED BEAM (MINIBEAM)*

This experimental brass-board was developed under the Lockheed Independent Research Program to illustrate the principle of an inertial translational proof-mass damper for structural vibrations. While the intended application is generally for low authority control (i.e., 10 percent to 20 percent damping), the scaling of this particular experiment (which uses off-the-shelf hardware components designed for other purposes) was such that over 50 percent damping was obtained.

6.1.1 Experimental Set-Up

A 40-in. long magnesium bar is clamped on a laboratory table (Fig. 1) allowing essentially only horizontal cantilevered structural oscillations with the first mode around 4.5 Hz. A 2-lb Ling shaker unit is mounted at the free end of the beam in a pivoted plexiglass cradle supporting the shaker caging, while the shaker stem is solidly attached to the beam. The cradle thus allows free, small horizontal motions of the shaker, but constrains its vertical motions which would otherwise produce excessive bending moments on its stem. As designed, this system is intended to represent an idealized one-dimensional proof-mass damper in the horizontal plane.

To implement a rate sensing device, an optical method is used. A laser beam (emitted from a helium-neon laser source at the root of the magnesium bar) is

*This experiment is shown and described on the DARPA/ACOSS videotape. Since its purpose is only to demonstrate a physical principle, no quantitative results will be given.

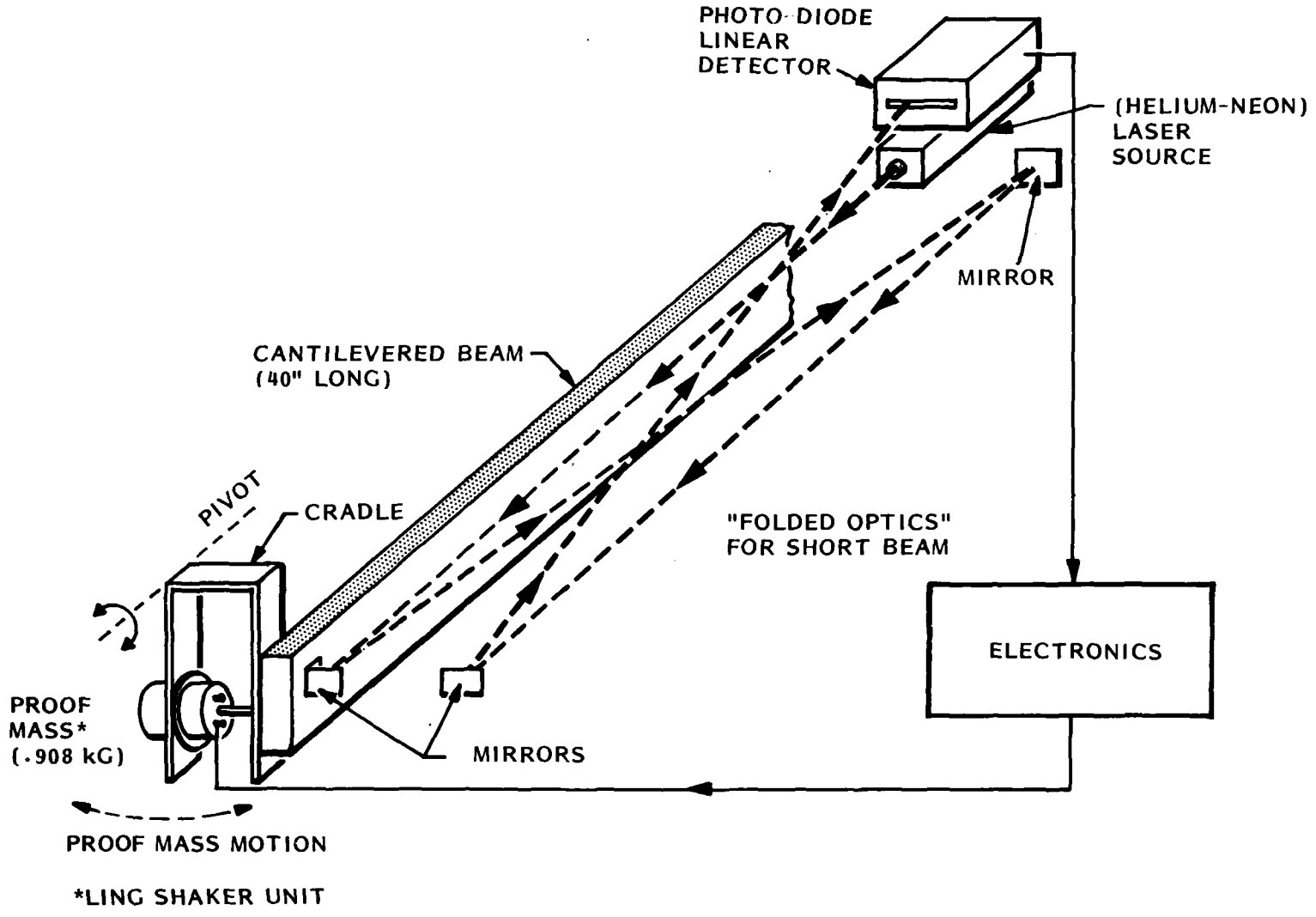

Fig. 1 Proof-Mass Damped Beam (Minibeam)

folded (reflected) several times by a system of mirrors, as shown in Fig. 2, in order to produce an oscillating spot corresponding to the beam's tip deflections. The spot is picked up by a linear detector, and via suitable electronic compensation, produces a tip-deflection rate signal used as feedback to drive the shaker with proper phase and amplitude.

6.1.2 Analytical Model and Actuator Dynamics

Let m be the mass of the shaker unit ("proof-mass damper") and let x, X respectively denote the inertial displacements of the shaker and of the beam tip, as shown in Fig. 2.

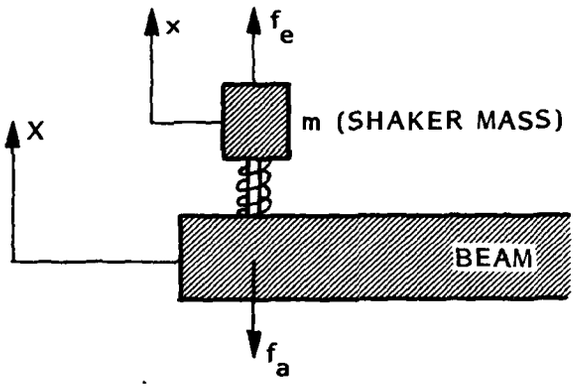

Fig. 2 Notation for Proof-Mass Dynamics

Let f_e denote the electromagnetic force applied to the shaker, f_a the actual force applied to the beam, and k the (weak) spring constant inherent to the caging of the shaker stem. Since f_e is proportional to the beam-tip rate, the equations of motion for the system are

$$\left.\begin{aligned} m\ddot{x} &= f_e = k\,(X - x) \\ f_e &= -f_e + k\,(x - X) \\ f_e &= D\dot{X} \end{aligned}\right\} \qquad (1)$$

In Laplace transformed variables we have then

$$(ms^2 + k)\, x = (Ds + k)\, X$$

and hence

$$x - X = sX \left(\frac{D - ms}{ms^2 + k} \right) \tag{2}$$

Substituting (2) into the middle equation of (1) yields, after some simple algebra, two equivalent forms for the force f_a applied to the beam tip:

$$f_a = -DsX \left[1 - \frac{k\,(1 - ms/D)}{k + ms^2} \right] \tag{3}$$

$$f_a = -Ds^2X \left[\frac{ms/k - m/D}{1 + ms^2/k} \right] \tag{4}$$

From these two expressions, it can be seen that:

1) for $S \gg (k/m)^{1/2}$, $f_a \sim -DsX$

2) for $S \ll (k/m)^{1/2}$, $f_a \sim ms^2X$

The above shows the characteristic property of proof-mass dampers (such as the Ling shaker) having a weak spring caging restraint. For sufficiently large frequencies, their behavior approximates that of an idealized inertial damper, whereas for sufficiently low frequencies, their effect is essentially to mimic the presence of an added mass m attached to the structure (beam).

Finally, the colocated loop-closure is produced by using the optical position sensor with a classical rate circuit compensation analogous to the one used for the maxibeam experiment described in the next section.

6.2 GYRODAMPED BEAM (MAXIBEAM)*

This experimental brass-board was developed under the Lockheed Independent Program to illustrate the principle of an inertial rotational gyro-damper for structural vibrations. The major hardware component for this experiment is a pair of identical single-gimbal control moment gyros (CMGs). CMGs are not off-the-shelf pieces of hardware and are generally unique, "few-of-a-kind" developmental items, as shown in Table 1, which lists CMGs built by the Bendix Corporation. The two CMGs used in this experimental brass-board are model no. MA-5-100-1, and are part of a set of 5 identical units built for LMSC in 1973. (The shared developmental cost at the time was $60,000 per unit.)

While gyrodampers would normally be sized and fabricated for specific spacecraft structural stabilization systems, this experimental brass-board had to be designed "in reverse". That is, given the two available Bendix CMGs, weighing approximately 40 lb each, a massive flexible support structure had to be designed to match the performance characteristics of these CMGs. Approximately 10 to 20 percent damping was obtained with this experiment.

6.2.1 Experimental Set-Up

A massive aluminum I-beam, weighing almost 400 lb, with 16 in. web and 6 in. flanges, 25 feet long, is cantilevered on a special 1000 lb support structure so that its "soft-axis" deflections are essentially constrained to occur in the horizontal plane, with the first mode around 1 Hz. At the free end of the beam, the two MA-5-100-1 Bendix CMGs are symmetrically mounted (Fig. 3) in a scissoring V-CMG pair, with gimbal axes parallel to the long axis of the beam. In the caged position (i.e., zero gimbal angles), the CMG angular momenta are equal and opposite in the horizontal plane, and hence cancel (zero stored momentum). When the beam oscillates horizontally, the V-CMG pair scissors so that the resultant

*This experiment is shown and described on the DARPA/ACOSS videotape. Since its purpose is only to demonstrate a physical principle, no quantitative results will be given.

Table 1

BENDIX CONTROL MOMENT GYROS

MODEL NO:	MA-1000	MA-2300	MA-500 AC	MA-500 DC	MA-2000	MA-5-100-1
TYPE	DOUBLE GIMBAL	DOUBLE GIMBAL	SINGLE GIMBAL	SINGLE GIMBAL	DOUBLE GIMBAL	SINGLE GIMBAL
PROGRAM	CMG R and D	Skylab	CMG Test	CMG R and D	ADV. CMG	Pointer Control
AGENCY	NASA LRC	NASA MSFC	Air Force	In-House	NASA MSFC	LMSC
UNITS BUILT	4	12	3	5	1	5
STATUS	Evaluation at NASA	Qualified	Partially Qualified	Partially Qualified	Evaluation at NASA	Evaluation at LMSC
MOMENTUM (ft-lb-sec)	1000	2300	250 - 750	250 - 750	1000 - 3000	5
OUTPUT TORQUE Max ft-lb	175	122	500	500	175	100
PIVOT TORQUE Max ft-lb	175	122	90	90	175	12
DECREES OF FREEDOM	2	2	1	1	2	1
GIMBAL FREEDOM (deg)	Unlimited – Slip Rings	$\pm 80^{\circ}$ $\pm 175^{\circ}$	$\pm 170^{\circ}$	$\pm 170^{\circ}$	Unlimited – Slip Rings	Unlimited – Slip Rings
GIMBAL RATE Max (deg/sec)	10	4, 7	57.3	57.3	5, 30	1146
WEIGHT (lbs)	230	418	145	155	558	38
APPROX. ENVELOPE	39" Diam. Sphere	41" Diam. Sphere	(Cylinder 20" Diam. x 32" Long)		44" Diam. Sphere	Cylinder 10" x 10" Long
ROTOR SPEED (RPM)	11,400	9,000	7,850	7,850	4,000 to 12,000	8,000
SPIN UP TIME (hrs)	$<$4 hours	$<$14 hours	$<$6 hours	$<$2.5 hours	$<$2.5 hours (to 8,000 RPM)	$<$0.1

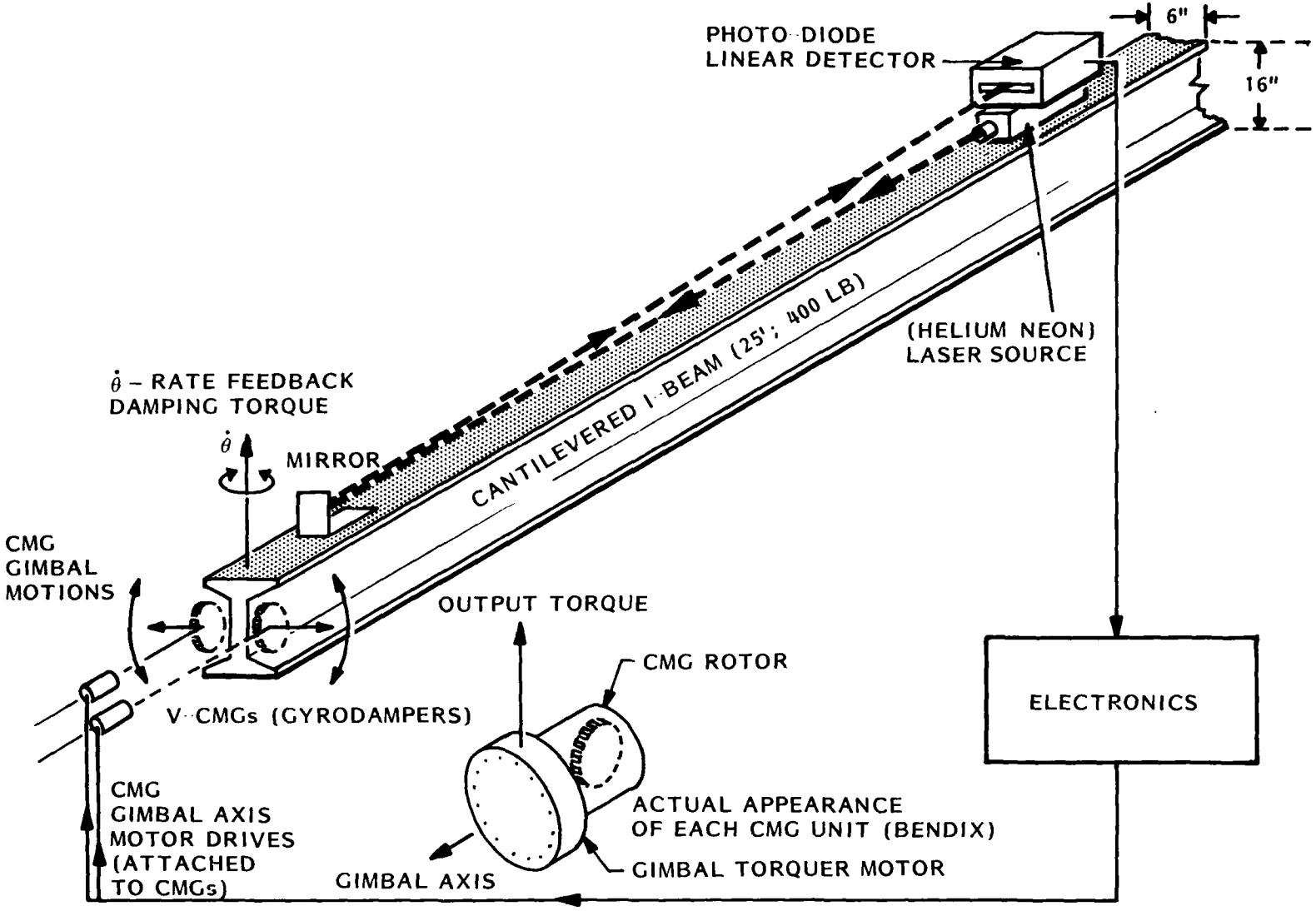

Fig. 3 Gyrodamped Beam (Maxibeam)

momentum (and hence the output torque) always lies along the vertical axis normal to the horizontal plane of beam vibrations. A summary of the maxibeam experimental data is given in Table 2.

To implement a rate-sensing device, an optical system is used. A laser beam, emitted at the root of the beam, is folded (reflected) once by a mirror colocated with the CMGs, and produces an oscillating spot picked up by a linear detector colocated with the laser source. The signal is then processed electronically to produce beam-tip rotational rates, and with suitable compensation, is used as (rotational) rate-feedback to drive the CMG gimbal torquer motors with proper phase and amplitude. (The CMG rotors have a constant 8000 rpm spin, and at 20 rad/sec gimbal rate, the output torque of each CMG is about 100 ft-lb; see Table 1).

Table 2

MAXIBEAM EXPERIMENT DATA

Beam

M = 154.6 kg (effective cantilevered mass)
L = 6.96 m
I = $4.375\ 10^{-6}$ m^4
E = $7.2\ 10^{10}$ Pa

Actuators

Total mass	=	34.5 kg
	=	20 rad/sec
Max gimbal sec	=	1650 rad/sec^2
Max output torque	=	120 nm

System Modes (cantilever beam with tip mass)

Mode No.	Frequency	Mode Shape at Tip (rotation) rad $kg^{-1/2}$
1	1.000	0.0244
2	7.064	-0.0884
3	20.86	0.1425
4	42.22	-0.1966

Control gain for 10% damping in first mode: Da = 2105 nm/rad-s^{-1}

6.2.2 Analytical Model and Actuator Dynamics

Consider a small rigid portion B of the oscillating maxibeam, with an orthonormal frame $\{\vec{e}_1, \vec{e}_2, \vec{e}_3\}$ attached to it as shown in Fig. 4. For simplicity of illustrating the basic principles involved, we assume that B can only undergo planar oscillatory rotations about $\vec{e}_1$, and that $\vec{e}_1$ maintains an inertially fixed orientation. Then the inertial angular velocity $\vec{\Omega}_B$ of B (i.e., of the frame $\{\vec{e}_1, \vec{e}_2, \vec{e}_3\}$) is

$$\Omega_B = \dot{\theta}\,\vec{e}_1 \tag{1}$$

where θ is the angle of rotation of B about $\vec{e}_1$. Consider first gyro no. 1, with constant speed rotor having angular momentum $\vec{h}_1$, gimbaled on $\vec{e}_3$, the gimbal angle σ being zero when h_1 is parallel to $-\vec{e}_2$. The total angular momentum H the gyro, expressed in the moving frame $\vec{e}_1, \vec{e}_2, \vec{e}_3$ is then given by

$$\vec{H} = h\,(\sin\sigma\,\vec{e}_1 - \cos\sigma\,\vec{e}_2) + J\dot{\sigma}\,\vec{e}_3 \tag{2}$$

where $h \equiv |\vec{h}_1| = \text{const}$, and J is the gyro's inertia about the gimbal axis (direction) $\vec{e}_3$.

Let $\vec{T}_g$ be the torque applied externally to the gyro (e.g., by the gimbal torquer motor). The equation of (gimbal) motion of the gyro is then

$$\frac{d\vec{H}}{dt} = \vec{T}g, \tag{3}$$

where d( )/dt denotes time differentiation w.r.t inertial space. If (˙) denotes time differentiation in the moving frame $\{\vec{e}_1, \vec{e}_2, \vec{e}_3\}$, and if we assume small motion linearized dynamics, then from (1), (2), and (3) we obtain:

$$\left.\begin{aligned} \frac{d}{dt}\; h\,(\sigma\vec{e}_1 - \vec{e}_2) + J\sigma\vec{e}_3 \;&=\; h\,(\dot{\sigma}\vec{e}_1 + \sigma\vec{\Omega}_B \times \vec{e}_1 - \vec{\Omega}_B \times \vec{e}_2) \\ &\quad + J\ddot{\sigma}\vec{e}_3 + J\dot{\sigma}\vec{\Omega}_B \times \vec{e}_3 \\ h\,(\dot{\sigma}\vec{e}_1 - \dot{\theta}\vec{e}_3) + J\ddot{\sigma}\vec{e}_3 \;&=\; \vec{T}_g \end{aligned}\right\} \tag{4}$$

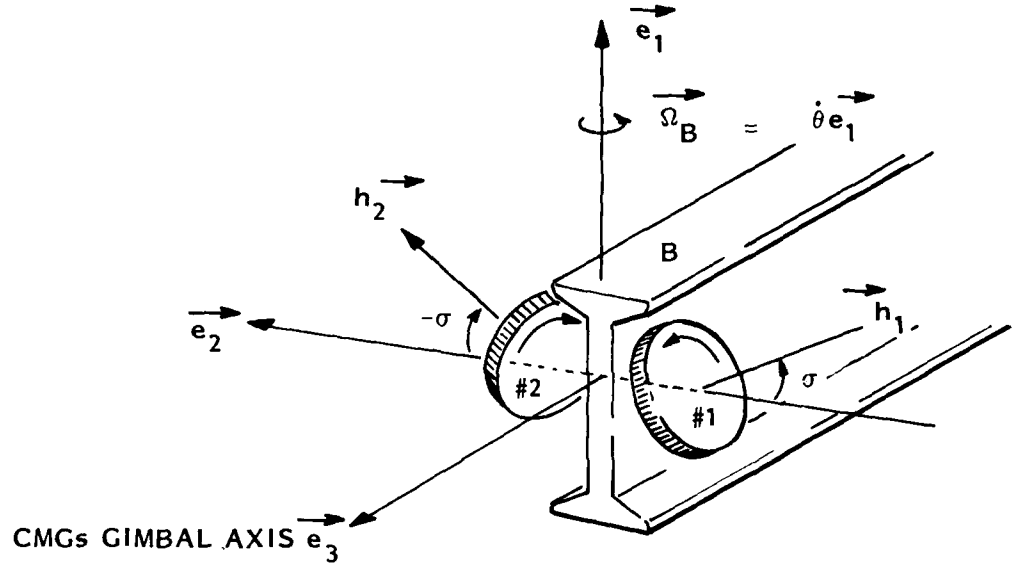

Fig. 4 Notation for CMG Dynamics

Assuming now that $\vec{T}_g = \vec{T}_g\vec{e}_3$ is an applied gimbal torque, projection of the last vector equation (4) along $\vec{e}_3$ results in

$$J\ddot{\sigma} = h\dot{\theta} + \vec{T}_g \qquad (5)$$

which represents the actuator (linearized) dynamics for each gyro. If, furthermore, $T_g \equiv -k_c\sigma - k_g\dot{\sigma}$, where $k_c > 0$, $k_g > 0$ are spring and dashpot constants, Eq. (5) represents a passive dissipative system driven by the input $\dot{\theta}(t)$. This passive gyro system will therefore absorb beam-rotational energy by opposing the $\dot{\theta}$ motion. However, the transmission of this energy is determined by the magnitude of h/J, which, in most practical cases of oscillating beams or structures, is too small for effective damping.

When two identical gyros are used such that zero gimbal angles correspond to gyro momenta alignments of $\vec{h}_1$ parallel to $-\vec{e}_2$, $\vec{h}_2$ parallel to $\vec{e}_2$, then the

counter-rotation of the rotors cancels the internally stored momentum for $\sigma = 0$. In addition, because of symmetry, the -induced gyro gimbal motions result in the classical "V-scissor" pairing of the momenta $\vec{h}_1$ and $\vec{h}_2$, i.e., the resultant total gyro momentum $\left(\text{w.r.t the moving frame } \{\vec{e}_1, \vec{e}_2, \vec{e}_3\}\right)$ always remains aligned with the $\pm e_1$ beam axis. This allows utilization of increased gyro gimbal travel. This travel is limited in practice due to the nonlinear relation between gyro momentum and gimbal angle, i.e.,

$$\left(\vec{h}_1 + \vec{h}_2 \cdot \vec{e}_1\right) = 2h \sin\sigma \tag{6}$$

where $h \equiv |\vec{h}_1| = |\vec{h}_2|$. Finally, the output torque $\vec{T}_B$ applied to the beam by the gyros is:

$$\left.\begin{aligned} \vec{T}_B &= -\left(\vec{h}_1 + \vec{h}_2\right) \cdot \vec{e}_1\vec{e}_1 = -2h\cos\sigma\dot{\sigma}\vec{e}_1 \\ &\cong -2h\dot{\sigma}\vec{e}_1 \end{aligned}\right\} \tag{7}$$

6.2.3 Control Equations for Active Augmentation of Passive Gyrodamper

The inertial absorption of the $\dot{\theta}$-rotational energy by the passive gyrodamper is limited in practice by the magnitude of h/J. To increase this energy dissipation, an angular rate sensor is added to the system to estimate the velocity which is fed back to the gyro's gimbal motor with the proper gain so that the colocated sensor/actuator pair will mimic a purely passive device. As is well known, this passive nature alone guarantees structural stability, i.e., this (idealized) device cannot excite the structure, but the structure can excite it. Such an actively augmented passive damper can be caricatured as a passive device with a "hearing aid" to magnify the $\dot{\theta}$ signal, and in this sense, is quite distinct from a purely active device which does not necessarily require either a colocated sensor or a rate feedback.

The maxibeam brass-board is an implementation of this concept for a system of two identical, coaxially gimbaled gyros (so-called V-gyros) as shown in Fig. 1.

Equation (5) remains valid for each gyro, but the gimbal torque T_g is no longer realized by passive springs and dashpots, but generated electronically by gimbal motors and will include a feedback team proportional to the sensor output $\dot{\theta}$. The control equations of each gyrodamper are now described by:

$$\underline{\text{Control Equation:}} \qquad \dot{\sigma}_c = \frac{D}{2h}\,\dot{\theta} \tag{8}$$

$$\underline{\text{CMG Rate-Servo and Caging Loops:}} \qquad T_g = \underbrace{k_g\,(\dot{\sigma}_c - \dot{\sigma})}_{\text{rate-loop}} \; \underbrace{-\,k_c\sigma}_{\substack{\text{caging}\\ \text{loop}}} \tag{9}$$

where $D > 0$, $k_g > 0$, $k_c > 0$ are constant gains, and $_c$, are, respectively, the commanded and actual gimbal rates. Substituting Eqs. (8) and (9) into (5), the gyrodynamics of each CMG are now given by:

$$J\ddot{\sigma} = h\dot{\theta} + (k_g D/2h)\,\dot{\theta} - k_g\dot{\sigma} - k_c\sigma \tag{10}$$

The transfer function corresponding to Eq. (10) is given by $(i^2 = -1)$:

$$\sigma/\theta = \frac{iK}{\omega_G^2 - \omega^2 + i\omega_1\omega},$$

where

$$\begin{aligned} K &\equiv \left|h + (k_g D/2h)\right|/J \qquad (11)\\ \omega_1 &\equiv k_g/J\\ \omega_G^2 &\equiv k_c/J \end{aligned}$$

and the gyrodamper bandwidth is the interval $\left|\omega_0,\ \omega_1\right|$, where $\omega_0 \equiv \omega_G^2/\omega_1$.

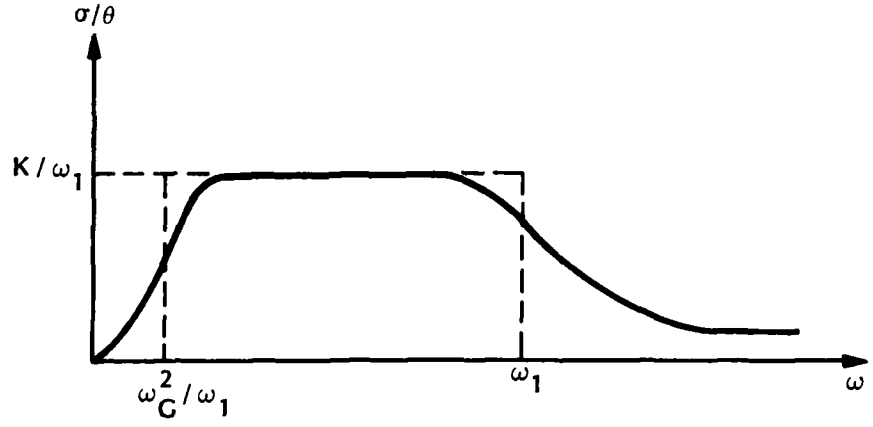

Fig. 5 Gyrodamper Transfer Function

The colocated loop-closure is finally produced by using the optical position sensor with a classical rate circuit compensation shown in Fig. 6. The compensator generates a rate signal up to 7 Hz to 10 Hz and is then rolled off. Curves a and b correspond to shifts in the second pole so that the relative damping of the 1 Hz and 7 Hz bending modes may be adjusted. The 21 Hz mode is not controlled.

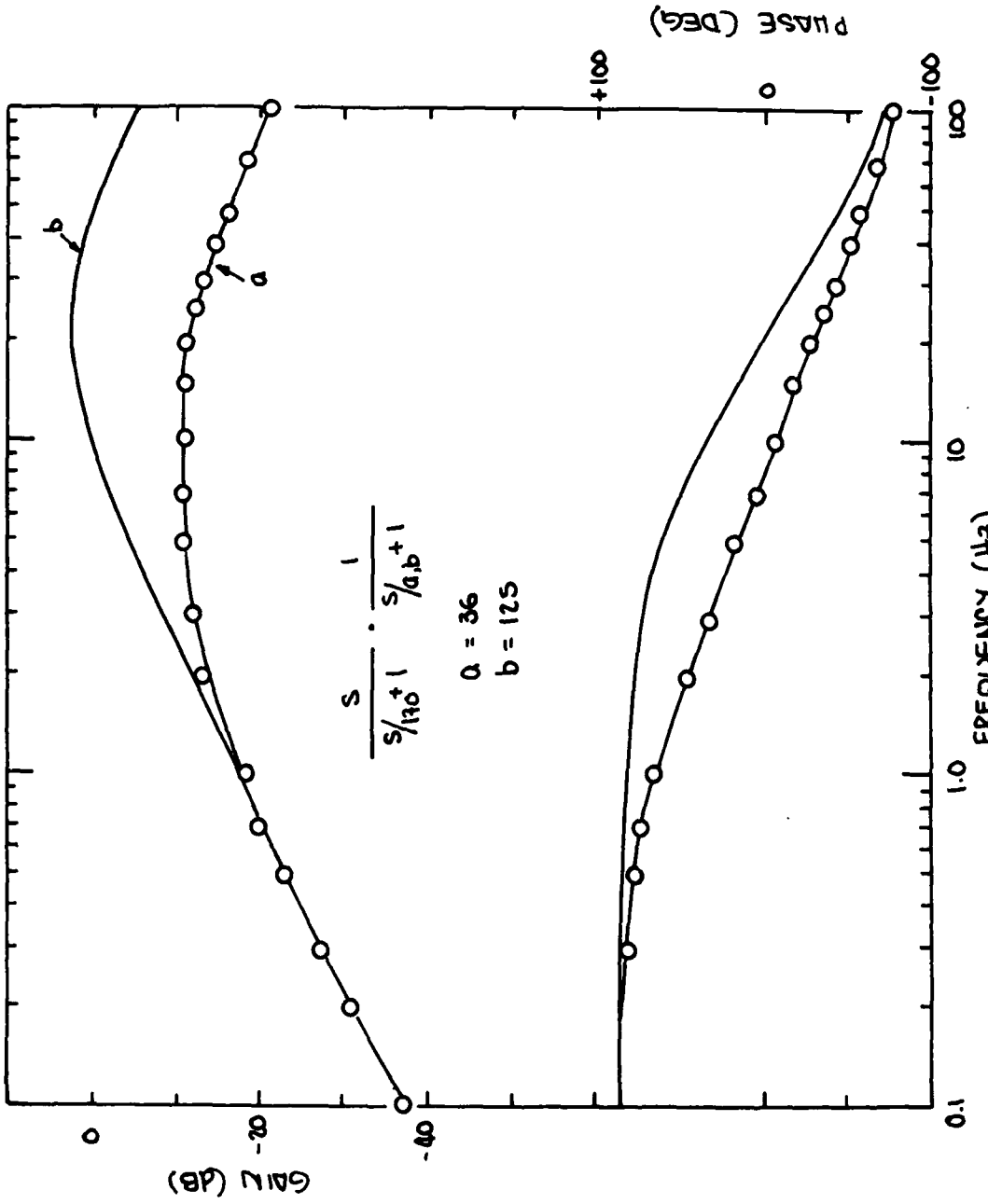

Fig. 6 Low Authority Compensation

6.3 TOYSAT EXPERIMENTS

6.3.1 Introduction

The next three sections describe experiments performed in the Space Systems Division's Modal Lab. The experiments were designed to test three of LMSC's basic control theories; optimal slewing, Low Authority Control, and High Authority or Modern Modal Control.

A photograph of the test specimen is shown in Fig. 1. The specimen consists of a rigid block of aluminum in the middle, with a long flexible bar of aluminum attached to each side. The central block is suspended from the ceiling by thin wires. The control is provided by two Electroseis linear actuators which act on the rigid central body. For these experiments, the linear actuators are commanded to give equal but opposite forces, resulting in a pure torque on the central body. There are two sets of sensors installed. On both ends of the flexible bar accelerometers provide information on the tip acceleration. Connected in parallel with the Electroseis linear actuators are linear potentiometers which give the amount of rotation of the central body. Small Ling shakers are also attached to each end of the flexible bar, however they are not used for control purposes; their only function is to provide a weight at the end of the flexible bar so as to lower the frequencies of the natural modes. For each experiment the control commands are generated differently. They will be described separately in each section.

An analytical model was developed in order to implement the control schemes. The model was used to generate a modal model; a truncated version is shown in Table 1. The values predicted by the analytical model were verified by performing a sine sweep of the test speciment. Agreement between analytically predicted and experimentally obtained frequencies was quite good. The biggest difference in frequency was around 5 percent. The analytical model was then adjusted to agree exactly with the experimental results.

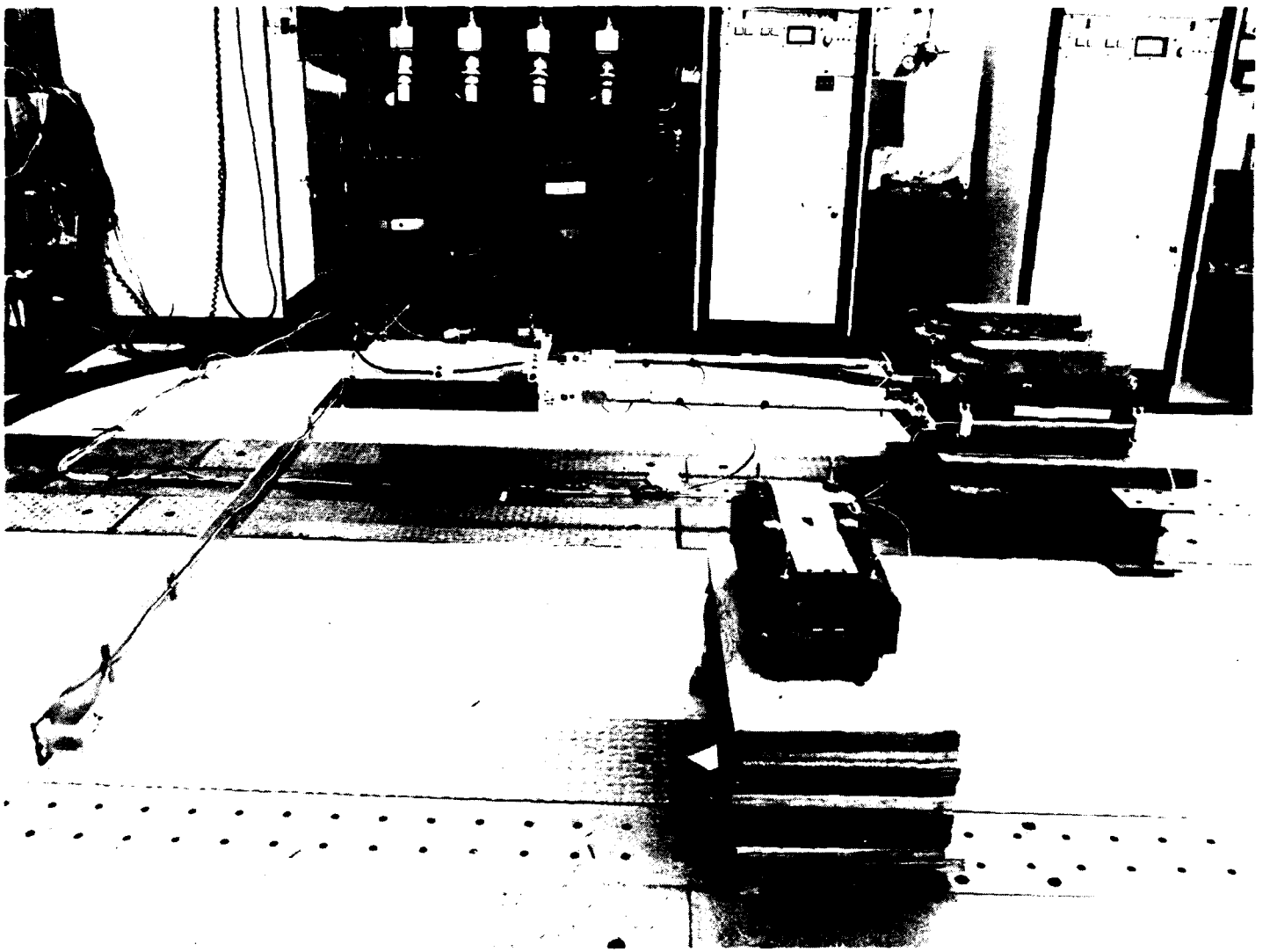

Fig. 1 TOYSAT Test Vehicle

Table 1

SYSTEM MODAL EQUATIONS

$$\frac{d}{dt}\begin{pmatrix} \theta \\ \dot{\theta} \\ q_1 \\ \dot{q}_1 \\ q_2 \\ \dot{q}_2 \end{pmatrix} = \begin{pmatrix} 0 & 1 & 0 & 0 & 0 & 0 \\ 0 & 0 & 0 & 0 & 0 & 0 \\ 0 & 0 & 0 & 1 & 0 & 0 \\ 0 & 0 & -w_1^2 & 0 & 0 & 0 \\ 0 & 0 & 0 & 0 & 0 & 1 \\ 0 & 0 & 0 & 0 & -w_2^2 & 0 \end{pmatrix} \begin{pmatrix} \theta \\ \dot{\theta} \\ q_1 \\ \dot{q}_1 \\ q_2 \\ \dot{q}_2 \end{pmatrix} + \begin{pmatrix} 0 \\ 1/J \\ 0 \\ \eta_1 \\ 0 \\ \eta_2 \end{pmatrix} T$$

θ is rigid body angle

q_i are modal amplitudes

w_i are modal frequencies

J is the total moment of inertia

η_i are the control influence coefficients

T is the control torque

Values:

$w_1 = 2.62$ Hz

$w_2 = 9.4$ Hz

$J = 135.05$ lb-in-sec^2

$\eta_1(0) = 1.53$

$\eta_2(0) = 0.78$

6.3.2 Optimal Slew Maneuver

The Optimal Slew as presented here is an open loop torque command to cause a rigid body angular displacement while leaving the first bending mode quiescent at the end of the maneuver. In general, more than one mode can be controlled at the end of the maneuver, but in this case only the first mode is considered. "Optimal" in the title is justified because the particular maneuvers shown here minimize the control energy used for the maneuver as well as accomplishing the desired objectives. Briefly, the control profile is a solution of the calculus of variations problem shown in equation (1).

$$\min_{u} \int_{o}^{t_f} u^2 \, dt \qquad (1)$$

subject to $x(0) = X_o$, $x(t_f) = 0$.

Here u is the control torque, and x is a state vector composed of the rigid body angle, the first modal amplitude, and both of their rates of change. For a more detailed description see "Optimal Feedback Maneuvering of Flexible Spacecraft" by John A. Breakwell, presented at the AIAA/AAS Astrodynamics Specialist Conference, Provincetown, Massachusetts, June 1979.

For these experiments, the commands to the linear actuators were provided by a PDP1145 digital computer. The desired profiles were approximated by small segments of constant output. Each command was divided into one hundred such segments. The output from the computer was fed through a digital to analog converter, and then smoothed by an eight pole butterworth filter set at 100 rad/sec before being input to the actuators.

The effectiveness of this slewing technique is demonstrated in Figs. 2 and 3. All slews are through 10 degrees. For comparison purposes, the responses to square wave torque commands are also shown. The tip acceleration output is filtered to show frequency content between 0.1 and 5 Hz. Both optimal slews show almost no residuals of the tip accelerations at the end of the maneuvers. What residual there is can be attributed to the 1 Hz symmetric mode, which was not controlled, and only insignificantly excited.

6.3.3 Low Authority Control

This version of Low Authority Control takes the form of a collocated rate feedback. The rate signal is obtained by differentiating the difference of the linear potentiometers attached to the central body. The signal is then rolled off twice for smoothing. Initially the roll off is set at 10.5 Hz, but a case is also described

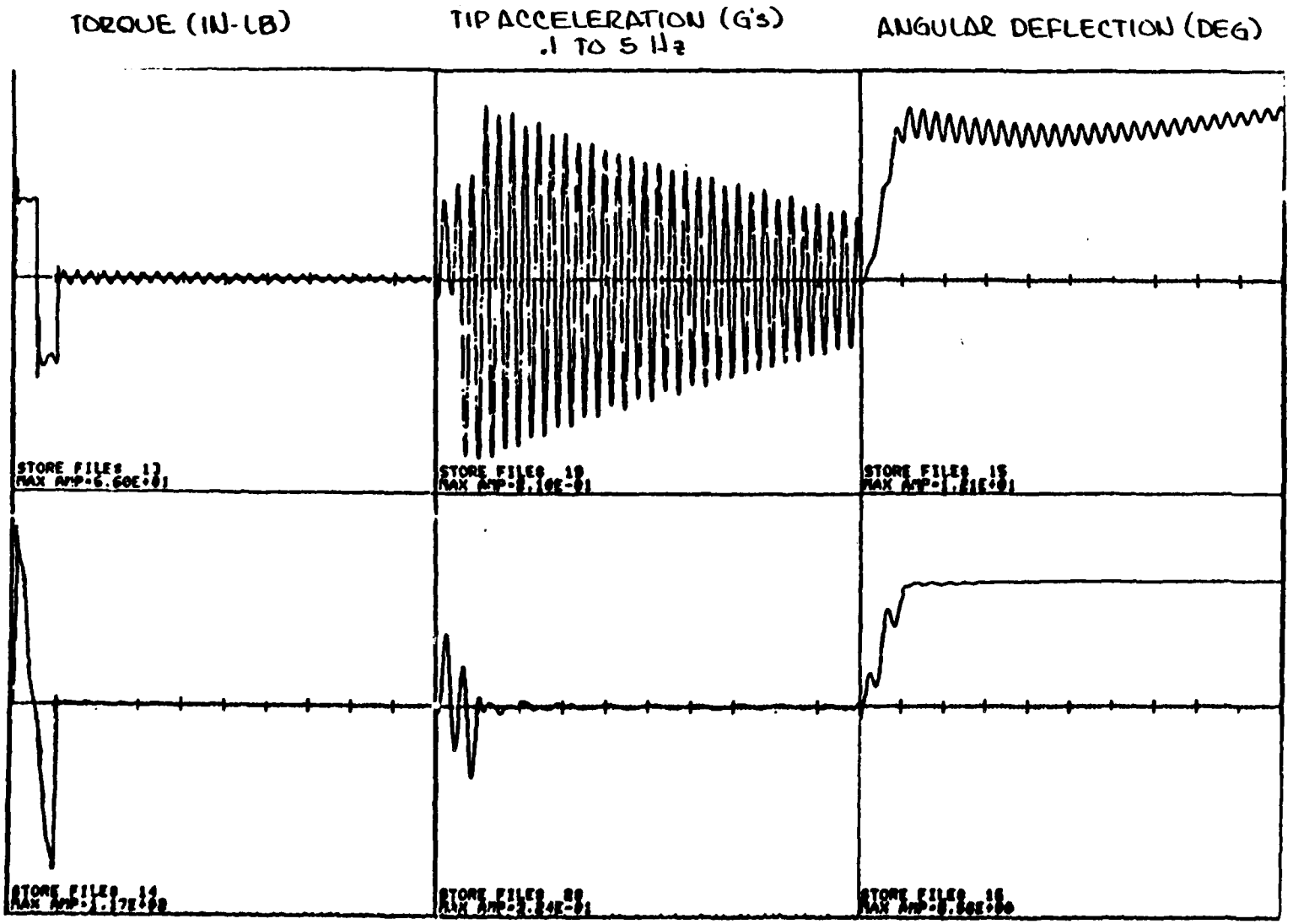

Fig. 2 Comparison of Rectangular and Optimal Slew Command Results
Command Period = 1.0 Second

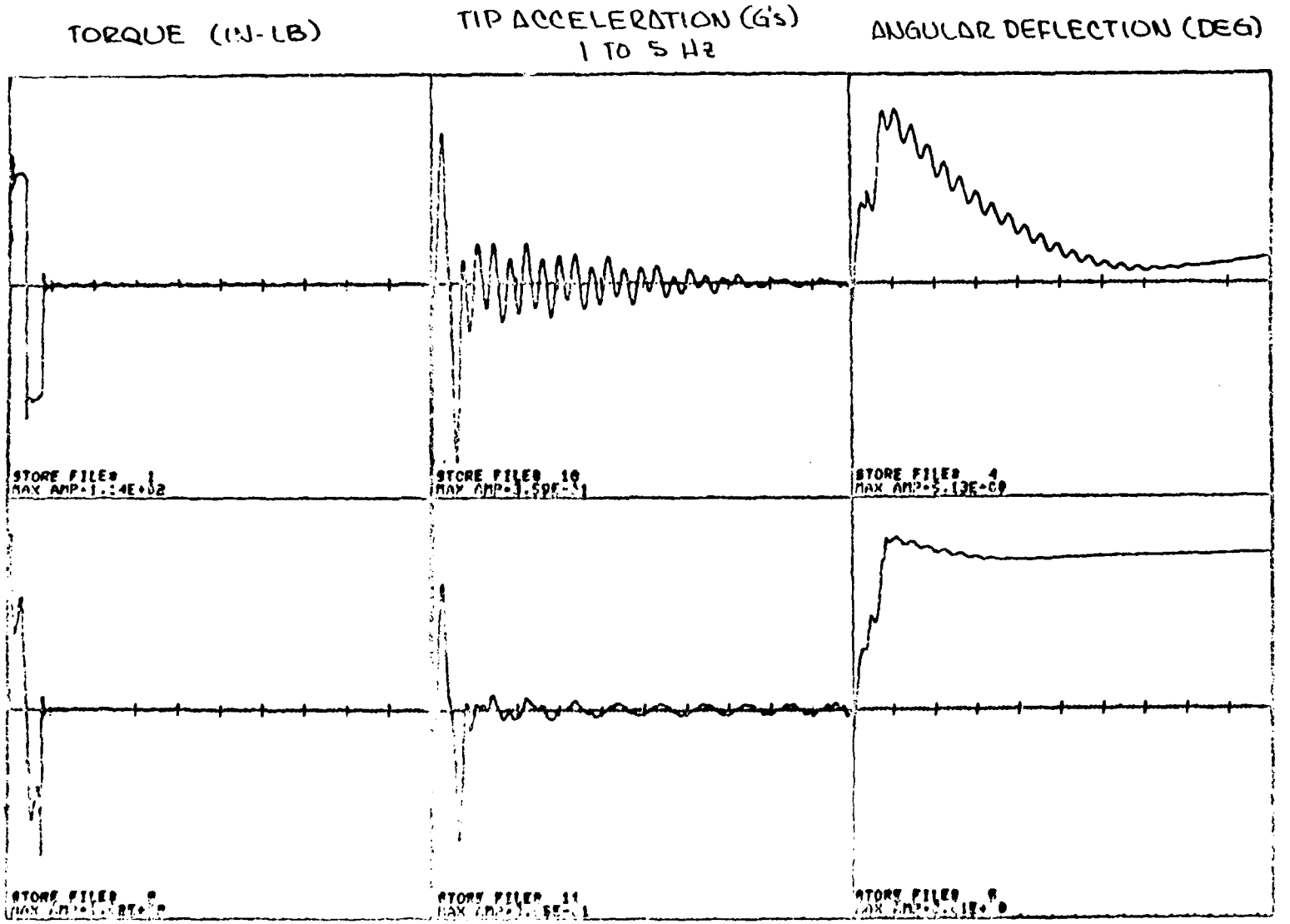

Fig. 3 Comparison of Rectangular and Optimal Slew Command Results
Command Period = 0.75 Second

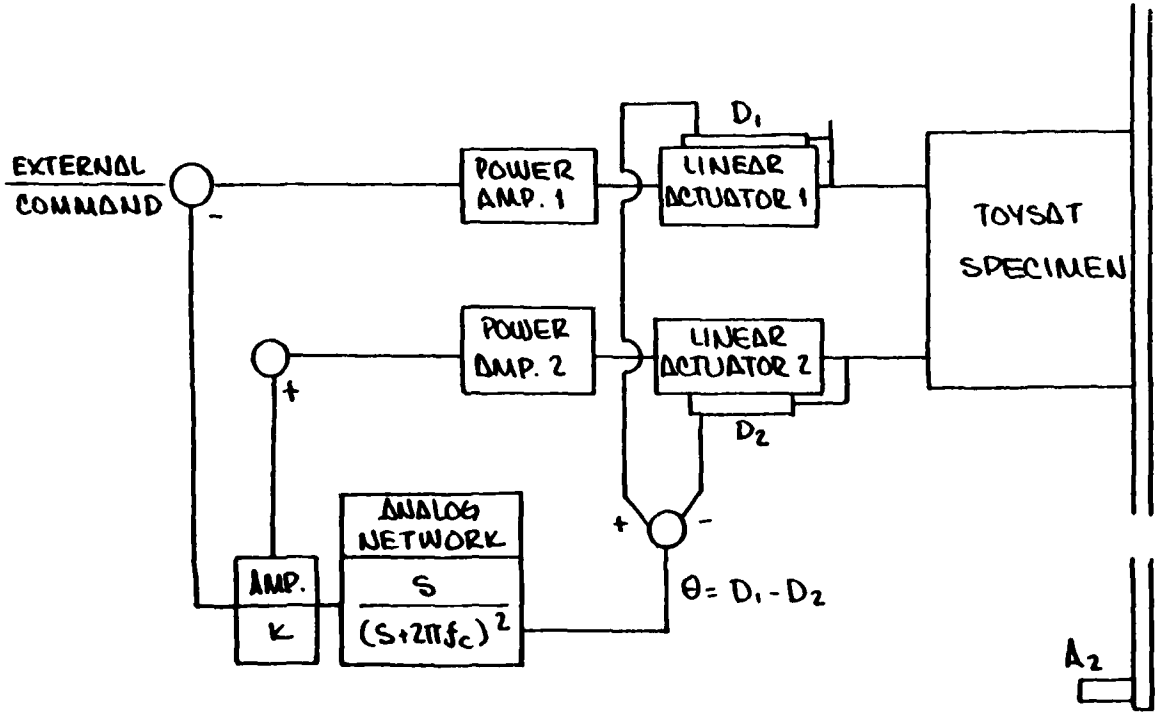

- K VALUES 0, 5, 10, 20 ; f_c = 10.5 Hz AND 18.9 Hz
- DAMPING AUGMENTATION ATTEMPTED FOR 2.66 Hz, 9.4 Hz ASYMMETRIC MODES

Fig. 4 Low Authority Control Experiment Block Diagram

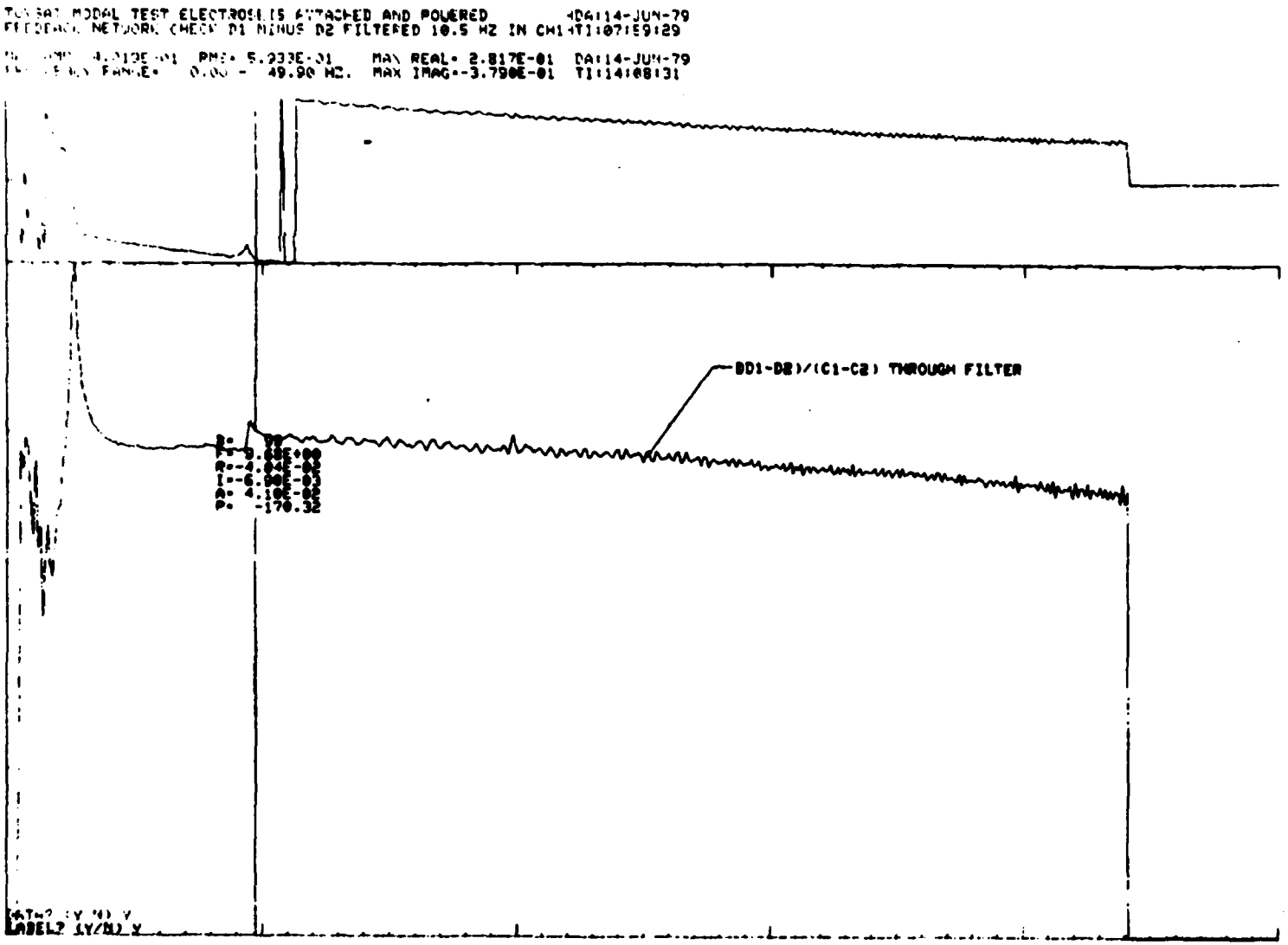

Fig. 5 Bode Plot of Transfer Function Between Filtered Rate Output and Actuator Input

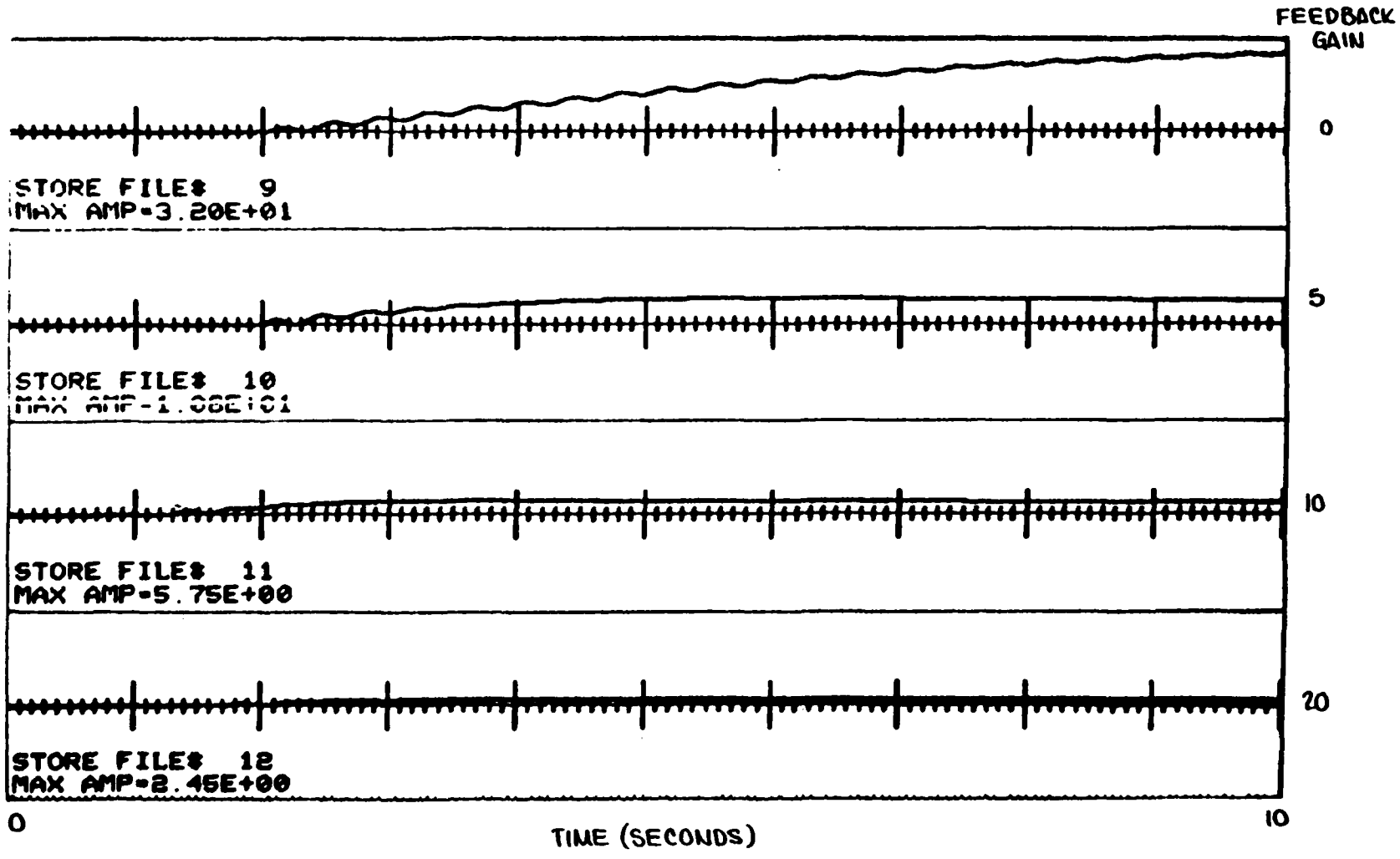

Fig. 6 Low Authority Control TOYSAT Angular Deflection (Degrees) Response to Impact Excitation

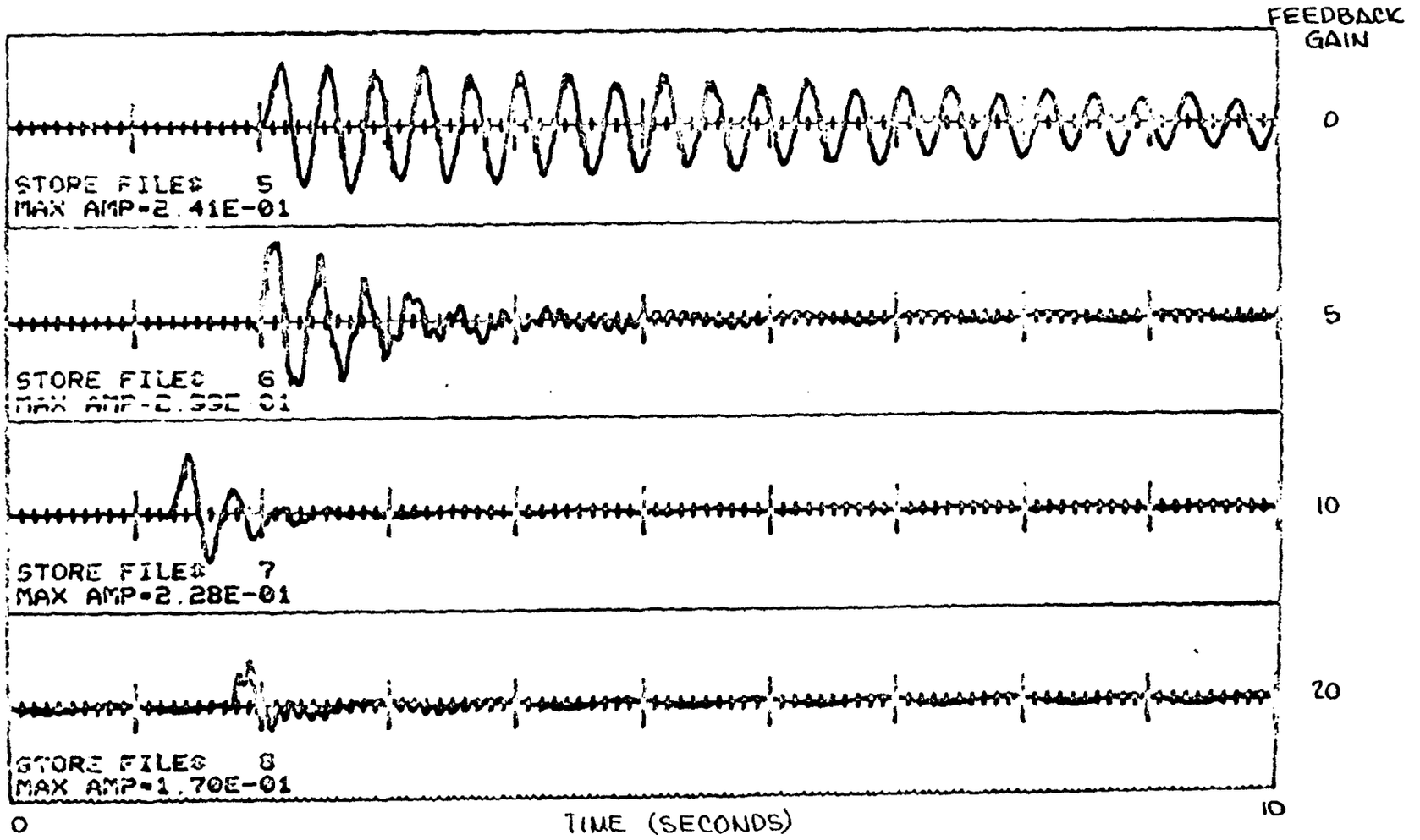

Fig. 7 Low Authority Control TOYSAT Tip Acceleration (G's) Response to Impact Excitation

with the double roll-off at 18.9 Hz. The signal is then multiplied by some gain, and input to the linear actuators. A block diagram of the system is shown in Fig. 4. Rather than picking the gains through the use of an analytical model, the testing capabilities of the Modal Lab were used. A sine sweep was performed to obtain a Bode plot of the transfer function between the output (the smoothed rate signal) and the input (the signal to the linear actuators). The Bode plot is shown in Fig. 5. Classical techniques were then used to predict the highest gain which would yield stability. The prediction was a gain of 10. Figures 6 and 7 show the result of the closed loop system acting on an excited TOYSAT. The gains were varied from 0 to 20. Because of the rate-feedback nature of the feedback loop, the angular displacement history exhibits some drift, however the tip acceleration histories show significant damping. The resulting modal dampings are shown in Table 2.

6.3.4 High Authority Control

The final TOYSAT experiment is a test of both Modern Modal Control and digital control. Measurements of the tip accelerations and the central angular deflection are processed by the PDP 1145 digital computer to provide estimates of the instantaneous modal amplitudes. These estimates are then multiplied by gains and fed back to the linear actuators. In addition to the PDP 1145, analog to digital and digital to analog converters are used to convert the measurement signals and the control commands respectively. Before the measurements are converted to digital signals, they are passed through a 100 Hz eight pole Butterworth filter which acts as an anti-aliasing filter. Also, before the commands are fed to the linear actuators, they are smoothed by a similar filter.

The formulation of the estimator and controller is shown in Figs. 8 and 9. The method used for dealing with the acceleration measurements makes the filter sub-optimal. The optimal, or Kalman formulation, is applicable only when measurement and state disturbances are uncorrelated, which is not the case here. The delay caused by the two Butterworth filters was quite significant, amounting to four time steps. The usual way of dealing with this sort of delay

Table 2

TOYSAT LOW AUTHORITY CONTROL EXPERIMENTAL RESULTS

Mode Description	Resonant Frequency (Hz)	Viscous Damping (%)	Feedback Gain, K
	f_c = 10.5 Hz		
First Asymmetric	2.600	0.3	0
	2.707	8.3	10
	2.714	18.7	20
Second Symmetric	8.97	2.3	0
	9.39	1.4	10
	9.00	1.2	20
Second Asymmetric	9.37	1.6	0
	9.56	2.5	10
	9.60	3.4	20
	f_c = 18.9 Hz		
First Symmetric	2.60	0.3	0
	2.63	4.4	10
Second Symmetric	8.97	2.3	0
	8.99	2.8	10
Second Asymmetric	9.37	1.6	0
	9.52	2.7	10

requires augmenting the state vector. Speed limitations on the PDP prevent this alternative. A simpler approach is used; it's described by Fig. 10.

The performance of this digital regulator is shown in Figs. 11, 12, and 13. The TOYSAT was manually excited, then the controller was turned on. Most of the tip acceleration dies out within one second – much faster than with the Low Authority controller. There is some drift apparent in the angular displacement. This is probably caused by the poor DC response of the linear actuators. Figures 14, 15, and 16 show the output of the estimator which was used to generate the actuator commands.

$$\dot{x}_N = Fx_N + Gu_N + \Gamma_c \omega$$

$$z_N = H_1 x_N + H_2 \dot{x}_N + v$$

$$x_{N+1} = \Phi x_N + \Delta u_N + \Gamma \omega$$

THEREFORE

$$\hat{x}_{N+1} = (\Phi - KH_1 - KH_2 F)\hat{x}_N + (\Delta - KH_2 G)u_N + Kz_N$$

$$u_{N+1} = C\hat{x}_{N+1}$$

Fig. 8 High Authority Control Formulation

$$\hat{X}_N = \begin{Bmatrix} \theta \\ \dot{\theta} \\ q_{f_1} \\ \dot{q}_{f_1} \\ q_{f_2} \\ \dot{q}_{f_2} \end{Bmatrix} \quad ; \quad z = \begin{Bmatrix} \frac{D_2 - D_1}{8.5} \\ \frac{\ddot{y}_2 - \ddot{y}_1}{2} \end{Bmatrix} \quad ;$$

U = TORQUE COMMAND
C = CONTROL MATRIX
K = FILTER MATRIX

$$; \quad G = \begin{Bmatrix} 0 \\ \frac{1}{J} \\ 0 \\ \eta_1 \\ 0 \\ \eta_2 \end{Bmatrix}$$

$$A = \begin{Bmatrix} \frac{\Delta t^2}{2J} \\ \frac{\Delta t}{J} \\ \frac{\eta_1}{\omega_1^2}(1 - CW_1) \\ \frac{\eta_1}{\omega_1}(SW_1) \\ \frac{\eta_2}{\omega_2^2}(1 - CW_2) \\ \frac{\eta_2}{\omega_2}(SW_2) \end{Bmatrix}$$

$$H_1 = \begin{bmatrix} 1 & 0 & \frac{\phi_1(0)}{b} & 0 & \frac{\phi_2(0)}{b} & 0 \\ 0 & 0 & 0 & 0 & 0 & 0 \end{bmatrix}$$

$$H_2 = \begin{bmatrix} 0 & 0 & 0 & 0 & 0 & 0 \\ 0 & R & 0 & \phi_1(\ell) & 0 & \phi_2(\ell) \end{bmatrix}$$

$$F = \begin{bmatrix} 0 & \Delta t & 0 & 0 & 0 & 0 \\ 0 & 1 & 0 & 0 & 0 & 0 \\ 0 & 0 & CW_1 & \frac{SW_1}{\omega_1} & 0 & 0 \\ 0 & 0 & -\omega_1 SW_1 & CW_1 & 0 & 0 \\ 0 & 0 & 0 & 0 & CW_2 & \frac{SW_2}{\omega_2^2} \\ 0 & 0 & 0 & 0 & -\omega_2 SW_2 & CW_2 \end{bmatrix}$$

$$\Phi = \begin{bmatrix} 0 & 1 & 0 & 0 & 0 & 0 \\ 0 & 0 & 0 & 0 & 0 & 0 \\ 0 & 0 & 0 & 1 & 0 & 0 \\ 0 & 0 & -\omega_1^2 & 0 & 0 & 0 \\ 0 & 0 & 0 & 0 & 0 & 1 \\ 0 & 0 & 0 & 0 & -\omega_2^2 & 0 \end{bmatrix}$$

$$\eta_i = \frac{\phi_i(0)}{2 m_2 b} \qquad CW_i = \cos \omega_i \Delta t \qquad SW_i = \sin \omega_i \Delta t$$

b = 7.875 INCH
R = 72.125 INCH
J = 135.05 LB SEC^2/IN
m_2 = .0104 LB SEC^2/IN
$\phi_1(0)$ = .251 $\quad \phi_1(\ell)$ = -.499
$\phi_2(0)$ = .127 $\quad \phi_2(\ell)$ = .359
$\omega_1 = 2\pi(2.66) \quad \omega_2 = 2\pi(9.91)$

Fig. 9 High Authority Control Formulation

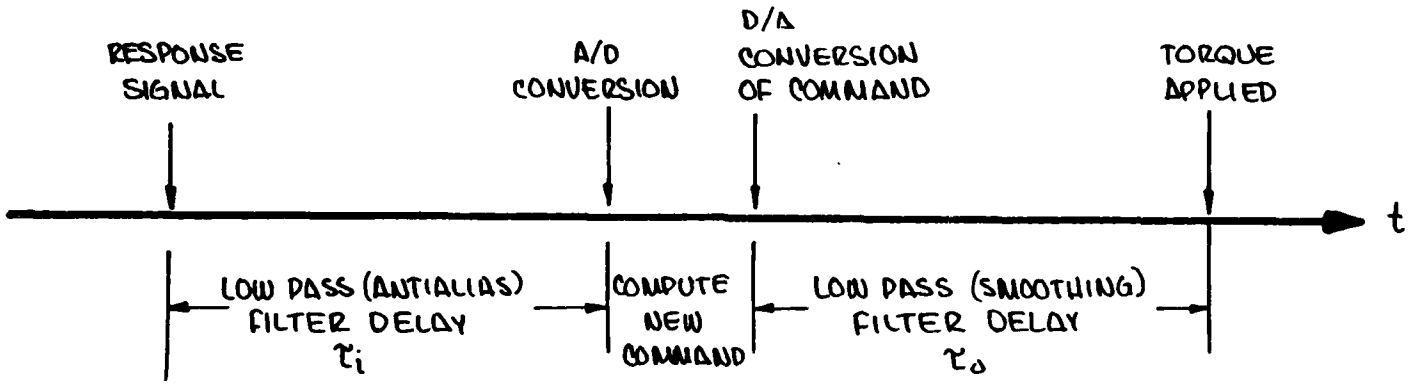

$$\text{FILTER DELAY} = \frac{N}{8 f_c}$$

N = NUMBER OF POLES IN FILTER
f_c = FILTER CORNER FREQUENCY (Hz)

APPROXIMATE CORRECTION FOR FILTER DELAY

$$C' = C\Phi^{\text{INT}\left(\frac{\tau_i + \tau_o}{\Delta t}\right)}$$

$$u_{NM} = C' \hat{x}_{N+1}$$

Fig. 10 Group Delay

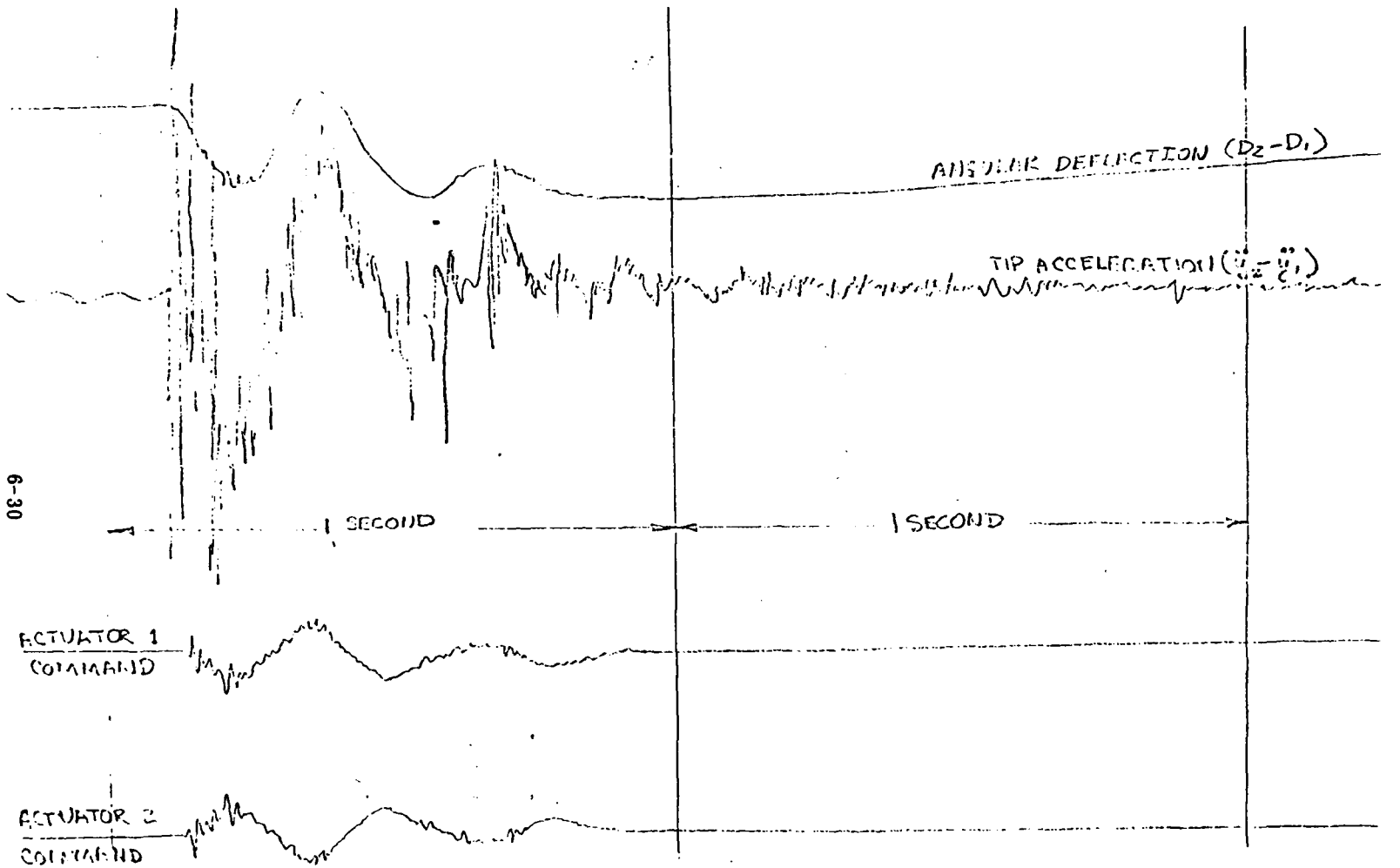

Fig. 11 Digital High Authority Control of Rigid Body and First Two Asymmetric Modes of TOYSAT Specimen

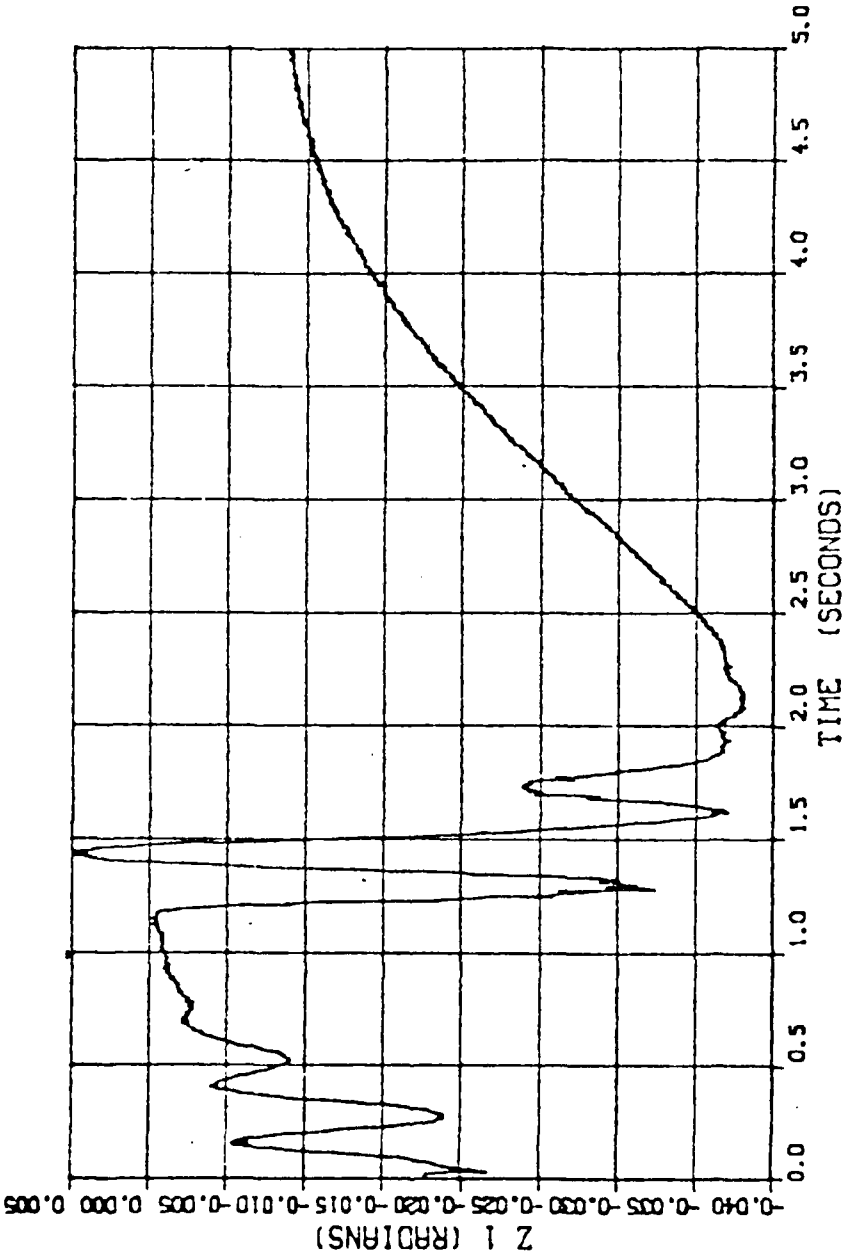

Fig. 12 Experimental Angular Deflection

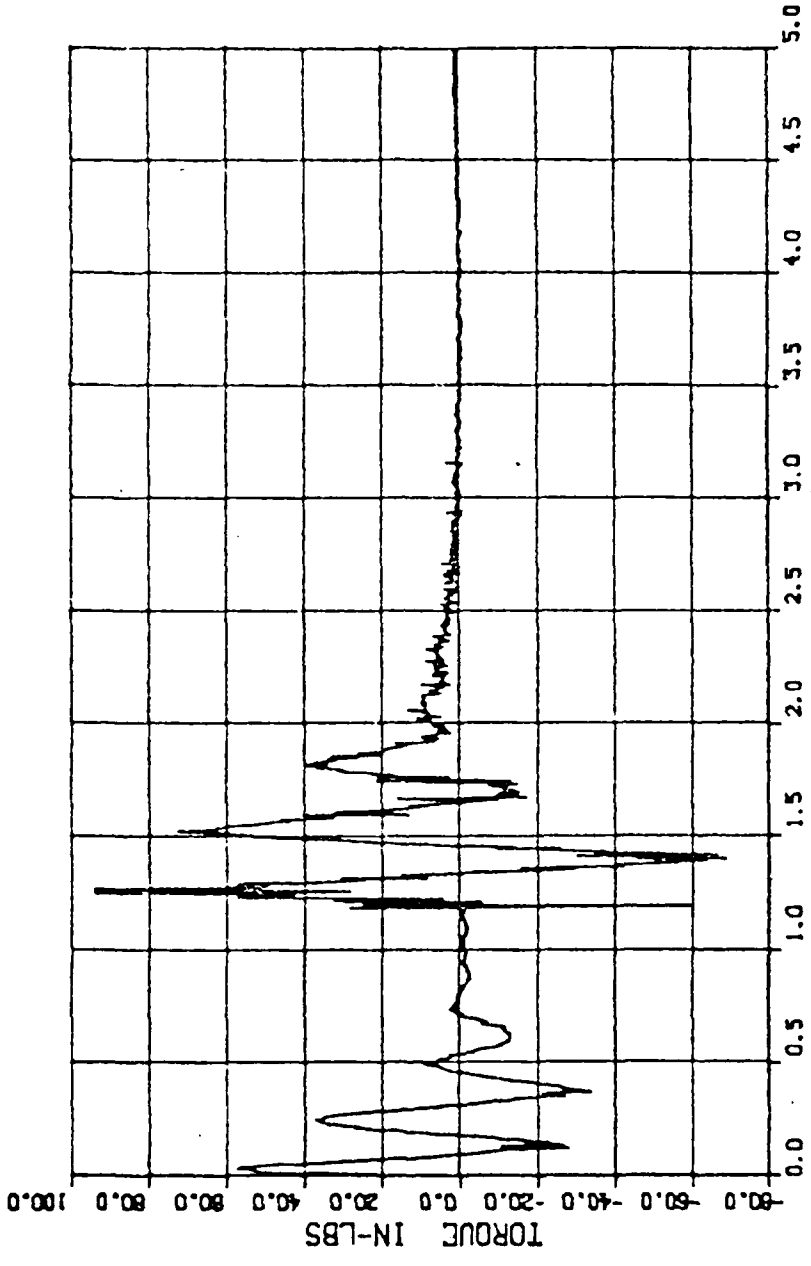

Fig. 13 Torque Command

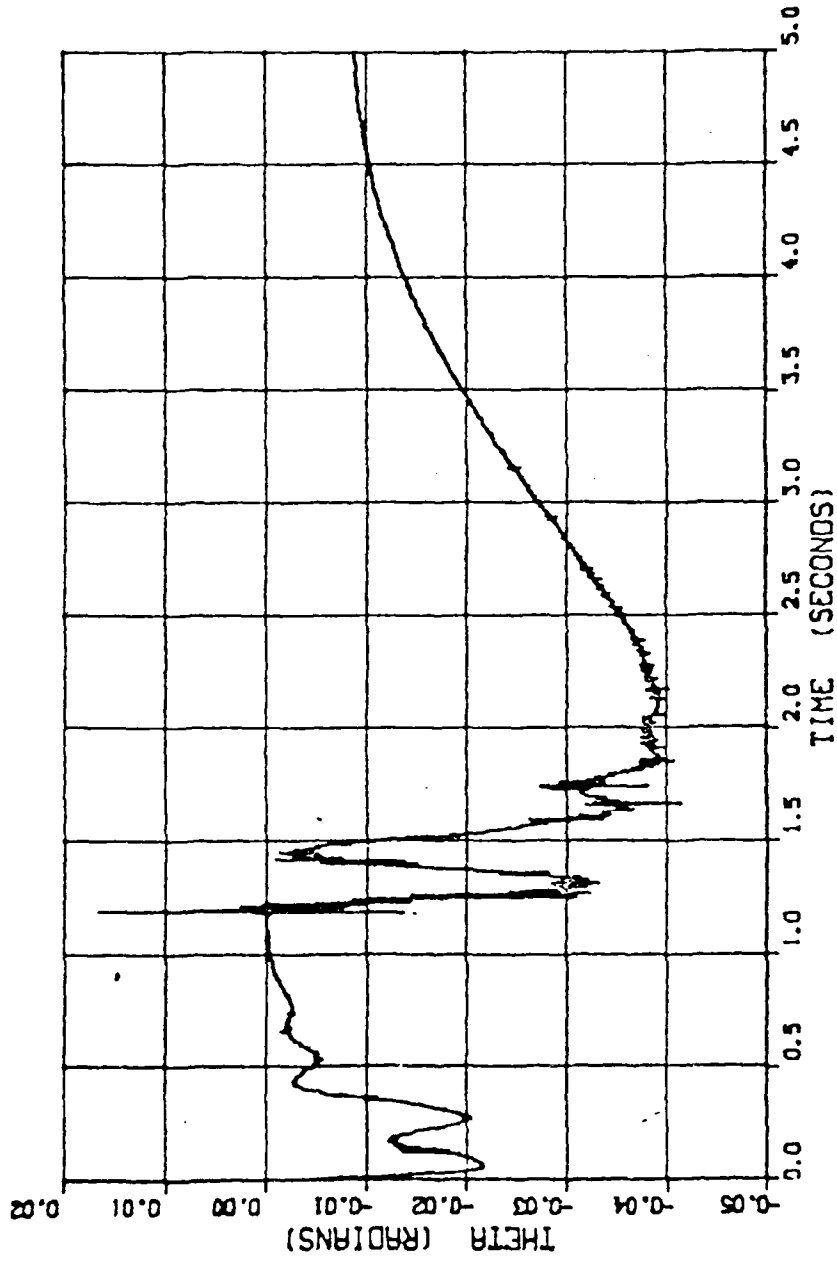

Fig. 14 Angular Displacement State

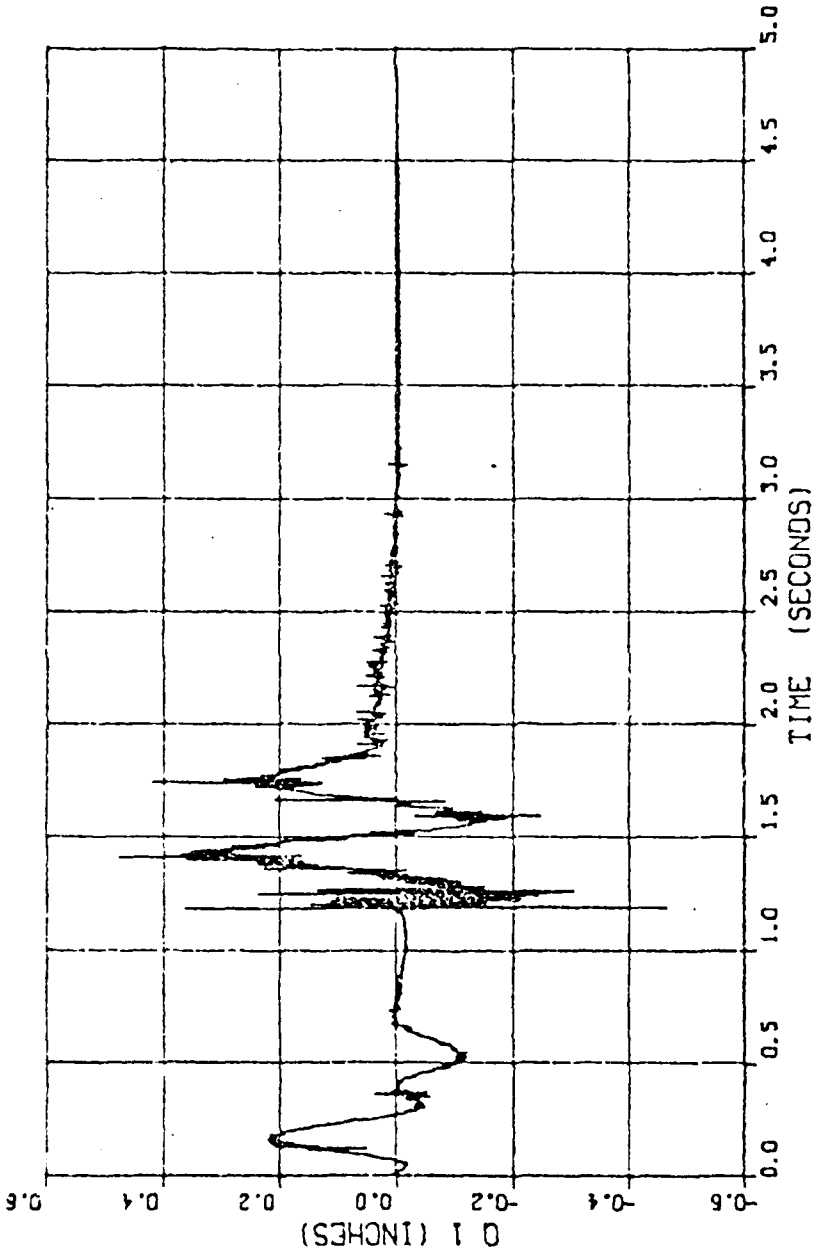

Fig. 15 Mode 1 Displacement State

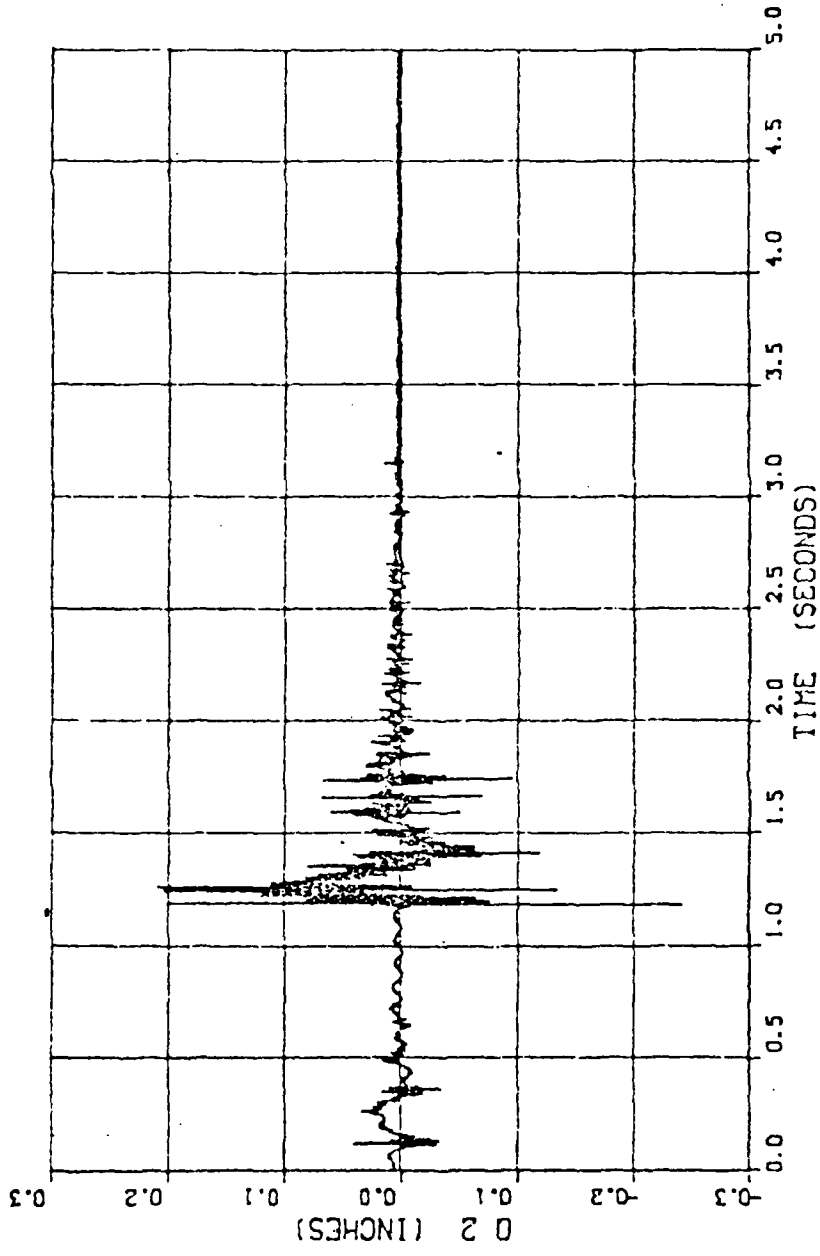

Fig. 16 Mode 2 Displacement State

The preceding results were generated rather quickly. It is anticipated that careful tuning of the gains could result in even better damping of the modal disturbances.

6.4 MICROVIBRATION SENSING

6.4.1 Introduction

A He-Ne laser Vibration Sensor has been developed which features a digital output for computational convenience, and which complements conventional vibration sensors (i.e. accelerometers) by sensing vibratory events at low frequencies from DC to beyond 50 Hz. Vibration amplitude resolution of the sensor is 0.08 μm; maximum amplitude and frequency product is presently limited to 0.05 m·Hz for 2 MHz electronic bandwidth. For example, the maximum measurable vibration amplitude for a 25 Hz vibration is 2 mm. The time delay of the sensor output to the actual vibration is less than 1 μsec which is nearly perfect for measuring the dynamics of structures and vibration sensing for the dynamic damping of structures (active control of structures). By electronically splitting the laser beam using a Bragg cell it is possible to simultaneously sample and hence monitor a large number of points to which retroreflectors have been affixed. Although the laboratory Vibration Sensor employed but two channels, it exhibited the basis for continuously sensing more than 50 independent vibrating targets.

The Vibration Sensor employs a low power He-Ne laser and two Bragg cells, one to provide a heterodyne offset frequency for use as a local oscillator, the other for generating multiple beams for various targets. Optical path variations due to the vibratory motion of each target is measured by comparing zero-crossings of the local oscillator signal with those of each target, identifiable by a specific Bragg frequency. The various differential zero-crossings provide the basis for the digital output of the Vibration Sensor. Experimental results compare well with theoretical predictions.

6.4.2 Theory

The Vibration Sensor conceptual layout diagram is illustrated in Fig. 1. The first Bragg cell translates the laser output frequency from ν_o to $\nu_o + \nu_a$. The frequency translated beam is directed by the second Bragg cell to two target retroreflectors which correspond to two driving frequencies ν_1 and ν_2, respectively. The laser beam incident upon the channel 1 target at range y_1 has a frequency $\nu_o + \nu_a + \nu_1$ which is different from frequency $\nu_o + \nu_a + \nu_2$ for the laser beam on channel 2 target at range $y_2(t)$. The returning signals $\nu_o + \nu_a + \nu_1 + 2\dot{y}_1/\lambda$ and $\nu_o + \nu_a + \nu_2 + 2\dot{y}/\lambda$ (where λ is the laser wavelength) are being shifted in frequency, when passed through the second Bragg cell again, by ν_1 and ν_2, respectively. A photodiode detector is used to sense the heterodyne beat between the optical local oscillator (LO) beam, which is derived from the laser output directly, and the vibration sensing beams.

The electric field of the laser beam on the photo-detector from channel 1 and channel 2 targets can be expressed as

$$\begin{aligned} E_s &= E_{s1} + E_{s2} \\ &= E_1 \exp \left\{ i \left[2\pi (\nu_o + \nu_a + 2\nu_1) t + 4\pi y_1 (t)/\lambda \right] \right\} \\ &\quad E_2 \exp \left\{ i \left[2\pi (\nu_o + \nu_a + 2\nu_2) t + 4\pi y_2 (t)/\lambda \right] \right\} \end{aligned} \tag{1}$$

The electric field of the optical LO can be expressed as

$$E_L = E_\ell \exp \left\{ i\, 2\pi\, \nu_o t \right\} \tag{2}$$

The resultant electric field on the photo detector is the sum of equations (1) and (2) or

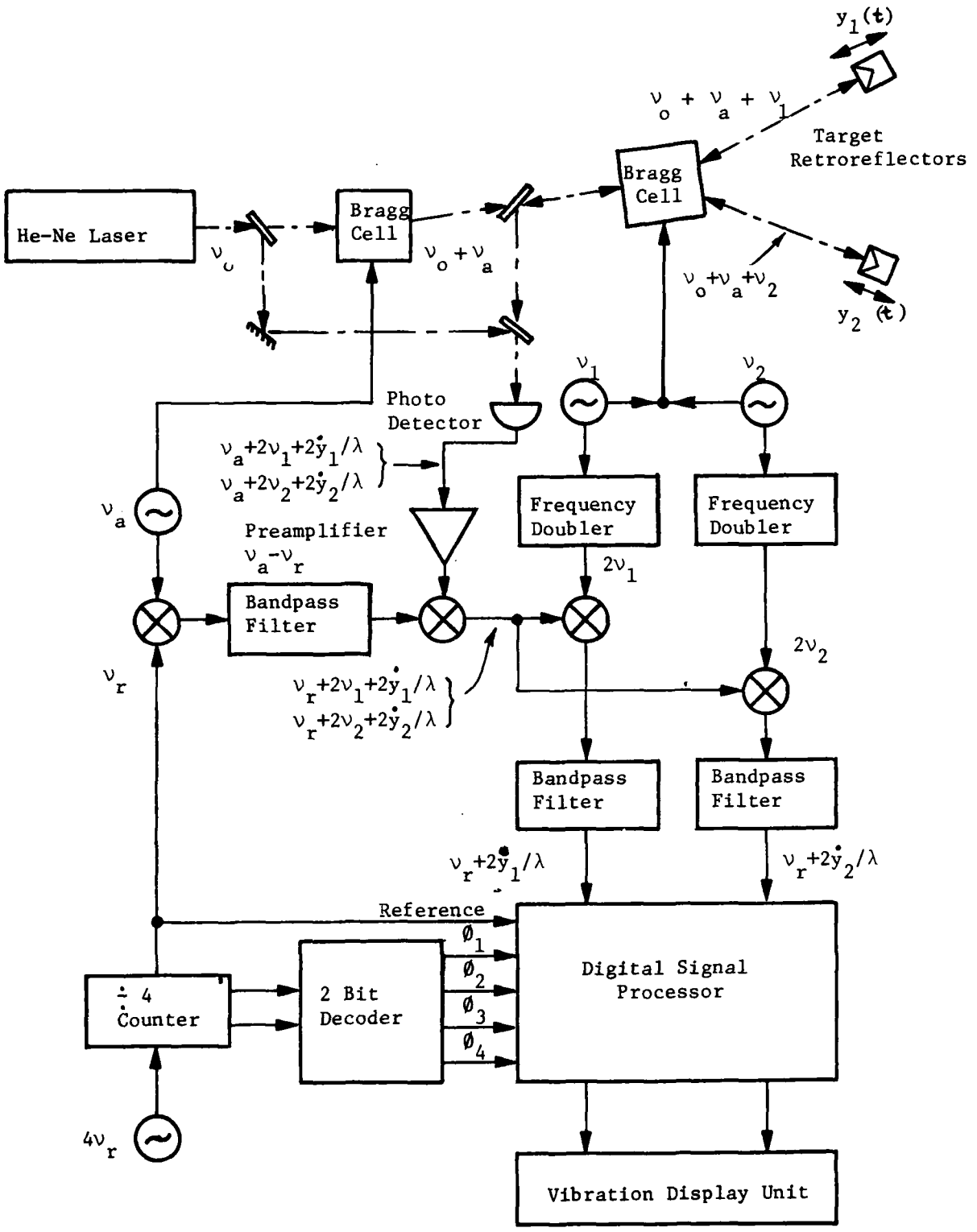

Fig. 1 Vibration Sensor (2-Channel) Conceptual Layout Diagram

$$E = E_s + E_L = E_1 \exp\left\{i\left[2\pi(\nu_o + \nu_a + 2\nu_1)t + 4\pi y_1(t)/\lambda\right]\right\} + E_2 \exp\left\{i\left[2\pi(\nu_o + \nu_a + 2\nu_2)t + 4\pi y_2(t)/\lambda\right]\right\} + E_\ell \exp\left\{i\, 2\pi\nu_o t\right\} \quad (3)$$

Optical power received by the photodetector is proportional to the product of equation (3) and its complex conjugate or

$$P \alpha EE^* = E_1^2 + E_2^2 + E_\ell^2 = 2E_1 E_\ell \cos\left[2\pi(\nu_a + 2\nu_1)t + 4\pi y_1(t)/\lambda\right] + 2E_2 E_\ell \cos\left[2\pi(\nu_a + 2\nu_2)t + 4\pi y_2(t)/\lambda\right] + 2E_1 E_2 \cos\left[4\pi(\nu_1 - \nu_2)t + 4\pi y_1(t)/\lambda - 4\pi y_2(t)/\lambda\right] \quad (4)$$

Since $E_\ell >> E_1, E_2$, equation (4) can be simplified to

$$P = P_1 + P_2 + P_\ell + P_{s1} + P_{s2}$$

where

P_1, P_2 = DC component of signal power

P_ℓ = Optical LO power $>> P_1, P_2$

$$P_{s1} = 2\sqrt{P_1 P_\ell}\cos\left[2\pi(\nu_a + 2\nu_1)t + 4\pi y_1(t)/\lambda\right] \quad (5)$$

$$P_{s2} = 2\sqrt{P_2 P_\ell}\cos\left[2\pi(\nu_a + 2\nu_2)t + 4\pi y_2(t)/\lambda\right] \quad (6)$$

The AC component of photo current is

$$I_s = I_{s1} + I_{s2} \quad (7)$$

$$= \frac{\eta q}{h\nu}(P_{s1} + P_{s2})$$

$$= \frac{2\eta q}{h\nu}\left\{\sqrt{P_1 P_\ell}\cos\left[2\pi(\nu_a + 2\nu_1)T + 4\pi y_1(t)/\lambda\right] + \sqrt{P_2 P_\ell}\cos\left[2\pi(\nu_a + 2\nu_2)t + 4\pi y_2(t)/\lambda\right]\right.$$

Here we have used equation (6) and (7),

where

η = quantum efficiency of the photo diode detector
q = charge of electron
$h\nu$ = laser photon energy

The mean square noise current can be approximated as

$$\overline{I^2}_n \approx B\left(\frac{2\eta q^2}{h\nu} P_\ell + \frac{4kTa}{R_L}\right) \tag{8}$$

where

B = electronic bandwidth
k = Boltzman's constant
T_a = equivalent temperature of preamplifier
R_L = resistance of detector load resistor

The power signal-to-noise ratio of the sensor is

$$\left(\frac{S}{N}\right)_1 = \frac{\overline{I^2}_{s1}}{\overline{I^2}_N} \approx \frac{2\left(\frac{\eta q}{h\nu}\right)^2 P_1 P_\ell}{B\left(\frac{2\eta q^2}{h\nu} P_\ell + \frac{4kT_a}{R_L}\right)} \tag{9}$$

for channel 1 target and

$$\frac{S}{N} = \frac{\overline{I^2}_{s2}}{\overline{I^2}_N} \approx \frac{2\left(\frac{\eta q}{h\nu}\right)^2 P_2 P_\ell}{B\left(\frac{2\eta q^2}{h\nu} P_\ell + \frac{4kT_a}{R_L}\right)} \tag{10}$$

for channel 2 target.

Assume a 0.4 mW single frequency He-Ne laser is used to measure vibrations of 50 targets, the signal-to-noise ratio of each channel can be calculated according to the typical values

$$\eta = 0.8$$
$$q = 1.6 \times 10^{-19} \text{ coul}$$
$$h\nu = 3.13 \times 10^{-19} \text{ joul}$$
$$P_\ell = 10^{-4} \text{ watt}$$
$$P_1 = 5 \times 10^{-9} \text{ watt}$$
$$B = 2 \times 10^{6} \text{ Hz}$$
$$k = 1.38 \times 10^{-23} \text{ j/°k}$$
$$Ta = 5\ 96 \text{°k (for an amplifier with 3 dB noise figure)}$$
$$R_L = 50 \text{ Ohms}$$

Yields the result according to Equation (9)

$$\left(\frac{S}{N}\right)_1 = \frac{2\left(\frac{0.8 \times 1.6 \times 10^{-19}}{3.13 \times 10^{-19}}\right) \times 5 \times 10^{-9} \times 10^{-4}}{2 \times 10^{6}\left(\frac{2 \times 0.8 \times 2.56 \times 10^{-38} \times 10^{-4}}{3.13 \times 10^{-9}} + \frac{4 \times 1.38 \times 10^{-23} \times 5\ 96}{50}\right)} = 125$$

This signal-to-noise ratio is more than what is required by the digital signal processor to process the signal. For a constant signal-to-noise ratio, the maximum number of channels can be measured by the sensor is proportional to the laser output power.

The phase modulation expression in Equation (1) for channel 1 signal $\exp\left\{i\left[2\pi(\nu_o + \nu_a + 2\nu_1)\,t + 4\pi y_1(t)/\lambda\right]\right\}$ can also be expressed in a frequency modulation form such as $\exp\left\{i\left[2\pi(\nu_o + \nu_a + 2\nu_1 + 2\,y_i(t)/\lambda)\,t + \theta_1\right]\right\}$, where θ_1 is constant. The Doppler frequency, $\nu_{d1} = 2\dot{y}_1(t)/\lambda$, for a sinusoidal vibration can be written as $\nu_{d1} = 4\pi\nu_{m1}y_{d1}\sin(2\pi\nu_{m1}t)/\lambda$, where ν_{m1} is the modulation frequency and y_{d1} is the amplitude of vibration. For a 2 MHz electronics bandwidth, the peak Doppler frequency is limited to 1 MHz or $4\pi\nu_{m1}y_{d1}/\lambda = 10^6$ Hz or $\nu_{m1}y_{d1} = 0.05$ m·Hz. Therefore, the maximum amplitude and frequency product of the vibratory targets is limited to 0.05 m·Hz for 2 MHz electronic bandwidth.

In order to separate two target signals from the photodetector output we can first mix with cos $[2\pi(\nu_a - \nu_r)\, t]$ to obtain cos $[2\pi(2\nu_1 + \nu_r)\, t + 4\pi y_1/\lambda]$ and cos $[2\pi(2\nu_2 + \nu_r)\, t + 4\pi y_2/\lambda]$, and then mix these with cos $[2\pi(2\nu_1)\, t]$ to obtain cos $\left[2\pi\nu_r\, t + 4\pi y_1/\lambda\right]$ or with cos $[2\pi(2\nu_2)\, t]$ to obtain cos $\left[2\pi\nu_r\, t + 4\pi y_2/\lambda\right]$.

Here ν_r is the frequency of the reference signal which is 4 MHz in this case. The signal cos $[2\pi(\nu_a - \nu_r)\, t]$ is a result of mixing the reference signal with the first Bragg cell driving signal and bandpassing at $\nu_a - \nu_r$. Signals cos $[2\pi(2\nu_1)\, t]$ and cos $[2\pi(2\nu_2)\, t]$ are derived from frequency doublers and in turn from oscillators at frequencies ν_1 and ν_2, respectively. Signals of both channels are centered at frequency ν_r but separately passed by each bandpass filter. The digital signal processor takes the reference signal and the output of two channels from the bandpass filters to process the vibration information of targets. By comparing the zero-crossings of cos $(2\pi\nu_r t)$ with cos $(2\pi\nu_r t + 4\pi y_1/\lambda)$ and cos $(2\pi\nu_r t + 4\pi y_2/\lambda)$ the displacement Δy_1 and Δy_2 can easily be determined. For every zero-crossing count difference there is a phase change of 2π radians or a displacement of $\lambda/2 = 0.32\ \mu m$. If four reference signals cos $(2\pi\nu_r t)$, cos $(2\pi\nu_r t + \pi/2)$, cos $(2\pi\nu_r t + \pi)$, and cos $(2\pi\nu_r + 3\pi/2)$ are used for zero-crossing comparison, the displacement resolution would be $\lambda/8$ or $0.08\ \mu m$.

6.4.3 Digital Signal Processor

A digital electronic circuit has been designed to measure the total phase difference between the reference signal (4 MHz) and the phase modulated heterodyne signal returning from targets. A zero-crossing counting technique is used to determine the phase difference in a multiple of 2π radians which corresponds to a displacement resolution of about 0.32 μm. A fine phase measurement system based on the zero-crossing timing has also been built in order to achieve a 0.08 μm resolution.

CLOCK CIRCUIT

All the timing signals needed for the digital circuit are derived from a 16 MHz oscillator. With a 4 bit binary counter and a 4 to 16 line decoder, the clock circuit is capable of generating 16 disjointed clocks. Each of them has a frequency of 1 MHz and pulse width of about 60 ms. The clocks used in the signal processor are illustrated in Fig. 2, where ϕ is used in the coarse phase measurement; ϕ_2, ϕ_2, ϕ_4 together with ϕ_1, are used in the fine phase measurement; ϕ_5 is used as the sampling signal for the output. In addition to the clocks mentioned above, the clock circuit also provide a 4 MHz reference signal for use as the carrier for the phase modulated target signals.

COARSE PHASE MEASUREMENT

The coarse phase measurement circuit consists of a reference channel and as many target channels as needed. Figure 3 shows the functional block diagram for a two-target system. Additional channels can easily be added. As shown in Fig. 3, the reference channel is just a 14 bit binary counter which continuously counts the number of zero-crossings (or the number of 2π radian phase change) of the 4 MHz reference signal. A 14 bit latch samples the content of the counter at the

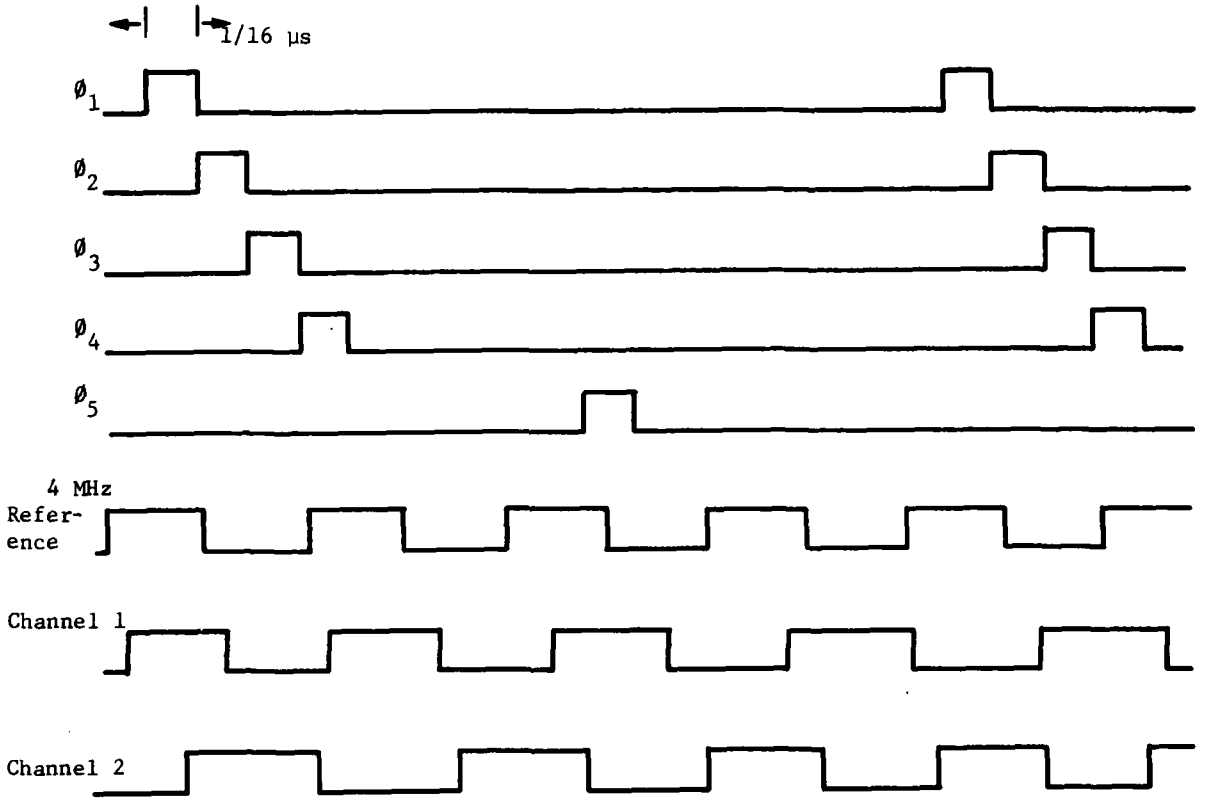

Fig. 2 Vibration Sensor Timing Diagram

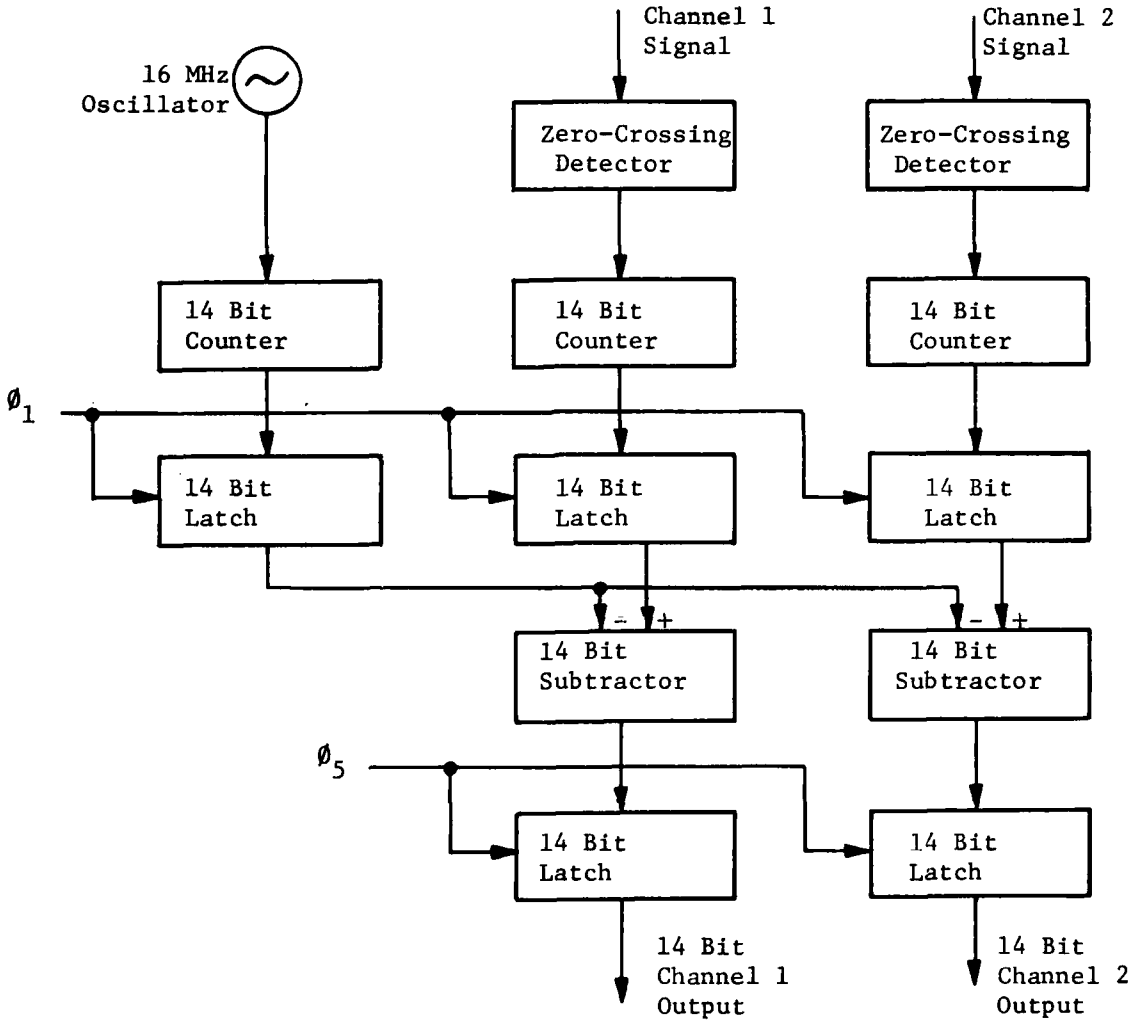

Fig. 3 Vibration Sensor Coarse Phase Measurement System

at the falling edge of clock ϕ_1. The output of the latch corresponds to the total phase change of the reference signal since the beginning of counting process. Signals from each target are first shaped by a zero-crossing detector then passed through a circuit identical to the reference channel to generate a binary number corresponding to the total phase change in the target signal. This number together with the one provided by the reference channel is fed into a binary subtractor to calculate the total phase deviation of the target signal due to the displacement of the target.

FINE PHASE MEASUREMENT

To achieve a phase resolution better than 2π radians, a circuit has been designed to determine the timing of zero-crossing of the target signal. As illustrated in Fig. 4, the least significant bit of the target counter in each coarse system is sampled at 4 different instances which are $\pi/2$ radians apart in terms of 4 MHz frequency. The output of the latches are then processed by a simple logical circuit to determine when the zero-crossing occurs and to encode this information into 2 bits. These two bits together with the 14 bits from the coarse system are sampled at the falling edge of clock ϕ_5 to provide a steady 16 bit output for the vibration sensor system. A graphic simulation of all the input and output signals of the digital signal processor is summarized and shown in Fig. 5

AD-A089 142 LOCKHEED MISSILES AND SPACE CO INC PALO ALTO CA PALO --ETC F/G 22/2
ACOSS THREE (ACTIVE CONTROL OF SPACE STRUCTURES). PHASE I.(U)
MAY 80 M G LYONS, J N AUBRUN, G MARGULIES F30602-79-C-0087
UNCLASSIFIED RADC-TR-80-131 NL

3 OF 3
AD A089142

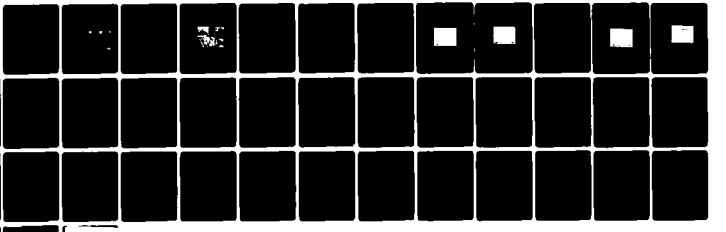

END
DATE FILMED
10-80
DTIC

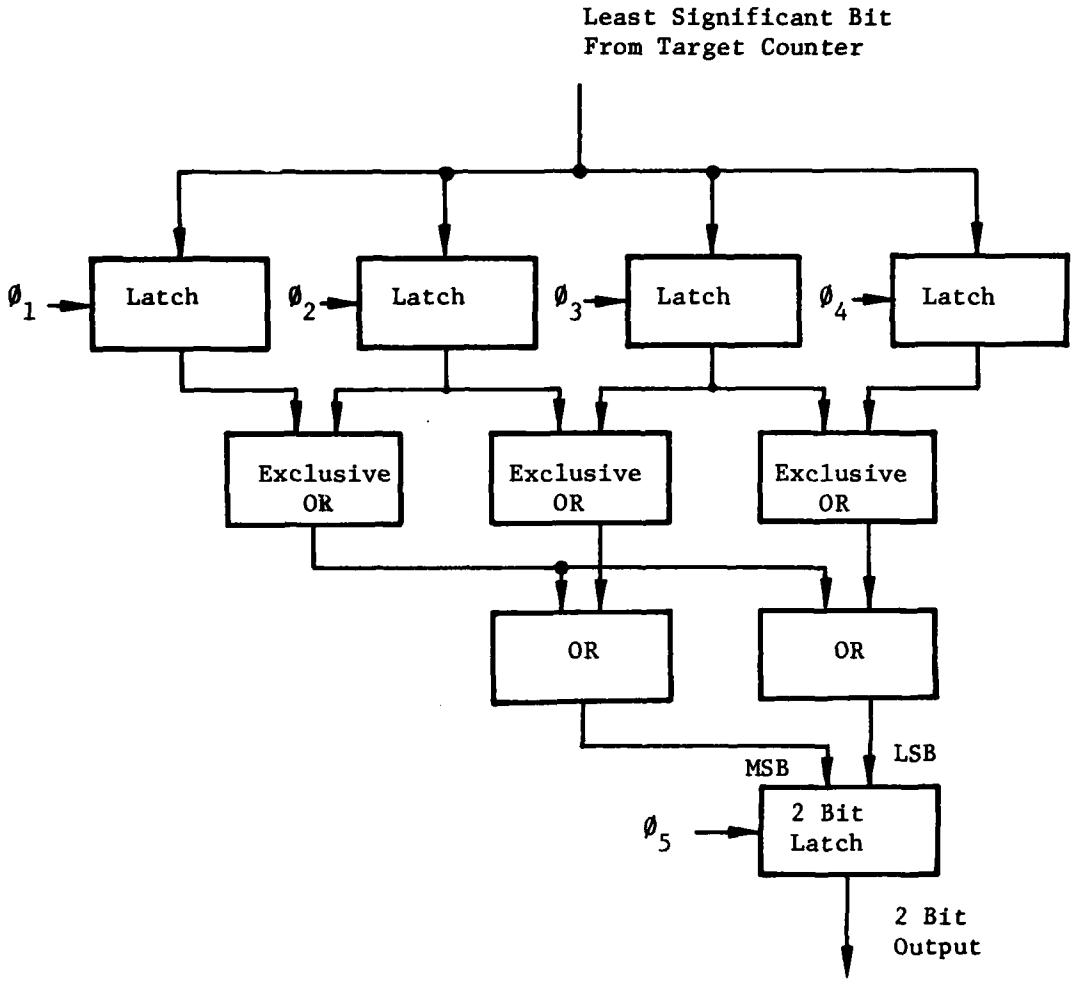

Fig. 4 Vibration Sensor Fine Phase Measurement System

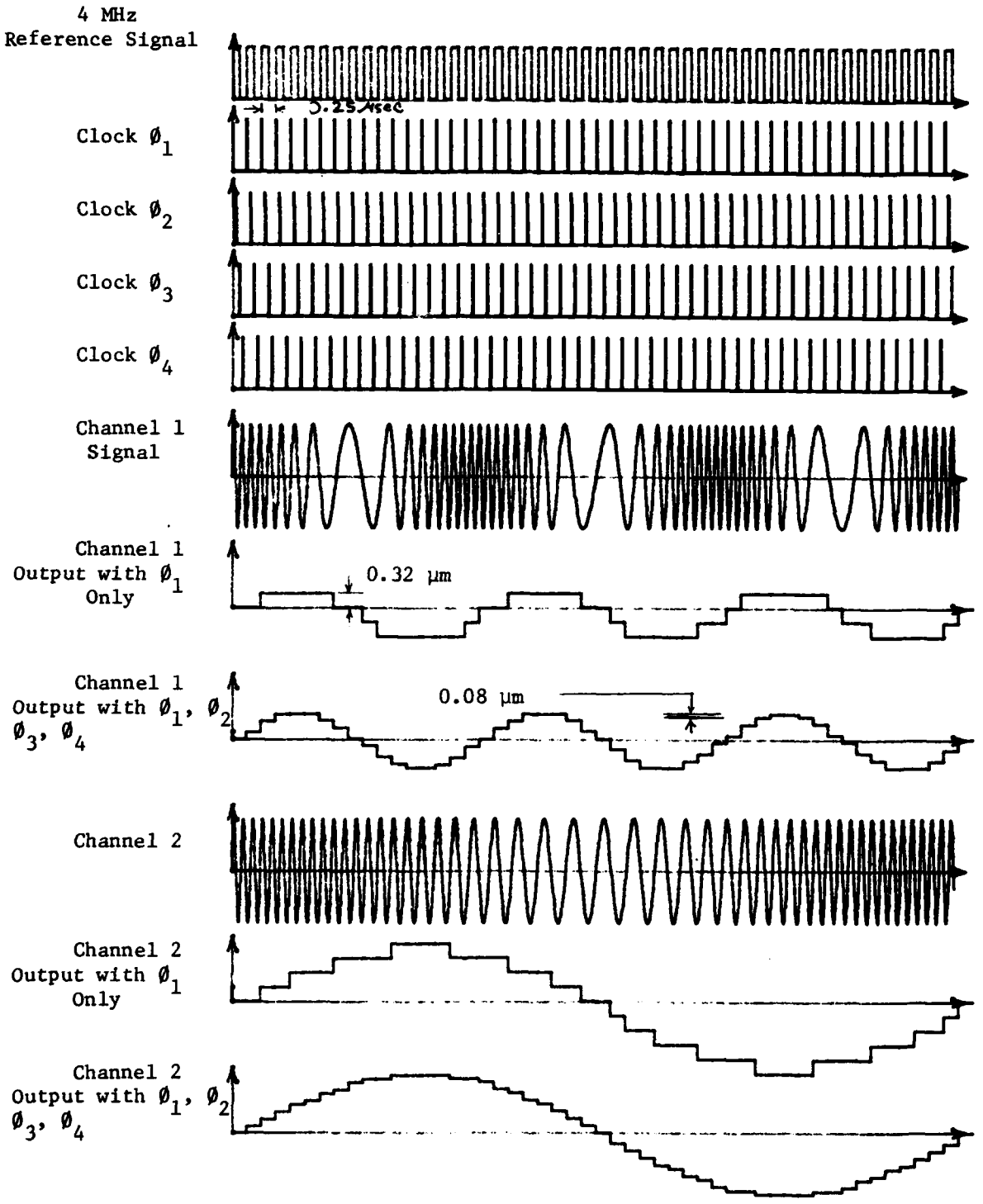

Fig. 5 Vibration Sensor Signal Simulation

6.4.4 Experimental Apparatus

The Vibration Sensor laboratory setup and the breadboard layout diagram are shown in Figs. 6 and 7, respectively. The Channel 1 target is a 1-cm retro-reflector driven by a shaker located on a separate Table 3 meters away from the sensor setup. The Channel 2 target is a PZT driven mirror set on the same platform with other optical components. A Hughes Model 3176H He-Ne laser with 4 mW output at 632.8 nm is used in the system. The reflectivity and transmission of all the beamsplitters used in the system are close to 0.5. The efficiency of the first Bragg cell, ϵ_1, is 0.8. The second Bragg cell efficiency can be expressed as $\epsilon_2 = 0.8/N$, where N is the number of channels. Because the Bragg cell can only take 3 watts RF power to reach 80 percent efficiency, the RF driving power for each channel is 3/N watts. Therefore, the Bragg cell efficiency for each channel is $\epsilon_2 = 0.8/N$. Two cylindrical telescopes are used in conjunction with the Bragg cell to generate a large number of target sensing beams for multiple targets vibration sensing purposes. Only one beam expander is used in Channel 1. The laser beam diameter after the beam expander is approximately 1 cm. The return signal power onto the photodetector can be calculated by

$$\begin{aligned} P_s &\approx P_o \times T_1 \times \epsilon_1 \times T_2 \times \epsilon_2 \times \epsilon_2 \times T_3 \\ &\approx .4 \times 10^{-3} \times 0.5 \times 0.8 \times .08/N \times 0.8/N \times 0.5 \times 0.5 \\ &\approx 0.128 \times 10^{-3}/N^2 \text{ Watt} \end{aligned}$$

where T's and R's are the transmission and reflectance of beamsplitters shown in Fig. 7 and $P_o = 4$ mW is the laser output power. For 50 channels, N = 50, the signal power is $P_s \approx 5 \times 10^{-8}$ Watt for $P_o = 4$ mW or $P_s \approx 5 \times 10^{-9}$ Watt for $P_o = 0.4$ mW. In our experiment N = 2 and the calculated power level is 32×10^{-6} Watt.

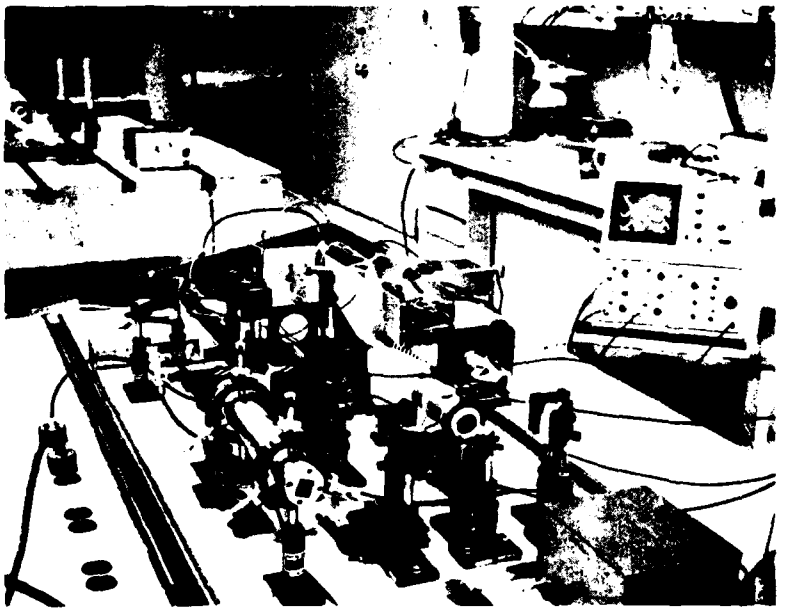

Fig. 6 Vibration Sensor Laboratory Setup

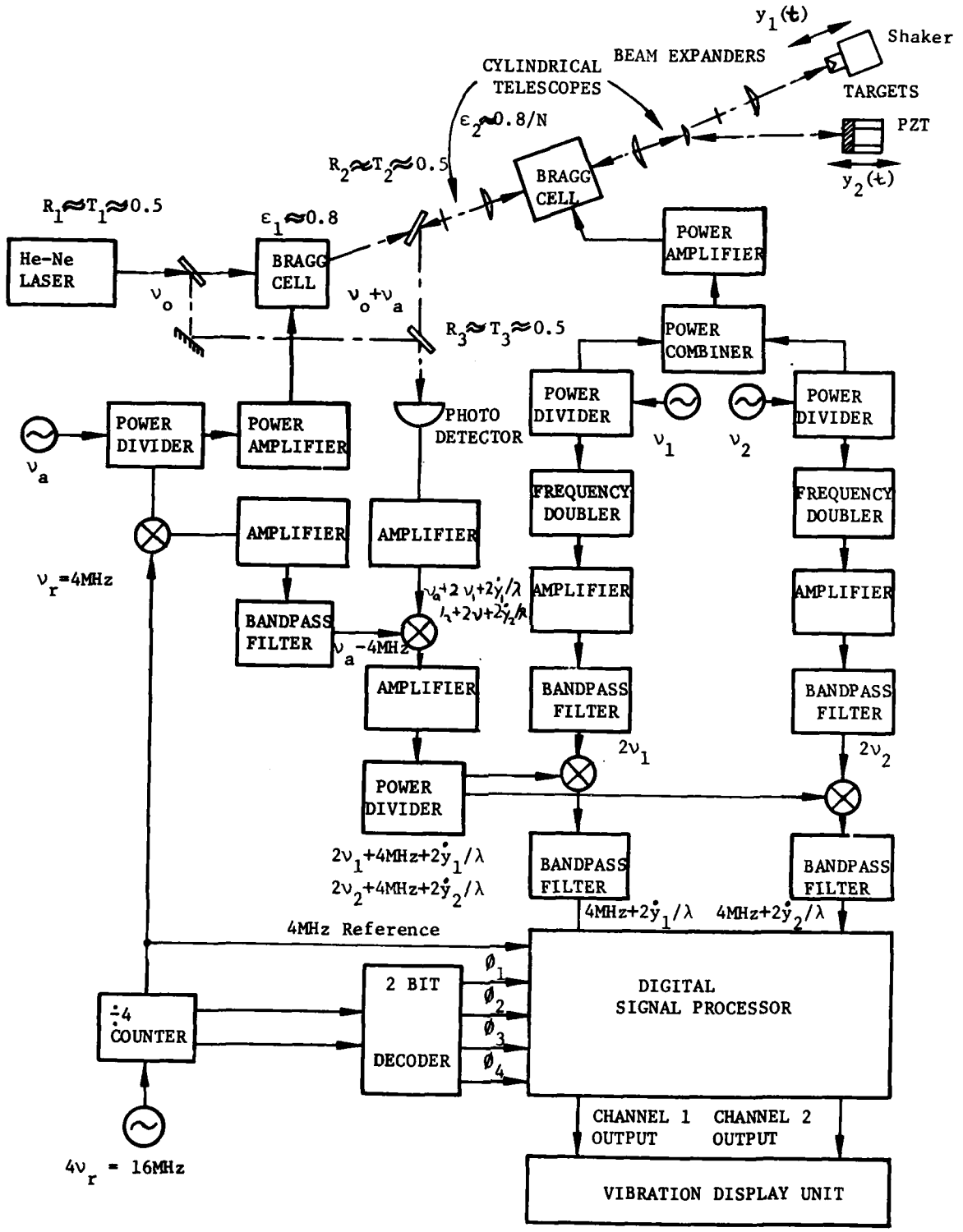

Fig. 7 Vibration Sensor (2-Channel) Breadboard Layout Diagram

The optical LO power onto the detector is $P_\ell = P_o \times R_1 \times R_3$ which is $P_\ell \approx 4 \times 10^{-3} \times 0.5 \times 0.05 = 10^{-3}$ Watt for $P_o = 4$ mW or $P_\ell = 10^{-4}$ Watt for $P_o = 0.4$ mW.

Two K&L Model 5B53-4/2-B/B bandpass filters centered at 4 MHz, one for each channel, are used in the system to restrict the input signal to the digital signal processor to a bandwidth of 2 MHz. A two-channel digital signal processor has been assembled and tested. Due to the availability of digital IC components, we use 16 bits instead of 14 bits in the entire coarse measurement system thus producing two 18 bit outputs. Two 16 bit Digital-to-Analog (D/A) converters are used to convert the lower 16 bits of each output into analog form for the display purpose.

6.4.5 Experimental Results

The oscilloscope trace of the displacement of two vibratory targets is shown in Figs. 8 and 9. In Fig. 8, the upper trace is the sensor output for Channel 1 target vibrating at 30 Hz and an amplitude of 1.5 mm. The middle trace is the sensor output for Channel 2 target which measures a 60 Hz vibration at an amplitude of 0.9 μm. It is noticeable that the "stair-like" waveform is a result of digital signal processing. Each step of the stair represents 0.08 μm displacement of target which is the resolution of the present system. The lower trace represents the driving signal to the PZT for Channel 2 target. Comparing the output of the Vibration Sensor with the driving signal of the target mirror indicates a time delay of about 1 nsec between the sensor output and the actual vibration. Of this, about 500 nsec is contributed by the digital circuitry (between the falling edges of input sampling clock ϕ_1 and output sampling clock ϕ_5), the rest of it is due to the settling time of the D/A converter. Power consumption for the two-channel digital signal processing system is about 10 watts with standard TTL components.

Although the output of the sensor system closely follows the actual vibration in general, we found a large number of glitches presented especially when the amplitude of the vibration is small. These glitches occurs at certain intervals of target displacement corresponding to even 2π, 4π, 6π, and 8π radian phase changes. Most of these glitches have been identified as being caused by the sampling of target signal counters while the counters are changing states. We have done experiments to sense such ill-conditioned triggering cases in the coarse system and delay the latch action whenever it occurs. This scheme seems to be able to eliminate glitches at 2π, 4π, and 6π intervals but those with an 8π interval still remain. At this time no effort is made to identify the cause of this problem. But we feel this can be solved with confidence after a careful examination of the digital signal processing electronics. The DC response of the sensor is shown in

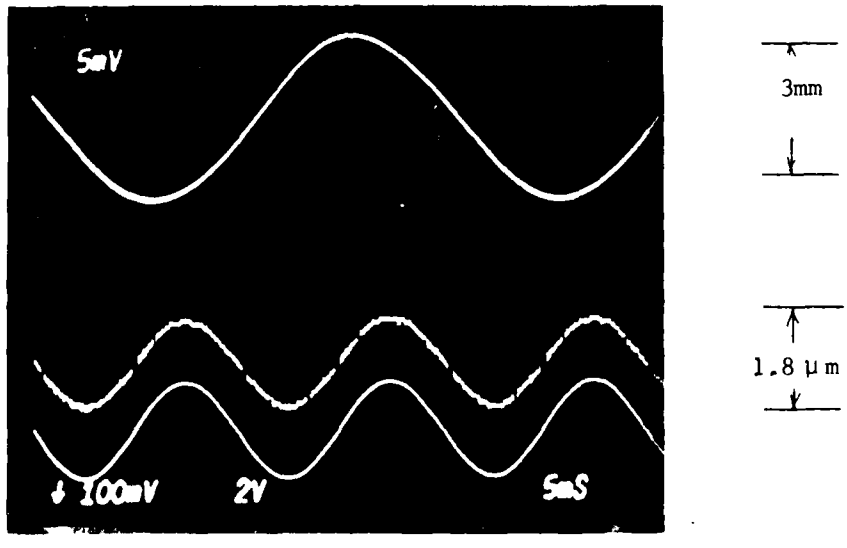

Fig. 8 Vibration Sensor Output for Two Vibratory Targets - Exhibition of Amplitude Range and Sensitivity of Sensor

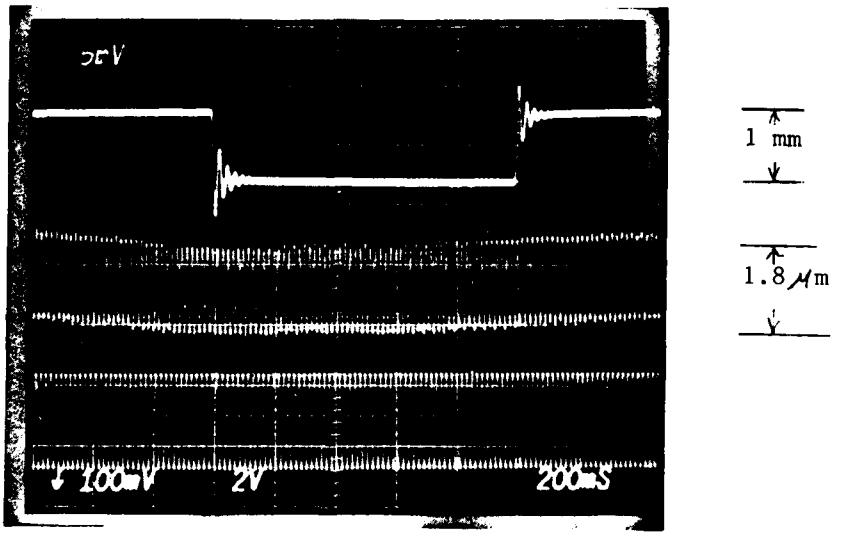

Fig. 9 Vibration Sensor Output for Two Vibratory Targets - Exhibition of AC and DC Response of Sensor

the upper trace of Fig. 9. The only difference between the Fig. 8 and Fig. 9 experiments is the driving voltage applied to the shaker for channel 1 target. In the Fig. 9 experiment, a 0.5 Hz square wave is applied to the shaker. The sensor measures the steady state DC displacement ($\sim$1 mm) as well as the transient behavior of the shaker.

As mentioned earlier, the signal processor provides a 18 bit digital output in 2's complement form. In other words, the output digits represent a decimal number between -131072 to +131071. With the least significant bit corresponding to 0.08 μm in displacement, this means a displacement range from -10.485 mm to +10.485 mm. It is worthwhile to mention that wider range can be achieved by simply using longer words in the signal processing electronics and the only limitation is that the vibration amplitude and frequency product must be under 0.05 m·Hz. Since we are only using the lower 16 bits in the display, the range shown on the oscilloscope is further restricted to -2.62 mm to +2.62 mm. Larger displacement causes a sudden jump from the largest representable value to the lowest value as can be seen in Fig. 10.

A reset button is built in the electronics to signal the beginning of the counting process. Hence the output of the electronics represents the displacement of the target relative to the target position when the reset button is released. At the present time we have no control on the zero displacement position relative to the vibration waveform. This causes a DC component associated with the output of the sensor.

The laser used in the system outputs three longitudinal modes spaced by 500 MHz which is shown in Fig. 11. Although the unstable laser is used in such a sensitive system we can still obtain reasonably good results. Because of the 500 MHz frequency spacing between laser modes and the destructive interference between them, we have observed that for every 30 cm displacement of target along the optical path of the vibration sensing beam there is a node point for the returning signal which limit the full range application of the sensor. The single frequency laser will be a solution to that problem.

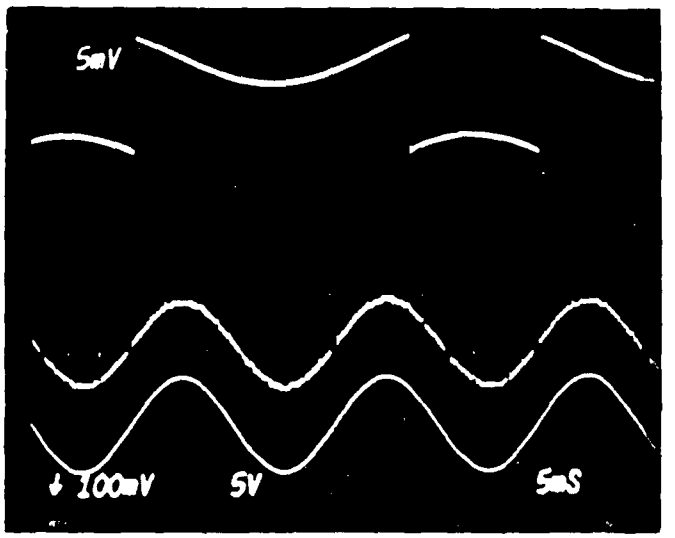

Fig. 10 Output Discontinuity of Vibration Sensor

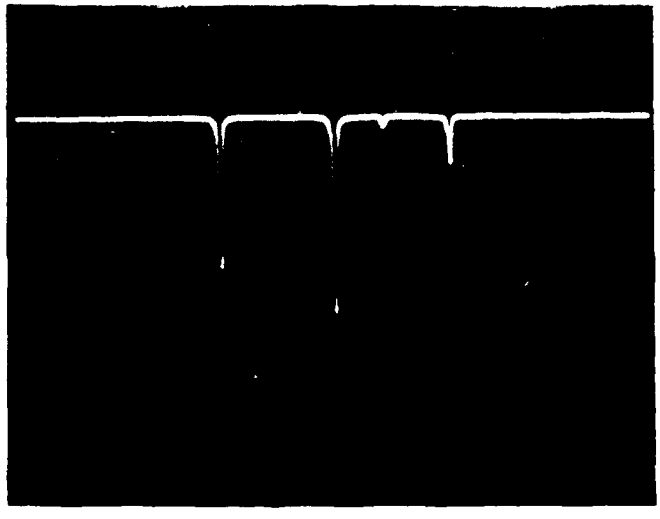

Fig. 11 Optical Spectrum Analyzer Output Shows 3 Longitudinal Modes of the Laser Used in the Vibration Sensor Experiment

6.4.6 Conclusions and Recommendations

After this very limited effort toward the development of the Vibration Sensor, we are satisfied with the outcome of this research. The concept of using zero-crossing counting technique in the sensing of low frequency, small amplitude vibration has been proved. The capability of the sensor for simultaneous sensing of multiple targets and wide frequency and amplitude coverage of the vibration has been demonstrated. The remaining problems which need to be done in the future concerning the Vibration Sensor are listed below:

1. Design and fabricate or purchase a stable single mode single frequency He-Ne laser with an output of 0.4 mW at 632.8 nm.
2. Remove the glitches from the sensor output.
3. Develop a second generation signal processor to handle larger amplitude and frequency range of vibration to provide improved resolution, to automatically adjust the system zero to the center of vibration, and to derive velocity/acceleration information of targets.
4. Incorporate the microcomputer and the graphical display into the system for real time display/control of vibrating targets.
5. Fabricate or purchase compact optics and electronics to minimize the size of the sensor.
6. Procure better quality optics such as cylindrical lenses, beam-splitters, Bragg cells, etc. in order to reduce the optical loss.
7. Verify the minimum required signal-to-noise ration experimentally.
8. Isolate the EMI problem.
9. Develop and demonstrate a 10-channel Vibration Sensor as a basis for the design of sensor with more channels.

Section 7
CONCLUSIONS AND FUTURE WORK

7.1 CONCLUSIONS

The integrated control design methodology presented in the previous sections has significant promise for large space structure applications. The approach is geared towards addressing specific issues such as low damping ratios, truncated modes and finite bandwidth actuators and sensors. The control laws have been optimized for minimal complexity to aid implementation on space based systems. Controller robustness with respect to modeling errors and truncation effects are discussed.

Application of the methodology to three simple structures illustrates that satisfactory closed loop systems can be obtained. The procedure, however, is not automatic but requires iteration based on designer's judgement. The techniques developed minimize the effects of truncation errors on control and observation spillover, but the stability of the closed-loop system must be examined on a case by case basis. It is also the belief of the authors that absolute stability will be impossible to assure with realistic sensors and actuators for unbounded modeling errors.

7.2 FUTURE WORK

The work performed during this phase has set a sound foundation for large space structures control design methodology. Further experience is required with some of the techniques already developed. Certain new methods must also be developed to provide a more complete basis for control design in complex space structures with densely packed modes.

The following specific tasks will aid the development of an integrated control methodology:

(a) The question of mode truncation and reduced order models is of fundamental importance in the study of dynamic systems in general, and large space structures in particular. The roles of system poles, zeros, and residues should be further studied. In addition, projection methods should be examined. The construction of models based on partial observed information (output) should be studied.

(b) The problem of collocated control should be further studied to yield a better understanding of mode controllability through this type of control. Actuators/sensors dynamics and their effect on the design should be considered too.

(c) Robustness properties of the system must be studied for various system operating conditions. For example, actuators, sensors dynamics, structural damping, etc.

(d) The question of actuators and sensors dynamics should also be considered. Sensitivity of actuators/sensors location to their dynamics should be examined.

(e) The concept of frequency-shaped cost functionals and its adaptation to a design tool should be further developed. In particular, a specific guideline for the selection of cost functionals should be developed.

(f) Design of ground based experiments including validation procedures for assuring adequate robustness demonstrations must be investigated further.

(g) Sensor and actuator designs to handle the micro-vibration control problems need further development.

Appendix A
MODAL STRUCTURE OF OSCILLATORY SYSTEMS

The oscillatory system is described by

$$\dot{x}(t) = Ax(t) + Bu(t)$$

where

$$A = \left[\begin{array}{c|c} 0 & I_n \\ \hline -A_o & 0 \end{array}\right] \qquad B = \left[\begin{array}{c} 0 \\ \hline Bu \end{array}\right]$$

and $A_o = A_o^T > 0$.

Let U be the $n \times n$ matrix of eigenvectors of A_o, i.e.,

$$A_o U = U\Lambda.$$

Define $z = Tx$

where

$$T = \left[\begin{array}{c|c} U^{-1} & 0 \\ \hline 0 & U^{-1} \end{array}\right]$$

leads to $\dot{z} = Fz + Gu$

where

$$F = \left[\begin{array}{c|c} 0 & I_n \\ \hline -\Lambda_o & 0 \end{array}\right] = TAT^{-1}, \quad G = TB$$

Since A_o is p.d. the diagonal elements of Λ_o are all positive, i.e.,

$$\Lambda_o = \text{diag}\,(a_1, a_2, \ldots, a_n)$$

$$a_i > 0 \quad \forall\ 1 \leq i \leq n$$

The eigenvalues of the matrix F are found from

$$\lambda_i^2 + a_i = 0 \qquad i = 1, 2, \ldots, n$$

to yield

$$\lambda_i = \begin{cases} \hat{j}\sqrt{a_i} & i = 1, 3, 5, \ldots, 2n-1 \\ -\hat{j}\sqrt{a_i} & i = 2, 4, 6, \ldots, 2n \end{cases} \tag{1}$$

where

$$j \triangleq \sqrt{-1}$$

Let

$$U_o = [u_1, u_2, \ldots, u_{2n}]$$

$$V_o = [v_1, v_2, \ldots, v_{2n}]'$$

be the $2n \times 2n$ matrices of right and left eigenvectors, respectively, of the matrix F_o; i.e.,

$$F_o U_o = U_o \Lambda_o$$

$$V_o F_o = \Lambda_o V_o$$

where $\Lambda_o = \text{diag}\,(\lambda_1, \ldots, \lambda_{2n})$ is the diagonal matrix of eigenvalues obtained via Eq. (1). Then, it can be verified that

$$U_o = \begin{bmatrix} 1 & 1 & 0 & 0 & \cdots & \cdots & 0 & 0 \\ 0 & 0 & 1 & 1 & & & 0 & 0 \\ 0 & 0 & 0 & 0 & & & 0 & 0 \\ \vdots & \vdots & \vdots & \vdots & & & \vdots & \vdots \\ 0 & 0 & 0 & 0 & & & 1 & 1 \\ \lambda_1 & \lambda_2 & 0 & 0 & & & 0 & 0 \\ 0 & 0 & \lambda_3 & \lambda_4 & & & \vdots & \vdots \\ 0 & 0 & 0 & 0 & & & & \\ \vdots & \vdots & \vdots & \vdots & & & & \\ 0 & 0 & 0 & 0 & & & \lambda_{2n-1} & \lambda_{2n} \end{bmatrix} \qquad (2)$$

and

$$V_o = \begin{bmatrix} 1/2 & 0 & \cdots & 0 & 1/2\,\lambda_1 & 0 & \cdots & 0 \\ 1/2 & 0 & & 0 & 1/2\,\lambda_2 & 0 & \cdots & 0 \\ 0 & 1/2 & \cdots & 0 & 0 & 1/2\,\lambda_3 & \cdots & 0 \\ 0 & 1/2 & & 0 & 0 & 1/2\,\lambda_4 & \cdots & 0 \\ \vdots & & & & & & & \\ 0 & \cdots & 1/2 & 0 & 0 & \cdots & & 1/2\,\lambda_{2n-1} \\ 0 & \cdots & 1/2 & 0 & 0 & \cdots & & 1/2\,\lambda_{2n} \end{bmatrix} = U_o^{-1} \qquad (3)$$

Then, since

$$\phi_z(t, 0) = U_o e^{\Lambda_o t} V_o ,$$

the modal analysis performed above, in conjunction with the use of Euler's equations for complex numbers, can be used to obtain the transition matrix in closed form. Therefore, the 2n x 2n transition matrix is given by

$$\phi_z(t, 0) = \begin{bmatrix} \bar{\alpha} & \bar{\beta} \\ \bar{\bar{\gamma}} & \bar{\bar{\alpha}} \end{bmatrix} \left[\begin{array}{ccc|ccc} \bar{\alpha}_1 & & 0 & \bar{\beta}_1 & & 0 \\ & \ddots & & & \ddots & \\ 0 & & \bar{\alpha}_n & 0 & & \bar{\beta}_n \\ \hline \bar{\gamma}_1 & & 0 & \bar{\alpha}_1 & & 0 \\ & \ddots & & & \ddots & \\ 0 & & \bar{\gamma}_n & 0 & & \bar{\alpha}_n \end{array}\right] \tag{4}$$

where the elements of the four n x n diagonal blaocks are given by

$$\left.\begin{aligned} \bar{\alpha}_i &= \cos \sqrt{a_i}\, t \\ \bar{\beta}_i &= \frac{1}{\sqrt{a_i}} \sin \sqrt{a_i}\, t \\ \bar{\gamma}_i &= \sqrt{a_i} \sin \sqrt{a_i}\, t \end{aligned}\right\} \quad i = 1, 2, \ldots, n \tag{5}$$

For evaluating the controllability matrix defined in Eq. (22) we need $\phi_z(0, t)$ rather than $\phi(t, 0)$; however, since

$$\phi_z(0, t) = \phi_z^{-1}(t, 0)$$

it can be easily verified that

$$\phi_z(0, t) = \begin{bmatrix} \alpha & \beta \\ \gamma & \alpha \end{bmatrix} \tag{6}$$

where each of the four n x n blocks is diagonal with elements given by

$$\left.\begin{aligned} \alpha_i &= \bar{\alpha}_i \\ \beta_i &= -\bar{\beta}_i \\ \gamma_i &= -\bar{\gamma}_i \end{aligned}\right\} \quad i = 1, 2, \ldots, n \tag{7}$$

Using (5) yields the required expression for the transition matrix $\Phi_Z(0, t)$.

Appendix B

INVERSE OPTIMAL CONTROL FOR GENERALIZED COLLOCATED CONTROL

Ever since Kalman (Ref 1) formulated the inverse optimal control problem in 1964, the subject has been of significant interest in control theory (Refs 2 through 5). The inverse optimal control theory attempts to derive a class of performance indices which are optimized by a prespecified control input. In its simplest form, the state and input penalty matrices of a quadratic performance index are determined for linear feedback control of linear dynamic systems (Refs 1 and 6 Sec. 4.2).

Past research has never exploited the full potential of inverse optimal control theory. Once the control law has been specified, obtaining the optimizing cost functional itself has little direct value. However, when combined with known and previously proven properties of optimal control laws, the derived optimizing function aids understanding of the feedback and the robustness properties of the control law. An optimizing function is derived for a specific class of systems and is used to study controller properties.

This appendix addresses purely oscillatory systems defined by all poles and zeros on the imaginary axis. Large space structures (LSS) can be approximately described by such systems because of their typically low damping ratios. Quadratic optimizing functions are derived for control laws which increase damping ratios in such systems.

Consider the linear dynamic system described by

$$\begin{cases} \dot{x}(t) = Ax(t) + Bu(t), \; x \epsilon R^{2n}, \; u \epsilon R^{m} \\ y(t) = B^{T}x(t), \; y \epsilon R^{m} \end{cases} \tag{1}$$

where

$$A = \begin{bmatrix} 0 & I_n \\ \hline -A_o & 0 \end{bmatrix} \quad B = \begin{bmatrix} 0 \\ \hline B_o \end{bmatrix} \tag{2}$$

and the $n \times n$ matrix A_o is symmetric and positive-definite (pd) i.e.,

$$A_o = A_o^T > 0 \tag{3}$$

Next, consider the set of admissible controls, $\mathcal{U}$, defined by

$$\mathcal{U} \triangleq \left\{u \in R^m: \; u = Ky, \; \mathrm{Re}\,[\lambda(A + BKB^T)] < 0\right\} \tag{4}$$

where $\lambda(\cdot)$ stands for the eigenvalue of the argument, and $\mathrm{Re}(\cdot)$ is the real part of a complex number.

Let the objective function to be minimized be quadratic in the state and control over an infinite time period, i.e.,

$$J(x,u) \triangleq \int_o^\infty \left[x^T(t)Qx(t) + u^T(t)Ru(t)\right] dt \tag{5}$$

with

$$Q \geq 0, \quad R > 0 \tag{6}$$

Problem: (inverse optimal control problem)

Given an admissible control, u^*, under what conditions on K, Q, and R is this control law optimal, ie.., when is

$$J(x,u^*) = \min_{u \in \mathcal{U}} J(x,u) \tag{7}$$

If such an optimal control u^* exists, then (Ref 2)

$$u^* = Ky = -R^{-1}B^T Px \tag{8}$$

where P is the $2n \times 2n$ pd solution of the algebraic matrix Riccati equation (ARE) given by

$$PA + A^T P - PBR^{-1}B^T P + Q = 0 \tag{9}$$

The inverse optimal control problem is, therefore, the following. Given an admissible rate feedback control law find for what, if any, weight matrices Q and R, the ARE in Eq (9) is solved

Let the $2n \times 2n$ symmetric P and Q matrices be partitioned as

$$P = \left[\begin{array}{c|c} P_{11} & P_{12} \\ \hline P_{12}^T & P_{22} \end{array}\right] \quad Q = \left[\begin{array}{c|c} Q_{11} & 0 \\ \hline 0 & Q_{22} \end{array}\right] \tag{10}$$

Then from the ARE in Eq (9), we find

$$P_{11} - A_o P_{22} - P_{12} B_o R^{-1} B_o^T P_{22} = 0 \tag{11}$$

$$P_{12} A_o + A_o P_{12}^T + P_{12} B_o R^{-1} B_o^T P_{12} = Q_{11} \tag{12}$$

$$P_{22}B_oR^{-1}B_o^TP_{22} - P_{12}P_{12}^T = Q_{22} \tag{13}$$

Since a rate feedback control law is used, we find from Eq (8) that

$$B_o^TP_{12} = 0 \longleftrightarrow P_{12} \in \mathcal{N}\left(B_o^T\right) \tag{14}$$

Therefore, P_{12} can be expressed as

$$P_{12} = N_1 \Phi N_1^T \tag{15}$$

where

$$N_1 \in \mathcal{N}\left(B_o^T\right) \tag{16}$$

$$\Phi = \Phi^T > 0 \tag{17}$$

The $n \times n$ matrix P_{12} as given in Eq (15) is symmetric and from Eq (17), psd. The latter condition is required to satisfy Eq (12) since $(-A_o)$ is a stable matrix.

Lemma 1:

For a dynamic system under a rate feedback control law, the $n \times n$ matrix P_{12} in Eqs (11) through (13) has to satisfy

$$P_{12} = 0 \tag{18}$$

Proof:

This is verified by observing Eq (13) where Q_{22} has to be at least psd.

Since $P_{12} = 0$, the resulting $2n \times 2n$ matrix P that solves the ARE will be a block diagonal matrix. This motivates the following form for the matrix P to be checked as a possible solution of the ARE.

Let

$$P = \alpha B(B^T B)^{-1} B^T + NEN^T \tag{19}$$

where

$$N \in \mathcal{N}(B^T), \quad N \in R^{2n \times (2n - m)} \tag{20}$$

$$N^T N = I_{2n - m} \tag{21}$$

$$\alpha \in R_+^1$$

$$E = E^T > 0 \quad E \in R^{(2n - m) \times (2n - m)} \tag{22}$$

It is clear that P in Eq (19) is symmetric. To show that it is also pd we note that

$$PB = \alpha B \tag{23}$$

$$PN = NE \tag{24}$$

Therefore, B and N are right eigenvectors of the matrix P corresponding to positive eigenvalues; therefore, P is pd. Similar results are obtained for left eigenvectors.

Using the form for P as given in Eq (19) the ARE can be written as

$$PA + A^T P - \alpha^2 B R^{-1} B^T + Q = 0 \tag{25}$$

Since

$$B = \begin{bmatrix} 0 \\ \hline B_o \end{bmatrix}$$

we find that to satisfy Eq (20)

$$N = \left[\begin{array}{c|c} 0 & I_n \\ \hline N_o & 0 \end{array}\right], \quad N_o \epsilon R^{n \times (n-m)} \tag{26}$$

where N_o is chosen such that

$$B_o^T N_o = 0 \longleftrightarrow N_o \epsilon \mathcal{N}\left(B_o^T\right) \tag{27}$$

$$N_o^T N_o = I_{n-m} \tag{28}$$

Let the symmetric matrix E in Eq (19) be partitioned as follows

$$E = \underbrace{\left[\begin{array}{c|c} E_1 & E_2 \\ \hline E_2^T & E_3 \end{array}\right]}_{n-m \quad m} \begin{matrix} \} \ n-m \\ \} \ m \end{matrix} \tag{29}$$

Theorem 1:

A necessary and sufficient condition for P in Eq (19) to solve the ARE in Eq (9) is that

$$Q = \left[\begin{array}{c|c} 0 & 0 \\ \hline 0 & \alpha^2 B_o R^{-1} B_o^T \end{array}\right] \tag{30}$$

$$E = \left[\begin{array}{c|c} \alpha I_{n-m} & 0 \\ \hline 0 & \alpha A_o \end{array}\right] \tag{31}$$

The 2n x 2n pd solution matrix P is given by

$$P = \left[\begin{array}{c|c} \alpha A_o & 0 \\ \hline 0 & \alpha I_n \end{array}\right] \tag{32}$$

Proof: (sufficiency)

$$P = \left[\begin{array}{c|c} 0 & 0 \\ \hline 0 & \alpha B_o \left(B_o^T B_o\right)^{-1} B_o^T \end{array}\right] + \left[\begin{array}{c|c} \alpha A_o & 0 \\ \hline 0 & \alpha N_o N_o^T \end{array}\right]$$

since, from Eqs (27) and (28)

$$\left[\begin{array}{c} B_o^T \\ \hline N_o^T \end{array}\right]^{-1} = \left[\begin{array}{c|c} B_o \left(B_o^T B_o\right)^{-1} & N_o \end{array}\right] \tag{33}$$

we get

$$P = \left[\begin{array}{c|c} \alpha A_o & 0 \\ \hline 0 & \alpha I_n \end{array}\right]$$

$$Q = \alpha^2 B R^{-1} B^T - PA - A^T P = \left[\begin{array}{c|c} 0 & 0 \\ \hline 0 & \alpha^2 B_o R^{-1} B_o^T \end{array}\right]$$

(necessity) from Eq (25)

$$Q = \alpha^2 B R^{-1} - PA - A P$$

Since

$$P = \left[\begin{array}{c|c} E_3 & E_2^T N_o^T \\ \hline N_o E_2 & \alpha B_o \left(B_o^T B_o\right)^{-1} B_o^T + N_o E_1 N_o \end{array}\right]$$

we find

$$Q = \left[\begin{array}{c|c} E_o^T N_o A_o + A_o N_o^T E_2 & A_o \left[\alpha B_o^T \left(B_o B\right)^{-1} B_o^T + N_o E_1 N_o^T\right] - E_3 \\ \hline \left[\alpha B_o \left(B_o^T B_o\right)^{-1} B_o^T + N_o E_1 N_o^T\right] A_o - E^3 & \alpha^2 B_o R^{-1} B_o^T - N_o E_2 - E_2 N_o^T \end{array}\right]$$

Since Q is block diagonal, then using Eq (33) and Lemma 1, we find

$$E_1 = \alpha I_n - m$$

$$E_2 = 0$$

$$E_3 = \alpha A_o$$

Once the solution to the ARE is obtained, one can find the optimal control as well. For the case where the sensors and actuators are co-located we have the following.

Corollary 1:

When the output feedback control law is chosen as

$$u = Ky \tag{34}$$

where K is a symmetric, $m \times m$ negative-definite (nd) matrix and the output is given through

$$y = B^T x \tag{35}$$

then

$$R = -\alpha K^{-1} \tag{36}$$

is the $m \times m$ control penalty matrix of the quadratic objective function

$$J = \int_0^\infty \left(x^T Q x + u^T R u \right) dt \tag{37}$$

Proof:

The optimal control that minimizes Eq (37) is given by

$$u^* = -R^{-1} B^T P x$$

using the solution matrix P from Eq (32) we find

$$u^* = -\alpha R^{-1} B^T x$$

hence

$$K = -\alpha R^{-1}$$

Appendix C
DESIGN OF CONTROL LAWS WITH FREQUENCY SHAPED COST FUNCTIONALS

The design problem treats a linear problem

$$\dot{x} = Fx + gu$$

$$y = Hx$$

and the following performance index is to minimized:

$$J = \frac{1}{2}\int_{-\infty}^{\infty} x^*(j\omega)A(j\omega)\ x(j\omega) + u^*(j\omega)B(j\omega)u(j\omega)\ \ d\omega$$

Note that the weighting functions are functions of frequency.

If the weighting functions $A(j\omega)$ and $B(j\omega)$ are assumed to be rational functions of squared frequency, ω^2, a systematic control design procedure, may be developed for positive semidefinite $A(j\omega)$ and positive definite $B(j\omega)$. This is not a serious limitation because a wide variety of functional forms may be approximated by ratios of polynominals. To develop a specific control design procedure, it is further assumed that $A(j\omega)$ has rank p, and $B(j\omega)$ is positive definite with full rank, q

$$A(j\omega) = P_1^*(j\omega)P_1(j\omega) \qquad (1)$$

$$B(j\omega) = P_2^*(j\omega)P_2(j\omega) \qquad (2)$$

P_1 and P_2 are pxn and qxq rational matrices. Define

$$P_1(j\omega)x = x^1 \tag{3}$$

$$P_2(j\omega)u = u^1 \tag{3}$$

If $P(j\omega)$ is a ratio of polynominals in $j\omega$ and the number of zeros does not exceed the number of poles, Eq (3) may be written as a system of differential equations with output x^1.

$$\dot{z}_1 = F_1 z_1 + G_1 x$$

$$x^1 = H_1 z_1 + d_1 x \tag{5}$$

D_1 is zero if the number of poles is at least one more than the number of zeros. Equation (4) may also be written in terms of a differential equation, again if the number of zeros does not exceed the number of poles.

$$\dot{z}_2 = F_2 z_2 + G_2 u$$

$$\dot{u}^1 = H_2 z_2 + D_2 u \tag{6}$$

The dynamic Eq (1) and the cost functional (16) may now be written in terms of an extended state vector.

$$\frac{d}{dt}\begin{bmatrix} x \\ z_1 \\ z_2 \end{bmatrix} = \begin{bmatrix} F & 0 & 0 \\ G_1 & F_1 & 0 \\ 0 & 0 & F_2 \end{bmatrix}\begin{bmatrix} x \\ z_1 \\ z_2 \end{bmatrix} + \begin{bmatrix} G \\ 0 \\ G_2 \end{bmatrix}^u \tag{7}$$

$$J_{ss} = E\, x^T \begin{pmatrix} z_1^T & z_2^T & u^T \end{pmatrix} \begin{bmatrix} D_1^T D_1 & 0 & 0 \\ H_1^T D_1 & 0 & 0 \\ 0 & H_2^T H_2 & H_2^T D_2 \\ 0 & D_2^T H_2 & D_2^T D_2 \end{bmatrix} \begin{bmatrix} x \\ z_1 \\ z_2 \\ u \end{bmatrix} \tag{8}$$

Defining appropriate vectors and matrices, Eqs (7) and (8) become

$$x^1 = F^1 x^1 + G^1 u \tag{9}$$

$$J = \lim_{T \to \infty} \frac{1}{2T} \int_0^T \begin{bmatrix} x^1 T_u T \end{bmatrix} \begin{bmatrix} A_T & N \\ N^T & B \end{bmatrix} \begin{bmatrix} x^1 \\ u \end{bmatrix} dt \tag{10}$$

The control law is obtained by solving the following modified algebraic Riccati equation

$$- S F^1 - F^1 S - A + (S G^1 + N) B^{-1} (S G^1 + N)^T = 0 \tag{11}$$

and

$$u = B^{-1} (S G + N)^T x^1 \tag{12}$$

Equation (12) is written in an equivalent form as

$$u = C_1 x + C_2 z_1 + C_3 z_2 \tag{13}$$

The generalized controller structure is then shown in Fig. 1. This controller has the form of a general dynamic compensator. The transfer function between the control input u and the state x is

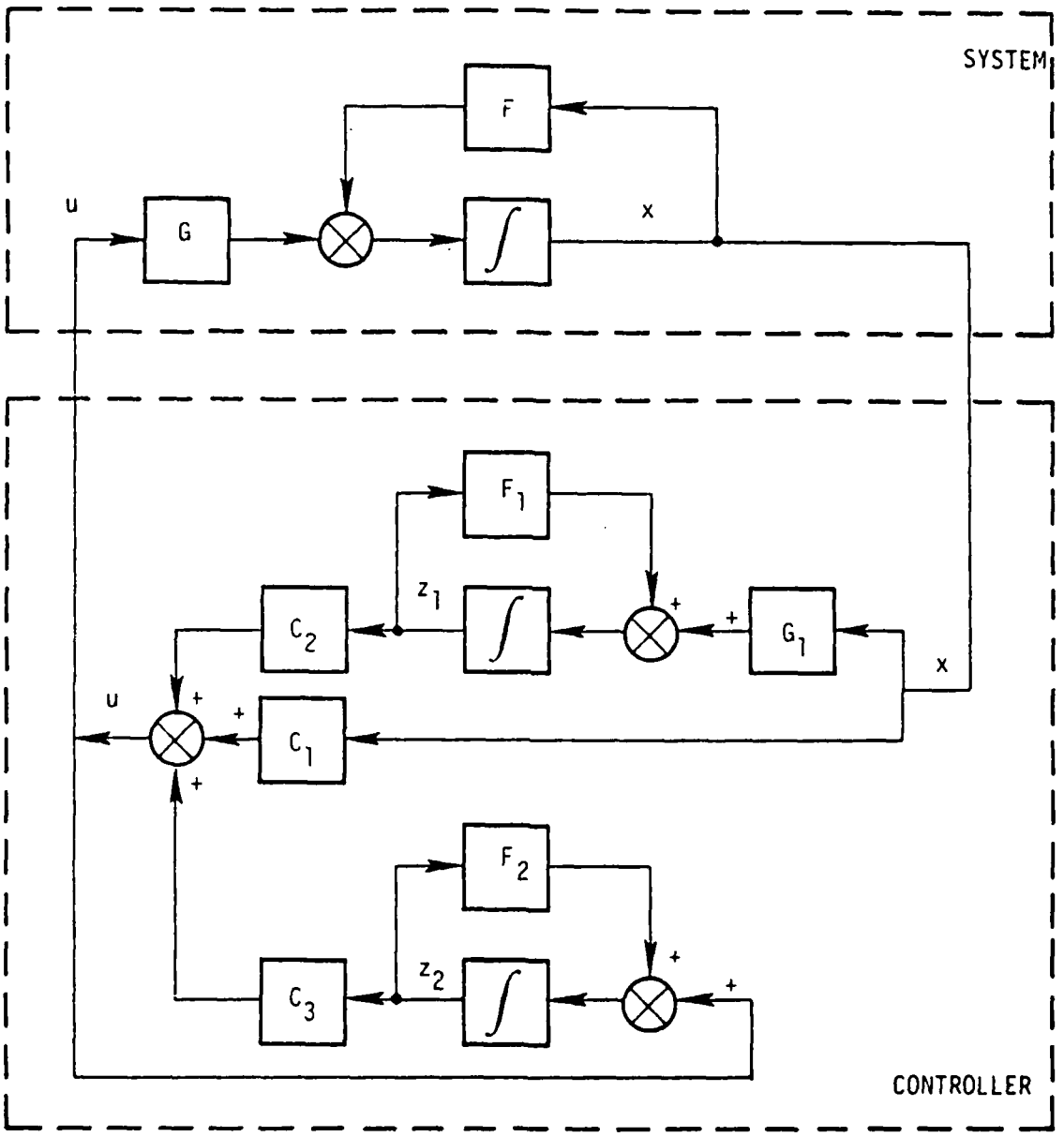

Fig. 1 Structure of the Generalized Controller

$$z_1(j\omega) = (j\omega I - F_1)^{-1} G_1 x \tag{14}$$

$$z_2(j\omega) = (j\omega I - F_2)^{-1} G_2 u \tag{15}$$

$$\left[I - C_3(j\omega I - F_2)^{-1} G_2\right] u(j\omega) = \left[C_1 + C_2(j\omega I - F_1)^{-1} G_1\right] x(j\omega) \tag{16}$$

or

$$u(j\omega) = \left[I - C_3(j\omega I - F_2^{-1} G_2\right]^{-1} \left[(C_1 + C_2(j\omega I - F_1)^{-1} G_1\right] x(j\omega)$$

The compensator may be expressed in an equivalent form shown in Fig. 2. Note that the transfer functions between x^1 and u and u^1 and u are

$$x^1(j\omega) = \left[H_1 (j\omega I - F_1)^{-1} G_1 + D_1\right] x(j\omega) \tag{17}$$

$$u^1(j\omega) = \left[H_2 (j\omega I - F_2)^{-1} G_2 + D_2\right] u(j\omega) \tag{18}$$

Therefore, the poles of $P_1(j\omega)$ and $P_2(j\omega)$ show up as compensator poles and zeros, respectively and directly influence the closed loop transfer function. This provides a direct relationship between the form of the frequency dependence shaping used in the cost function and the structure of the overall compensator.

If the number of zeros in $P_1(j\omega)$ exceeds the number of poles, Eq (5) must be modified. For example, if $P_1(j\omega)$ has one more zero than poles, Eq (5) may be written as

$$\dot{z}_1 = F_1 z_1 + G_1 x$$

$$x^1 = H_1 z_1 + D_1 x + D_{11} \dot{x} \tag{19}$$

Using Eq (1), this may be written as

$$\dot{z}_1 = F_1 z_1 + G_1 x$$

$$x^1 = H_1 z_1 + D_1 x + D_{11} (Fx + Gu)$$

$$= H_1 z_1 + (D_1 + D_{11} F) x + D_{11} Gu \tag{20}$$

Therefore when $P_1(j\omega)$ may have k_1 more zeros than poles, a more general form for Eq (5) is

$$\dot{z} = F_1 z_1 + G_1 x$$

$$x^1 = H_1 z_1 + D_1 x + \sum_{i=0}^{k_1 - 1} D_1 \, i \, u^{(i)} \tag{21}$$

where $u^{(i)}$ is the i^{th} derivative of u. Equations (6), (7), and (8) are also modified in a similar way.

Selection of Weighting Matrices

It appears that a solution can be guaranteed if $B(j\omega)$ is positive definite and $A(j\omega)$ is positive semi-definite at all but a finite number of discrete frequencies (though this is not a necessary condition). It should be pointed that that even under these constraints, the solution may not be easy to find and in fact may not even be causal. The total class of weighting functions for which a causal may be found will be subjects of future research.

Appendix D
MINIMUM-ENERGY CONTROL

Consider the linear dynamic system described by

$$\dot{x}(t) = A(t)\,x(t) + B(t)\,u(t)\ ,\ x\ R^n\ ,\ u\ R^n \tag{1}$$

Next, define the controllability matrix by

$$W(t_o,t_1) \triangleq \int_{t_o}^{t_1} \Phi(t_o,\tau)B(\tau)B'(\tau)\ \Phi'(t_o,\tau)d\tau \tag{2}$$

where prime indicates transposition (real or complex), and $\Phi(.)$ is the transition matrix. Then we have the following.

THEOREM

For a controllable system described by Eq (1), the controllability matrix is nonsingular and the input that transfers the initial state x_o to a desired final state $x(t_1)$ in a finite time $t_1 > t_o$ is given by

$$U^*(t) = B'(t)\Phi(t_o,t)W^{-1}(t_o,t_1)\ \Phi(t_o,t_1)x(t_1)-x_o \tag{3}$$

Furthermore, this input requires the minimal control energy. This minimal energy is given by

$$J^* \triangleq \int_{t_o}^{t_1} ||u(\tau)||^2\, d\tau = x_o'\, W^{-1}(t_o,t_1)x_o \tag{4}$$

for a system whose final state is the origin $x(t_1) = 0$.

PROOF:

First we prove that the control in Eq (3) transfers the initial state x_o to the desired final state $x(t_1)$. The solution to Eq (1) is given by

$$x(t) = \Phi(t,t_o)x_o + \int_{t_o}^{t} \Phi(t,\tau)B(\tau)u(\tau)d = \Phi(t,t_o)\left[x_o + \int_{t_o}^{t} \Phi(t_o,\tau)B(\tau)u(\tau)d\tau\right] \tag{5}$$

where we have used the property

$$\Phi(t,\tau) = \Phi(t,t_o)\Phi(t_o,\tau) .$$

Using Eq (3) in Eq (5) we find

$$x(t_1) = \Phi(t_1,t_o)\left\{x_o + \left[\int_{t_o}^{t_1} \Phi(t_o,\tau)B(\tau)B'(\tau)\Phi(t_o,\tau)d\tau\right] \cdot W^{-1}(t_o,t_1)\left[\Phi(t_o,t_1)x(t_1)-x_o\right]\right\}$$

Using the definition in Eq (2)

$$x(t_1) = \Phi(t_1,t_o)\left\{x_o + W(t_o,t_1)W^{-1}(t_o,t_1)\left[\Phi(t_o,t_1)x(t_1)-x_o\right]\right\}$$

$$= \Phi(t_1,t_o)\left[x_o + \Phi(t_o,t_1)x(t) - x_o\right]$$

and using the fact that

$$\left[\Phi(t_o,t_1)\right]^{-1} = \Phi(t_1,t_o)$$

we obtain the result.

Next we show the minimal energy property. Let $\{u(t)\}$ be any control sequence that transfers the initial state x_o to $x(t_1)$, then we have to show that

$$\int_{t_o}^{t_1} \|u(t)\|^2 \, dt \geq \int_{t_o}^{t_1} \|u^*(t)\|^2 \, dt \tag{6}$$

Define

$$\overline{x} = \Phi^{-1}(t_1,t_o)x(t_1) - x_o - \Phi(t_o,t_1)x(t_1) - x_o$$

then, by the assumption that both control sequences transfer x_o to $x(t_1)$ we have from Eq (5)

$$\overline{x} = \int_{t_o}^{t_1} \Phi(t_o,\tau)B(\tau)u_1(\tau)d = \int_{t_o}^{t_1} \Phi(t_o,\tau)B(\tau)u^*(\tau)d$$

Subtracting

$$\int_{t_o}^{t_1} \Phi(t_o,\tau)B(\tau)\left[u_1(\tau) - u^*(\tau)\right] d\tau = 0$$

which implies

$$\left\langle \int_{t_o}^{t_1} \Phi(t_o,\tau)B(\tau)\left[u_1(\tau)-u^*(\tau)\right]d\tau,\ W^{-1}(t_o,t_1)\overline{x} \right\rangle = 0$$

where $\langle .,. \rangle$ is the usual inner product.

Since $\langle x,Ay \rangle = \langle A'x,y \rangle$ we have

$$\int_{t_o}^{t_1} \left\langle u_1(\tau)-u^*(\tau),\ B'(\tau)O'(t_o,\tau)W^{-1}(t_o,t_1)\overline{x} \right\rangle d\tau = 0$$

and using Eq (3) this becomes

$$\int_{t_o}^{t_1} \left\langle u_1(\tau)-u^*(\tau),\ u^*(\tau) \right\rangle d\tau = 0$$

Consider now

$$\int_{t_o}^{t_1} \|u_1(\tau)\|^2 d = \int_{t_o}^{t_1} \|u_1(\tau) - u^*(\tau) + u^*(\tau)\|^2 d\tau$$

$$= \int_{t_o}^{t_1} \|u_1(\tau) - u^*(\tau)\|^2\, d + \int_{t_o}^{t_1} \|u^*(\tau)\|^2\, d\tau$$

$$+ 2 \int_{t_o}^{t_1} \left\langle u_1(\tau) - u^*(\tau),\, u^*(\tau) \right\rangle d\tau$$

$$= \int_{t_o}^{t_1} \|u_1(\tau) - u^*(\tau)\|^2 \, d\tau + \int_{t_o}^{t_1} \|u^*(\tau)\|^2 \, d\tau$$

Since

$$\int_{t_o}^{t_1} \|u_1(\tau) - u^*(\tau)\|^2 \, d\tau \geq 0$$

we conclude

$$\int_{t_o}^{t_1} \|u_1(\tau)\|^2 \, d\tau \geq \int_{t_o}^{t_1} \|u^*(\tau)\|^2 \, d\tau$$

Finally

$$J^{*'} = \int_{t_o}^{t_1} \|u^*(\tau)\|^2 \, d\tau$$

$$= \int_{t_o}^{t_1} x' \, W^{-1}(t_o,t_1)\Phi'(t_o,\tau)B(\tau)B'(\tau)\Phi(t_o,\tau)W^{-1}(t_o,t_1)\bar{x} \, d\tau$$

$$= \bar{x}' \, W^{-1} \, x = x_o' \, W^{-1} \, x_o$$

Since it is assumed that

$$x(t_1) = 0 .$$

MISSION
of
Rome Air Development Center

RADC plans and executes research, development, test and selected acquisition programs in support of Command, Control Communications and Intelligence (C^3I) activities. Technical and engineering support within areas of technical competence is provided to ESD Program Offices (POs) and other ESD elements. The principal technical mission areas are communications, electromagnetic guidance and control, surveillance of ground and aerospace objects, intelligence data collection and handling, information system technology, ionospheric propagation, solid state sciences, microwave physics and electronic reliability, maintainability and compatibility.